Excess Pore Pressures under Cyclically Loaded model Jack-up Foundations

by

Yu Sheng HSU

A dissertation submitted for the degree of

Doctor of Philosophy

at

University of Cambridge

England

Wolfson College

April 1998

To My Parents, family and Winnie

SUMMARY

Excess pore pressures under cyclically loaded model jack-up foundations

Numerous centrifugal modelling research programmes have been carried out at Cambridge University to observe the drained response of circular foundations on sand. In this new series of centrifugal tests, the effects of excess pore pressure under spud-can foundations of a scaled model three-leg offshore jack up structure subjected to horizontal cyclic loadings were studied. The medium dense to dense sand layer under the foundation was saturated with viscous silicone oil to ensure that the transient flow could be measured and was close to the prototype response. The viscosity of the silicone oil used was about 3-4 times more than required for the prototype, to investigate the possibility of inducing liquefaction. The test series has shown that macroscopic partially drained behaviour was different from that expected in the drained or undrained conditions. Observations in the centrifuge tests indicate that there was a reduction of vertical and rotational stiffness of soil when the vertical loading during a cyclic event falls below its initial value (before the start of the cyclic event). Thus, structural design methods should if possible avoid the use of a single fixity value for design. However, the centrifuge experiments have shown that despite numerous cyclic loadings at different frequencies and amplitudes, the foundation of the model jack up structure did not fail.

A comparison between the performance of non-skirted and rigid vertical skirted flat spuds subjected to similar cyclic loadings was carried out to deduce the effects of suction under skirted foundations. The rigid vertical skirted foundation did not have increased fixity. The non-skirted foundations settled more than the skirted ones. During the pull-out event, much greater and more reliable suction forces were induced under the skirted foundations.

The excess pore pressure behaviour under the foundation is extremely complex. There is no evidence of pore pressure building up in any of the events conducted in the nine tests. However, the excess pore pressure is a function of the cyclic loading amplitude, the cyclic frequency and the position under the foundation. Both double and single frequency pore pressure behaviours are present. The maximum and minimum pore pressure values do not coincide with the maximum and minimum loads. This pore pressure behaviour can be explained through the Characteristic State Concept (Luong and Sidaner, 1981). The excess pore pressure data can also be used to predict vertical permanent deformation and cyclic settlement profile.

PREFACE

The work described in this thesis would not have been possible, without the financial support of Esso Exploration and Production UK Limited (EEPUK) and the Health and Safety Executives (HSE), and without the skilful management of the EEPUK contract by J.D. Murff and P. Wong of Exxon Production Research (EPRCo). I would like also thank M. Thompson, N. Brown and M. Birkinshaw of HSE, N. Baltrop of W.S. Atkins, C.K. Lau formerly at W.S. Atkins, and P. Laws of Marine and Technology Support Unit (Matsu). I would like to thank EEPUK and HSE for giving me permission to include the testing programme and typical test data from the experimental test reports and would like to stress that any opinions or interpretations expressed in this thesis are those of the author and do not purport to represent opinions of the organisations involved.

I am also grateful to my supervisor, Prof. A.N. Schofield, for giving me the chance to carry out research at the University of Cambridge and whose leadership in the Soil Mechanics Group has created a dynamic and friendly environment. I wish to thank my project manager, Dr E.T.R. Dean and the consultant, Dr R.G. James for their invaluable judgements, advice, patience and suggestions during my experimental work. I would like to thank the Cambridge University Engineering Department (CUED) staff members involved in the project in particular; C.H. Collison, P. Ford, J.A. Chandler, T. Albett and S.G. Chandler for their technical support, and N.H. Baker, A.Brand and B. Perry for the electronics support. I would also like to thank the academic staff and research students of the Soil Mechanics Group who have provided me with support, intellectually motivating discussions and great friendship.

Under the present arrangements for management of centrifuge operations and contracts, a company called Andrew N. Schofield and Associates Limited (ANS&A) undertakes many of the contracts such as the EEPUK contract referred to; within ANS&A, I would like to thank J.A. Curtis and K. Wilkinson.

I certify that, except where specific reference is made in the text to the work of others, the contents of this dissertation are original and have not been submitted to any other University. This dissertation is the result of my own work and includes nothing which is the outcome of work done in collaboration.

Yu Sheng Hsu

April, 1998

DEFINITIONS OF SYMBOLS USED IN SEVERAL PLACES IN THE TEXT

Roman (Lowercase)

c	soil cohesion
d	depth
e	void ratio
e_c	eccentricity
g	earth's gravity acceleration
h	horizontal displacements
h_s	sample height
i	hydraulic gradient
k	secant stiffness
k_{FL}	permeability
n	material parameter
q'	deviatoric principal stress
q_o	overburden stress
q_p'	deviatoric stress at peak shear stress
p'	mean effective principal stress
p_p'	mean effective stress at peak shear stress
s_i	approximate inclination factor
t	time
t_f	footing space
t_p	prototype time
t_m	model time
u	pore pressure
u_{EQ}	equilibrium static pore pressure
u_{XS}	excess pore pressure
v	specific volume
Δv	change in vertical displacements
v_p	permanent vertical deformation
x	horizontal displacements
y	vertical displacements
z	depth of position of interest below seabed

Roman (Uppercase)

A	area
A_1	effective area of fluid entering the region below the spud-can foundation
A_2	bottom area of spud-can foundation
B	width or diameter of foundation
B'	reduced width
C_r ,C_v	constants
D	depth between sea surface and bed
E	elastic modulus
G_s	specific gravity of solids
G_r	rotational stiffness
G_v	vertical stiffness
H	horizontal load
ΔH	horizontal load amplitudes (i.e. H_{MAX} - H_{MIN})
ΔH_1	horizontal load amplitude measured at leeward spud can tip
ΔH_2 , ΔH_3	horizontal load amplitude measured at windward spud can tips
H_1	horizontal load reaction at leeward spud can tip
H_2 ,H_3	horizontal load reactions at windward spud can tips
H_{MAX}	maximum horizontal force applied
H_{MIN}	minimum horiozntal force applied
H_T	total (Global) horizontal loading consisting of wind, current and wave loading
I	moment of inertia
K	bulk modulus
L	length
L_m	length for model
L_p	length for prototype
M	moment reaction
ΔM	moment reaction amplitude (i.e. M_{MAX} - M_{MIN})
ΔM_1	moment reaction amplitude measured at leeward spud can tip
ΔM_2 , ΔM_3	moment reaction amplitude measured at windward spud can tips
M_1	moment reaction at leeward spud can tip
M_2,M_3	moment reaction at windward spud can tips
M_c	slope of effective stress locus of critical states plotted in (p',q) space
M_{MAX}	maximum moment reactions measured

M_{MIN}	minimum moment reactions measured
N	increase in gravity level due to centrifuge
N_γ, N_q, N_c	bearing capacity factors
P_A	excess pore pressure at A
P_B	excess pore pressure at B
Q_{FL}	quantity of flow
T_p	time period for prototype
T_m	time period for model
V	vertical load
ΔV	vertical load amplitude (i.e. V_{MAX}-V_{MIN})
ΔV_1	vertical load amplitude measured at leeward spud can tip
ΔV_2 , ΔV_3	vertical load amplitude measured at windward spud can tips
V_1	vertical load reaction at leeward spud can tip
V_2, V_3	vertical load reactions at windward spud can tips
V_m	maximum value of vertical load
V_{MAX}	maximum vertical load measured
V_{MIN}	minimum vertical load measured
V_p	total preload value usually twice working vertical load
V_T	total (global) vetical reaction response
V_w	working vertical load
W	weight of jack-up structure and legs

Greek

α, β	parameters depending ont he shape of the foundation
β_i	angle of inclination
δ	lateral displacement of deck
Γ	Ordinate of critical state line
δ'	angle of friction between soil and structure
ε_v	volumetric strain
ε_s	shear strain
ϕ'	effective angle of internal friction of soil
ϕ_c'	critical angle of friction
ϕ_{MAX}'	maximum shearing angle of friction
ϕ_{PEAK}'	peak angle of friction

γ'	submerged unit weight of saturated soil
γ_w	unit weight of water
η	ratio of deviatoric stress over mean effective stress
φ'	dilation angle
κ	slope of swelling line in (p',v) space
λ	slope of compression line in (p',v) space
μ	frictional coefficient
ν	poisson's ratio
θ	angle of rotation
ρ'	submerged mass density of saturated soil
ρ_b	bulk mass density of saturated soil
ρ_w	bulk mass density of water
σ	total stress
σ'	effective stress
σ_a'	effective deviatoric stress
σ_r'	effective radial stress
σ_v	total vertical stress
σ_v'	effective vertical stress
τ	shear stress
τ_{MAX}	maximum shear stress
ψ	state parameter

CONTENTS

1. INTRODUCTION

1.1 Background

Jackup platforms are mobile offshore structures deployed at offshore locations and are often associated with exploration of oil and gas. Conventional jackup platforms are not piled to the sea bed or equipped with a bottom mat. They usually consist of a hull supported on three-legs or a multi-pod with spud-cans as the foundation. A typical jackup installation and large spud geometry are shown in fig. 1.1 and fig. 1.2 respectively. To provide additional moment fixity for jackup structures, existing spud-can foundations are fitted with skirts (fig. 1.3) as described by Geir Svan∅ (1993). This modification utilises the suction capacity within the enclosed soil in the skirted spud for short duration unloading and also increases the effective foundation area.

This has generated some discussions (Dean, 1991, Dean et al, 1995 City University) about excess pore pressure behaviour generation under both skirted and non-skirted spudcan foundation especially when the jackup structure is subjected to cyclic loading. There is also concern about the possibility of liquefaction occurring under spudcan foundation as experienced by structures subjected to earthquake or dynamic loading.

1.2 Severity of Extreme Storm Conditions

A review of jackup operations by McClelland (1981) revealed that mobile jackup rigs are more prone to accidents than other engineering structures. A third of these accidents are related to foundation problems. This has been greatly reduced in recent years from the historical point of view, implying that the reliability inherent in present design practice is extremely high. However, accidents as the result of extreme storm conditions can still occur. Thus, design of offshore jack up platforms in harsh waters of the North Sea is largely governed by extreme storm environmental loading, serviceability criteria and economic limits. The ability to predict accurately the safety of jack up under extreme storm loading remains an important factor in the continued safe and economic exploitation of hydrocarbon resources offshore.

One reported example of jackup failure in relation to extreme storm conditions includes the following: On 9 August 1980, a total loss of US$ 30 million was incurred when a three-leg rig, located off Texas was struck by hurricane Allen. It overturned and disappeared into the sea. In another incident dated June 1974, off Madagascar, one leg of the (three-leg) Gato Salcatico jackup penetrated deeper below the sea floor during a storm causing physical damage. The unit was later salvaged but at a cost of US$ 4 million.

Efthymiou et al (1990) gave a summary of the survival experience of five fixed offshore platforms subjected to extreme storm conditions (see in Table 1.1). The Overload Ratio is defined as the ratio of the calculated environmental load (base shear), 'experienced' by the platform (by performing back calculations of the collapsed or survived platform) during the hurricane, to the design environmental load. This numerator has been estimated using hindcast winds, waves and currents for the individual hurricanes, 'best belief' kinematic models and realistic values of hydrodynamic coefficients. The denominator is the environmental load as used in the original (1960s) design of the platforms. It can be seen in Table 1.1 that the notional overload ratio ranges from 2.56 to 4.50. Two platforms with overload ratio of 4.50 collapsed. Thus, estimation of environmental loading used in the original design was not as accurate as required.

The problem in the 1960s lay in the underestimation of storm loads from the natural sea environment and soil mechanics strength calculations. Storm loading consists of wind-driven waves having different wavelengths, amplitudes and periods, travelling at different speeds and in different directions, plus storm-driven and tidal currents. This complexity is reflected in the resulting wave particle motions which affect loading. Moreover, with known water particle motions, there is still the problem of estimating the magnitude of loading. This problem has also defied theoretical solution and reliance has had to be placed on extensive measurement programmes. There was an urgent need to acquire knowledge about the foundation response to such extreme storm conditions because the foundation behaviour will dictate the stress levels experienced in the structural members when environmental loads exceed estimated design load values.

A joint industry study was co-ordinated by Noble Denton (Osborne, et al., 1991) who were advised by R.G. James to analyse spud fixity by an elasto-plastic method, using a yield locus equation that he had developed from studies of fixity of small model foundations in the

Cambridge Soil Mechanics Laboratory. He proposed that more test data should be obtained to check the equation that he had proposed.

Attempts at observation have been made; for example the objective with the Kolskaya rig (McCarron and Broussard, 1992) was to evaluate and determine the degree of spud-can rotational restraint ('fixity') offered by a sand sea floor during an extreme storm conditions, which then did occur on 12 December 1990 at the Hod location in the North Sea. The estimated elevated weight of the jackup structure and legs (W) was about 13,600 tonnes = 136 MN. The global wave load experience by the jackup was estimated to be in excess of 13 MN. This implies that during those extreme storm conditions, the H_{MAX}/W ratio was more than 1/10.

In recent years, several instrumented jack ups have experienced severe storms. However, it would be ideal if it was possible to instrument all jackup rigs which were installed in regions where severe storm conditions are expected. Soil-structural interaction behaviour could be investigated and pore pressure transducers could also be attached to the bottom of the spuds or buried in the ground to measure pore pressure generation. Since it is not economically viable to instrument all jack-up rigs, close attention has been paid to the possibility of numerical and physical models, in particular of centrifuge modelling of spud-can foundation behaviour near failure.

1.3 Centrifugal Modelling

Extreme loading can be applied repeatedly and safely in model tests. Cambridge University has pioneered centrifuge model studies of the undrained and drained response of circular spud footings in clay and dry sand respectively (Silva Perez, 1982). Dr R.G. James, as a Cambridge University Engineering Department Assistant Director of Research, with responsibilities for the development of the Cambridge Geotechnical Centrifuge Centre (CGCC), continued these studies with centrifuge tests undertaken under his supervision (Tan, 1990). Subsequently, several tests have been carried out in which a model jackup structure or an individual spud-can foundation have been subjected to vertical, horizontal and moment loading, by applying a horizontal monotonic or cyclic loading. These studies have helped designers draw some conclusions about bottom fixity under spud-can foundations that could justify the use of certain jackup structures in deeper and/or more exposed water. Esso

Exploration and Production UK Ltd (EEPUK) with technical management by Exxon Production Research Company (EPRCo), funded a series of tests (Tsukamoto, 1994) in which three leg rigs and single leg were fitted with a variety of different conical or flat bases, and tests were made to study spud fixity.

Up to now, some work has been conducted investigating excess pore pressure under gravity platforms but little work has been related to model spud-cans and their effect on the fixity of jackups. The generation of transient pore pressure cannot at present be predicted confidently using numerical models. This is because a transient pore pressure problem must be treated as a consolidation problem in which excess pore pressure generated by consolidation may cause permanent deformation to occur, and in some cases, deformation may create tension cracks causing excess pore pressure to dissipate or altering drainage path lengths. Full-scale experiments to study such behaviour would be very expensive. Laboratory model tests under earth's *1g* gravity do not reproduce correct stress levels. Laboratory element tests, such as triaxial tests, do not take account of pressure gradients or of interactions between elements. A theoretically correct and practical way of testing the transient pore pressure behaviour under the spud-can foundation is to conduct centrifuge model tests.

In the centrifuge model experiments undertaken by Tan (1990) there was at one point an indication of possible liquefaction, which could not be followed up at the time within the scope of Tan's work. However, it was a cause of concern, and led to further funding for the tests reported in this thesis.

In 1993, a total of nine tests, financed by the EEPUK and the UK Health and Safety Executive (HSE), were carried out by the author, with assistance in the direction of research by Dr R.G. James and Dr E.T.R. Dean, using a new jackup testing package on the Cambridge University 10m Balanced Beam Centrifuge. The principal result of a very large number of test loading cycles on many spud can model foundations, was that the engineers whose responsibility for deployment of jack ups in the North Sea had a very large body of model test data. The data also provided the present author with the possibility of selecting from this large body of work, a subset of the data which is presented herein. After an overview of seven tests designated YSH3 to YSH9 (Dean, et al., 1994 Confidential Reports), this thesis will concentrate on the data observed in the last two tests, the eighth and ninth tests, designated YSH8 and YSH9. Tests YSH8 and YSH9 are three-leg jackup model experiments conducted respectively on non-skirted and skirted circular spud-can foundations. Both tests are conducted at an acceleration 61 times that of the earth's gravity on an oil-saturated sand

specimen. Some efforts were made to create similar loading magnitude conditions at the hull in both tests (Dean et. al, 1995 OTC).

The nine tests represent nine prototype jackup rigs with heights ranging from 12.7 to 25.4 m (from hull connection to spud-can foundation). These prototypes are classified as smaller size jackups for near shore explorations compared with those installed in the northern North Sea. However, the cyclic load levels (H_{MAX} /W) applied to them at prototype levels will most likely match storm conditions, or in some cases are more severe than those experienced in the North Sea. For the model tests, the ratio of maximum horizontal force divided by net weight of the model (H_{MAX} /W) was up to 19%. Prototype cyclic loading periods ranges from 1.5 to 578 seconds. These are realistic values which could be experienced in the North Sea. However, it has to be accepted that the centrifuge soil conditions are less complicated than in reality, where there may be non-homogeneous soil conditions and the effects of scouring.

Table 1.2 to 1.8b lists the full range of tests and the reports that were written for the report to EEPUK and HSE. These are confidential to EEPUK, HSE, Andrew Schofield & Associates Limited and to Cambridge University. Fig. 1.4a, 1.4b 1.4c and 1.4d, show the complexity and details of the large body of data that were reported. One major outcome of this extensive series of tests is that in many loading events in the range of $2\ \% < H_{MAX}/W < 19\ \%$, there was no further liquefaction such as was reported by Tan (1990). While liquefaction may remain a concern to operators, the evidence of the work in this thesis shows that liquefaction is not easily provoked.

In the nine tests, a total of 271 horizontal cyclic events were conducted with varying magnitudes and frequencies. No build up of positive pore pressures or foundation failure was observed.

Permanent vertical deformation was experienced, even at small loads. Observations made from the tests (described in later chapters) will provide crucial ideas about partial drained fixity in relation to cyclic loading. Excess pore pressure data under the spud-can foundation could explain whether soil is hardening or softening. It also correlates with the permanent vertical deformation of the spud-can foundations. Comparison of the non-skirted and skirted foundation provides evidence that higher positive pore pressure generation under skirted foundations reduces fixity. However, the skirted foundation has longer drainage paths reducing permanent settlement, increasing effective stresses around the skirt and also providing reliable high pull out strength.

1.4 Theoretical Interpretation

Environmental lateral loading is made up of the wind, wave and current loading. The maximum of each of these three loads may not necessary coincide with each other during a severe storm. In modelling, the extreme storm conditions can be simplified by applying an equivalent total cyclic horizontal loading, H_T , to the hull of a simple three-leg jackup model as shown in fig. 1.5. The maximum (equivalent) horizontal force over the weight of the structure ratio (H_{MAX}/W) is often used as an indication of the level of loading.

1.4.1 Fixed and Pinned conditions

For jackup operations, it is essential to know the fixity conditions of the jackup rig during extreme storm conditions. The complexity of the detailed analysis of an independent leg jackup unit (ILJU) can be approximated while still retaining some essential features of the soil-structural interaction problem (Dean *et al.*, 1992). Fig. 1.6 shows a single leg of a three-leg jackup, which acts as a simple beam with flexural rigidity, *EI*, and length, *L*. When subjected to a horizontal load (*H*), at the top of the leg, the foundation fixing moment (*M*), is related to rotation, θ, by a secant stiffness, *k*, as shown below:-

$$M=k.\theta \qquad (1.1).$$

k will in general vary with *M* or θ due to the non-linearity of the soil response. For a beam with displacement, δ, at one end and rotation, θ, at the other. It may be shown that:

$$\theta = \frac{H.L^2}{2EI}\left(1-\frac{kL}{kL+EI}\right) \qquad (1.2),$$

$$\frac{\delta}{L} = \frac{H.L^2}{3EI}\left(1-\frac{3}{4}\frac{kL}{kL+EI}\right) \qquad (1.3),$$

A relationship between M and H for a given secant rotational stiffness, k, can be obtained by substituting θ with Moment, M:

$$M = \frac{HL}{2}\left(\frac{kL}{kL + EI}\right) \qquad (1.4),$$

The degree of spud-can restraint, better known as 'fixity' is the description of the expected global response or stiffness of the system. No moment fixity (k =0) implies a pinned condition and full moment fixity ($k = \infty$) indicates full moment restraint. The two idealised foundation conditions are namely, fixed (or encastre), and pinned, as illustrated in fig. 1.7. The function, $\left(\frac{kL}{kL + EI}\right)$, is equal to zero for a pinned condition and for fixed condition, the same function tends to unity. Comparing the variation in horizontal displacements, the horizontal displacement, δ, for the pinned single leg is four times that of the fixed condition.

1.4.2 Load paths

The three-leg jackup structure can be idealised as a model with three simple beam columns and the hull representing a rigid beam as shown in fig. 1.8. Each side of the equilateral triangular hull is of length $2\sqrt{3}\,t_f$. The total horizontal loading consisting of wind, current and wave loading, H_T, is applied from the windward direction, and the figure shows a three-leg jackup with one leeward leg, Leg No. 1, and two windward legs, Leg Nos. 2 and 3. At each foundation, three restraints are considered, vertical, shear, and moment fixity. The reactions under each leg will vary depending on the total horizontal load (H_T) applied and the fixity conditions of the foundations. The three load components for legs 2 and 3 (windward legs) are assumed to be identical. Considering the moment and force equilibrium of the model, and taking account of the horizontal displacement, δ, of the hull relative to the foundations and the eccentricities, M_1/V_1 and M_2/V_2, of the vertical reactions at the foundations, the vertical reactions under legs 1, 2, and 3 (note that $V_2 = V_3$) are obtained as:

$$V_1 = \frac{W.(t_f + \delta - M_2/V_2) + H_T.L}{3t_f + (M_1/V_1 - M_2/V_2)} \qquad (1.5),$$

$$2V_2 = \frac{W.(2t_f - \delta + M_1/V_1) - H_T.L}{3t_f + (M_1/V_1 - M_2/V_2)} \qquad (1.6),$$

and:

$$W = V_1 + V_2 + V_3 = V_1 + 2V_2 \quad (1.7),$$

$$H_T = H_1 + H_2 + H_3 = H_1 + 2H_2 \quad (1.8).$$

Fig. 1.9a shows the V_T-H_T global response of the structure subjected to environmental loading. Note that the vertical load, V_T, prior to cyclic lateral loading is equivalent to the weight of the structure, W, and will remain constant throughout all horizontal loading events. The corresponding load paths between the windward and leeward legs are as shown in fig. 1.9b. It can be seen that the variation of vertical load (ΔV_1) under the leeward leg, Leg 1, is twice that of the windward legs. The variation of moment and horizontal loads under each leg is similar in magnitude and direction.

The corresponding load paths for the three-leg jackup structure can be further investigated for two simplified cases, namely that of pinned and fixed conditions for all the foundations. For both situations, the lateral deflection, δ, will be considered small in relation to the footing spacing, t_f ($\delta \ll t_f$ such that $\delta \approx 0$). It will be deduced that in pinned conditions where $M_1=M_2=0$:

from equations (1.5) and (1.6),

$$V_1 = (W.t_f + H_T.L)/3t_f \quad (1.9),$$

$$V_2 = (W.t_f - H_T.L/2)/3t_f \quad (1.10),$$

note that $\Delta V = V - V_w$ and ΔH_1, ΔH_2 *and* ΔH_3 are close to $H_T/3$,

$$\Delta V_1 = (\Delta H_1).(L/t_f) \quad (1.11),$$

$$\Delta V_2 = \Delta V_3 = -(\Delta H_2).(L/2t_f) \quad (1.12),$$

$$M_1=M_2=M_3=0 \quad (1.13).$$

As for the fixed conditions, considering equilibrium of the hull together with the upper half of the legs (noting that the moments in the legs at mid height is zero), and taking δ=0, it will be shown that:

$$V_1 = [W.t_f + (H_T.L/2)]/3t_f \quad (1.14),$$

$$V_2 = [W.t_f - (H_T.L/4)]/3t_f \quad (1.15),$$

hence,

$$\Delta V_1 = (\Delta H_1).(L/2t_f) \quad (1.16),$$

$$\Delta V_2 = -(\Delta H_2).(L/4t_f) \quad (1.17).$$

Thus, depending on the foundation conditions, the load path of the leeward leg is different from that of the windward ones as illustrated in fig. 1.10a. Fig. 1.10b shows the relationship between the lateral displacements, δ, of the rigid deck and the lateral force for the two idealisations.

1.4.3 Yield locus

It is interesting to plot load paths and to relate them to limiting behaviour of the foundation under combined loads. There is a wide variety of possible equations in use to describe such limiting behaviour. Each equation will define a theoretical yield locus. Most equations are based on Terzaghi's theory of bearing capacity with suitable modifications to take into account of the influence of lateral and moment loads, footing geometry and depth of penetration. Roscoe and Schofield (1956) drew a limiting yield locus for a flat plate on clay under constant vertical load, V and moment, M. Some distinct behaviour of flat non-skirted and skirted spud-can foundations was highlighted in relation to a three dimensional yield locus in Osborne et al (1991) and Dean et al (1992). With reference to the yield locus as defined by Osborne et al (1991), equation 1.18 is as shown below:-

$$\{[M/(B.V_m)]^2+\beta^2.(H/V_m)^2\}^{0.5}=\alpha.V/V_m.(1-V/V_m) \qquad (1.18)$$

where α and β are parameters depending on the shape of the foundation and can be 0.35 and 0.625 respectively for a shallow cone semi-rough foundation. As illustrated in fig. 1.11, the three dimensional limiting yield locus is an ellipsoid with the maximum value of vertical load (V_m) and vertical (V) horizontal (H) and moment (M) loads are combined load paths. This yield locus is similar to the cam-clay yield surface developed by Schofield and Wroth (1968) which implies that combinations of vertical, horizontal, and moment loads outside the yield surface can only be approached by a process of "hardening" in which the yield locus is enlarged.

The design of the Independent Legs Jackup (ILJU) is based on a standard feature which is introduced in installation by which vertical loads are increased by pumping a large weight of water into the hull during the operation called 'spudding in' or 'preloading'. Preload is usually twice the working load value (V_p). Subsequently, water is discharged reducing that load to its working value, V_w, (with negligible horizontal or moment loading) as shown in fig.

1.12a before commencing operation of the oil drilling activities. Fig. 1.12b shows the formation of the yield locus during the preloading process, ignoring the moment axis. The yield locus presented is a two dimensional elliptical yield surface after vertical unloading to the working load, V_w . This will provide greater horizontal and moment capacity. The maximum vertical load, V_m , value is equal to the preload value, V_p . During operation the yield locus will alter when there are elasto-plastic deformations (dotted yield surface illustrated in fig. 1.12b).

The three dimensional load paths, as described in the earlier section 1.4.2, can be plotted within a two dimensional yield locus of limiting behaviour of the foundation under combined loads as described by Equation 1.18. This is achieved by converting the Moment and Horizontal forces of a typical load path into a function, $\{[M/(B.V_m)]^2+\beta^2.(H/V_m)^2\}^{0.5}$, and plotted as the x-axis. As the left hand side of Equation 1.18 is always positive, all the load paths will be plotted in the positive space of the yield locus. The yield locus and stress paths are plotted in fig. 1.13. As described by Dean et al. (1992), the paths OA and OA' are related to the fixed condition and OB and OB' represent the pinned condition. A typical load path may start close to the fixed conditions at low horizontal load levels and gradually tend towards the pinned condition at high load levels. A typical load path is shown schematically (path OC or OD). Note that the gradient of the idealised pinned condition is much greater than that of the fixed condition. The maximum vertical load (V_m) is assumed to have a linear relationship between vertical load and vertical displacement of each respective leg (after each horizontal loading event).

1.5 Previous work on Cyclic Loading and Pore Pressure Generation

Tan (1990) performed cyclic combined (vertical and horizontal only) loading tests on a single spud-can foundation sitting on oil saturated sand. Monotonic testing (on dry sand) performed in Tan's research provided the experimental data for the formulation of a two-dimensional empirical limiting yield locus for vertical and horizontal loads. He also demonstrated in one test the possibility of pore pressure build up leading to liquefaction as shown in fig. 1.14. The liquefaction was induced when horizontal cyclic loads were applied while the vertical load was reducing and vertical displacement restricted.

This idea was extended to include moment loading, forming a three dimensional limiting yield locus. In theory, any load path within this yield locus will show elastic and linear behaviour. More practically, when load paths start to venture near but within the limits of the locus, the load paths tend to become non-linear but still elastic. When the load path passes the yield locus, plastic deformation will either cause the yield locus to extend in size for a hardening case or reduce its size when softening. This has been studied and documented in numerous papers (e.g. Tan, 1990; Shi, 1988). The soil behaviour is effectively fully drained for sand and undrained for clays. For a real jack up foundation, even at quasi static range of loading i.e. for prototype frequency loading of less than 0.12 Hz, there are differences in soil behaviour between drained and undrained situations. These two limits are conditions clearly defined in most stress path and element tests. The stress path tests, therefore, do not accurately simulate this macroscopic partial drainage behaviour under the spud-can foundation. Effects of large magnitude cyclic loading are clearly evident in both analytical models and experimental results. The exact nature of this behaviour is not fully understood and introduces significant uncertainty. There is a need to develop reliable prediction methods for higher magnitude loading. Fixity of offshore structures inferred from site measurements for both ambient and storm conditions has indicated that at storm levels, the compliant structure shows distinctive reduction in fixity and also an increase in the natural period of the structure. This degradation of stiffness is sometimes said to be related to the sand scouring under the foundation, but also may be due to the effects of cyclic loading.

The experiments presented herein will give a general idea of the behaviour of the foundation subjected to both low and high intensity cyclic loading. It will be demonstrated that realistic three-leg jackup model subjected to cyclic loading develops plastic deformation even when load paths are cycling well within the yield locus. It is still quite difficult to predict the pore pressure behaviour despite extensive tests conducted in the nine test series. However, the data does give a certain theoretical framework to the transient flow of excess pore pressure generated under spud-can foundations and its effects on the fixity of jackup structures.

1.6 Objectives of Research

Both skirted and non-skirted spud-can foundations can generate and sustain both negative and positive excess pore pressure during a cyclic loading situation and will increase or reduce the effective stress in the soil respectively. The apprehension related to the

possibility of pore pressure building up during extreme loading scenarios causing liquefaction especially in loose sand arose from Tan's (1990) work, which is related to single spud foundation on oil saturated sand subjected to combined vertical and horizontal loads. The cyclic behaviour of three-leg jackup model foundations are more complicated as simultaneous moment loading is also involved, and the loads applied to each foundation are affected by interaction between foundation and structure stiffness. However, the previous work on sand and clay has formed a good basis for understanding the behaviour of soils, especially the formation of a three dimensional limiting yield locus for drained soil. The experimental data does show that considerable settlement has occurred in all tests. This is a consequence of the cyclic loading and it seems to be related to the difference in drainage paths and frequency of the unloading and loading process.

The aim of the research is to predict transient excess pore pressure generation using the physical framework developed from the experimental data and also to investigate the effects on fixity. The research summarises the findings observed from the comparison of non-skirted and skirted spud foundations. The scope of work presented in this thesis includes (i) overall vertical settlement of three-legs, (ii) pull out test, (iii) moment fixity due to horizontal cyclic loading, (iv) effects of load paths in relation to the yield locus as described above, and (v) pore pressure generation.

1.7 Outline of Thesis

The thesis consists of seven chapters. Chapter 1 gives an introduction to the research involved. Chapter 2 is a literature review related to both spud-can foundation and soil cyclic loading behaviour. Chapter 3 describes the experimental apparatus and the procedure of the tests. Chapter 4 gives a detailed account of the observations and interpretations of experimental results. Chapter 5 compares the response of flat non-skirted and skirted spud-can foundations. Chapter 6 contains a summary and some suggestions for future research.

2. BACKGROUND AND LITERATURE REVIEW

2.1 Summary

Excess pore pressure effects have been studied extensively in element testing like triaxial tests. Numerous papers (Lee and Focht, 1975, Ishihara, 1993, Seed, 1979) have reported the build-up of excess pore pressure due to cyclic loading. These load cycles cause degradation of soil structure due to slip of particles, with reduction of effective stress and increase of pore pressure. Liquefaction occurs when load paths migrate towards zero effective stress. The published research involves variable frequency loading and in general, pore pressure generation depends on cyclic shear strain and is less dependent on frequency. Tests on loose samples are, in most cases, in undrained conditions. In the case of dense sand, the dilation effects initiate negative excess pore pressure development and actually increase stiffness. This theoretical framework developed from investigation of element response to cyclic loading, has been applied to predict soil behaviour via finite element or finite difference programmes. However, it is found that despite the large amount of work done in developing this theoretical framework, the computer programmes cannot accurately or confidently predict the generation of excess pore pressure during cyclic loading either of sand or clay.

2.2 Primary Considerations

In this study, the investigation of excess pore pressure effects under spud-can foundations is restricted to medium dense sand (B.S. 100/170). Although a preliminary desk study of excess pore pressure has been conducted by Dean (1991), prior to this centrifuge test series, the conceptual models and estimation of excess pore pressure have not been validated by any full-scale experiment or centrifugal modelling. This chapter outlines some preliminary theoretical considerations related to the behaviour of sand under spud-can foundations.

2.2.1 Terzaghi's principle of effective stress

In soil mechanics, the behaviour of real saturated soil is idealised to the behaviour of an ideal continuum which consists of two phases and behaves quite differently from that of single phase materials. The two phases are (i) fluids which fill the voids, and (ii) the soil skeletal structure. The soil particles are often assumed to be incompressible. For a water saturated soil, it can also be convenient to assume the water is incompressible. In this circumstances, volumetric strains of the two phase material occur in association with movement of water into or out of the void spaces. Shear and volume strains occur by slipping or crushing and other processes which result in changes of positions and orientations of particles relative to one another. Any applied stresses on a saturated soil material is shared between the skeletal network, which carries the effective stress, σ', and the fluid, which carries the pore pressure, u, following Terzaghi's principle of effective stress:

$$\sigma=\sigma'+u \qquad (2.1).$$

The effective stresses are transmitted through the soil skeletal structure by normal and tangential forces across inter-particle contacts, and it is properties and events at these contacts, with effects of geometric arrangements and interlocking behaviour of particles and inter-particle contacts, which dominate soil constitutive behaviour and strength. The pore pressure is transmitted through the pore fluid for incompressible particles and incompressible pore fluid, it is generally assumed that changes of pore pressure at constant effective stress have negligible effect on particle geometry or contact parameters.

Under static equilibrium conditions in a saturated sea bed, the pore pressure will be equivalent to the hydrostatic pressure with reference to the ground water free surface which is the same as the overlying sea surface,

$$u_{EQ} = \rho_w.g.(z+D) \qquad (2.2)$$

where u_{EQ} is the equilibrium static pressure, z is the depth of position of interest below the seabed, D is the depth between sea surface and sea bed, ρ_w is the mass density of water and g is the acceleration due to the earth's gravity.

Before the spud arrives, the total vertical stress, σ_v, at depth, z, below the sea bed is given by:

$$\sigma_v = \rho_w.g.D + \rho_b.g.z \qquad (2.3),$$

where $\rho_b = (Gs+e).\rho_w /(1+e)$ is the bulk mass density of the saturated soil. The in-situ vertical effective stress, σ_v', can be obtained by subtracting the static equilibrium pore pressure, u_{EQ}, from the total vertical stress, σ_v, giving:

$$\sigma_v' = (\rho_b - \rho_w).g.z = \rho'.g.z \qquad (2.4),$$

where ρ' is the buoyant mass density of soil. When the footing is lowered onto the sea bed, additional total stress is introduced due to the buoyant weight of the footing and attached structure, and later due to any wave or other loading applied to the structure. Additional pore pressures are generated in the soil. These additional pressure will gradually dissipate in association with interstitial pore fluid flow and macroscopic deformations of the foundation, but may increase in further load applications. If, at a given time, the actual pore pressure at a given position in the foundation is u, then the excess pore pressure at that position and time, here denoted as u_{xs}, is given by

$$u_{xs} = u - u_{EQ} \qquad (2.5),$$

where u_{EQ} is the hydrostatic pressure at that position.

For a cohesionless soil (i.e. c'=0), the Mohr-Coulomb failure criterion is that the shear strength $|\tau_{MAX}|$ on a plane in any soil body is:

$$\text{within the soil: } |\tau_{MAX}| = c' + \sigma'.tan(\phi') \qquad (2.6),$$

where c' is cohesion which is equal to zero for cohesionless soil, σ' is normal effective stress on the plane and ϕ' is the effective angle of internal friction of soil which is made up of two components, ϕ'_c, critical angle of friction and φ', which is the dilation angle. The dilation

angle, which is due to the interlocking effects of sand particles, depends on a variety of factors including relative density and average stress level. The critical angle can be simply described as the angle of repose of a heap of dry sand formed by pluviation.

Similarly, the maximum shear strength between soil and structure interface is expressed by:

$$\text{at a soil-structure interface:} \qquad |\tau_{MAX}| = \sigma'.tan(\delta') \qquad (2.7),$$

where δ' is the angle of friction between the soil and structure. That angle may depend on the nature of the structural surface and on the amount of local soil disturbance near the interface, as well as, on mean stress level, soil density and other factors. If the pore pressure, u, increases positively without any change in the corresponding total stress, then the effective stress, σ', will reduce and the shear strength ,$|\tau_{MAX}|$, within the soil material will reduce. This will result (i) if $|\tau_{MAX}|$ reduces below the applied shear stress, τ, then shear failure can occur, and (ii) if the effective stresses and therefore the shear strength reaches zero, then the soil is said to be liquefied.

On the other hand, if the excess pore pressure is negative, the effective stresses can be higher, and so the strength can be increased. Negative excess pore pressure, u_{xs} , is often referred to as pore suction, even though the actual pressure, $u_{xs} = u - u_{EQ}$, may be positive.

2.2.2 Generation and dissipation of excess pore pressure

Rapid application of load during preloading, or in rapid cyclic loading induced by waves, the wind, or collision of boats against the legs, can induce positive or negative excess pore pressure within the soil in the vicinity of the spud-can foundations. When loading is applied slowly to the soil material (Bolton, 1991, Atkinson, 1993, Lambe and Whitman, 1979), volumetric changes will occur with sliding of one particle relative to other, or in other places particles may roll relative to one another. These and other particulate processes cause changes in the geometry of the void spaces. Pore pressure gradients induce pore fluid movement. However, in rapid loading, there is less time for interstitial fluid flow, and excess pore pressures are induced which initially prevent the changes of pore volumes.

The following are some major features related to excess pore pressure development in soil:-

(a) Rapid volumetric compression of a saturated soil element will initially induce positive excess pore pressure which will prevent compaction. Conversely, a decrease in total stress, which under drained conditions would result in the expansion or dilation of the soil body, would in rapid loading induce pore suctions.

(b) Low stress level rapid shearing would induce positive excess pore pressure which will initially counteract the tendency for the soil skeleton to contract. Conversely, at high levels of shear relative to the normal stress, drained shearing causes volumetric expansion, and rapid shearing induces pore suctions.

(c) Soil behaviour depends not only on the stress history but also on density. Loose sand tends to contract under rapid shearing inducing positive excess pores pressure; dense sand will experience pore suctions.

(d) Below a spudcan the soil will experience cyclic loading with rotation of major principal stress direction, unlike the experience of cyclic loaded triaxial test specimens in a laboratory.

(e) The overall effective foundation stiffness may depend on both the lateral and vertical effective stresses; the stiffness may also depend on a variety of other factors including the stress and strain history.

(f) As time passes pore fluid will flow, driven by the gradients of excess pore pressures. The direction and rate of flow will be determined by the global boundary conditions and by local features. The applied load will gradually transfer from the pore fluid to the soil particles. The effective stress will simultaneously change, and changes of pore volume will be equal to the total change of element volume. The associated deformations of the soil body will continue until all pore pressure have returned to equilibrium values.

Conceptual models describing pore pressure behaviour seen in laboratory element tests have developed from the Critical Voids Ratio concept (Casagrande, 1936), to concepts of Critical State Soil Mechanics (Roscoe, Schofield, and Wroth, 1958; Roscoe and Schofield, 1963; Schofield and Wroth, 1968), and to concepts of Characteristic States (Luong and Sidaner, 1981) and a Steady States Line (Castro, 1969; Been and Jeffries, 1985). However, such models only give a local view of the pore pressure in one element. The global characteristics of excess pore pressure generated under spud-can foundations require pore pressure gradients to be captured in a solution of a boundary value problem. It is essential to be able to create a physical model such that all parts of the foundation soil layer in a model are at the same

stresses and density as the corresponding parts of the full-scale prototype. Interactions between different parts of the model must occur in the same way as the corresponding interactions occur between different parts of the full-scale prototype. This enables the correct reproduction of full-scale behaviour. This can be achieved using centrifuge modelling techniques which are becoming more widely used.

2.2.3 Darcy's law

Darcy's experiment as shown in fig. 2.1 demonstrated that the flow rate, dQ_{FL}/dt, through sand at moderate flow velocities (sufficiently slow to give laminar flow), where Q_{FL} is the quantity of flow, varies in direct proportion to the cross-sectional area, A, of the specimen and to the difference between the hydrostatic head at the two ends of specimens, and is inversely proportional to the length, dL, of the column of sand tested. These relationships can be written as:

$$dQ_{FL}/dt \propto (A.\Delta h_s)/\Delta L \qquad (2.8),$$

$$dQ_{FL}/dt = k_{FL}.(A.\Delta h_s)/\Delta L = k.A.i \qquad (2.9),$$

where k_{FL} is the permeability of the specimen and i is the hydraulic gradient. However, Darcy's experiment (1856) was conducted under 1g conditions which leads to the belief that the hydraulic gradient depends on the difference in water head as the driving force and the length of the sample which limits speed. But the reason for the flow is because there is a gradient of pore pressure between the two ends of the sample. The rate of flow depends on the excess pore pressure gradient, $\Delta u_{xs}/\Delta L$, across the soil body:

$$\Delta u_{xs}/\Delta L = \rho_w.g.i \qquad (2.10),$$

where Δu_{xs} is the difference in excess pore pressures at the two ends of the soil body (this difference is independent of pore pressure datum value), where $g = 9.81 m/s^2$. By modifying Darcy's law, an alternative equation relating flow rate and the gradient of excess pore pressure can be developed:

$$dQ_{FL}/(A.dt) = (k_{FL}/(g.\rho_w)).(\Delta u_{xs}/\Delta L) \qquad (2.11).$$

Under a higher gravity condition, the excess pore pressure between the two ends of the sample in fig. 2.1 will be N times greater than that at $1g$ and the rate of flow will be N times larger. Thus, function $k_{FL}/(g.\rho_w)$ is independent of the increase in gravity level. This implies that the above equation is still valid at higher g-levels.

2.2.4 Liquefaction of soil

Shaking of ground and rapid cyclic loading can cause loss of strength and stiffness which is called soil liquefaction. Sandy soils tend to be most susceptible to liquefaction (Committee on Earthquake Engineering, 1985). In extreme cases, for example in a strong earthquake, excess pore fluid pressures within the foundation soil can cause pore water to make channels and carry soil particles to the surface. This phenomenon is known as sand boils. Laboratory tests on soil samples subjected to oscillatory straining demonstrate pore pressure build up in saturated soil. Under such rapid loading, the soil particles will tend to rearrange their positions to create a closer packing. In this undrained condition, water cannot drain from soil during straining (i.e. no volume change), gravity loading is transferred from the mineral skeleton to the pore fluid with a reduction in the capacity of soil to resist loading.

Fig. 2.2 illustrates a correspnding pair of (p' , q) and (p' , v) plots. Starting at (p_o', v_o) on a normal consolidation line due to isotropic consolidation, the figure shows a few cycles of undrained Δq loadings which brings the effective stress point over the the critical state line or phase transformation line before inducing dilatant shear. Note the on-going increase of excess pore pressure causing effective stress to reduce. The influence of the first stress cycle caused an increase in the apparent pre-consolidation pressure. The p' values will fall due to the remaining stress cycles and this correlate with positions on κ-lines which are falling cycle by cycle, whilst the volume, v, remains constant. This behaviour is called cyclic mobility.

Laboratory element tests (Seed, 1979) have pinpointed those factors that have a major influence on cyclic pore pressure generation. However, the susceptibility of soils to liquefaction depends not only on generation of pore pressure but also on the creation of hydraulic gradients. All reported cases of liquefaction are phenomenon occurring at near zero effective stress in the presence of a high hydraulic gradient:

(a) Saturated granular soils without clayey fines are more susceptible to the build up of pore pressure. Fig. 2.2b shows that when κ (gradient of recompression line)

increases, as it will from sand to clay, the excess pore pressure induced by cycles of shearing reduces (dotted and solid line respectively).

(b) The higher the content of the most fine particles (fine silt and clay) which contributes to plasticity, the lesser the susceptibility to cyclic pore pressure build-up.

(c) Density of cohesionless soil is a very important factor. Generally, excess positive pore pressures build up rapidly in loose sand and a point may be reached where soil loses much of its initial resistance to shear. Pore pressure build-up occurs even in denser sand, but at a slower rate; although significant cyclic and permanent strains may develop, the soil can retain its shear resistance.

(d) Other factors affecting the degree of pore pressure build up include amplitude of oscillatory straining (there is a threshold of cyclic shear strain that must be exceeded before build-up of pore pressure can begin); past history of stressing; size, shape and gradation of particles; confining pressure acting on soil; age of the deposit; fabric of soil; the boundary considerations; overconsolidation ratios of the soil.

Fig. 2.3 illustrates three plots of Δu versus time corresponding to different cyclic loading. Fig. 2.3a shows Δu trending upwards with identical cycles when the excess pore pressure, reached its ceiling, the pore pressure phenomenon is known as 'liquefaction'. Fig. 2.3b shows no upward trend but rather cycles of Δu increasing in size, cycle by cycle, this behaviour is called cyclic mobility which will cause progressive loss of stiffness at some locattions and increasing load transfer elsewhere, giving rise to enhanced amplitude of response. Fig. 2.3c shows no upward trend with simple repeated Δu cycles which induces a negligible changes in soil state cycle by cycle. Fig. 2.3c represents the excess pore pressure behaviour observed in the test series.

As mentioned in the earlier section, when Tan (1990) contributed to the study of spud-can foundations subjected to cyclic loading he demonstrated that liquefaction is attainable for a spud-can foundation with a short drainage path under the foundation. The situation in which liquefaction was induced was achieved by introducing horizontal cyclic loading to the foundation while keeping the vertical displacement near fixed. Then, as a result, the vertical load reduced during cycling, eventually reaching a liquefaction state.

2.2.5 Contraction, dilation and critical states of sand

When a soil element is subjected to cyclic shear, sands exhibit dilatancy or densification and a highly non-linear stress-strain relationship. These phenomenon depend primarily on the relative density of the sand, amplitude of the shear strain, and the state of stress. Sands with low relative density decrease in volume with the application of cyclic shear, whereas the opposite is true for sands with a high relative density.

This can be studied in detail by exploring the mobilised angle of internal friction of sand, ϕ'. Its variation depends on the stress level and density as mentioned previously. Shear box tests are often employed to investigate the effects of relative density of sand and the normal effective stress applied on strength. Some of the observations gathered from numerous shear box tests often applied in theoretical soil models are as follows:-

(a) A particular sand of varying density tends to have roughly an unique ultimate angle of friction, often known as the critical angle of friction, ϕ_{crit}'.

(b) Dense soils as shown in fig. 2.4 usually display a peak strength that is higher than their ultimate failure strengths. Beyond this peak, thin rupture zones can be detected in the previously uniform soil within which the density falls towards some critical value below which it will not drop. The soil samples dilate (become larger) and there is a reduction in density.

(c) Soils with an initial loose density (also shown in fig. 2.4), on the other hand, require a high magnitude of straining to mobilise their ultimate strength. Even after straining, no peak is observed. The soil sample contracts (becomes smaller) as it is sheared, and the density rises towards the same order of 'critical' density as that observed in the rupture zones of dense samples.

(d) The magnitude of the 'peak' strength for dense soils is related to the rate at which the soil dilates.

The above-mentioned phenomena can be described by simple shear box tests. Consider a shear box test as shown in fig. 2.5. The shear box applies normal effective stress, σ' and shear stress, τ, on a slip plane. Drained tests demonstrate that, at peak strength, during a shear displacement, dense sand may dilate by an amount y. Taylor (1948) proposed two factors contributing to the strength of soil. They are (i) frictional resistance between particles and (ii) interlocking which causes volume increase during shear distortion. Taylor found that,

$$\tau.dx = \mu.\sigma'.dx + \sigma'.dy \qquad (2.12),$$

$$\tau/\sigma' = \mu + dy/dx \qquad (2.13),$$

implying that (Strength) is (Friction) plus (Interlocking). μ was interpreted as frictional coefficient. dy/dx was interpreted as a dilative component of strength. Dense sand on the shear plane dilated into a loosened critical state at it which it continued to shear without further dilation. The shear box test is repeated with varying initial density. Fig. 2.6a shows schematically how peak strength decreases as the initial void ratio increases i.e. it becomes a looser sample. Fig. 2.6b schematically how the amount of dilation or compression varies with respect to the initial state of the specimen. The variation of ϕ ' (which is arc sine of the ratio of τ/σ') will be higher for denser soil samples (fig. 2.6c).

As described earlier, eqn. 2.6 can be rewritten as

$$\tau'/\sigma' = \tan(\phi'_{crit} + \varphi') \qquad (2.14),$$

For triaxial tests, this is analogous to,

$$q'/p' = M_c - d\varepsilon_v / d\varepsilon_s \qquad (2.15),$$

M_c is related to the critical stress ratio and the other function, $d\varepsilon_v / d\varepsilon_s$, is known as the rate of dilation. Therefore at peak point at a particular stress as shown in fig. 2.7, the eqn. can be modified to,

$$q'_p = M_c . p'_p - p'_p (d\varepsilon_v / d\varepsilon_s)_p \qquad (2.16).$$

The above equation demonstrates that peak stress ratio increases with peak rate of dilation. Therefore, it is expected that the peak rate of dilation depends on initial state or overconsolidation ratio and the dilation angle is higher for more overconsolidated sample shearing at constant p'.

Sand can be defined in two states, described in detail in section 2.3.2, they are found either on the wet or dry side of the critical state line. When shear stresses increase, sand on the wet side (which is related to loose or lightly overconsolidated samples) tends to compress, on the other hand, sand in the dry side (related to dense and overconsolidated sand sample) will

dilate or expand after a small compression. Ultimately, it will reach a state (Critical state) where indefinite shear strains can occur without further volumetric strains. As mentioned earlier, dry side or dense sand will reach peak shear stress before reaching ultimate state. This peak states of soil recognised during shearing of dilative soil can be explained as due to the friction between grains and the interlocking effect. This peak shear stress (for a given normal stress) will increase with increasing rate of dilation. Fig. 2.7 shows a typical drained shear test of an overconsolidated or dense soil. The dilation angle φ' is maximum when rate of dilation, $\delta v/\delta h$ is the maximum. Been and Jefferies (1985) introduced the concept of the state parameter, ψ, which is the difference between the actual void ratio and the critical void ratio (at the same mean isotropic stress level). Loose test specimens as shown in fig 2.8 will contract during loading (the state-parameter is defined as positive), where as dense samples will dilate and, as described earlier, the volume increase or decrease stops when the critical state line has been reached. Thus, the amount of dilation or contraction depends on the state parameter value.

2.3 Conceptual Behaviour of Sand

The behaviour of sand can be described mathematically assuming that the soil behaves plastically, or derived from experimental observations like element testing. Generally, the study of soil behaviour is concluded either in the drained or undrained condition as is seen in the development of critical state concept models. Schofield and Wroth (1968) formed a conceptual framework for the understanding of soil behaviour. In which the state of soil at anytime can be represented uniquely in a space with parameters v, p' and q. This space is limited by a state boundary. Soil can exist in states inside this boundary. A critical state is a state of the soil when it can deform continuously without any change in volume or effective stress. The response of soil element to changes in stress and/or volume is reflected as state path of soil within the limiting space. Projections of three-dimensional stress-volume space, q-p'-v, stress conditions can be described in terms of stress ratio, $\eta=q/p'$. At failure, $\eta=M_c$, where M_c represent the slope of effective stress locus of critical states for triaxial compression tests only plotted in (p',q) space.

$$M_c = 6.\ sin\ \phi'/(3 - sin\ \phi') \qquad (2.17).$$

For the Granta Gravel critical state model, predicted undrained (curve a) and drained (curve b) responses in monotonic triaxial compression are as shown in fig. 2.9a. Note that for triaxial extension test, $M_c = 6.\ sin\ \phi'/(3 + sin\ \phi')$.

The tendency to change volume due to shear and the nature of volume change is controlled by the compressibility of soil structure in relation to the virgin compression (isotropic) and the rebound (or recompression) curves. As illustrated in fig. 2.9b, curve (a) represents the rebound and recompression curve indicating the elastic volume strain condition, where as curve (b) represents the work hardening compression consisting of both the plastic and elastic volumetric strains. The plastic strains are caused by particle re-arrangement due to slippage at grain contacts. After slippage soil elements must experience a mean principal effective stress, p', which is greater than that previously experienced. The following is a brief account of two simple soil models that were developed by Schofield and Wroth (1968).

2.3.1 Critical state soil mechanics

Two models were introduced by Schofield and Wroth (1968), namely Granta-gravel and Cam-clay. In Granta-gravel, the material behaviour is assumed to be rigidly plastic but allowing for strain hardening and strain softening. The Granta-gravel soil model was not intended for modelling sand behaviour but to introduce a slightly more complex soil model for introduction to the clay model. The only difference between Granta-gravel and Cam-clay is that in Cam-clay, part of the volumetric strain is recoverable, whilst the shear strain remains purely plastic, thus implying that Cam-clay is then an elastic-plastic model for soil.

In recent years this difference between these two models has disappeared when curves are plotted as a graph of (v_κ, p', q) as shown in fig. 2.10. Since $v_\kappa = (v - \kappa . ln\ p')$ corresponds to the recompression curves for the soil, therefore, if κ is zero, then the Granta-gravel curves are observed; for valid values of κ, the Cam-clay curves are described.

2.3.2 Cyclic loading of sand

The critical state concept was also proven to be useful in the development of a framework for describing the cyclic response of soils. The classical critical state theory has a single 'critical state line', e.g. Schofield and Wroth (1968), which uniquely defines the states

of failure for a given soil. However, the state of failure of soil is dependent on the stress history preceding failure, e.g. monotonic or cyclic loading, and hence a soil may have several "critical states" as defined below:-

2.3.2.1 Critical state line

As defined by Schofield and Wroth (1968), when soil and other granular materials are continuously distorted until they flow as a frictional fluid, it will come into a well-defined critical state determined by two equations, $q = M_c \, . \, p'$ *and* $\Gamma = v + \lambda \, . \, ln \, p'$. The constants M_c , Γ, and λ represent basic soil-material properties.

2.3.2.2 Steady state and cyclic limit line

Two cases of critical states which appear to be independent of stress history are the steady state and the cyclic limit state. Steady state is a state of failure where soil deforms continuously at constant volume and constant effective stress. It corresponds to Casagrande's (1976) concept of critical void ratio for sands. The failure state is established by numerous drained and strain controlled triaxial tests on both initially loose and dense sand samples. He showed that all specimens tested at the same effective confining pressure approached same density when sheared to large strains. The cyclic limit state is the failure stated induced by cyclic loading as defined by Sangrey et al. (1978). It constitutes the upper bound of non-failure behaviour for very large number of cycles. For sands, laboratory data indicates that the cyclic limit state coincides with that of the steady state. An important draw back, especially in former days when the laboratory techniques were not refined, is that it proved to be very difficult to measure the steady state line relating the critical void ratio of a specific sand-type to the logarithm of the mean isotropic stress level (Berg, 1994).

2.3.2.3 Characteristic stress ratio

Luong and Sidaner (1981) performed cyclic and transient loading of both drained and undrained tests on sand and studied the specific stress ratio for a specific density at which there is no change in specific volume or stress ratio. this specific stress ratio is known as the "Characteristic stress ratio". They explained the experimental based on their concept as shown in fig. 2.12b. The region between the characteristic stress ratio lines CL was known as the subchracteristic region. The region above the characteristic stress ratio was called surcharacteristic region. A stress path in the subcharacteristic and surcharacteristic region causes a contraction and dilative response of sand respectively.

2.3.2.4 Phase transformation line

In a series of undrained triaxial tests on saturated sand sample, Ishihara et al. (1975) discovered that whenever stress ratio exceeded a specific value, upon unloading, large pore pressures were generated. Ishihara et al. (1975) described this specific stress ratio line in q-p' plot as the "line of phase transformation". There is a dramatic change in behaviour of sand when such a ratio is exceeded.

The phase transformation line, steady state line, characteristic state line, steady state line and cyclic limit line all relate to the same general phenomenon but each defined by a slightly different criterion. This "critical state" line is essential in defining the two states in which the sand may be found. The two states are contractive and dilative soil. A contractive soil when loaded to failure from initial stage would show either a continuing positive pore pressure or decrease in void ratio. On the other hand, dilative soil, prior to failure will exhibit a decrease in pore pressure or a continuing increase in void ratio. The "critical state" line (as illustrated in fig. 2.11) is an approximate division between dilative and contractive soil.

2.3.3 Characteristic states

The characteristic state theory developed by Luong and Sidaner (1981) is one of the available theories to explain the appearance of double frequencies in the pore pressure transducer traces.

In triaxial tests on sand, they were able to establish a characteristic stress ratio for a sand in a specific state of density which is similar to the Critical State stress ratio developed by Schofield and Wroth (1968). A stress ratio is defined as, q/p', where q is the deviatoric stress; $\sigma_a'-\sigma_r'$ in triaxial test nomenclature, and p' is the mean effective stress, or $(\sigma_a'+2\sigma_r')/3$, where σ_a' is the axial effective stress and σ_r' is the characteristic state that causes compaction. Shearing at a characteristic ratio caused no volume change, and shearing above it caused rapid dilation. It is not necessary that the critical and characteristic stress ratios are equal. In the case when they are equal, $q/p'=M_c$. This is similar to the theory of stress-dilatancy developed by Rowe (1962), with zero dilatancy at the critical state or the 'characteristic ratio'. However, where drainage is not allowed (i.e. undrained conditions) and volume change is prevented, cycling at less than the characteristic stress ratio causes positive

pore pressure to develop; cycling above the stress ratio causes negative pore pressure (suction).

The double frequency behaviour could be explained by plotting a shear stress, τ', against effective stress, σ_v', as illustrated in fig. 2.12a. The dotted line represents the magnitude of the total stress which in this simple explanation is assumed to be constant. The corresponding pore pressure and shear stress time plots are as shown in fig. 2.13. As explained in Terzaghi's principle of effective stress, the pore pressure, u, is equal to the difference between the total stress, σ_v, and the effective stress, σ_v'. There are two characteristic lines representing the characteristic state, where the sample will contract if the state of stress is between the two critical lines. Typical tests conducted by Luong and Sidaner (1981) are as shown in fig. 2.12b. The plot in fig. 2.12a is different from that of the characteristic state theory, this is because the q vs. p' plot is more suitable for higher stress levels like those developed during an earthquake. However, the double frequency behaviour developed is very similar in both types of plots. The state of stress starts at point O, where there is a nominal effective stress. When the shear stress is increased in a particular direction, pore pressure will increase as it travels below the critical state line (point P). When the state of stress crosses the critical state line, the sample starts to dilate. It continues to dilate inducing suctions until the applied shear has reached its peak (point Q). Then, when the applied shear stress reduces (i.e. the state of stress goes below the critical state line), the pore pressure starts to increase slowly (point R). As the shear stress increases in the opposite direction, state of stress is similar (points O, P', Q' and R'), forming a 'figure of eight'. The 'figure of eight' may migrate towards the left (i.e. near zero effective stress), if the amplitude of shear stress reduces with cycling inducing liquefaction. On the other hand, if it migrates towards the right, the soil will be strengthened. The pore pressure behaviour vs. shear stress cross plot is illustrated in fig. 2.14. It is quite clear that there are double frequency traces.

2.4 Macroscopic Study of Foundation Design on Sand

The macroscopic study of foundation design has evolved from the use of bearing capacity factors by Terzaghi (1943) and others to the application of a yield locus limiting behaviour and finite elements analysis. The use of the limiting yield locus is very popular in the industry due to its simplicity of use. This works quite well for clay but applying plasticity

in sand has been more complicated and has led to non-associated flow properties (Lade, 1993). In design of shallow foundations, since sand is a very permeable material, the undrained effects are usually ignored unless the structure is a huge caisson.

2.4.1 Modes of failure

Modes of failure related to jack-up installations, as illustrated in fig. 2.15 are as follows:-

(a) Liquefaction due to the generation of positive excess pore pressure, the soil under the spud-can weakens, causing a reduction of shear strength and in some extreme cases may cause soil flow, leading to differential settlement.

(b) One typical example of structural failure related to the spud-can foundation is as follows. The structure may be designed with pin-joints at the foundation but the details of the foundation may provide some fixity. This makes the structure more rigid and may induce fatigue problems. Another typical structural failure may be due to excessive settlement of the foundation, and this induces higher stresses at hull to leg connections (Murff et al., 1991, Murff et al., 1992, Wong et al., 1993, Dean et al., 1995 OTC).

(c) Punchthrough can occur at the peak vertical load during preloading, in some cases, large vertical displacements will occur with a rapid reduction of vertical resistance from the soil.

(d) Overturning and toppling of the jack-up unit, is perhaps due to extreme wave load conditions, causing one leg to lift off the sea bed and destabilising the structure.

(e) Partial sliding can occur during horizontal loading, when one of the legs slides.

(f) Full sliding can occur if the entire structure slides.

The mode of failure depends on a variety of factors, including, (i) the compressibility and strength of the foundation soil(s), (ii) the depth of penetration of foundation, (iii) the geometry of the footing, (iv) the density of sand, (v) the pore water pressure, (vi) the soil permeability, which may be different in different flow directions, (vii) the rate of loading, particularly with respect to the drainage conditions, (viii) the nature of the loading; static, quasi-static and dynamic/transient cyclic, (ix) the loading history, and (x) the geometry of soil strata.

In the study of ultimate loads of small shallow foundations on uniform dry sand, Vesic (1973) identifies three general classes or modes of vertical bearing capacity failure. They are as follows:-

(a) General failure; this kind of failure has a well-defined slip line pattern extending from one edge of the footing to the surface. Initially, when the vertical load increases, small vertical displacements occur. After the peak vertical load is reached, large vertical displacements occur with a rapid reduction of vertical resistance from the soil, implying an obvious yielding point. This kind of failure in homogeneous soil is related to stiff materials such as very dense sand,

(b) Punching Shear; as the load increases the vertical settlement of the footing is accompanied by a compression of the soil immediately underneath. Continued penetration is made possible by vertical shear around the footing perimeter. The soil outside the loaded area is not affected. There may be small sudden vertical movements (jerks) of the foundation in which case the yield point is not definite. This kind of failure is usually associated with deep foundation failure or failure on compressible (loose) soil materials,

(c) Local Shear; in the failure surface geometry, local shear retains some of the characteristics of both general shear and punching shear modes. The failure pattern consists of a wedge and slip surfaces at the edges of the footings and bulging at the sides similar to general shear. However, the vertical compression under the footing is significant and the slip surfaces end somewhere in the soil mass. This type of failure is associated with medium dense soils.

2.4.2 Vertical bearing capacity

The numerical study of ultimate bearing capacity of shallow foundations started with the calculation of hardness of metals assuming a plane strain case i.e. indentation tests by Prandtl (1920) using plasticity theory. This was extended to the case of weightless materials with internal friction by Reissner (1924) and then to axially symmetrical case by Hencky (1923). Caquot and Kerisel (1949) then applied these theories into foundation analysis problems attempting to apply plasticity analyses to soils with weight. Terzaghi suggested the supposition of the weight term with the other two terms of the bearing equation as shown:-

$$V/B=0.5.\gamma'.B.N_{\gamma} + q_o.N_q + c.N_c \qquad (2.18).$$

After this approach was inspired by Terzaghi (1943), it made a lasting impact on the subsequent generation in solving shallow foundation problems (Meyerhof, 1951, Hansen, 1975). However, the plasticity problem is simplified by applying the limit equilibrium method to obtain approximate solutions for the stability of foundations. This is widely used in practice and there are numerous solutions presented by the relevant literature, for example, Steedman(1984).

The mode of failure for vertical loading only is assumed to be that of general shear as mentioned in the previous section. As it is difficult to accurately model foundations which include shape differences, effects of overburden shear resistance etc. in numerical solution, semi-empirical methods are also implemented to give a conservative solution. Thus, factors like foundation shape, shear resistance of overburden can be included.

Limit analysis can also provide a solution to foundation problems. This uses the upper and lower bound theorems of associated flow plasticity. In this kind of analysis, the soil is assumed to be perfectly plastic, ignoring the work-hardening or work-softening effects. At the yield locus, which in this case acts as plastic potential, the associated flow rule applies. The collapse load can be calculated quite accurately by assuming a suitable choice of stress and velocity fields either from failure mechanisms inferred or conducting model tests. The striking feature of these two bound theorems is that no matter how complex the geometry of the foundation of loading conditions, it usually produces solutions that are very close (necessarily) to the actual solution.

The method of characteristics based on plasticity theory can be applied in predicting the bearing capacity of footings on sand. In this analysis, soils are assumed to be ideal rigid plastic materials with a Coulomb failure criterion. The stresses in the plastic failure zones are considered to satisfy both equilibrium and a failure criterion. This differs from the bearing capacity methods which employ the superposition concept, in which contributions of soil self-weight and surcharge to footings are expressed in the form of bearing capacity factors as used previously. Moreover, soil behaviour is in fact non-linear, and thus, the superposition does not generally hold. A hyperbolic differential equation can be formulated by substituting the Coulomb failure criterion into equilibrium equations with respect to stress components. Solving the equations along the characteristic lines, stress components within the plastic zones can be determined. Sokolovski (1960) adopted a finite difference approximation which obtain fair agreement between theoretical and experimental work. Computations for method

of characteristics are very sensitive to the roughness of the cone-soil interface and do not take account of the stress-strain relationship of the soil. Only part of the soil near the footing is assumed to be in the state of plastic equilibrium, and the region with partial stress distributions near the plastic region are not considered.

2.4.3 Combined loading bearing capacity

This approach is then extended into solving foundation problems related to combined loading. This is of importance in the offshore industry as most of offshore structures are subjected to high horizontal overturning forces created by the environmental conditions. Combined loading includes the effects of eccentricity and of inclination of applied load.

In a three-leg offshore structure subjected to environmental cyclic loading, the variations of load, better known as 'load paths', under each spud-can foundation can be quite different. For this research, cyclic loading is assumed to be applied only in the direction as shown as fig. 2.16. The numbering systems of the legs are also shown in this figure. Leg 1 is known as the leeward leg and Leg 2 and Leg 3 are known as the windward legs. The general load paths for the windward and leeward legs are as shown in fig. 2.17. The load paths are different because in the study of element testing, it is well-known that the soil properties like shear modulus are stress history dependent. Moreover, the excess pore pressure generated would be different depending on their stress history. Thus, it is expected that the excess pore pressure generated under the leeward leg would be different from that of the windward ones.

2.4.3.1 Moment loading

Meyerhof (1953) published a theory to explain behaviour of foundations with combined loading. He postulated an approximate means of estimating bearing capacity of foundations under eccentric loading. He extended the theory to include horizontal loads. His approach is based on foundation always tilting towards the side of eccentricity i.e. the contact stresses are greater on that side. The assumed contact pressure distribution is identical to that for a centrally loaded foundation of reduced width. Therefore, a strip of width, B, carrying a vertical load with an eccentricity, e_c, the load will be assumed to act centrally on a reduced width, B', of the foundation (fig. 2.18). This effective contact width is as follows:-

$$B'=B-2e_c \qquad (2.19).$$

This solutions was found to compare favourably with experimental data by Ramelot and Vandeperre (1950). But later work by Lee (1965) which consisted of making careful measurements of effective width concluded that Meyerhof's effective contact concept leads to reasonable but conservative, simple and useful means of estimating bearing capacity of strip footings subjected to vertical and moment loading.

It has to be noted that the case of rectangular or circular footings is more complex as eccentric loading makes it a three-dimensional problem, this is also compounded by the variation of calculating means that for any eccentricity, e_c, vertical load, V and moment capacity, M can be found. These two components can be varied and plotted in vertical load vs moment over breadth space resulting in an interaction diagram or locus.

2.4.3.2 Inclined load

The work of Junikis (1956) (Meyerhof, 1956) on foundations subjected to inclined load concluded that the shape of rupture surfaces is a logarithmic spiral. This confirms the theoretical approach and experimental research of Meyerhof (1953, 1965) who included the horizontal load component to his eccentrically loaded solution. Meyerhof stated that bearing capacity of surface footings will decrease rapidly with greater inclination, β_i (as illustrated in fig. 2.19), to zero. Meyerhof suggested an approximate inclination, s_i, factor for surface footings on cohesionless material to be applied in classical Terzaghi's equation. Hansen (1961), on the basis of circular rupture lines, also postulated inclination factors. As described above, interaction locus can also be derived from the Meyerhof and Hansen's inclined load theory

2.4.4 Yield locus concept

Shi (1988) and Tan (1990) were able to obtain a interaction locus based on their centrifuge tests on circular spud-can footings subjected to both eccentric and horizontal loads. Shi's (1988) results showed that the interaction diagrams based on the theoretical considerations of Hansen and Meyerhof is very conservative. This is expected since the theories are based on plane strain strip footings which might be conservative for three-dimensional problem of rectangle and circular footings.

The interaction diagrams based on Hansen and Meyerhof theoretical concepts are based on ultimate state which are perfectly plastic models in continuum terms. They provide points of failure. Thus, a work hardening elasto-plastic model can be introduced to completely describe the quantitative behaviour of footings when subjected to combined loads and in particular with regard to the prediction of displacements.

A footing when loaded vertically in sand will exhibit a very stiff behaviour during vertical unloading and nearly traces its path when reloaded vertically. Thus, the interaction diagram of the footing can be regarded as a yield locus which contains a space at different tangent stiffness with parameters derived elastically. Thus, the shape of the yield locus and the behaviour within it may be defined. But in order to create a complete elasto-plastic work-hardening model, displacements predicted beyond the yield locus when plastic deformation is taking place must be considered. It is well known that sand demonstrates non-associated behaviour at the yield surface. Thus, the flow rule at the yield locus may not follow normality and has to be defined. From a physical point of view, it is possible for the footing to heave due to dilation.

The extensive use of good experimental data, both at 1*g* (Butterfield and Gotardi, 1994, Silva Perez, 1982) and centrifugal tests (Shi, 1988, Tan, 1990, Tsukamoto, 1994), has helped to explore the effects of combined loading (i.e. the corresponding elastic and plastic strains) in relation to this yield locus concept. They have been used to validate conceptual and theoretical models based on different methods in assessing bearing capacity. This is of importance especially for structures designed to resist high horizontal loading for offshore structures like the jack-up structure and offshore gravity structures.

2.4.5 Finite element analysis

For problems involving complicated geometries, loadings and material properties (Zienkiewicz, 1977 and Logan, 1992), it is in general, not possible to obtain analytical mathematical solutions. Analytical solutions are those given by a mathematical expression that yields the values of the desired unknown quantities at any location in a body and are thus valid for an infinite number of locations in a body. But because of the complicated shapes, loadings and material properties, these analytical solutions in general require the solution of ordinary or partial differential equation. The basic principle of the finite element method is as

follows; instead of requiring a direct solution of differential equations, the finite element formulation of the problem results in a system of simultaneous algebraic equations for solutions. This numerical method yields approximate values of the unknowns at discrete numbers of points in the continuum. The process of modelling a body by dividing the body into an equivalent system of smaller bodies or finite elements, interconnected at nodal points or nodes common to two or more elements and/or boundary lines and/or surfaces is known as discretization. In the finite element method, instead of solving the problem for the entire body in one operation, one formulates the equations of each finite element and combine them to obtain the solution of the whole body. Briefly, the solution for a structural problem determines the displacements of each node and stresses within each element making up the structure that is subjected to applied loads. In non-structural problems, the distribution of unknown variable could be temperature or fluid pressures due to thermal or fluid fluxes.

With the continuing fall in price of computing equipment and the development of more powerful microcomputers, the finite element method has evolved into a popular technique of analysis. This is demonstrated in its application in structural engineering and the aircraft and car industries. As it is the engineer's responsibility to predict mechanical behaviour of materials like wood, plastic, steel, concrete, etc., conceptual models for the respective materials have to be developed. These models describe simplification of real behaviour and are sufficiently accurate for purposes of engineering analysis and design. However, soil behaviour conforms less to the models of material behaviour that are mentioned. This is because the two-phase material consists of soil particles and water. The response are inherently more complex. Another complicated factor is the non-uniform distribution of soil properties in an typical deposit (such as stiffness and strength). Soil properties always vary with depth below the ground surface and have to be considered in engineering design (Britto and Gunn 1987). Terzaghi's effective stress principle is the first conceptual model successfully to account for two-phase nature of soil. Other theories like critical state soil mechanics can also be incorporated in the finite element method to describe soil behaviour.

In the classical approach, calculations of deformation and failure are done separately. In the calculations for failure, a perfectly rigid plastic stress-strain assumption is applied, resulting in a factor of safety based on experience or design code. However, in the prediction of deformation, a linear elastic model is often applied to represent the average elastic behaviour of the soil. However, it is well known that soil behaviour is non-linear. In the modern approach, both failure and deformation characteristics can be calculated by the same analysis

based on a complete constitutive model and numerical solution of a boundary value problem. There are a few types of numerical analytical methods available, namely, (i) unified general expression for specific problem, (ii) finite element methods which study the effects of the elements both from the microscopic and macroscopic points of view within a sound constitutive framework, and (iii) solution of differential equations representing the boundary value problem with the use of the finite difference method. It also has to be emphasised that numerical analyses requires good and accurate soil parameters which is obtained from accurate laboratory testing on high quality undisturbed soil samples.

There are many numerical software packages or programmes that could be applied to give good predictions of deformations for most soil mechanics problems concerning monotonic loading in either drained or undrained cases. Certain numerical software has coupled capabilities which can take into consideration draining or suction. As mentioned, this modern approach requires a complete constitutive model and accurate parameters input, obtained from laboratory tests. Both laboratory testing and the constitutive model development are closely related. The most appropriate constitutive model should be chosen qualitatively depending on the boundary value problems and the major properties of the soil. Calibration with the model parameters are tested and should be checked with experimental results. The finite element model must capture the important features of the physical situation, without irrelevant detail. It is essential to apply a suitable constitutive model with justifiable simplification. Some knowledge of the physical behaviour being modelled must be taken from small or large scale testing and compared with finite element methods.

2.5 Present Design Approach to Foundation Design

The essence of foundation design is to identify the associated problems or hazards and environmental impact, assess the probability of such dangers, make economical judgements and take actions to prevent the mode of failures described earlier. Engineers in the offshore oil industry have to also decide which is the most economical offshore structure having the minimum construction, deployment, operating costs with the greatest yield in oil production.

Bjerrum (1973) identified several geotechnical problems involved in foundations in the North Sea. In general, ultimate failure, stability problems, serviceability design and soil structural dynamics issues have to be considered. After reviewing the role of modern geotechnical analysis in foundation design, Poulos and Hull (1989) classified analysis method into three-levels which depends on the level of sophistication. They stressed the need to use soundly based soil mechanics theory to better understand foundation behaviour. Foundation design in the past involves three analysis; (1) overall stability to ensure adequate safety against failure, (2) ensuring that deformations are within tolerable limits* at design load conditions depending on the structure type and its functions and (3) stress analysis within the foundation provides information for its structural design. These analyses are often separate, unconnected and involve different analytical methods, assumptions and soil parameters. In many cases, the methods employed are empirical or highly simplified which may not accurately reflect the mode of behaviour of the foundation. Modern analytical methods provide geotechnical engineers with the opportunity to adopt a more logical design approach including all the three main aspects within a common analysis. This kind of technique does not always involve complicated computer analysis. In many cases, it is possible for designer to use results derived from soundly-based analyses. Charts, equations and numbers in tabular form are used extensively, where geotechnical requirements which do not justify a more comprehensive computer analysis. Poulos classified analysis methods into three categories (as illustrated in Table 2.1) depending on their level of sophistication. The use of the appropriate category is a function of the available geotechnical data and the significance of the project. The various facts involved in application of theoretical analyses are method of analysis, magnitude of soil parameters, method of modelling the soil profile and variation of parameters with depth. The primary purpose of analysis is to predict response of foundations to the anticipated design loadings. The predictions involve several steps as summarised in fig. 2.20.

Jack-up structures are often preferred at site specific locations due to their mobility and fast deployment. The jackup is a hybrid type of structure (Vugts, 1993). Its numbers are about twice as many as any other type of offshore exploration platforms. Originally, its use is to locate exploration wells. This has been extended to act as accommodation unit or support unit or development wells adjacent to fixed platform and now as permanent production platform.

* The tolerable limits are related to the acceptable strength criterion of the structural members for the design extreme environmental load cases. Any foundation deformations, change of foundation fixity and sliding of foundations affecting stresses in the most critical structural members must be taken into consideration.

2.5.1 Static loading

Jack-up units are bottom founded structures. Their response reflects the bottom fixity conditions and support provided by the foundation. Foundation design considerations of mobile jack ups are different from other offshore fixed structures platforms or gravity structure due to the fact that the foundations are not custom-designed for a specific site. Thus, they must be designed to remain stable, regardless of soil conditions. Offshore soils around the world exhibit a wide range of engineering properties.

The design loads can be divided into two types: gravity loads and environmental loads. Gravity loads are usually known with greater certainty. These usually consist of two components, (a) the operational light ship weight plus (b) variable loads. Environmental loads are known with less accuracy. They are estimated on the basis of probability and statistical data for a specific geographical region. These components were discussed briefly in the earlier section 1.2.

Foundation preloading has been used widely as a method to proof test the foundations of jackup rigs and has been adopted as standard operating procedure. The main aim of preloading is to force additional penetration of the footing to a level where total bearing capacity exceeding an acceptable margin of safety and anticipating highest load for the design storm. The prediction of footing performances involves two important facets: (a) investigation of the geotechnical subsurface conditions and (b) prediction of bearing capacity of footing as a function of footing penetration.

Techniques for marine geotechnical site investigation will not be discussed in this thesis. Traditionally bearing capacity analysis of individual footings served at least two purposes, (a) to predict footing penetration below sea floor and (b) evaluate the risk of a foundation failure caused by "punchthrough". General classical bearing capacities theories are used for analyses as described in section 2.4. Now, it is possible to analyses footing penetration using non-linear large-strain finite element (Nystrom, 1984). Other factors which may strongly influence foundation performance includes:-

(a) eccentric and inclined loading

(b) cyclic loading

(c) rate and extent of soil collapse into the hole created by the penetrating footing

(d) effects of rig placement adjacent to a fixed platform

(e) soil structural interaction behaviour.

In relation to the soil structural interaction behaviour, the emphasis of foundations has moved from ultimate failure criterion to predicting fixity response involving the kinematics behaviour of the foundation. A model with zero fixity will result in higher bending moment in the legs at hull connection and higher horizontal displacement at deck level, inducing higher secondary effects. The evaluation of bottom fixity can be done in three ways: (1) full scale measurements, (2) numerical modelling and (3) centrifuge tests. The first is the most expensive and environmental conditions corresponding to survival ones may not be warranted during the recording period. The second may be the most efficient but computing power required to analyse a three-dimensional structure with a complicated soil constitutive model, rendering this approach less cost effective. Moreover, validation with site or centrifuge data is indispensable to confirm the effectiveness of the constitutive soil models applied in numerical modelling. The third could provide a complete model (within the apparatus constraints) with the prototype soil and environmental conditions. It has to be stressed that the centrifuge method may not achieve the complexity of varying soil conditions at specific site. However, centrifuge tests could provide sound information (Tan, 1990, Murff et al., 1991, Dean et al., 1992, Murff et al., 1992, Wong et al., 1993, Tsukamoto, 1994) about structural interaction behaviour for specific soil conditions. This could be demonstrated in its use to validate information gathered from the recent joint industry study on foundation fixity of jack-up units (Noble Denton and Associates, 1987, Osborne et al., 1991).

2.5.2 Cyclic loading

Cyclic loading can be divided into two categories, either dynamic or non-dynamic. Dynamic effects are usually considered when cyclic frequency exceeds 0.12 Hz. However, the emphasis on the thesis is related to non-dynamic or quasi-static cyclic loading effects.

In practice, to design for cyclic loading, soil specimens are taken from specific location and depths. They are then subjected to different cyclic stress paths and load cycles which the soil will most likely be subjected around the vicinity of the foundation. These results are then usually input into numerical models as soil parameters or as a user-defined soil model. Design of foundation will be based on the residual and degraded strength and efforts have to be put in to ensure that such methods will produce conservative results. Sometimes, the

laboratory results are combined to create a sophisticated parameters. As presented in the paper by Perol and Meimon (1989), an advanced soil model for behaviour under cyclic loading incorporating a comprehensive structural model (which is a 2-D reduction of the real structure) is analysed with realistic loading history accounting for real wave loading. It is essential that any analyses has to include the effects the soil-structural interaction response to give a more accurate picture of the foundation behaviour.

In the present design of jack-up structures, the foundation design is evaluated with respect to the maximum preload applied to ensure that punching shear will not occur. Monotonic combined load analysis is also performed at working load level to ensure that severe storm levels does not cause failure. To predict the kinematic behaviour of the jack-up structure, non-linear springs at foundation are assumed. In some cases, the load paths under the foundation are plotted to ensure that they do not exceed the yield locus defined by numerical or empirical models.

Another approach to evaluate the effects of cyclic storm loading, is to ensure that the most severe storm conditions will not exceed conditions at preload level and extreme monotonic combined load conditions. In certain conditions, excess pore pressure generated under the foundation (especially in sand) is assumed to be negligible as the drainage paths are assumed to be too short for jack-up foundation to have any impact on the stability of the foundation.

To verify assumptions and to study cyclic behaviour in the soil structural interaction context, it is essential to obtain data from either field work or centrifuge tests to validate assumptions and theoretical solutions. Information could be obtained confidently in a controlled manner in a centrifuge environment. Monitoring in field may lead to numerous technical and economical problems. Moreover, the environmental loading conditions are quite random and haphazard. Recent centrifuge work (Dean et al., 1995 CUED, Dean et al., 1995 OTC) sponsored by the industry could provide some useful knowledge about cyclic behaviour of spud-can foundation on sand.

2.6 Discussion and Conclusion

The chapter has demonstrated that in element testing, the generation of positive excess pore pressure at constant total stress will induce a reduction of effective stress, undermining strength. On the other hand, negative excess pore pressure increases effective stress. Negative excess pore pressure can be generated either by reduction of isotropic load or during the shearing of a very dense sample, causing dilation. Positive excess pore pressure is generated by compression of soil element and during the initial part of a shearing process. In the partial drainage situation, any changes in excess pore pressure will cause fluid to move in or out of the element causing void ratio changes. The subsequent change in density will cause reduction in magnitude of the generated excess pore pressure. Negative excess pore pressure will result in a less dense sample after drainage has occurred, whereas positive excess pore pressure will result in a denser material. This soil behaviour can be implemented in numerical models like finite element to predict the macroscopic behaviour of foundations subjected to monotonic loadings, which is essential in calculating the stiffness of foundation for the structural analysis. This will produce a more realistic design for jack-up structures.

Classical methods like use of bearing capacity formulas and characteristic methods apply drained or undrained soil conditions to predict failure loads and modes. These methods only produces failure criterion and do not predict or provide information about the stiffness of foundations.

3. EXPERIMENTAL APPARATUS AND PROCEDURES

3.1 Background

In recent years, several centrifugal modelling studies related to the response of circular spud footings have been conducted at the University of Cambridge; these include studies performed by Silva Perez (1982), Lau (1988), Shi (1988), Tan (1990), and more recent industrially sponsored work, Dean et al (1992) and Tsukamoto (1994), all related to the drained bottom fixity of spud-can foundation. The tests were conducted either in the Cambridge University 2 m Drum or 10 m Beam Centrifuge. The gravity levels, density of specimens, size and type of the spud-can foundation and loading are varied to perform a parametric study of the performance of circular shallow foundations. The tests were performed either on a single leg spud or a three-leg model jack-up rig.

In this new series, to capture the partially drained transient pore pressure behaviour of the spud-can foundation, the pore fluid (which is usually water) is replaced by 200 centistokes (cs) (at 25^{o}C) Silicone oil. Water is used in the previous work.

3.2 Scaling Relations

By using a centrifuge to increase the gravity level to N times that of the earth's gravity (known as $1g$), a physical model N times smaller than the corresponding full size 'prototype' will experience (Schofield, 1980) the same stress levels as that of the full-size prototype in earth's gravity. This is essential because stress-strain behaviour and strength of soils is stress-dependent. The scaling relations relevant to this test series are as listed in Table 3.1. For example, at a centrifugal acceleration of Ng, L_m denoting model length and L_p, prototype length, the prototype distance is related to model distance by, $L_p = N.L_m$.

3.3 Applications of Silicone Oil in Centrifuge

Saturated cohesionless material is made up of the soil particle skeleton with pore fluid in the void spaces between particles. Externally applied load applied to a granular soil element will result in changes of void shapes and void volumes, changing structure of aggregate, and therefore, creating volumetric and shear strains and changes in stiffness. Volumetric change indicates that pore fluid is either expelled or sucked into the soil element, inducing excess pore pressure gradients between different points and regions within the soil mass. According to the effective stress theory, the changes of pore pressure due to an imposed total stress will cause the effective stress to vary accordingly. The effects on effective stress depend on several factors which are interrelated. Excess pore pressure dissipation involving moderate fluid flow velocities, has a rate proportional to the excess pore pressure gradients, which is the difference of excess pore pressure between two points divided by their distance apart. According to Darcy's law, as the pore fluid flows, excess pore pressures change until a new equilibrium situation is reached. The slow dissipation process of excess pore pressure is studied in consolidation theory. Both positive and negative excess pore pressure can be developed during and after some of the events.

Quasi-static cyclic wave loading application due to offshore environmental conditions is usually within the cyclic prototype frequency range less than 0.12 Hz and does not involve inertial effects in offshore structures. However, offshore wave (quasi-static) loading may lead to partially drained conditions in foundation soils. This is particularly important in jack-up foundations, and in the past, when water was used in centrifuge tests, they could only simulate 'fully drained' conditions. Table 3.1 show the summary of the scaling effects in the centrifugal model. In relation to time effects, as experienced from past centrifuge tests, excess pore pressure gradients, du_{xs}/dx, is N times larger in the prototype. The time required for a given degree of consolidation is N^2 times shorter in a model compared to a prototype. This is because pore fluid velocities in a model are N times faster over a distance which were N times smaller. Previous models with water as pore fluid were unable to develop significant excess pore pressure for model cyclic loading periods with the sensitivity of the technical apparatus that was available. To investigate the development and effects of the excess pore fluid pressure in the soil beneath and around spud-can footings with the available transducers, the rate of consolidation and dissipation of excess pore pressure has to be slowed down by using a more viscous pore fluid in the model. The pore fluid used was be 200 cs (at 25^{o}C) silicone oil. As the viscosity varies with temperature, it is essential to check the

temperature of pore fluid before and after the test. If the viscosity is, say 270 cs, the consolidation rate will be slowed down 270 times compared with consolidation using water. This is slow enough to allow data of transient pore pressures to be observed.

3.4 Models and Prototypes

3.4.1 Prototype

The higher gravity environment produced by the centrifuge allows stresses and strains to be correctly scaled, as demonstrated in numerous research studies. Moreover, the acceleration in a centrifuge does not alter engineering material properties. Thus, the centrifuge allows the modelling of soil with real anisotropy, and real dependence of stress-strain behaviour on stress history or path reversal, and other real aspects of physical behaviour which are not yet well described by the study of constitutive relations. The higher gravity environment allows each element within a centrifuge model to be subjected to correct conditions. So it is expected for the elements to yield, rupture, or crack just as in the prototype (Schofield, 1976).

One limitation of centrifuge modelling is the variation of gravity levels with respect to the radius from the centre of the centrifuge, but this effect will not be significant if the depth of the soil layer is very much smaller than the radius from centre of centrifuge to the centroid of soil layer which is the case in this test series (Taylor, 1995).

The scaling of time in centrifuge has some conflicts. When investigating dynamic behaviour in earthquake tests (Schofield, 1981) the prototype time is scaled up by N times that of the model. In fluid flow, dynamic or inertial effects depend very much on the Reynolds number, which takes into account the relative velocity between the fluid and solid phase and does not scale with higher gravity level; so long as the Reynolds number is lesser than 1.0, the inertial effects are minimal. In contrast, in the study of consolidation, time is scaled up by N^2. Thus, it is essential to identify the correct scaling relation for time.

In Soviet centrifuge model studies of the stability of high embankments at construction time and during subsequent periods of gradual consolidation, Malushitsky (1981) demonstrated that by testing a set of models at different scale levels (all equivalent to the same prototype in

terms of stresses and scale), time for a process such as failure of mine waste heap could be fitted to a scaling relationship of time, N^x. The power, x, is equal to a value between 0 and 2. He simply used modelling of models to find an empirical value x and then used the value he determined for the scaling of time.

With this time factor, the frequency of loading or actuation can be determined. Then, the method of loading and required power can be selected. In many cases, the loading frequency required to directly model diffusion is too fast or require too much power and in some cases the instrument available is not sensitve enough to collect the relevant information. Moreover, higher loading frequnecy could create inertial effects which are not present in the prototype. Thus, the loading frequency must be reduced to a manageable level without causing significant changes in the disspation of pore pressure occuring during the loading (Taylor, 1995). In granular materials, where significant pore pressure changes would occur, the viscosity of the pore fluid can be increased to retard the pore pressure dissipation. For dynamic events in sand, it is normal to increase pore fluid viscosity by the scaling factor, N, to match the time scaling factors for inertia and diffusion. In contrast, if dynamic effects are not relevant or not of primary interest, then there can be freedom to choose a different pore fluid viscosity but permeability of the 'prototype has to be scaled accordingly. The relationship between the consolidation times of a prototype with water as pore fluid and a model saturated with silicone oil of viscosity say 270cs is given below:-

$$T_p=(N^2/270)T_m \qquad (3.1).$$

This also implies that to reproduce the prototype period, T_p, the period of cyclic loading in the model, T_m, has to be multiplied by the factor $(N^2/270)$. Thus, for this viscous oil test series, the period of cyclic loading at model scale has to be calculated from realistic prototype period values which could range from 10-20 seconds for a single extreme wave and 4-8 hours for a storm of many waves.

For the present test series, the soil phenomenon of interest is partial drainage and the partial consolidation during cycling. The tests were to be compared with previous commercially sponsored tests on dry BS 100/170 sand. The same experimental apparatus (modified for the beam centrifuge) was to be used as previously. Therefore, the same technical apparatus constraints applies. For these reasons, the use od BS 100/170 sand was specified in the

commercial contract for the partially drained tests. In the tests, a pore fluid viscosity of say 270cs silicone oil was selected for tests at say 61g (which is the case for tests series YSH8 and YSH9). As the foundation width (B= *76.2mm*) to grain size (d_{50} =*0.14mm*) is greater than 100, the corresponding prototype would be represented by sand in the tests but with a permeability equal to 61/270 times that which would be the case if the model pore fluid had had a viscosity of 61cs.

As a result, extra precautions has to be taken when extrapolating the test results to other prototype materials. For example, rock flour or silts are found at some locations in the North Sea. If it had been practical to use rock flour with silicone oil of viscosity 61 cs in tests at 61g and assuming that the presence of silicone oil instead of water does not alter the soil's mechanical properties, then the prototype soil would have been rock flour with water as the pore fluid. And if silt with 270cs siliicone oil were used for the test, then permeability would have been less than in tests on sand, and it may be possible to speculate that more significant pore pressure build up might have occured during cyclic loading.

3.4.2 Modelling of models

In model studies at Cambridge, it has sometimes been possible to simulate modelling of models. An example is Mair's (1979) study of tunnel construction in soft clay. In the experimental studies of the two-dimensional plane section tunnels the validity of the modelling of models was explored with identical effective stress-histories at geometrically similar levels. It was concluded that good agreement between their deformation behaviour was obtained, thus achieving modelling of models. When modelling of models is achieved, the word "prototype" is given a new value because tests have confirmed a perfect scaling relationship. However, even if modelling of models is not achieved, there is still the possibility of numerical analysis of the model test data. Jack-up tests involve complicated stress distributions (a) between windward and leeward legs and (b) with the ground below any one spud-can foundation. Load cycles involve different response after different stress history, such as many small wave load cycles and a few large wave-loads. The tests are already complicated. It is not feasible to undertake modelling or models. However, it will be shown that excess pore pressures around the vicinity of the spud-can foundation do not change drastically with variation of frequency and load magnitudes and this will confirm that inertial effects are minimal.

3.4.3 Modelling limitations

Limitation created by the size and scale of the model and instrumentation may pose a difficult problem in centrifugal modelling. This includes the effects of machine limits, however, the crucial problems related to the test series are (i) the effects of the boundary of the container, (ii) the particle size effects which depend on the size of the model compared with the size of the particles and (iii) the technical limitations which is control by the size of the instruments. Taking, for example, the size of the pore pressure transducer, they are equivalent to oil barrels buried into the grounds at prototype level. These effects are not thought to have any significant effect on the test series.

3.5 Description of Apparatus

Due to the refurbishment of the 2 m drum centrifuge at the time of this study and the availability of good test equipment on the 10m beam centrifuge, the series of model tests reported in this thesis were conducted in the beam centrifuge. A new three-leg jack-up model, the respective loading equipment and supporting structure was redesigned to suit the beam centrifuge.

3.5.1 The Experimental package

Fig 3.1a illustrates the experimental package. This consists of three main components, (i) a modified steel joist (upper beam) housing the horizontal actuator and junction boxes, bolted to a 300 mm deep cylindrical tub extension, (ii) a 250 mm deep rigid steel support extension holding a central lower beam with a vertical air jack supporting the three-leg jack-up model via a yoke, and (iii) a 850 mm diameter steel tub containing the sand sample saturated with 200 cs oil. Fig. 3.1b shows the assembled package before it is lowered into the centrifuge pit.

3.5.2 The three-leg jack-up model

The three-leg jack-up model is made of duraluminium, 424.6 mm high and with legs about 215 mm apart as illustrated in fig. 3.2. It hangs on a yoke which is supported by a vertical jack which moves the model jack-up vertically up and down. In this test series, the

self-weight of the jack-up is more than adequate to simulate the preloading and working load values. However, at the end of all the cyclic events, it is the general procedure to try to locate the yielding point of the vertical loads vs. displacement curve by reloading the jack-up model. The self-weight under the high gravity plus the additional effort put in by the air jack is not adequate to cause yielding of the sand in some cases.

3.5.3 Sand Specimen

Two types of sand were used in this test series. These were placed in the 850 mm diameter tub in two layers. The bottom layer, which functioned as a drainage layer, consisted of about 90 mm depth, coarse B.S. 14/25 Leighton Buzzard sand. The bottom layer of sand acts as a drainage layer for the top layer which eases draining and saturating. The top layer is of 200 mm depth, medium dense to dense, fine Leighton Buzzard sand. The sand for this test series is B.S. 100/170 Leighton Buzzard. The sand was supplied by David Ball Ltd. A summary of the sand properties is as shown in Table 3.2, which is compiled from the triaxial tests performed by Tan (1990). In addition, a comparison between water and oil saturated sand of triaxial tests was conducted by Eyton (1982) and Bielby (1989), who concluded that oil saturated samples showed maximum shearing angles (ϕ_{MAX}') of around 2^{o} lower and critical shearing angles (ϕ_{c}') of around 1.5^{o} lower, than corresponding water saturated specimens.

The density of the sand specimen can be calibrated by pluviating sand from a hopper at different heights and flow rates into a container with fixed volume. Generally, sand particles dropped at a high rate with a short falling height will produce a very loose sample. If poured at a high height at a slow rate, the sample will be dense.

3.5.4 The Pore fluid

The oil used in this test series of centrifuge tests is 200 cs (at 25^{o}C) silicone oil supplied by Dow Corning Limited (200 Fluid) i.e. 200 times more viscous than water. Silicone oil is a relatively inert fluid with a specific gravity of 0.97 (at 25^{o}C/15.6^{o}C). It has special properties including thermal stability, high dielectric strength, water repellent, low surface tension and it is essentially non-toxic. However, the viscosity of silicone oil varies significantly with temperature. Tests were thus conducted prior to centrifuge tests using a

viscometer to ascertain the effect of temperature on viscosity. The results were verified with the material specification provided by the supplier. This also implies that it is essential to measure the temperature of the fluid at the start and end of the each test. Generally, the more viscous the oil, the slower the rate of saturation should be. To increase the rate of saturation to a practicable level, the temperature of the soil sample and the oil entering the sample is heated up to 75°C with the use of a water bath. At that temperature, the viscosity of the 200 cs (at 25°C) silicone oil will have fallen to about 70 cs. After each test series, the silicone oil is drained from the soil sample and filtered, and the viscosity checked again with a viscometer before reuse in the next test series.

3.5.5 850 mm diameter tub and water tank

An 850 mm diameter tub (400mm depth) is used for this particular series of centrifuge tests. It has four holes situated at the bottom of the tub side for saturation and draining purposes. The holes are all covered with a permeable geotextile material prior to pouring sand, to prevent the escape of soil particles which may cause the holes to clog. A pressure lid of diameter greater than 850 mm is available such that when sealed against the top of the tub a vacuum can be applied to the tub and its contents. The tub and pressure lid were designed to safely resist the external pressure exerted when a vacuum of 30" mercury is applied inside the tub. A water tank was fabricated from steel plates welded together and lagged with rock wool with hardboard on the outside. It acted as a hot water bath, accommodating the tub during the saturation process. Industrial convection water-heaters with a three phase AC voltage supply were installed near the bottom of the water bath.

3.5.6 Instrumentation

Three types of instrumentation were used in the test series. They were namely, pore pressure transducers, load cells and displacement transducers.

3.5.6.1 Pore pressure transducers

Miniature pore pressure transducers (PPT) manufactured by Druck Ltd (as illustrated in fig. 3.3) were used to measure the variation in the fluid pressure. The 7 bar PPT model type are about 6 mm in diameter and 15 mm in length with sintered copper porous stone covering the diaphragm. Pore pressure in the region of the PPT will cause the crystal silicon

diaphragm to deflect depending on the pressure magnitude, this will be picked up by the active strain gauge bridge diffused into the diaphragm.

It is essential to position the transducers such that characteristics of the pore pressure generation in the soil surrounding the spud-can be captured. The leads of the pore pressure transducers are often coiled into a circular bundle after each centrifuge test, resulting in the leads having the tendency to curl up when resting on a flat surface. Thus, it was difficult to place the pore pressure transducer at a specified position. In the first centrifuge test, one of the pore pressure positioned about 30 mm below the sand surface floated to the surface. In the subsequent tests, to ensure that the pore pressure transducers will remain in the intended positions, some steps was taken to reduce this effect. Instead of coiling the leads into a circular bundle after a centrifuge test, the pore pressure transducer leads are straightened and strapped to an open slot trunking with cable ties.

3.5.6.2 Load cells

The total load cells are designed in house. They can measure Vertical, Horizontal and Moment loadings acting on a model foundation such as the spud. Spud-can foundations of two type of geometry, conical and flat spuds of diameter 57.8mm, were employed in the first seven tests (YSH1-YSH7). However, in the last two tests, designated tests YSH8 and YSH9, a flat spud of 76.7mm diameter and a skirted flat spud of same diameter were required respectively. A 76.7mm diameter cylinder with one closed end and an end tip was glued to the bottom of the 57.8mm diameter flat spud as shown in fig. 3.4a. In the last test (YSH9), this 76.7 mm diameter flat spud was modified by attaching an annular ring (of 18mm depth) around it as shown in fig. 3.4b (see also fig. 3.4c). A hole is drilled in the spud to allow fluid trapped within the skirt to escape during the preloading process. A valve is attached and is initiated by air pressure to close that hole after the landing and preloading event.

Basically, the load cell is made up of three webs; two vertical and one horizontal. Strain gauges are attached to all three webs to measure the extension or compression of the webs (as shown in the schematic diagram, fig. 3.5). Taking the average compression of the two vertical webs gives the vertical load; the difference of the two verticals gives information about the moment load. The horizontal webs measure the shear acting upon the spud i.e. horizontal loading. Before each test series the load cells are calibrated by attaching weights on to the load cells, with different eccentricities to calibrate the two vertical webs. However, the horizontal shear web is also slightly affected by this eccentric loading. When horizontal shear

loading is applied to the cell and the voltage measured relates mainly to the shear web but some coupling with vertical webs values is needed to give the shear load. For a given load combination, the offset voltage read outs can be used to calculate a calibration matrix. The load cells requires a input voltage of 5 volts and has a 1000 gain amplifiers. Due to the effects of electrical noise, in tests YSH8 and YSH9, the output voltage were reconditioned using an analogue filter attached in the junction box.

Before all the apparatus were assembled, and electrically and hydraulically connected up to the centrifuge, a simple calibration process was performed on the model three-leg jack-up rig. The jack-up rig was held tightly against the rigid tub extensions. The spud was taken off exposing the core of the load cell. A stub was attached to the load cell and with the help of a series of lever systems, vertical and moment load was applied. The horizontal load was applied by means of a spring balance.

3.5.6.3 Displacement transducer

The displacement transducer used in all the tests is the Linear Variable Differential Transformer (LVDT). It has a DC voltage input of 10 volts applied across lines at +5V and -5V. The electrical output varies with the position of a ferrite ore within the transducer body. In the test series, the LVDTs are situated at positions on the hull of the model jack-up structure to gather information about the displacements and rotations of the hull (as illustrated in fig. 3.6). Displacements and rotations of the individual footings were not measured. The horizontal and vertical displacements and rotations of the spud cans were deduced using the measured hull displacements and calculating the relative motions of the spuds using the elastic beam bending theory for measured loads at the spud cans. The conversion can be found in appendix A of Dean et al. (1994), see also Tsukamoto (1994).

3.5.7 Pressure vessel, oil container and other accessories

During saturation (which will be described in section 3.6), the oil will flow from an oil container open to the atmosphere, via a needle valve, to a pressure vessel, and then via pipes to oil inlet holes at the base of the 850 mm diameter tub. The weight of the oil container is monitored, to measure the amount of oil entering the pressure vessel. The function of the pressure vessel is to remove all the air from the silicone oil before entry into the tub. A constant pressure gradient between the pressure vessel and tub is maintained by adjusting three components, by adjusting the height of the pressure vessel (above the tub), by

controlling the vacuum in pressure vessel employing a fine vacuum tuner, and by using the needle valve to control the leak introduced into the pressure vessel. Vacuum gauges are installed at appropriate locations to monitor pressures of different components of the vacuum system. They are also employed to monitor the pressure gradient between the tub and pressure vessel. This will control the rate of oil flow to minimise the risk of piping.

3.5.8 Data Acquisition

Fig. 3.7 illustrates a summary of the data signal processing applied in the test series. Two types of data acquisition method were employed for the test series, namely the Labtech software sampling and recording digital data and the Racal system. Both systems are installed in the centrifuge control room. Power is supplied (12 volts) to the junction box and the corresponding output voltage is fed into the two systems in parallel.

3.5.8.1 Labtech software

This is commercially available software used as a tool for data acquisition. Labtech version LTN7.11 was used at the time of this test series. Analogue values are obtained from the junction boxes and fed into the 486 computer via an analogue-to-digital converter (ADC Card). The software allows offsets and calibration equations to be applied to the raw data so that corresponding pressures or forces can be calculated from the voltage outputs. This is then be written to a text file (*.PRN) as raw voltage data or calculated channels and/or onto the screen as a meter reading and/or plotted in graphs. This is essential especially at the preloading and unloading stage where the preload value has to be achieved and known so that the working load can be set at half that preload value. The software is also used at 1g level to check the integrity of the loading system, investigate traces of electrical interference, and the accuracy and sensitiveness of the instrument. The maximum sampling rate for about 25 analogue input channels and 100 digital outputs including calculated channels is 20 Hz. The sampling rate is varied in the test series for each respective event depending on the resolution required. This is also essential to limit the size of each text file.

3.5.8.2 Racal Systems

The Racal system consists of two magnetic tape recording and reading systems (Racal A and Racal B). They are employed to record the analogue voltage outputs from junctions boxes. The Labtech software could only allow a maximum sampling rate of 20 Hz and was not able to provide good resolution for the model loading frequency of 2 or 4 Hz.

The sampling rate depends on the speed of recording and the length of the tape. Generally, recording at a higher speed for the same period event will give better resolution. Application of the Racal system requires the voltage inputs to be conditioned. This was done by adjusting the gains and maximum amplitude on the Racal system panels. For this test series, only 25 channels were available and the 26th channel was a common channel for the synchronisation of Racal A and B. Speech input was applied at the start and end of each event via a microphone, and includes the event number and a short description of the event. This was for the purpose of synchronisation and identifying the event when digitising. To digitise the analogue readings, "Global Lab" software, incorporating a hardware interface which drives and reads the magnetic tape automatically, is employed. It allows the digitising of one magnetic tape at any time and the raw data is written into a text file.

3.5.9 Computer control motor

The computer control motor (demonstrated in a flow chart, fig. 3.8a) consists of a 386 computer and the appropriate Digital to Analogue cards to send voltage pulses to the servo motor at the centrifuge arm via a Quickbasic programme. LVDT readings and data from the strain gauge on the top horizontal lever arm is read to into the Quickbasic software to monitor the horizontal displacement of the actuator block and the horizontal force within the top horizontal lever arm. Limits are set within the programme to ensure that the maximum and minimum force or displacement are not exceeded. The software consists of two main options. The first is applying a horizontal sinusoidal cyclic loading (to the hull or horizontal support point) by specifying the voltage output to the servo motor driving a lead screw, frequency of loading and the number of cycles. The other option is for applying horizontal 'move to'. This is essential in the case where there is a need to move the hull horizontal to a specified position. A typical example is the need to move the hull to a position close to the original landing site before retraction. In some tests, the horizontal 'move to' is applied to observe the dissipation rate of excess pore pressure. This is essentially a displacement control system applied at the hull level (not at the individual leg). It would be ideal if there were a closed loop control providing the choice of force control but due to time constraint and the fact that when checking the cyclic option of the Quickbasic programme, good sinusoidal displacement curves were all that was obtained for the model frequency of loadings; the programme was not modified to include force control. The voltage output and the corresponding horizontal hull displacement amplitude can be calibrated at 1g, however, this is quite different from that at higher g-level. Fig. 3.8b illustrates the horizontal actuator

sitting on a modified channel with the motor enclosed on one and junction boxes on the other end.

3.5.10 CCTV camera

Two CCTV cameras and a light source (as already illustrated in fig. 3.1) were installed within the rigid supporting piece to observe the motion of the legs and the spud-can foundations during all the events in a particular test. This was recorded during a test on video and was also used to spot any possible failures with distinct failure mechanisms during landing.

3.6 Oil Saturation Procedure

3.6.1 Placing of the sand and pore pressure transducers

Two layers of soil were required in this test series. The bottom layer, better known as the drainage layer, is made up of BS 14/25 Leighton Buzzard sand of depth about 90 mm. This drainage layer is poured onto the tub by pluviation at a very slow rate, to ensure high density.

In this experiment, the second layer is made of dry fine sand, pluviated from a hopper into the 850 mm diameter tub to a depth of about 120mm as stated in section 3.6.3. The height of pluviation and the flow rate of hopper are adjusted depending on the sand density required. The pouring process is interrupted only by the placing of the pore pressure transducers at the appropriate depth from the top of the tub.

As mentioned in section *3.5.6.1*, the leads of PPTs are straightened using an open slot trunk. The lead will still curl a bit, the part of the lead closest to the tub wall is moved until the transducer is stationary over the intended position, a cable tie is attached and the lead held firmly to the wall . When all pore pressure transducers at the specified depth are placed, the sand pouring operation continues. The positions of pore pressure transducers in a typical test were under legs. They are situated such a manner so as to capture the excess pore pressure behaviour. It would have been ideal to ensure that PPTs are placed symmetrically under the

footing but due to the limited number of PPTs and junction boxes, more PPTs cannot be accommodated. Fig. 3.9 shows the layout of the PPTs for the test series.

3.6.2 Initial check

The plugs of the pore pressure transducers are put into a plastic bag which is then sealed. This will prevent oil or sand particles from coming in contact with the plugs. This is then placed into a container which rests on the sand sample at a location remote from the model jack-up test site. The pressure lid as shown in fig. 3.10 is then sealed over the mouth of the tub and a vacuum system is then set up. The sealant used is a gasket sealant which is effective up to a temperature of over 100^{o}C. Isolating the pressure vessel, a vacuum is applied to the tub to check for leaks. When inspection shows no leak, the tub pressure is allowed to return to atmospheric very slowly.

3.6.3 Saturation process

Subsequently, the oil feeding system is connected up (as shown in fig. 3.10). The tub with the sample and sealed pressure lid is moved into the water tank. The water tank is then filled and the temperature raised to about 75 ^{o}C. Vacuum is then applied to both the pressure vessel and the enclosed tub. The pressure vessel is raised to a suitable height. Closing the valve feeding oil into the tub, the pressure vessel is filled with silicone oil and the vacuum applied so as to ensure that air is evacuated before feeding oil into the tub. Then, the valve is opened to start the saturation process. The fine vacuum tuner is used to control the vacuum to ensure that there is a pressure gradient between the tub and the pressure vessel. It is adjusted such that the rate of flow from the pressure vessel to the tub is maintained at constant practical level and also prevents partial or localised liquefaction of the sand sample.

The needle valve is then opened to fill the pressure vessel. Ideally, the valve should be adjusted to ensure that quantity entering the tub is equivalent to that entering the pressure vessel. However, this is difficult to achieve. Precautions have to be taken to monitor the air leak from the oil container when introducing oil into the pressure vessel. The oil feeding process is monitored by weighing the oil container feeding the pressure vessel. The oil is preheated before entering the tub by circulating hot water through a pipe work system with the oil pipes fastened to it. If there is no leakage, the oil feeding process can be left unattended except when refilling of the oil container is required. The oil feeding process is

stopped when the oil surface, seen through laminated polycarbonate windows in the lid, is more than 6 mm above the sand surface. Then, with all the valves closed, the vacuum is switched off and the hot water from the water tank allowed to drain. The tub and pressure vessel are then allowed to slowly return to atmospheric pressure via natural leakage. The lid is then removed and the top surface of the tub is then cleaned with inhibisol to remove the gasket sealant. This saturation operation has to be completed at least a week before the test date.

3.6.4 Discussion on saturated specimen

The vacuum system evacuates the air from the silicone oil and sand before the oil enters the tub and flows into the sand. This allows a very high degree of saturation to be achieved. This is essential to simulate the soil conditions under the ocean. However, the hydrostatic pressure in the sea cannot be achieved by filling the tub with silicone oil to a model depth due to height and weight constraints. The excess pore pressure data will not be affected as long as there is adequate pore fluid over the sand surface all the time. In all the tests conducted, estimated 93% ± 5% degree of saturation was achieved. This is computed from measured volumes and weights of sand particles and silicone oil. By applying the vacuum, all pore pressure transducers and copper sintered porous stone are also sufficiently de-aired, ensuring the sensitivity of pore pressure transducers are not affected by the pressure of air.

To prevent partial and local liquefaction during saturation, the rate of flow of silicone oil has to be sufficiently slow. The temperature is raised to 75 ^{o}C, (reducing viscosity from about 200 cs at 25 ^{o}C to 75 cs at 75 ^{o}C) to ensure that the period of saturation can be reduced to a week without causing 'piping' of the sand specimen. The method of saturation is suitable for both loose and dense samples. Post test investigation (described in section 3.9) showed that the positions and depths of the pore pressure transducers were close to the initial locations. The effects of drawing air out of the sand specimen and introduction of oil into the pores did not cause any significant settlement during the saturation process. However, in the case of loose samples, there is a significant settlement after the saturation process. This is most likely to be due to the vibration and movements induced when handling the tub into the water tank. To investigate the possible problem of settlement due to application of vacuum in loose samples, a brass cylindrical container 85 mm diameter and 122 mm depth was filled with a very loose sand sample. A rigid rig holding an LVDT is placed over the centre of the container

measuring the settlement when a vacuum is applied. The container and its accessories are then placed in a desiccating glass chamber and a vacuum applied at different rates for about two hours. The results show no settlement of the sand sample. The experiment showed that the significant settlement for loose sand samples is most likely due to shocks and vibrations induced when transporting and placing the tub in the water bath.

This sample preparation method ensures that air within the dry sand samples, any instruments installed especially PPTs and the pore fluid is evacuated of air before introduction into the pores of the sand particles. This will ensure the sensitiveness of the pore pressure transducers simulates the 100% degree of saturation of in the sea bed.

3.7 Pre-test Preparation

Before each test, the rigid support piece holding the vertical actuators and three-leg jack-up model was bolted to the 300 mm deep tub extension with the modified channel attached (refer to fig. 3.1). The lever system applying horizontal load to the three-leg model was checked physically and the upper horizontal lever arm attached to the horizontal lead screw actuator removed isolating the jack-up model. This upper horizontal lever has a strain gauge so that horizontal load applied to the hull could be measured. This was used to verify that the sum of horizontal shear load of all three-legs were nearly equal to that applied. The sum of shear load will be less than that applied because of friction in the rose joints and pivot. The wires of the load cells, horizontal load cell and the LVDTs on the hull and the horizontal actuator are connected to one junction box. Precautions were taken to ensure that the wires were placed as far away from the servo motor as possible. Power is supplied to the junction box and loadings and displacements at zero load were measured. Calibration of the load cells was then conducted as indicated in section *3.5.6.2*. Plates of known thickness were then used to check the accuracy of calibration factors of the LVDTs. If the load cells and LVDTs are functioning well, the tub extensions are then jointed with the tub containing the oil saturated sand. The wires of the PPTs are then connected to the second junction box via holes within the rigid support system. The wires for all the instruments should be long enough to allow for the final settlement of the jack-up model. However, precautions are taken to ensure that the wires are not long enough to tangle with any parts of the experimental package. Then, power is supplied to the second junction box and the pore pressure at *1g*

(close to zero) is noted. The whole experimental package is then placed onto the wedge and swinging platform. The weight is measured and counterbalance weight required computed. Subsequently, the required counter balance weight is placed on the other swinging platform lowered into the pit and attached to the arm of the centrifuge. Then the swinging platform with the experimental package is transported and lowered into the pit very slowly, so as to minimise disturbances. After locking, the swinging platform to the centrifuge arms, all the electrical and hydraulic services are connected and checked.

The voltages of the instruments are checked again to ensure that they are similar to those recorded before loading up. The hydraulic air lines are checked for air leakage by moving the vertical air jack-upwards, a metallic block is placed around the vertical jack shaft to ensure that the yoke will not lower the jack-up model onto the sand surface. Subsequently, the air pressures were changed to check for leakage. As the three-leg model is isolated from the horizontal lead screw actuator driven by a servo motor, the computer controlled horizontal loading programme was then loaded and checked by applying cyclic loading with different frequencies and displacement amplitudes. The movement of the actuator block was monitored via the real time display of the Labtech software.

3.8 Centrifuge Tests

For each test, after the apparatus and counter balance weights were assembled and loaded onto the centrifuge, the temperature of the specimen was measured with a portable thermometer. The air pressure within the vertical air jack (lower chamber) was increased to 120 PSI. and the metallic block preventing the yoke from lowering was removed. The horizontal lever arm was reconnected. The apparatus was then taken up to the appropriate g-level. At this g-level, the zero readings of the load cell are taken into account by applying appropriate offsets for the rest of the test. The preloading event is undertaken. This was achieved by reducing the air pressure within the lower chamber of the vertical air jack, allowing the jack-up model to lower due to its self weight.

When landing is initiated, the pressure within the lower chamber of air jack was reduced further so that the weight of the jack-up model is transferred to the model sea bed. This continues till the maximum vertical preload value was achieved. The vertical load was then

reduced to achieve a normal working load (half the preload value). The Racal data acquisition recording the voltages output on two magnetic tapes of the instruments were running throughout the entire test, speech input was initiated at the start and end of each event. In addition, the Labtech data acquisition with different sampling rates (frequencies) is initiated with a sampling frequency depending on the loading frequency at the beginning of each horizontal and vertical loading event. The Labtech data acquisition software also provides real time plotting of graphs and meter readings. A series of horizontal cyclic loading events with different amplitudes and frequencies were applied to the model jack-up rig. The vertical working load was then reduced to a specified load and more horizontal cyclic load events were applied. This was usually repeated for another reduced vertical working loading. At the end of all the horizontal events, the jack-up model was moved back to the original horizontal position at landing event then reloaded by reducing the lower air chamber of the vertical jack and if yield has not occurred, pressure is increased in the upper air chamber of the vertical jack in order to increase the vertical load to a specified maximum value.

The pull-out or retraction event was initiated by increasing the air pressure within the lower chamber of air jack to 120 PSI. When the jack-up model has been lifted off the sand surface and the top of the hull had been held back to the soffit of the central beam, the centrifuge motor is stopped. The apparatus is allowed to swing down slowly. When the centrifuge arm has stopped turning, the metallic block is replaced and the upper horizontal lever arm disconnected. The temperature of the pore fluid is measured again with the portable digital thermometer and temperature is noted. The swinging arm platform with the experimental apparatus is then brought up from the centrifuge pit. The experimental package is removed from the swinging platform. After disconnecting the plugs of the PPTs, the rigid support tub extensions including the modified channel or joist are detached from the tub.

3.9 Post-test Investigation

After the separation of the tub extensions and tub containing the sand sample. Most of the pore fluid is allowed to drain average period of more than a day. The surface profile of the sand specimen is surveyed, especially the location within and around the foot prints where heave has occurred. The position of the footprints are noted. The post-test surface

profile survey and the locations of the footings were recorded. The site investigation process is initiated, the process consisted of (i) obtaining the void ratios of a few sand specimens, (ii) locating the pore pressure transducers and (iii) finding the approximate thickness of the fine sand layer.

To measure the void ratio, a sample was obtained using a cylindrical thin wall (38 mm diameter) brass sampler. The sample obtained was then trimmed with a cheese wire cutter and the dimensions noted. Attempts were made to remove the silicone oil within the sample. Inhibisol is used to wash the sample and then filtered to remove both excessive inhibisol and silicone oil. This process was repeated at least five times. Then, the 'cleaned' sample was placed into a drying bottle and placed in an oven to remove all inhibisol. The dry weight can be obtained and thus void ratio estimated.

The final locations of the pore pressure transducers were extremely important, as it was essential to capture the excess pore pressure generation pattern. These were located by careful excavation removing sand within and around the footprints with a spatula, as illustrated in fig 3.11. The positions and depths (with reference to the top of the tub) of the PPTs were recorded for all the transducers. When all the PPTs are removed, the fine sand layer is removed and the surface profile of the coarse layer is surveyed, providing information about the approximate thickness and volume of the fine sand layer. Thus, an approximate void ratio can be deduced and compared to that obtained from the sampler. However, it is essential to make the point that the sampler is not an accurate way of obtaining void ratio due to sample disturbance. Moreover, intact core sample is hard to obtain.

When the fine sand has been removed, the coarse sand and leftover silicone oil trapped in the pores are not removed. Instead they are re-used for subsequent tests. The silicone oil drained off filtered via the geotextile material covering the holes situated at the bottom of the tub are collected in containers and re-used for the next test. However, the variation of viscosity with temperature is checked with a viscometer to ensure the consistency of silicone oil for all the tests performed.

4. EXPERIMENTAL OBSERVATIONS AND INTERPRETATION

The objective of the experiments is to investigate the behaviour of the soil and the excess pore pressure generation under the spud-can foundations in partially drained conditions employing viscous pore fluid. This new series of centrifuge tests consists of nine tests, designated YSH1 to YSH9. Table 4.1 shows an overview of each test conducted. The tests are arranged such that when (i) different gravity levels were applied to the three-leg jack-up model, different sizes of spud-can foundations were used to simulate modelling of models, (ii) the same gravity levels were applied, the same size spud-can foundations with different geometries were employed. Typical examples are conical, flat or skirted flat spuds.

The primary objective for the test series was to measure the magnitude and wave shapes of excess pore pressure responses to cyclic loadings and to assess their effects on stiffness, settlement and ultimate strength of a jack up. Additional and related objectives included: (i) observe the prototype pull-out strengths, (ii) estimate plastic settlements via data from pore pressure transducers (PPTs), (iii) investigate the general load path patterns and effects of fixity, (iv) compare effects of drained and partially drained conditions, (v) validate results by modelling of models, (vi) investigate variations of excess pore pressure with respect to load amplitudes and frequency of loading, and (vii) study the effects of excess pore pressure on stiffness and settlement. In this chapter, the observations made are from data observed in tests YSH3 through to YSH9 only.

4.1 Pull-out Strength

As described in section 3.8, when all the horizontal cyclic loading events on the hull had been completed, the foundation was reloaded to the highest possible vertical load and the pull-out and retraction procedure was then initiated. The aim of reloading is to probe for any possible yielding point in relation to the vertical load and displacement. Pull-out and retraction was done by pulling the yoke upwards using the air jack via the vertical supporting point. Simultaneously, the load cell measurements at the spud-can foundations and the

displacements of the legs and hull were monitored. It was expected that the pull out strength might be dependent on the rate of pull out due to drainage effects during pull-out. However, in these test series, the rate of pulling could not be varied due to apparatus limitations. In all the oil saturated tests, suctions developed, of varying magnitude under each spud-cans. Only in the water saturated test YSH6 was pull-out slow enough for full drainage to occur during the pull-out operation.

It can be deduced from the pull-out results that the movement of the foundation is related to consolidation and shear effects. This can be summarised by the following equation:-

Rate of uplift x fooring area = rate of inflow of water stored in pores beneath footing + rate of plastic flow of particles with their pore water (4.1)

The equation showed that with a steady rate of uplift, the commencement of plastic flow due to liquefaction implies a loss of suction to bring down the first term of the right hand side of the equation. At that stage, the liquefied soil can form a thin disc beneath the footing. All that suction is lost when the plastic flow leads to "pipe" conducting seawater beneath the footing. Table 4.2 shows a summary of the prototype pull out strength measured in all the tests. In Test YSH6, the soil was saturated with water, and there was no evidence of any suction. The tension in the legs developed during a pull-out event is mainly due to the excess negative pore pressure generated under the spud-can foundation. It is interesting to note that if the excess negative pore pressure can be sustained, the seepage flow net would also induce high effective stress around the outskirts of the foundation. Fig. 4.1 sketches a possible pattern of progressive suction reduction of a non-skirted foundation. In this model, the upward movement of the foundation must cause parts of the soil directly under the spud-can to fluidise, starting at the edge of the foundation and slowly making its way inwards towards the centre of the foundation. As this reduces the effective suction area, the effective stress level of the soil directly under the spud-can may not play a part in the pull-out test. The pulling out action may cause the soil directly under the spud to fluidise or pipe. However, the surrounding soil, especially at the outskirts of the spud-can, will have a certain degree of increase in effective stress, increasing the skin friction between the side walls of the spud-can and the surrounding soil. This is evident in the pull-out strength of the skirted foundation. There are great variations in the pull-out strength for the spud foundation without skirts. The skirted spud test YSH9 developed an altogether greater suction than the non-skirted spuds, except in the case of test YSH7. Pull-out strength clearly is a function of the depth of

penetration of foundation, as is revealed in test YSH7 where the excess negative pore pressure and tension measured is the greatest; the non-skirted spud in test YSH7 has the greatest penetration. These tests will be discussed in greater detail in section 5.2.

Figs. 4.2 and 4.3 show plots of relevant measurements taken during a retraction operation (Test YSH3). Fig. 4.2 illustrates a plot of vertical displacements of Leg 1, 2 and 3 against the corresponding vertical forces measured. Fig. 4.3 shows time plots of vertical displacements, vertical load and the pore pressure measurement under the spuds respectively. The observed retraction operation with reference to Leg 2 could be divided into five stages (A-B, B-C, C-D, D-E and E-F) as indicated in the time plots.

The three-leg model was moved as close to its initial landing position as possible and unloading process is initiated. Before the first stage, A-B, unloading would have proceeded without much upheaval. At stage A-B, the centre of gravity of the three-leg model was probably not coinciding with the line of action of the force, this will cause the structure to move laterally to a more appropriate position especially when the vertical load is reduced, implying rapid decrease in effective stress under the spud-can. High shear stresses and moments at the foundation level were therefore induced causing change in pore pressure under the spud.* At point B, the pull up effort would start to induce tension in all the legs and simultaneously pore pressure starts to fall. The stage B-C shows a linear variation of vertical displacement with time (also known as the rate of pull-out). At point C, the maximum measured tension. The maximum excess pore suction occured at point X (fig. 4.3b and fig. 4.3c). Stage C-D illustrates a rapid reduction of excess suction and tension as pore pressure dissipates. This dissipation could also be other reasons like development of crack or soil failure. It will continue to reduce at a high rate till point D where the pore pressure will resume its equilibrium value and the legs would not be in tension. Simultaneously, the vertical displacement time plot shows a gradual increase in gradient and reaching its maximum gradient at point D (fig. 4.3a). It is noted that maximum suction does not necessarily coincide with maximum tension force. This could be due to the drainage path between the foundation level (contact area) and the position of the pore pressure transducer. Comparing the data obtained from all three-legs without skirts, all three-legs go into tension at about the same time (i.e. point B). Stage D-E shows no tension in the legs but the

* This is similar to the excess pore pressure data observed in Taylor's (1979) work in tunelling. In that case, the release of air pressure within a centrifuge model tunnel in clay induces positive pore pressure around the immediate vicinity of the tunnel. However, the author explained that this positive pore pressure was probably due to the boundary restriction of the strong box which is most likely not the exmplanation in this situation as the footing is quite far from the edge of the tub.

movement of the spud-can (close to point D) may induce some excess pore pressure under the spud. The vertical displacement time plot maintains the maximum gradient from point D as there is no resistance under the spud. At point E, the three-leg structure would be firmly held up against the soffit of the central beam. Stage E-F will show no tension in legs and pore pressure returns to equilibrium (hydrostatic) value. Note that tension was induced at the same time for three-legs but maximum tension for each individual leg occurred at different times. This may be either be due to small rig rotation or it was an effect of instability: pulling on three objects always results in one object coming out first. The difference could be due to different penetration depth.

Referring to Table 4.2, test YSH7 has the greatest amount of pull out force for all the non-skirted test events. Note that in one instance the tension stress generated exceeded 100 kN/m^2. The maximum available suction is approximately 100 kPa+u_{EQ}. This is most probably due to the greater penetration depth. Fig. 4.4 illustrates the maximum tension stress developed at the foundation level (for tests YSH3-YSH9) with respect to the ratio of penetration depth over diameter of spud. It is reasonable to say that at greater penetration depth, the drainage path is longer, time for progressive loss of suction is longer, and thus, resulting in a greater suction strength. The graph also show a distinct non-linear behaviour.

4.2 Plastic Settlement due to Cyclic Loading

Turning back now from the pull-out data, and considering the vertical loading, as described in section 1.5, the yield locus defines a limiting yielding condition such that all load paths within the yield locus will produce only elastic strains. However in practice, if the load path starts to venture near the limits, yielding will occur resulting in permanent deformations. The yield locus will either increase in size due to work hardening or it will decrease in size due to work softening depending on the load paths. Fig. 4.5 demonstrates this work hardening or softening effects. Load path 0-1-2 is known as the preloading effect where the foundation is loaded to twice the working vertical load. This response will cause permanent settlement (fig. 4.5a) to occur and the soil underneath the foundation to be compacted resulting in the expansion of the yield locus with a peak value, V_p, as illustrated in fig. 4.5b. When the foundation is unloaded to its normal working vertical load (load path 2-3), the response will be elastic and the size of the yield locus will not change. Environmental

loadings will cause the foundation to behave in either load paths 3-4h or 3-4s. These load paths will cause the foundation to response elastically if the magnitudes are such that the load paths are within the yield locus with V_p as peak vertical load. However, if the load path (3-4h) is such that the horizontal load increases with the vertical load, when the load path hit the yield locus, permanent deformations (settlement, v_{p2}, plus horizontal movement as shown in fig. 4.5c) will occur causing the yield locus to expand (peak vertical load is V_{m2}). This phenomenon is known as work hardening. On the other hand, if the load path 3-4s hit the yield locus, the foundation will start to heave (v_{p1}) resulting in a smaller yield locus with peak vertical load, V_{m1}. Tan (1990) proposed a yield locus based on data from monotonic loading experiments. Plasticity methods have also been employed to define this distinct yield surface of similar geometry.

This yield locus concept is analogous to the cam-clay model developed by Schofield and Wroth (1968). This concept developed defined conditions of dilative and contractive materials which was extended to the study of cyclic loading. However, it is well known in element cyclic loading tests that plastic strains can still occur within the elastic yield locus. Tan (1990) explained this phenomenon in his centrifuge test results by using a multi-loci yield locus within the original yield limiting locus. The experimental data in all the tests YSH3 to YSH9 showed that at very small load amplitudes ($\Delta V/V_p$ < 7.7%) at varying frequencies, the permanent settlement is negligible.

By observing the fluid movement under the spud-can foundation, we can make some conclusions about the plastic settlement of the foundation. This is done by inferring the volume changes directly under the spud-can foundation affecting vertical displacement from experimental pore pressure data.

4.2.1 Estimation of permanent vertical displacements

Pore pressure transducers recording the pore pressure behaviour under the spud-can act as settlement gauges and provide some information which could be relevant to the permanent vertical deformation of the spud-can foundation. To visualise this permanent displacement, the pore fluid flow between transducers has to be obtained. Fig. 4.6 shows the flow of pore fluid by employing the pore pressure data of PPT A (directly below the centreline of spud-can) and PPT B (situated at about the same depth as A and near the outskirts of the spud-can foundation). The data of PPT D (which is directly below PPTA) are

not used. It is assumed that the vertical pore fluid movement between positions A and D will not cause any vertical settlement under the spud-can foundation. Seepage flow into or out of position D from the surround may cause settlement but this is also assumed to be not significant, having negligible effects on vertical settlements.

As mentioned in Section 2.2.3, the difference in pressure head between points will cause fluid to move, this quantity of flow can be represented by hydraulic gradients between the pore pressures measured derived from eqn. 2.9. The mass flow rate out of the region below the spud is:-

$$dQ_{FL} / dt = k_{FL} /(\rho_w .g).(P_A - P_B) / L.A \qquad (4.2)$$

where P_A and P_B are excess pore pressures measured at positions A and B respectively, L is the horizontal distance between A and B, ρ_w is the density of water and g is the earth's gravity. Therefore with reference to Eqn. 4.1, the movement of the foundation is related mainly to the rate of inflow or outflow of water stored in pores beneath footing. The above equation (Eqn. 4.2) assumes that no shear flow at constant volume (i.e. no global shear mechanism). This assumption may be valid because due to the preloading effect, the cyclic load paths are suppose to be showing elastic response.

This assumes that pore pressures all around the outskirts of the spud-can foundation are similar to that of position B. With reference to fig. 4.6, the effective depth for pore fluid movement affecting vertical displacement is assumed to be d. Thus, the effective area of fluid entering the region below the spud-can foundation is assumed to be A_1 . And A_2 represent the bottom area of the spud-can foundation.

$$A_1 = \pi.d.B \qquad (4.3)$$

$$A_2 = \pi . B^2 / 4 \qquad (4.4)$$

where B is the diameter of the spud-can foundation.

The quantity of pore fluid (Q_{FL}) moving into or out of the effective region directly below the spud-can foundation will influence the plastic vertical deformation. The quantity of pore fluid for a single loading cycle can be calculated by integrating the region enclosed between the pore pressure traces of positions A and B ($\int (P_A - P_B).dt$) as shown in fig. 4.7 (shaded area). Thus, the plastic vertical deformation (v_p) can be calculated as follows:-

$$Q_{FL}=A_2 . v_p \quad (4.5)$$

$$Q_{FL} = k_{FL} . \int (P_A - P_B).dt / (L.\rho_w .g). A_1 \quad (4.6)$$

$$v_p = k_{FL} . \int (P_A - P_B).dt / (L.\rho_w .g). A_1 /A_2 \quad (4.7)$$

Table 4.3 shows the comparison of the estimated and the measured permanent vertical settlement. It could be seen that this simple approach employing the pore pressure data of two positions A and B give good prediction of permanent vertical settlement. This implies that global shearing is negligible in this case, since global collapse is not approached. It suggests that pore pressure generation due to the shearing may be a localised effect occurring near the contact area. The corresponding excess pore pressure generated in the soil around the spud-can foundation due to cyclic loading causes pore fluid flow under the spud-can to flow, which allows the permanent vertical settlement to occur. The excess pore pressure behaviour due to the cyclic loading is as described in fig. 2.3c where the excess pore pressure reduces to zero immediately after a load cycle is finished and that there are zero excess pore pressures after the shaking. There is no connection between these transient excess pressure pulses and the possible occurrence of long-term consolidation settlement due to dissipation of a steady component of excess pore pressure (which is not seen in these tests).

Despite the fact that an insufficient number of pore pressure transducers were placed in the soil to capture the extensive pore pressure behaviour around the spud-can foundation, good correlation between the experimental behaviour and that predicted by the above conceptual model were obtained. Moreover, the model prediction were good for load paths under the spud-can foundation for each leg, even though the load paths at the leeward leg and windward legs, were quite different. This also suggests that settlement was by punching shear rather than general shear, with most compaction occurring immediately below the spud.

4.2.2 Pore pressure effects

Fig. 4.8a shows that the excess pore pressure generated depends on the variation of vertical load and the frequency of loading (for the leeward leg i.e. Leg 1 in test YSH8). At constant frequency, the higher the magnitude of vertical load variation, the greater the excess pore pressure generation. Small amplitudes of vertical load variation produce little permanent vertical settlement, but after $\Delta V/V_p > 0.25$ the loading cycle approaches near to the yield locus, and the resulting permanent settlement begins to be greater. If the magnitude of

vertical load variation is kept constant, there is less time for drainage as loading frequency increases and the excess pore pressure magnitude would be bigger. Fig. 4.8b shows that at constant vertical load amplitude, more drainage is expected with lower frequency and this produces higher permanent vertical settlement. This behaviour could be summarised by the fact that the load amplitude depends only on the magnitude of the vertical load amplitude not frequency or rate of loading. Thus, at constant frequency of loading, increase in vertical load magnitude signifies increase in load amplitude, resulting in increased excess pore pressure generation and permanent settlement. Consequently, if the load amplitude is kept constant with varying frequency of loading, higher frequency will allow less drainage, and will induce higher excess pore pressure, resulting in lesser permanent settlements. Excess pore water pressure caused by loading cycle returns to zero when cycles are completed. No excess pore pressure exists immediately after shaking.

A hypothesis can be defined to explain the pore pressure and permanent settlement behaviour in relation to the magnitude and frequency of load application. Figs. 4.9a and 4.9b show two flow charts which explains the effects of pore pressure and vertical permanent settlement with respect to the load amplitude applied to the three-leg model system and the frequency of input. If the same load amplitude is applied to the three-leg model at different frequency as illustrated in fig. 4.9a, higher frequency will produce less drainage, higher pore pressure, absorbing the load changes and protecting or retaining some of the fabric of the soil skeleton. However, at lower frequency, the load changes may produce similar initial excess pore pressure (as load amplitude is the same) but more drainage and quick dissipation will result in lower excess pore pressure being measured. The load changes will be transferred to the soil skeleton most rapidly. Fig. 4.9b shows the effects of varying the load amplitude at constant frequency of load application. It is obvious that higher load amplitude will induce higher excess pore pressure because of greater load changes, and there also produce greater settlement.

4.3 Load paths, Moment and Horizontal Capacity

4.3.1 Load paths

Fig. 4.10 shows a typical leeward foundation's (*V-H-M/B*) load paths for a model frequency of 0.568Hz (prototype frequency=0.0412Hz) cyclic event with $\Delta H/W$ of about ±15.2%. Fig. 4.11 illustrates a similar load paths for a model frequency of 0.0284Hz (prototype frequency=0.00206Hz) cyclic event with $\Delta H/W$ = ±18.7%. Note that in both events for the leeward leg when H_l = -0.05 kN, V_l = 1.1 kN, M_l /B = -0.05 kN, there is a distinct change in gradient especially for the M vs. V plot (fig. 4.10a for faster cycle and fig. 4.10b for slower cycle). The change in gradient implies that moment over breadth capacity is reduced considerably when vertical load has reduced below the working load.

Note that for both M vs. V (fig. 4.10a and fig. 4.11a) and H vs. V (fig. 4.10b and fig. 4.11b) plots for the windward legs in both cases at the point when the vertical load is minimum, the load paths change gradient quite gently, forming a U-shape. This creates also the hysteresis for the load path loop. At the other end when vertical load is maximum, however, the loading and unloading gradients were just slightly altered. This implies that plastic yielding and permanent deformation occurs only when the vertical load is near the minimum vertical value. This also indicates that the horizontal and rotational stiffness will have different stiffnesses in its loading and unloading cycle. This will be demonstrated in the discussion of rotational stiffness (see below). Under the leeward leg, the H vs. V plots for both rates of loading showed not much hysteresis. And for the M vs. V case, the same phenomenon for the windward legs occurred when the vertical loads is at its minimum (the U-shape end). The hysteresis effect is slightly more prominent in the slower cycle, suggesting that rotational stiffness for the vertical unload and loading cycle will be different.

To investigate this phenomenon further, consider the loading sequences in a single load cycle. Fig. 4.12 demonstrates the loading sequences on the foundation and the corresponding applied stresses transferred to the soil under the foundation. During a single cycle, when vertical load is above the vertical working load value, the average effective stresses (stage A-E) will be increased under the footing. The applied moment would causes certain effective area to be stressed only. The increasing vertical and moment loads during the loading cycle (stages A-C), implies that the eccentricity, e_c = M/V, of the vertical load induced is close to

the centre of the foundation. Effective area will be slightly smaller than the maximum effective area when $M=0$. Consequently, the increasing vertical load and moment will also increase vertical stress (fig. 4.12, Stage C) and causing soil under the foundation to increase in effective stress. It will reach its maximum eccentricity and vertical load at stage B.

Subsequently, when the vertical load is reduced just below the vertical working load (Stage C-E), the eccentricity of vertical load start to increase faster because of the decreasing vertical load and increasing moment (in the opposite direction). The consequence is a more rapidly diminishing effective area and the possible reduction (depending on the rate of reduction of effective stress to the change in vertical load) in effective stress around the vicinity of the foundation due to the reduced vertical load. However, it is possible that the vertical load can be unloaded to a value such that the reduced effective area causes the vertical stress under the effective area to increase. This may result in vertical stresses exceeding the vertical stress during the maximum vertical load stage. This will cause greater rotation deformation comparatively. Moreover, the resulting increased effective stress under the foundation may be restricted to a small area not increasing the horizontal or moment capacity.

4.3.2 Moment and horizontal capacity

Tests YSH1 through to YSH7 were affected by electrical interference problems on the highly sensitive (1000 amplifiers gain) load cells. Interference was due to the servo-motor used. The problem was only rectified in tests YSH8 and YSH9 by applying an analogue filter in the load cell signals via the junction box. The signals of the electrical interference were analysed and thought to have little effect on the maxima and minima values of the load cell data. Thus, load paths of a particular horizontal cyclic event can be summarised by taking the differences of the maximas and minimas of the respective loads measured i.e. Vertical force (ΔV), Horizontal force (ΔH) and Moment over Breadth ($\Delta M/B$), better known as load amplitudes. The comparisons of these secant load paths will give a simplified view of the load paths, a measure of the horizontal and moment over breadth capacity for a given vertical load amplitude in a cyclic event.

Data from Leg 1 in tests YSH3-YSH9 are presented in Fig. 4.13. The plots show Vertical load amplitude (normalised with the Vertical Preload value) against normalised Horizontal and Moment over Breadth load amplitudes. Each point indicated in the graph shows the respective load amplitudes for a single horizontal cyclic event at a particular frequency. The frequency of loading does not seem to affect the general load path behaviour except for the drained test YSH6. The data points provided show that gradient for horizontal over vertical load amplitudes i.e. $\Delta H_1 / \Delta V_1$, is linear with gradient about 0.27 (fig. 4.13a). This is compared with the gradients of pinned and encastre conditions defined in Section 1.4 which are 0.25 and 0.50 respectively. The initial part of the Moment over Breadth curve (fig. 4.13b) is linear and has a gradient ($\Delta M_1 / \Delta V_1$) of 0.75. And when the normalised vertical load amplitude is greater than 0.5, the gradient reduces to 0.5.

As the behaviour of the foundations under windward legs (Leg 2 and Leg 3) are similar, only the data of Leg 3 is employed. Fig. 4.14 shows similar plots for Leg 3. The gradients for normalised horizontal ($\Delta H_3 / \Delta V_3$)and moment over breadth ($\Delta M_3 / \Delta V_3$) load amplitudes over vertical load amplitudes are 0.75 and 1.25 respectively. The $\Delta H_3 / \Delta V_3$ ratio is compared with that defined in Section 1.4 which is 0.503 and 1.01 for the idealised pinned and encastre conditions respectively. This gradients shows a higher degree of fixity at low vertical load amplitude variations, when normalised vertical load amplitude exceeds 0.25, both horizontal and moment over breadth capacity drops slightly. A possible explanation for the more scattered data for Leg 2,3 compared to Leg 1 could be that as vertical load amplitudes are of smaller magnitudes, the effects of electrical interference may be more detrimental especially for tests YSH3-YSH7.

With relation to the yield surface for the spud-can foundation as mentioned in the first chapter, the load amplitudes curves shown in fig. 4.13 and 4.14 actually represent the secant gradient (as illustrated in fig. 4.15a) of the load paths. It could be deduced from those figures that at higher variations of vertical load amplitude, the reduction in gradient in the normalised moment over breadth load amplitude curve, implies that the rotational fixity of the spud foundation is tending (shown in fig. 4.15b) towards a pinned condition; resulting in a reduction in moment over breadth capacity. With respect to the normalised horizontal load amplitude curve, the vertical load amplitudes applied are not high enough to create a distinct change in gradient.

To investigate this behaviour in detail, instead of the respective load amplitudes, the load maxima and minima of all the horizontal cyclic events are plotted. The general load paths of all the horizontal cyclic loading events in all the respective tests are plotted in fig. 4.16 and 4.17. Curve of the yield locus outlined in section 1.4 with maximum vertical load (V_m) equivalent to the preload value (V_p) are also drawn. With reference to normalised horizontal to vertical load plots, it could be seen that at high vertical loads (i.e. greater than half the preload value), the general load paths are linear. However, at lower vertical loads, for example, when normalised vertical load for Leg 1 is below 0.3 as shown in fig. 4.16, (except for test YSH6) there is a change in gradient. In this example, the change in gradient can also be found in the normalised moment over breadth load amplitude plot. This indicates that at higher vertical loads (i.e. above working load value), the variation of horizontal and moment over breadth forces with the vertical load amplitude is linear and of high fixity.

Fig. 4.17a,b show that behaviour of the spud-can foundations under the windward side corresponds to the behaviour within the yield locus as mentioned in section 1.4. When the load paths are well within the yield locus, the load paths are linear, however, when they approaches the yield locus, the load paths start to bend. Note that this discussion is with reference only to the Moment vs. Vertical load plots (Fig. 4.17b and fig. 4.17b).The windward side clearly shows a S-shaped path. In the case for the leeward side, due to the greater variation of vertical loads, the general load path pattern differs from that of the windward sides. But when the load is reduced just below the working load, the load path started to bend well within the yield locus. This suggests that soil must be softening at this point.

4.4 Drained and Partially Drained Effects

Fig. 4.18 and 4.19 shows general load path plots using the technique outlined in the last section. By plotting the maxima and minima of load paths conducted for every horizontal cyclic event (when working vertical load is half the preload value), a simplified load path pattern can be plotted. This simplified load path will vary depending on the configuration of the three-leg model. The load path patterns for the leeward and windward legs are very different. Test YSH6 was conducted with water as the pore fluid. The simplified load paths are compared with those of tests YSH8 and YSH9, which are oil saturated specimens. It is

clear from both figures fig. 4.18a and fig. 4.18b that for tests YSH8 and YSH9, the curve for the leeward leg (Leg 1) change gradient distinctly when the normalised vertical load (V_l / V_p) is about 0.4. However, for test YSH6, there does not seem to be such distinct change in gradient.

Therefore, it could be deduced that in drained cyclic conditions, as long as the load paths (for vertical loading less than the vertical working load value) does not approach the initial yield locus created by the preloading event, the load paths could be expected to be linear.

This phenomenon is also clearly shown in the load paths under the windward legs as illustrated in fig. 4.19 (in this case, Leg 3). Note that test YSH6 was conducted to verify that the loading conditions for Tsukamoto's (1994) tests were truly drained. The drained data shows consistency with the data provided by drained monotonic behaviour where load paths are quite linear well within the yield locus.

4.5 Modelling of Models

To investigate the modelling of models in relation to excess pore pressure generation during cyclic loading, the excess pore pressure generated for tests YSH4 and YSH8 is compared at prototype level. In both cases, the diameter of the spud-can foundation is identical, the pore pressure transducers designated PPTA is found directly under the spud-cans. However, position A in test YSH4 at prototype level was deeper than that as recorded in test YSH8. Thus, some discrepancies in excess pore pressure generation are expected.

To explore this phenomena of modelling of models, it is assumed that pore pressure generation is a function of the frequency of loading and the magnitude of the change in vertical load. In this chapter, it is assumed that the effects of horizontal loads applied at surface are negligible to pore pressure effects under footings. Thus, a ratio of vertical load amplitude over the pore pressure generated amplitude at A is plotted against the frequency loading. As shown in fig. 4.20a, at higher frequency loading (i.e. greater than 0.284 Hz) for test YSH8 at model scale, the data show good correlation between the leeward and windward legs. At lower frequency loading, the excess pore pressure generated is quite small and difficult to measure, therefore, the great variation in ratio at 0.0284Hz.

To compare tests YSH4 and YSH8, we convert the units to prototype levels. The graph fig. 4.20b shows a plot of the Prototype frequency against the ratio of vertical stress amplitude over the excess pore pressure amplitude at position A. The plot showed that the data points for test YSH4 has higher ratio values than test YSH8. This is expected because prototype position at A for test YSH4 is deeper than that of YSH8, thus, the excess pore pressure generated will be lower. Therefore, the plot for YSH4 will translate downwards if the correct excess pore pressure amplitude data is used at the same prototype depth.

4.6 Pore Pressure Variation

In this section, the general pore pressure trend is outlined, the detailed investigation of pore pressure behaviour will be discussed in the next chapter in relation to the comparison between behaviours of skirted and non-skirted spud foundations. Pore Pressure varies with respect to the frequency and amplitude of horizontal load cycles. However, the pore pressure behaviour is very sensitive to the variations in the vertical load. Shear stresses will cause shear strains to develop which will induce excess pore pressure, however, in this situation where the variation of vertical load is great especially for the heavily loaded leg, Leg 1, the effects on excess pore pressure due to shear may not be as significant.

The effective theory works well for an small element, however, when taken into consideration of a global view point problem for the spud-can foundation, the pore pressure behaviour is much more complex. Negative pore pressure can be induced in two ways, one is created by suctions when the vertical load has been reduced during unloading and the other could be induced by the shear distortion of dense soil under the spud-can creating dilation. The amount of suction created by dilation is difficult to determine and could be quite localised. Predictions based on consolidation theory may not be able to identify and take into consideration the effects of dilation zones. In this study, only the data obtained from test YSH8 will be considered. The positions of the pore pressure transducers under each leg, obtained by physical measurements after each test, were as illustrated in fig. 3.9.

For all cyclic loading events with the starting working load half the preload value, the pore pressure time plots showed a distinct pattern for each cyclic at all frequencies and

magnitudes of load application. There is no traces of build up or reduction of excess pore pressure. The peak values of pore pressure traces did not coincide with the peak load values. The pore pressure behaviour under the leeward leg (Leg 1) is quite different from that of the windward legs (Leg 2 and Leg 3). This is because of the different load paths occurring under each spud-can foundation as mentioned in section 2.4.3. All foundations will experience similar magnitudes and direction of horizontal and moment loads, but the foundation under the leeward leg will have a bigger variation in vertical load, which is about twice that of the windward legs. Moreover, at the same instant, time that the leeward leg is being vertically reloaded, the windward legs will be vertically unloading, and vice versa.

4.6.1 Limitations of the pore pressure measurements

The limitations of the pore pressure measurements made are as follows:-

(a) the pore pressure transducers are prone to positional changes due to the stresses and deformations of the soil.

(b) there is a physical scaling effect when a pore pressure transducer is used in a higher gravity environment, a scaled-up transducer is effectively a huge oil drum in the prototype level.

(c) the wires of the pore pressure transducers may provide a lesser resistance of flow for the pore fluid. However, the pore pressure generated is affected in a small region in the vicinity of the spud-can foundation and would usually take a shorter path rather than that of the wires.

(d) the pore pressure transducers are placed in only one side of the soil. This will not provide the entire pore pressure generation picture under the foundations due to their load paths.

4.6.2 Pattern of pore pressure directly under the foundation

A survey of the pore pressure generated directly under the spud-can foundation (at position A which is about 30-40 mm from the sand surface) with respect to its corresponding vertical loading showed that pore pressure behaviour of the leeward leg (Leg 1) and the windward legs (Leg 2 and Leg 3) can be quite different. The pore pressure patterns can be classified into two main types, elliptical and double cyclic traces. In the test designated YSH8, the three-leg model is subjected to horizontal cyclic loading at the hull level with

different model frequencies varying from 0.0284 Hz to about 4 Hz (prototype frequencies ranging from 0.00206 to 0.29 Hz) and different magnitudes of displacements.

For the pore pressure transducers directly under the windward legs i.e. Leg 2 and Leg 3, all the variation of vertical loads and frequencies showed double cyclic i.e. horizontal figure 'eight' (as illustrated in fig. 4.21a) pore pressure patterns. Under the leeward leg (Leg 1), the situation is quite different, most of the pore pressure patterns showed a elliptical type of pattern (shown in fig. 4.21a). However, when the vertical load variation is very large and at very low model frequency i.e. about 0.0284 Hz, double frequency pore pressures traces are developed (fig. 4.21b). The orientation of the ellipses varies and at times, the shapes of the ellipses are distorted.

A hypothesis for understanding pore pressure behaviour under the leeward leg where greatest variation of vertical load occur can be established by making some assumptions. The excess pore pressure generated depends on the rate of loading and the magnitude. Fig. 4.22 shows typical more fast and very slow vertical loading of the spud-can foundation with different stages in a single load cycle. Stages B-C-D and F-G-H represent region of slow rate of change of loads, where excess pore pressure under the foundation (location A) will tend to the equilibrium value. Unloading will induce negative excess pore pressure and positive excess pore pressure will be induced by compression. Dilation will also cause excess negative pore pressure to occur. Fig. 4.22a shows the corresponding pore pressure behaviour for a faster frequency loading. Stage A-B represent dilation of soil as it is loaded above the working load. It will continue to dilate till the start of stage B where the rate of change of magnitude decreases rapidly. Thus, pore pressure tends towards equilibrium value at stage C. When the load starts to decrease pore pressure will be close to equilibrium value as shown in stage D, the unloading will cause rapid decrease in excess pore pressure, reaching minimum value at stage E. Then as the rate slows down, the pore pressure tends towards its equilibrium value at stage G, however, sudden reloading will cause the pore pressure to shoot up to a maximum positive pore pressure value at stage I and the value will start to fall and the cycle continues.

For the very slow cycle (illustrated in fig. 4.22b), the pore pressure behaviour generated must allow for some dissipation which would not occur fully in the higher frequency loading. Similar to the last example, the pore pressure will start to fall due to dilation to stage B. Dissipation will cause the pore fluid pressure to return towards the equilibrium value at stage

C. The unloading (stages C to G) will only contribute a minimum quantity of negative excess pore pressure with the greatest suction at stage F. The sudden reversal of load will cause pore pressure to shoot up at stage H until dilation occurs again.

The unloading will induce maximum suction at stage F for slower cycles and stage E for faster cycle. When reloading commences the maximum pore pressure is generated at stage H for slower cycle and stage I for the faster cycle.

Under the windward legs, the pore pressure behaviour shows double frequency cyclic behaviour which is described in section 2.3.3 (figure 'eight' pattern). Thus, the windward legs demonstrated sensitiveness to the cyclic shear forces applied. This is also due to the fact that the change of vertical load is only about half that of the leeward leg. The corresponding experimental data cross plots between pore pressure and vertical load are shown in fig. 4.21. The unloading both in the rapid and slow cycles seems to cause pore suction to occur directly under the footing. Pore fluid will flow into the pores increasing the void ratio. However, this also depends on the excess pore pressure induced around the vicinity of the footing. If suction is also induced around the vicinity void ratio will change considerably. The pore pressure data collected for location B demonstrated that excess pore pressure induced are of smaller magnitudes and does not coincide with the peak values of the PPT directly under the foundation. However, if the surrounding excess pore pressure is close to the equilibrium value, large quantity of pore fluid would be introduced, depending on the frequency and magnitude of the cyclic loading.

4.6.3 Change of rotational stiffness

Fig. 4.23a and fig. 4.23b show that the moment-rotation response at the leeward and windward foundations respectively. By rotating fig. 4.23b through 180^{o}, it can be seen that the responses have similarities to those in fig. 4.23a. When cyclic loading is applied to the structure, the foundation will go through a variation of vertical, horizontal and moment loadings depending on the geometry of the hull and legs and the direction of loading of the hull. Especially for the leeward leg, when the foundation was unloaded vertically to a value just below the initial vertical working load, there is a distinct change of stiffness as shown in the moment vs. rotation plot, as shown in fig. 4.23a irrespective of the frequency of loading. The magnitude at model scale has to be such that $\Delta M/B > 0.2$kN. The stiffness stays low when the foundation continues to unload to a minimum value. Reloading due to application

of horizontal displacement in the opposite direction results in low stiffness till it increases abruptly at about the same vertical load value when change of stiffness occurs during unloading. As discussed in the section 4.6.2, the pore pressure data seems to indicate that the windward legs are sensitive to the shear load applied. The moment-rotation response shows considerable stiffness but at the larger rotations, the stiffness reduces. It is interesting to note that the change of stiffness always occurs during unloading and the change of stiffness is similar to that that occurred for the leeward leg. This rotational stiffness can be compared with the elastic rotational stiffness based on elastic half space solutions established in Murff et al. (1992). The following is the elastic rotational stiffness equation:-

$$\Delta M = C_r . B^3 . G_r . \Delta\theta \qquad \text{[kNm]} \qquad (4.8),$$

$$C_r = 1/[3(1-\nu)] \qquad (4.9),$$

$$G_r = 4100 + 11.5. (V_p/A) \qquad \text{[kN/m}^2\text{]} \qquad (4.10),$$

where V_p/A is the preload vertical stress which is about 454.4 kN/m^2, therefore, G_r=9326.8 kN/m^2. Taking poisson's ratio, ν, as 0.2 (for sand) and model diameter of spud-can, B, as 0.0767m, the model elastic rotational stiffness, $\Delta M/(B.\Delta\theta)$, is equal to 23 kN. This is plotted as a line in fig. 4.23a and fig. 4.23b. In fig. 4.23b, the elastic stiffness seems to describe the secant rotational stiffness of the curves (for windward legs 2 and 3) quite well. In the case of the leeward leg (fig. 4.23a), the line can be used to represent secant stiffness of the curves when the vertical load is less than the working load value.

The excess pore pressure generation observation can be applied to explain the rotational behaviour of the foundation (see later). However, it is important to look at the external load application on foundation before studying excess pore pressure data. The following discussion will only concentrate on the behaviour of leeward leg.

4.6.3.1 Effects of loading of soil

The cyclic loading applied to the three-leg structure will induce stresses from under the spud-can foundation to the soil. This stresses at the foundation level are often interpreted as the three load components, V, H and M. With this loads we could roughly estimate the stress acting upon the soil. Take a typical example, the behaviour of leeward leg of test YSH8 event 12, illustrated in fig. 4.24 demonstrates the variation of magnitude and change of load direction during cyclic loading. It is observed that when vertical load is maximum i.e. 1.82 kN, the model eccentricity (e_c) would be about 16.7 mm. Subsequently, at the minimum

vertical load value i.e. 0.63 kN, the eccentricity is about 29 mm, almost twice that at higher vertical load. This reflect the fact that effective area supporting the load would have changed drastically depending on the sequence of loading. The effective area at maximum load is much greater than at minimum vertical load level (as shown in fig. 4.24). In this event, the effective area at maximum vertical load is about twice that of the minimum vertical load. Assuming that the moment loads are similar (magnitude is about the same but in opposite direction) in both maximum and minimum cases, the forces on smaller effective area will induce greater rotation. However, if the shear is equal in magnitude but opposite in direction, the vertical stress induced by the reduced effective area may effectively increase to an extent the resistance against shear (note that the vertical stresses under the effective area at the minimum vertical load is about 1.2 times that at maximum vertical load). However, that does not seem to explain the sudden change of stiffness when unloading causes vertical load to go just below the working vertical load. The probable explanation is via fluid movement under the leeward leg.

4.6.3.2 Probable causes for the change in stiffness

It was observed especially under the leeward leg that the change of stiffness is very drastic. The soil gave stiff response when vertical load is above working load. However, when the vertical load is lower than the working load, stiffness fell drastically.

This phenomenon could be explained as follows. When unloading commences, pore pressure (observing PPT A's excess pore pressure in fig. 4.25a,b) starts to fall. As the vertical load falls below the initial vertical working load, the maximum suction causing the minimum pore pressure would have been achieved. This value seems to correspond to the change of stiffness and also the maximum rate of change of the loads. In both cases PPT B's excess pore pressure traces are close to the equilibrium value. Thus, drainage would occur transferring pore fluid into the soil under the foundation. This will result in both uplift and the increased void ratio under the spud-can foundation. By doing so, the pore pressure will also start to increase while the vertical load continues to decrease. At minimum vertical load, the rate of change of load is zero, therefore, the pore pressures tends to zero. Consequently, the reduction of vertical load would result in the decrease of effective stress around the vicinity of the spud-can foundation despite the suction occurring. Thus, the possible reduction in stiffness. The reloading of the spud-can foundation will cause the excess pore pressure to increase rapidly due to the increased void ratio, thus, a possible cause for the reduction of

stiffness. The stiffness will resume its stiffer value when the excess pore pressure are dissipated quickly, creating both settlement and decreased void ratio.

Another observation deduced from pore pressure experimental data could be used to explain the change in stiffness. This is carried out by observing the hydraulic gradient created between PPT A and PPT B. The hydraulic gradient between A and B is obtained by converting the difference in pressure between A and B into fluid head and divided by the drainage length. Assuming that the drainage length is constant, the volume of liquid flowing in or out from under the foundation is a function of the difference in pressure between locations A and B. The higher the hydraulic gradient between the two points, the greater the volume change. Positive hydraulic gradient in this case signifies, that the excess pore pressure at A (P_A) is greater than that at B (P_B), which will result in more settlement. Fig. 4.26a and fig. 4.26b shows time plots of the difference between pore pressure data at locations A and B. The vertical load variation is also superimposed. Two zones could be defined for each cycle, namely, loading and unloading. It is clear that a lot of pore fluid movement had occurred under the footing where the stiffness is low. During the unloading stage, a lot of fluid has moved into the region under the foundation causing uplift resulting in increased void ratio, softening the soil conditions. Thus, causing reduction in stiffness. However, upon reloading, the large quantity of pore fluid is removed under the foundation. This will create a higher positive pore pressure preventing the soil from strengthening instantly. After the dissipation of this positive pore pressure, the subsequent loads does not seem to induce much fluid flow until the point of softening begins again within the unloading stage.

Note that the vertical settlements superimposed with the sum of the difference in excess pore pressure between A and B (function of hydraulic gradient) against time shown in fig. 4.27a and fig.4.27b. The patterns are very similar which also confirms the accuracy of the estimation of plastic settlement using the pore pressure data as shown in section 4.2.1. Fig. 4.27a is for a single cycle of test YSH8 Event 12 and fig. 4.27b is for three cycles of test YSH8 Event 19.

The pore pressure traces in fig. 4.27 showed that for the faster cycle, having a greater variation change in pore pressure implies greater volume changes under the spud-can. This is measured by the settlement indicated 'x' in fig. 4.27b. This is then compared to the slower cycle where the loading variation is very similar. The settlement for the slower cycle is noted

as 'y' in fig. 4.27a. As 'x' is greater than 'y', that indicates that the faster cycle has a greater change in volume. However, the settlement of every single cycle showed that the slower cycle has a greater permanent settlement. This implies that in the faster cycle, the volume of pore fluid entering and leaving the region below the footing is similar and there is less time to dissipate. Thus, there is greater cyclic change in volume but not as much permanent settlement as that of the slower cycle.

4.6.3.3 Effects of frequency of loading

For the leeward legs, its clear from fig. 4.23a that when loading and unloading above the working vertical load values, the soil under the spud-can is stiff and when the vertical load falls below the working load, the soil start to soften and in certain cases zero rotational resistance was reached. At the windward legs, the moment-rotation data show similar behaviour for monotonic loadings, i.e. distinctive S-curve behaviour. Note that for the windward legs, the stiffness seems to vary with frequency loading, secant rotational stiffness reduces at higher frequency cyclic loading. However, for test YSH8 Event 24, the cyclic loading at frequency at 2.24Hz seems to indicate a increase in secant stiffness of the foundation. This could be a result of a denser state under the soil due to the continuous compacting. The change of gradient in stiffness is more distinctive when the vertical load is below the vertical working load and this change of gradient seems to begin at the similar vertical load levels as for the leeward leg.

4.7 Conclusions

The conclusions attained from the observations made as described in this chapter is as follows:-

(i) Pull-out strength depends on the rate of retraction, the size or diameter of the spud-can foundation, and the depth of penetration. With the presence of skirts, the penetration depth can be assumed to be that extending from the soil surface to the tip of the skirt. In this experimental series, the rate of pull-out rate cannot be varied due to apparatus limits. Suction was induced under the spud-can foundations for all soil samples saturated with viscous oil.

Tension in legs is induced by negative excess pore pressure induced under the spud-can and also the high skin friction around the buried vertical part of the foundation. The loss of suction and tension during the retraction process were probably due to the formation of a cavity directly under the foundation causing soil to pipe. Subsequently, soil failure around the outskirts of the spud-can foundation occurred due to drainage, reducing the effective stress around the spud. In a real ocean deployment of a jack-up, the formation of cavity will be inhibited by the depth of spud-can below the sea level. If the water depth is high, failure can only be due to inadequate skin friction.

(ii) Plastic deformations under the spud-can foundation due to cyclic loading depend on the number of cycles, frequency of loading and the magnitude of applied load. Volumetric deformations can be correlated with excess pore pressure gradients. These hydraulic gradients induce pore fluid flow causing volume changes. In this test series, only two pore pressure transducers were employed to predict the settlement; after a few cyclic events under both leeward and windward legs, the predictions were close to that measured in the experiments. The data seems to indicate that excess pore pressure induced depends primary on the vertical load amplitude and frequency of loading.

(iii) Comparing the drained and partially drained load paths, despite lack of more drained case data, the load paths created by the drained situation are linear except when it is approaching the yield locus. It seems to be less stiff (in relation to the observations of load paths) compared with the linear parts of the partially drained load paths.

(iv) The pore pressure amplitudes for location A and the corresponding plastic settlement per cycle are related to the change of vertical load and the frequency of loading.

(v) The load paths plotted in the *V-H-M* load space could be correlated with the stiffness response of the respective load components. They also highlight parts of the cyclic cycle where permanent deformations are likely to occur. Hysteresis effects of the load paths vary with the frequency of loading. The general secant load paths indicate that there is loss of stiffness at higher load amplitudes.

(vi) The sudden reduction of rotational stiffness for the leeward leg (and also the windward leg) when the vertical load is below the vertical working load may be associated with pore fluid moving into the soil under the foundation causing a looser soil specimen

during the unloading phase. When reload occurs, the excess positive pore pressure is induced and requires time to dissipate. Thus, stiffness will not recover immediately. The pore fluid movement increasing void ratio is created by suction. At higher vertical loads i.e. greater than the vertical working load, there are volumetric changes occurring at localised areas but do not cause such distinct change in density as due to suction. Different load paths in the next chapter will explain the asymmetry between loading and unloading.

(vii) If any global shear flow is negligible, the excess pore pressure differences between locations A and B is an indicator of the fluid flow between the region beneath footing and the surrounding soil. This indicator can be correlated with the vertical settlement profile with time during cyclic loading.

5. COMPARISON BETWEEN SKIRTED AND NON-SKIRTED SPUD

In the last two tests YSH8 and YSH9, special efforts were made to investigate and compare the foundation behaviour between a skirted and non-skirted flat spud-can foundation of a three-leg jack-up model subjected to the similar horizontal loading events. Fig. 5.1a and 5.1b illustrates the vertical loading and the respective vertical displacements of the respective spud foundation at the preloading stage for tests YSH8 and YSH9 respectively. The initial part of both sets of curves differs because of the effects of the tip for test YSH8 and the skirt in YSH9. The skirt mobilised a high resistance before full contact of the base of the spud-can is made. When full contact is achieved, the stiffnesses of the curves are quite similar in both tests. The curves for legs 1, 2 and 3 are dark lines, and there is a faint line calculated by applying the vertical bearing capacity formula established by Murff et al. (1992) as follows; given a value of friction angle, ϕ'_{peak}, for the soil conditions, the bearing capacity can be predicted as:-

$$V_p /(\gamma . A . B) = 0.3 N_\gamma [1 - e^{(-\alpha (v_p /B))}] + N_q (v_p /B) \qquad (5.1),$$

$$N_q = e^{(\pi . \tan \phi')} . \tan^2 (45+\phi'/2) \qquad (5.2),$$

$$N_\gamma = 2(N_q + 1) \tan \phi' \qquad (5.3),$$

where, γ is the submerged unit weight, A is the area of the spud, B is the diameter of the spud; α was determined by Murff et al. (1992) based on the combination which provided the best visual match to the experimental load-displacement curves for the flat transition. Following Murff et al. (1992) dense case, α is taken as 26 (for dense sand) respectively. N_γ and N_q are the bearing capacity factors for plane strain case. V_p and v_p are the vertical preload load and the corresponding plastic deformation respectively. For a fixed value α=26, variation of angle of friction showed that the faint lines fitted the dark lines of data best when ϕ'_{peak} is about 39^o. The predicted faint curve is also plotted in fig. 5.1a and fig. 5.1b and matches the experimental data well. Comparing this ϕ'_{peak} with the ϕ'_c from element testing (Tan, 1990) shown in table 3.1, which is about 32^o with a dilation angle, ψ, of about 11^o. This indicated good correlation with laboratory results. A summary of the prototype elasto-plastic and plastic stiffnesses are as shown in table 5.1. The elasto-plastic stiffness can also be predicted

by equations developed by performing data analysis of the tests performed on the same sand type for other centrifuge tests as mentioned in Murff et al., 1991 and Murff et al., 1992. The equations are:-

$$\Delta V = C_v \,.\, B.\, G_v \,.\, \Delta v \quad [\text{kN}] \qquad (5.4),$$

$$G_v = 36600 + 24.9\,(V_p\,/A) \quad [\text{kN/m}^2] \qquad (5.5),$$

$$C_v = 2/(1-\nu) \qquad (5.6),$$

where ν is the poisson's ratio for sand, taken as 0.2 so that C_v = 2.5. Inputting the parameters prototype V_p = 7814.1 kN, A = 17.19 m^2, B = 4.68 m to give G_v =47917.2 kN/m^2, the elastic vertical stiffness, $\Delta V / \Delta v$, is equal to about 0.56 MN/mm. This compares well with the experimental data in table 5.1. This indicates that the properties of the sand for both tests (YSH8 and YSH9) are similar.

In both tests (YSH8 and YSH9), the hull horizontal load amplitudes for each respective event are also very similar as illustrated in Fig. 5.2. In the following discussion, attention is focused on the effects of horizontal cyclic loading for events 3-25 when the working vertical loading is half the preload value, unless specified.

5.1 Vertical Settlements

The cumulative overall settlement versus events for the two tests YSH8 and YSH9 show, in fig. 5.3, that the non-skirted spuds for all three-legs tend to settle more (about twice that of the skirted spuds).

As the load amplitudes of both tests are similar, the comparison of the excess pore pressure generated under the spud-cans can be related to the plastic settlement of the foundation. Fig. 5.4a plots cyclic excess pore pressure amplitude for different frequencies with respect to the vertical load amplitude for Leg 1. It is clear that the cyclic pore pressure amplitude for the skirted spud has magnitude about twice (or more) that of the non-skirted spud. Fig. 5.4b shows the corresponding permanent settlement per cycle against the cyclic vertical load amplitude for both type of spuds. The comparison is consistent with the hypothesis established in section 4.2.2. If applied load levels are similar, faster frequencies inducing

higher excess pore pressure, or the use of skirts will result in lesser settlement. A reason for the lesser settlement for the skirted foundation could be the fact that the skirt could be assumed as a deeper spud foundation extending down to the tip of the skirt. The soil required to be mobilised to cause permanent settlement is deeper and will be stiffer.

At first sight, this might indicate that the non-skirted foundation is more beneficial, but prototype settlement of 0.3m (compared with 0.15m for skirted foundation) for Leg 1 at prototype scale implies that the hull of the prototype jack-up structure has to be raised, increasing the leg lengths and inducing higher stress at the hull connections. In respect of the yield surface, the increase in settlement will have the benefit of increasing the yield surface size. However, to benefit from the increased yield surface size, the working load has to be increased or otherwise, the load paths especially for large load amplitudes will be within the softening zone as shown in fig. 5.5. Increasing the weight of the hull, will also add more stresses to the hull connections.

5.2 Pull-out Capacity

The suction forces measured from the tests are tabulated in Table 5.2. The table shows that the average suction forces created by the skirted spuds are about 4.6 times greater than non-skirted spuds. The lower pull-out strength of non-skirted spuds could be due to the shallower founding depth causing faster dissipation. The loads for the non-skirted spuds vary considerably. The variation may be due to the differences in pull-out rate and force in each leg caused by rig rotation during the pull-out evemt. Another possibility is the randomness in the development of cracks. This will have greater proportionate effect if the embedment depth is small. The pull-out tensions for three-legs in the skirted foundation are very similar, but in the non-skirted case, there are variations between legs. The pull-out strength is suction induced by cavitation forming under spud-can. Cavitation is due to the creation of vacuum under the foundation i.e. about 100 kPa, equivalent to one atmospheric pressure. The hydrostatic head offshore from the water surface to the foundation level as shown in fig. 5.6. It depends on the depth of the sea, and cavitation may not occur at the foundation level. In that case, failure may be due to the different mechanism of liquefaction or piping of soil immediately below the foundation reducing the effective suction area as described in section 4.1.

As the fluid (oil) surface which is about 6 mm above soil surface represents shallow water, the maximum suction stress required to cause cavitation is only about one atmospheric pressure i.e. 100 kPa. From table 5.2, the pull-out strength of each leg for test YSH9 exceeded 100 kPa by about 20% (which also occurred in test YSH7 shown in table 4.2). This indicates that there may have been additional strength due to other sources. One possibility is the skin friction around the skirt. For deeper foundation like test YSH7, the longer drainage path will allow high negative pore pressure to be sustained in the soil around the spud-can. This will increase effective stress around the outskirts of the foundation inducing higher skin friction and thus, higher pull-out strength.

Simple seepage theory assuming cavitation under the spud-can is used to predict and compared the experimental pore pressure data obtained at positions A, B, C and D. The foundation level is assumed to possess a suction capacity of 100 kPa. Via simple seepage analysis, flow nets are drawn to calculate the predicted pore pressure at locations A, B, C and D. In the case of the skirted foundation, it is assumed to be a deeper foundation than the non-skirted one. The soil within the skirt is not considered; the experimental pore pressure data at the respective locations are supposed to coincide with the maximum suction experienced. Table 5.3 shows a summary of the prediction and corresponding experimental pore pressure data. The data match the prediction quite well. Thus, in this situation, the assumption of cavitation under the foundation level appears to be reasonable.

The pull-out strength is dependent on the depth of the foundation and the pull-out rate. The Vertical load vs. time plot is as shown in fig. 5.7. As described in the earlier chapter, the pull-out rate is difficult to vary (apparatus limitations). The skirted spud-can sustained a higher suction force for a longer period than the non-skirted spud foundation. This is attributed to the longer drainage path for skirted foundation. The skirts prevent fast dissipation, thus, sustaining a higher negative pore pressure for a longer period.

5.3 Pore Pressure Generation

As mentioned in the earlier section 5.1, a skirted foundation seems to preserve the soil skeleton despite generating higher pore pressure amplitudes. The lesser settlement could

be due to the skirt extension providing a longer path preventing full dissipation and/or also the deeper foundation should provide a stiffer response.

The excess pore pressure amplitudes generated during each horizontal event for both the tests are as shown in fig. 5.8. As the input load magnitude and frequency to the structure is similar in both cases, the excess pore pressure generation for skirted foundation is at least double that of the non-skirted foundation.

The excess pore pressure behaviour related to the settlement of the foundation is also investigated for test YSH9 and compared with test YSH8. As shown in chapter 4, both plastic and elastic settlements can be predicted by observing the pore pressure data at locations A and B. In this case, Leg 1 of Event 12 of both tests, YSH8 and YSH9, are investigated and compared. Fig. 5.9a shows the time plots of the experimental excess pore pressure at locations A and B with the vertical load variation superimposed for test YSH9 only. The differences of the experimental pore pressure values (for test YSH9 only) at A and B are also plotted in fig. 5.9b. The behaviour of the skirted foundation will be similar to the non-skirted one. Fig. 5.10 demonstrates the cumulative differences in excess pore pressure gradient between A and B, i.e. an approximate integral of $\int (P_A - P_B) \, dt$, for a single cycle for both tests YSH8 and YSH9. The variation of vertical displacements are also superimposed. It is clear that for test YSH9 the experimental profile of the pore pressure data, matches the settlement profile. It is interesting to note that the settlement profiles for both tests YSH8 and YSH9 are almost identical, despite the great differences in the pore pressures. A potential reason for this phenomenon is the longer drainage length for test YSH9 imposed by the skirt. The quantity of pore fluid flowing in or our the region under the spud-can foundation depends on the cumulative head difference, drainage length, permeability and the area entering into the region. The skirt also reduces the access for fluid entering into the region under the foundation.

The pore pressure data demonstrated again that the moment stiffness for test YSH9 will change drastically in the same way as mentioned in the last chapter. Fig. 5.11 shows the moment/rotation cross plot for tests YSH8 and YSH9, for Event 12 Leg 1 only. It illustrates that rotational stiffness is undermined when large pore fluid movement is induced. It is interesting to note for test YSH9 Event 12 that when the moment is at the minimum value when vertical load is reduced, the suction induced also causes high effective stresses to develop around the skirts causing stiffer response. However, the sudden reversal of vertical

load caused considerable generation of positive pore pressure, reducing the all-round effective stresses.

5.4 Load Paths and Moment Fixity

5.4.1 Load paths

The *V-H-M* load paths for test YSH8 and YSH9 Event 12 are compared in fig. 5.12. These load paths represent the response of foundations subjected to large magnitude loadings at slower cycles. The windward legs in both tests showed load path loops with hysteresis similar to those described in section 4.3.1. There would most likely be deformation when the vertical load is at the lowest. The windward legs load paths for both tests are very similar.

For the leeward leg, especially for the M vs. V plot, the hysteresis effects for test YSH9 is very much more than that of the test YSH8. Comparing tests YSH8 with YSH9, the rotational stiffness for the vertical loading cycle would be different from the unloading cycle. This is evident in fig. 5.11. As mentioned before, when vertical load is at the minimum, deformations occur. The H vs. V plot showed similar behaviour in both cases.

5.4.2 Moment and horizontal load capacity

Fig. 5.13 show similar amplitude plots as described in section 4.3.2. In this case, the plots are related to tests conducted at different starting vertical working load. In both tests, after the preloading operation, the vertical load is unloaded to half the preload value. A series of horizontal load events were performed, followed by vertical unloading to a quarter of preload value. Another horizontal loading test series was performed. Then it is vertically unloaded to one-eighth of the preload value and the last series of horizontal loads is applied. Each point plotted in the graph represent the difference in the maximum and minimum horizontal and moment load response in a single horizontal event. The legends are divided into categories related to the starting working load which was either half, one-quarter or one-eighth of Vertical Preload value (V_p), and whether it is skirted or non-skirted foundation. The secant load amplitudes are plotted in fig. 5.13. It is obvious from the horizontal load amplitude vs. vertical load amplitude plot (fig. 5.13a), that when ΔV_l < 0.8 kN, all data

points showed linear behaviour. However, when ΔV_1 exceeds 0.8 kN, in both tests, the horizontal load capacity of some events (especially those at one-eighth of preload value) reduces considerably. In the moment amplitude vs. vertical load amplitude plots, the data points showed linear behaviour at low vertical variations. The moment load amplitude reduces considerably for the one-eighth preload starting load when ΔV_1 exceeds 0.4 kN. This is expected. Lower working level implies that the load paths may be cycling near the softening zones. The graphs for YSH8 test at half preload showed that in both plots fig. 5.13a and fig. 5.13b, the plot is linear.

To study the effects of different vertical working loads, tests YSH8 and YSH9 are compared at the same vertical working load. Fig. 5.14a shows (for working load at half preload value) that the horizontal capacity of the skirted foundation fell when ΔV_1 exceeded 0.8 kN. In fig. 5.14b, the moment capacity for the skirted spud also starts to reduce when ΔV_1 exceeds 0.8 kN. This implies that when horizontal loading of a structure increases, a skirted spud may tend towards a pinned condition more rapidly than the non-skirted one. The plots at one quarter preload value, fig. 5.15, showed linear behaviour, with no drastic change in gradient for both tests, YSH8 and YSH9. A likely reason is that the load paths are cycling well within the yield locus, showing elastic behaviour. When the starting working load is at one-eighth of the preload value, the graph showed that test YSH9 may have slipped when ΔV_1 was about 0.8 kN. This is represented by a drastic drop in horizontal and moment load amplitudes in both figures, fig. 5.16a and fig. 5.16b. For test YSH8, there is sign of reduction in the horizontal and moment load amplitudes at ΔV_1 =0.8 kN but the result is not as drastic as that for the skirted foundation.

As described in section 4.3.2, instead of plotting the respective load amplitudes, the load maxima and minima of all the horizontal cyclic events are plotted. The general load paths of all the horizontal cyclic loading events for 1/4th and 1/8th vertical preload value are plotted in fig. 5.17 and 5.18. As already indicated in fig. 5.15, the general load paths for both skirted and non-skirted foundations at starting working vertical load of 1/4 preload showed similar behaviour. When the starting working vertical load is reduced to 1/8 preload value, fig. 5.18a showed that at low vertical loads (i.e. below starting working vertical load during cyclic loading) the skirted foundation showed higher horizontal capacity. Moment capacity illustrated in fig. 5.18b seems to be lower for the skirted foundation at both lower and higher vertical loads during cyclic loading (i.e. general load paths are much flatter than the non-

skirted one). Moreover, at certain instances when vertical load is low, the moment capacity is reduced to zero.

5.5 Hull Stiffness

In this section, the secant hull stiffness of the jack-up structure is compared between tests YSH8 and YSH9. The secant hull stiffness is calculated by dividing the net hull horizontal load, calculated as the sum of the horizontal loads measured at spud cans, by hull displacement, as shown in fig. 5.19. As the horizontal load is similar in both cases, the model hull stiffness response for test YSH8 of each event is plotted against the corresponding event for test YSH9 as illustrated in fig. 5.20. If both structures are identical with the same foundation and soil conditions, the secant hull stiffness should be identical. However, in this case, the data indicate that stiffness for the skirted foundation, test YSH9, were slightly lower than that of the non-skirted spud. This is most likely due to the greater excess pore pressure generated under the spud-can foundation causing more pore fluid movement under the skirted foundation.

5.6 Conclusions

The tests YSH8 and YSH9 were designed such that the initial soil conditions and the applied loading amplitudes were similar. This allowed direct comparison between the non-skirted and skirted foundation. The comparison demonstrated the effects of excess pore pressure affecting foundation behaviour in a partially drained soil condition. The following is a summary of the comparison:-

(i) The permanent vertical settlement for the skirted foundation is about half that of the non-skirted one. The lesser settlement could be due to the longer drainage path and the stiffer soil conditions at the bottom of the skirt, which may be assumed as a deep foundation.

skirted one). Moreover, at certain instances when vertical load is low, the moment capacity is reduced to zero.

5.5 Hull Stiffness

In this section, the secant hull stiffness of the jack-up structure is compared between tests YSH8 and YSH9. The secant hull stiffness is calculated by dividing the net hull horizontal load, calculated as the sum of the horizontal loads measured at spud cans, by hull displacement, as shown in fig. 5.19. As the horizontal load is similar in both cases, the model hull stiffness response for test YSH8 of each event is plotted against the corresponding event for test YSH9 as illustrated in fig. 5.20. If both structures are identical with the same foundation and soil conditions, the secant hull stiffness should be identical. However, in this case, the data indicate that stiffness for the skirted foundation, test YSH9, were slightly lower than that of the non-skirted spud. This is most likely due to the greater excess pore pressure generated under the spud-can foundation causing more pore fluid movement under the skirted foundation.

5.6 Conclusions

The tests YSH8 and YSH9 were designed such that the initial soil conditions and the applied loading amplitudes were similar. This allowed direct comparison between the non-skirted and skirted foundation. The comparison demonstrated the effects of excess pore pressure affecting foundation behaviour in a partially drained soil condition. The following is a summary of the comparison:-

(i) The permanent vertical settlement for the skirted foundation is about half that of the non-skirted one. The lesser settlement could be due to the longer drainage path and the stiffer soil conditions at the bottom of the skirt, which may be assumed as a deep foundation.

(ii) The pull-out capacity of the skirted foundation was found to be about 4.6 times that of the non-skirted foundation. The variation of magnitudes of pull-out strength for the non-skirted foundations was large. The skirted foundation has consistent pull-out capacity. Simple seepage analysis with the assumption of full suction (to cause full suction, -100KPa) under the foundation is able to predict the pore pressure conditions close to its vicinity. The skirted foundation is assumed as deep foundation, the full suction created at the foundation level contribute to most of the tension strength measured. The rest of the load component must be due the increase in skin friction, due to increase in the effective stresses around the skirt, holding the foundation in place.

(iii) Settlement is dependent on the magnitude and frequency of the applied cyclic load. But if the excess pore pressure amplitudes generated (which is a function of the loading frequency) is greater, at the same load magnitude, it is most likely that the resulting settlement will be less. This is most likely due to the shorter time for dissipation. And in the case of the skirted foundation, the skirts created a longer drainage path compared with the non-skirted one.

(iv) The load paths indicate that the stiffness of the loading and unloading part within a single cyclic cycle for the skirted foundation would be quite different. It also seems to indicate that the moment and horizontal capacity for the skirted foundation (especially at lower starting working load levels) may be lower than that of the non-skirted one. The stiffness variation is similar to that established in the last chapter where the pore fluid movement under the foundation is more (affecting settlements) when vertical load is below the working vertical load.

(v) The hull stiffness for structures with skirted foundation may be slightly lower than for the non-skirted foundations.

6 CONCLUSIONS AND FUTURE WORK

A study of cyclic behaviour in a soil-structural interaction problem has been made to establish the effects of excess pore pressure generated, due to change of magnitude of wave loading and of its frequency of application. In this study, cyclic loading is referred to as quasi-static cyclic loading that has a maximum prototype frequency of about 0.12 Hz where the effects of inertial forces can be ignored. Experiments captured this pore pressure generation, using more viscous oil as pore fluid to slow down the dissipation rate.

Horizontal cyclic loading was applied at the hull level to a three-leg jack-up model in a high gravity environment. The large amount of data obtained could not have be gathered in the field without a fleet of small prototype size jack-ups (for near shore exploration) subjected to load levels similar or in some cases greater than the North Sea severe conditions. Pore pressure transducers were buried under the spud-can foundations to observe the excess pore pressure generation pattern. It differed with respect to load magnitudes under the leeward and windward legs. This pore pressure data was related to settlement data of the leeward (heavily loaded) leg 1. One conclusion of this study is that it would be hard to conduct three-leg jack-up tests in field conditions because the load paths under the windward and leeward legs are very different. Single leg model tests did provide information about soil behaviour like stiffness and excess pore pressure generation but before single leg data could be used it would have been essential to develop a programme to simulate the correct stress history under the foundations of a three-leg rig. Moreover, as the hull ties the three legs together, there is probably a behavioural relationship between the windward and leeward foundations i.e. if the leeward leg is weakened by the loading and soil conditions, more loads will be transferred to the windward legs, keeping the structure stabilised.

It has to be emphasised that the excess pore pressure behaviour observed and reported in the thesis is that of medium dense silica sand. It is likely that if similar tests have been carried out with loose silica sands, calcareous sands or with silt, larger excess pore pressures and larger deformations would have been recorded.

6.1 Overview of Tests YSH3-YSH9

6.1.1 Permanent settlements

The experimental data with respect to the tests YSH3-YSH9 revealed that if horizontal cyclic loading is kept the same irrespective of the rate or frequency of loading, higher frequency will induce greater excess pore pressure due to less drainage, resulting in lesser settlement per cycle. At lower frequency loading, lesser excess pore pressure is induced due to more drainage, resulting in more settlement. If the magnitude of load is increased keeping frequency of loading constant, more settlement per cycle will be expected and greater excess pore pressure generation is induced due to greater plastic strains. This implies that if due to environment, a series of waves with high frequency but within the non-dynamic range, apply load to a jack-up structure, not much permanent settlement will be expected. However, if wave loading is of lower frequency but of the same magnitude of loads, more permanent settlement is expected. In cases when a series of wave has the same frequency of loading but of varying loading magnitudes, when load magnitude increases, more plastic strains will be induced, developing more permanent settlement and higher excess pore pressure amplitudes.

6.1.2 Suction due to pull-out

In each test (YSH3-YSH9), a pull-out event was conducted after all the horizontal cyclic loading events are completed. All the pull-out events for tests YSH3-YSH9 demonstrated that for all oil-saturated samples, suction is developed under the spud-can, inducing tension in legs. The pull-out strength is dependent on the depth of penetration and diameter of foundations, and the rate of pull-out. For safety reasons, the pull-out rates were not varied.

For shallow non-skirted spud cases, the suctions developed under legs are inconsistent and of small magnitude, due to formation of tension cracks or rotation of the spud-can during pull-out. For the skirted spud case, the suctions developed are substantial and very consistent between legs, which implies reliable pull-out strength in the event of a large overturning wave load.

The maximum suction under the spud-can is reached when cavitation occurs under the foundation. The occurrence of cavitation depends also on the depth of water above the sea bed. In these test series, the suction required to create cavitation is close to one atmospheric pressure. Skirted and deeper spud-can foundation demonstrated that tension or pull-out strength in legs can be greater than the magnitude contributed by cavitation. This additional contribution must be due to high effective stress developed around the outskirts of the spud-can.

In the study of cyclic loading, depending on the magnitude of load amplitudes, vertical unloading forms part of a cyclic loading cycle, thus its related to pull-out. Suction under a spud-can induced by vertical unloading can cause drainage to occur, altering the void ratio of the soil directly under the foundations.

6.1.3 Load paths

The load paths within the *V-H-M* load space in the partially drained case are very different for the leeward and windward legs. The load paths for the lightly loaded legs show loops with hysterisis. This hysterisis due to the difference of the loading and unloading parts of a single load cycle is evident in the rotational stiffness behaviour. There are also signs of yielding when the vertical load (which is sensitive to the soil effective stress under the footing) is at a minimum. In the case of the heavily loaded leg, the load paths hysterisis behaviour is dependent on the frequency of loading and the length of drainage path. At higher frequency loading or restricted drainage paths (like for skirted foundation), the hysterisis effect is more prominent, implying difference in foundation behaviour during the loading and unloading part of a single cycle. Yielding at low vertical loads is also present.

6.1.4 Moment fixity

The moment fixity is related to the rotational stiffness of the foundation. The centrifuge test series revealed that the change in rotational stiffness for the heavily loaded foundation is subtle. The rotational stiffness could approach zero when the vertical load is reduced below the vertical working load. The softening of the foundation is most likely due to fluid flowing into the soil under foundation when unloading below the working vertical load. Sudden loading will causes high excess positive pore pressure to be developed, reducing effective stress. However, when the vertical load during cyclic loading exceeds the

vertical working load, dilation under the foundation is prominent, allowing greater rotational stiffness higher than predicted by an elastic space solution (Murff et al., 1992). This dilation zone is confined to a limited region and did not cause much fluid movement.

An explanation for the change in rotational stiffness is as follows. When vertical load is at a minimum, the mean effective stress under the foundation is also at a minimum. The increasing moment will cause deviatoric stresses to increase, causing soil to deform when it reaches the yield surface. This results in lower stiffness when vertical load is less than working vertical load. This behaviour under the heavily loaded leg seems to be independent of the frequency of loading, and is observed in the experimental data.

Although the rotational stiffness of the lightly loaded legs can be described by the elastic space solution shown in Murff et al. (1992), there is still a problem with reduction of stiffness when the vertical load is at its minimum. With respect to structural design, it may be necessary to take into consideration the variation in stiffness of soil in the unload and load part of a single cycle.

6.1.5 Comparison of Skirted and Non-skirted Spud-can foundation

A comparison between a skirted and non-skirted foundation showed that a non-skirted foundation has greater settlement than a skirted foundation. Thus, for long term deployment, the jack-ups with non-skirted foundation may have more need to be jacked up to accommodate such settlement. The reason a skirted foundation has less settlement is most probably due to the stiffer soil materials under the skirt and the longer drainage path created by the skirts preventing fast dissipation. This is evident in the test results. Excess pore pressure generated under the skirted foundation is about twice that of the non-skirted ones.

6.2 Impact on Present Design Method

In conservative, ultimate limit, structural design of jack-ups, pinned conditions are often assumed under the foundation. To provide a more realistic design, especially in the case of deep sea deployment or deployment in harsher storm conditions, studies have been

performed to establish a realistic moment fixity condition for the foundation. The foundation behaviour of a single leg can be treated as three springs for resisting vertical, and horizontal translation and rotation. The stiffness of the foundations can be considered as either elastic or non-linear springs. This foundation stiffnesses are applied to the three spud-can foundations of a three-leg jack-up for the purpose of structural analysis. The results obtained from this study indicate that there is a need to identify the leg with the greatest variation in vertical loads which will depend on wave direction. One leg may be more heavily loaded with waves in a given direction, and less loaded if the storm comes from a different direction. The other two legs are the lightly loaded legs whose foundation stiffness can be described by the elastic space solution developed by Murff et al. (1992). But in the case of the heavily loaded leg, it has to be assumed that when vertical load is below the working vertical load, the secant rotational stiffness should be close to zero and when vertical load exceeds the working vertical load a higher stiffness could be employed. This condition for foundations should be applied, to provide more realistic structural analysis especially for the hull to leg connections.

6.3 Future Work

As mentioned earlier in section 2.4.5, with the reducing prices and increasing speed and power of computer technology, it is not too difficult to imagine that numerical modelling using finite element methods or finite difference methods with high quality laboratory testing on good quality soil specimen will continue to be a popular option to study geotechnical problems. The research highlighted in this thesis showed that excess pore pressure data is closely linked to soil deformation under the foundation. This implies that physical modelling, both field and the centrifuge tests, are still absolutely essential and cannot be ignored. Future work should involve the use of physical models to calibrate numerical models such that real life situation can be modelled more accurately.

REFERENCES

Atkinson, J.H., 1993, *An Introduction to the Mechanics of Soils and Foundations*, McGraw-Hill.

Been, K., and Jeffries, N.G., 1985, "A State Parameter for Sands", *Geotechnique* 35, No. 2, 99-112.

Berg, P. van den, 1994, *Analysis of soil penetration*, Delft University Press.

Bielby, F., 1989, "Triaxial tests on Oil Saturated Sand", Part 2 Project Report, Cambridge University Engineering Department.

Bjerrum, L.,1973, "Geotechnical problems involced in foundations of structures in the North Sea", Geotechnique 23, No. 3, pp 319-358.

Bolton, M.D., 1991, *A Guide to Soil Mechanics*, Hong Kong.

Britto, A.M., and Gunn, M.J., 1987, *Critical State Soil Mechanics via Finite Elements*, Ellis Horwood Ltd, Chichester.

Butterfield, R., and Gotardi, G., 1994, "A complete three-dimensional failure envelope for shallow footings on sand", *Geotechnique* 44, No. 1, pp. 181-184.

Caquot, A., and Kerisel, F., 1949, Traité de mécanique de sols, Paris.

Casagrande, A., 1936, "Characteristics of Cohesionless Soils affecting Stability of Earth Dams", J. Boston Soc. Civil Engineers.

Casagrande, A., 1976, "Liquefaction and cyclic Deformation of Sands a critical review", *Harvard Soil Mechanics Series* No. 88, 5th Panamerican Conference on Soil Mech. and Found. Engrg., Buenos Aires.

Castro, G., 1969, "Liquefaction of Sands", Ph.D. Thesis, Harvard University.

Committee on Earthquake Engineering, 1985, *Liquefaction of Soils During Earthquakes*, National Research Council, National Academy Press, Washington D.C.

Darcy, H., 1856, Les Fontaines Publiques de la Ville de Dijon, Dijon.

Dean, E.T.R., 1991, "Some Potential Approximate Methods for the Preliminary Estimation of Excess Pore Pressures and Settlement-Time Curves for Submerged Circular Spud Foundations subjected to Time-Dependent Loading", Technical Report CUED/D-Soils/TR240, Cambridge University.

Dean, E.T.R., Hsu, Y.S., James, R.G., Saskura, T., A.N. Schofield, and Y. Tsukamoto, 1995, "Centrifuge modelling of jackups and spudcans on drained and partially drained silica sand", Technical Report CUED/D-Soils/TR291, Cambridge University Engineering Department.

Dean E.T.R., Hsu Y.S., James, R.G., and Schofield, A.N., 1994, "Test YSH3 : 3-Leg Jackup Model with Conical Spuds on Dense Sand", Confidential report, ANS&A Centrifuge Testing for Esso Exploration and Production UK Limited Contract EP-022R Task Order 4-022.

Dean E.T.R., Hsu Y.S., James, R.G., and Schofield, A.N., 1994, "Test YSH4 : 3-Leg Jackup Model with Flat Spuds on Medium Dense Sand", Confidential report, ANS&A Centrifuge Testing for Esso Exploration and Production UK Limited Contract EP-022R Task Order 4-022.

Dean E.T.R., Hsu Y.S., James, R.G., and Schofield, A.N., 1994, "Test YSH5 : 3-Leg Jackup Model with Conical Spuds on Dense Sand", Confidential report, ANS&A Centrifuge Testing for Esso Exploration and Production UK Limited Contract EP-022R Task Order 4-022.

Dean E.T.R., Hsu Y.S., James, R.G., and Schofield, A.N., 1994, "Test YSH6 : 3-Leg Jackup Model with Flat Spuds on Dense Water-saturated Sand", Confidential report, ANS&A Centrifuge Testing for Esso Exploration and Production UK Limited Contract EP-022R Task Order 4-022.

Dean E.T.R., Hsu Y.S., James, R.G., and Schofield, A.N., 1994, "Test YSH7 : 3-Leg Jackup Model with Flat` Spuds on Dense Sand", Confidential report, ANS&A Centrifuge Testing for Esso Exploration and Production UK Limited Contract EP-022R Task Order 4-022.

Dean E.T.R., Hsu Y.S., James, R.G., and Schofield, A.N., 1994, "Test YSH8 : 3-Leg Jackup Model with Large Flat Spuds on Dense Sand", Confidential report, ANS&A Centrifuge Testing for Esso Exploration and Production UK Limited Contract EP-022R Task Order 4-022.

Dean E.T.R., Hsu Y.S., James, R.G., and Schofield, A.N., 1994, "Test YSH9 : 3-Leg Jackup Model with Large Skirted-flat Spuds on Dense Sand", Confidential report, ANS&A Centrifuge Testing for Esso Exploration and Production UK Limited Contract EP-022R Task Order 4-022.

Dean E.T.R., Hsu Y.S., James, R.G., and Schofield, A.N., 1994, "Final Report", Confidential report, ANS&A Centrifuge Testing for Esso Exploration and Production UK Limited Contract EP-022R Task Order 4-022.

Dean, E.T.R., Hsu, Y., James, R.G., Schofield, A.N., Murff, J.D., and Wong, P.C., 1995, "Centrifuge Modelling of 3-leg jackups with non-skirted and skirted spuds on partially drained sand", Paper OTC 7839, *Offshore Technology Conference*.

Dean, E.T.R., Hsu, Y.S., James, R.G., Sasakura, T., Schofield, A.N., and Tsukamoto, Y., 1995, "Centrifuge modelling of jackups and spudcans on drained and partially drained silica sand", Proc. of the fifth Int. Conf. on the Jackup Platform: Design, Construction and Operation, City University.

Dean, E.T.R., James, R.G., Schofield, A.N., Tan, F.S.C. and Tsukamoto, Y., 1992, "The bearing capacity of conical footings on sand in relation to the behaviour of spudcan footings on jackups", *Predictive Soil Mechanics*, Proc. of the Wroth Memorial Symposium, Oxford.

Efthymiou, M., and Graham, C.G., 1990, "Environmental Loading on Fixed Offshore Platforms", *Environmental Forces on Offshore Structures and their Prediction*, Society for Underwater Technology, vol. 26, 293-320.

Eyton, D.G.P., 1982, "Triaxial Tests on Sands with Viscous Pore Fluid", Part 2 Project Report, Cambridge University Engineering Department.

Geir SvanØ, 1993, "Skirted Spud-cans- Extending Operational Depth and Improving Performance", Proc. of the Fourth Int. Conf. on the Jack-up Platform, London.

Hansen, J.B., 1961, "A general formula for bearing capacity", Danish Geotechnical Institute Bulletin.

Hansen, B., 1975, "Bearing capacity of footings in theory and experiment", Proc. 1st Baltic Conf. Soil Mech. Fdn. Eng., Vol. 1.

Hencky, H., 1923, "Über einige statisch bestimmte Fälle des Gleichgewichts in plastischen körpem", *Z. f. ang. Math. u. Mech.*, vol. 3, 241.

Hsu, Y.S., Collison, C.H., Dean, E.T.R., and R.G. James, "Techniques for saturating sand with oil", Proc. of the Int. Conf. Centrifuge 94, Singapore.

Ishihara, 1993, "Liquefaction and flow failure during earthquakes", Geotechnique 43, No. 3, pp. 351-415.

Junikis, A.R., 1956, "Rupture surfaces in sand under oblique loads", J. Soil Mech. Fdn. Eng., ASCE, SM1.

Jeyatharan, K., 1991, "Partial Liquefaction of Sand Fill in a mobile Arctic Caisson under Ice Loading", Ph.D. Thesis, Cambridge University.

Lade, P.V., 1993, "Initiation of static instability in the submarine Nerlerk berm", Canadian Geotechnical Journal, vol. 30, pp. 895-904.

Lambe, T.W., and Whitman, R.V., 1979, *Soil Mechanics*, John Wiley & Sons

Lau, C.K., 1988, "Scale Effect in Tests on Footings", Ph.D. Thesis, Cambridge University.

Lee L.K., 1965, "Foundations subject to moment", Proc. 6th Int. Conf. Soil Mech. Fdn. Engg., Vol. 2.

Lee, K.L., and Focht, J.A., 1975, "Liquefaction Potential at Ekofisk Tank in North Sea", Journal of the Geotechnical Engineering Division, ASCE, GT1, pp. 1-18.

Luong, M.P., and Sidaner, J.F., 1981, "Undrained Behaviour of Cohesionless Soils under Cyclic and Transient Loading", Proc. Int. Conf. on Recent Advances in Geot. Earthquake Engrg. and Soil Dynamics, vol. 1, St. Louis, pp. 215-220.

Logan, D.L., 1992, *A First Course in the Finite Element Method*, 2nd ed., PWS-KENT, Boston.

Mair, R.J., 1979, "Centrifugal modelling of tunnel construction in soft clay", Ph.D. Thesis, Cambridge University.

Malushitsky, Y.N., 1981, *The centrifugal model testing of waste-heap embankments*, Cambridge University Press.

McCarron, W.O., and Broussard, M.D., 1992, "Measured Jack-up response and spudcan-seafloor interaction for an extreme storm Event", Proc. of the sixth Int. Conf., vol. 1, *Behaviour of Offshore Structures*.

McClelland, B., Young, A.G., and Remmes, B.D., 1981, "Avoiding jack-up rig foundation failures", Symp. on Geot. Aspects of Coastal and Offshore Structures, Bangkok.

Meyerhof, G.G., 1951, "The ultimate bearing capacity of foundations", *Geotechnique*, 28, No.3, Vol. 2, pp. 281-307.

Meyerhof, G.G., 1953, "The bearing capacity of foundations under eccentric and inclined loads", Proc. 3rd Int. Conf. Soil Mech., Vol. 1, pp. 440-445.

Meyerhof, G.G., 1956, "Discussion of rupture surfaces in sand by Junikis, A.R.", J. Soil Mech. Fdn., ASCE, SM3.

Meyerhof, G.G., 1965, "Shallow foundations", J. Soil Mech. Fdn. Div., ASCE, SM2, pp. 21-31.

Murff, J.D., Hamilton, J.M., Dean, E.T.R., James, R.G., Kusakabe, O., Schofield, A.N., 1991, "Centrifuge Testing of Foundation Behavior Using Full Jackup Fig Models", Paper OTC 6516, *Offshore Technology Conference*, pp. 165-178.

Murff, J.D., Prins, M.D., Dean, E.T.R., James, R.G., and Schofield, A.N., 1992, "Jackup Rig Foundation Modelling", Paper OTC 6807, *Offshore Technology Conference*, pp. 35-46.

Noble Denton and Associates, 1987, "Foundation fixity of jack-up units : a Joint Industry Study", confidential report, Noble Denton and Associates, London.

Nystrom, G.A., 1984, "Finite-strain axial analysis of piles in clay", *Analysis and Design of Pile Foundations*, ASCE.

Osborne, J.J., Trickey, J.C., Houlsby, G.T., and James, R.G., 1991, "Findings from a joint industry study on foundation fixity of jackup units", Paper OTC 6615, *Offshore Technology Conference*.

Perol, C., and Meimon, Y., 1989, "Cyclic Storm Loading Soil-Structure Interaction for a Three Independent Leg Jack-Up", Marines Structures, (UK), Vol. 2, Nos. 3/5, pp. 403-423.

Prandtl, L., 1920, "Uberdie harte plastischer Korper (on the hardness of plastic bodies), Nachr. Kgl. Ges. Wiss. Gottingen, Math.-Phys. Klasse, referred to by Terzaghi, K. (1943).

Poulos, H.G., 1988, *Marine Geotechnics*, Unwin Hyman, London.

Poulos, H.G., and Hull, T.S., 1989, "The Role of Analytical Geomechanics in Foundation Engineering", *Foundation Engineering: Current principles and practices*, vol.2, ASCE, pp. 1578-1605.

Ramelot, C., and Vandeperre, L., 1950, "Travaux de la commission d'etude des foundations de pylônes", compt. Rend. Rech., I.R.S. LA. Brussels, No. 2.

Reissner, H., 1924, "Zum Erddruckproblem", Proc. 1st Int. Cong. Applied Mech., Delft, referred to by Terzaghi, K. (1943)

Roscoe, K.H., and Schofield, A.N., 1956, "The Stability of Short Pier Foundations in Sand", *British Welding Journal*, August, 343-354.

Roscoe, K.H., and Schofield, A.N., 1963, "Mechanical Behaviour of an Idealised 'Wet Clay'", Proc. 2nd European Conf. Soil Mech., 47-54.

Roscoe, K.H., Schofield, A.N., and Wroth, C.P., 1958, "On the Yielding of Soils", *Geotechnique* 8, 22-53.

Rowe, P.W., 1962, "The Stress-Dilatancy Relation for Static Equilibrium of an Assembly of Particles in contact", *Proc. Roy. Soc. Series A*, vol. 269, 500-527.

Sangrey, D.A., Castro, G., Poulos, S.J., and France, J.W., "Cyclic loading of sands, silts and clays", Proc. ASCE Spec. Conf. on Earthq. Engg. Soil Dynam., Pasdena, vol. 2, pp. 836-851.

Schofield, A.N., 1976, "The role of centrifuge modelling", *Offshore Soil Mechanics*, Cambridge University Engineering Department.

Schofield, A.N., 1980, "Cambridge Geotechnical Centrifuge Operations", *Geotechnique*, vol. 30, No. 3, 227-268.

Schofield, A.N., 1981, "Dynamic and Earthquake Geotechnical Centrifuge Modelling", Int. Conf. on Recent Advances in Geo. Earthquake Eng. and Soil dynamics, St. Louis.

Schofield, A.N., and Wroth, C.P., 1968, "Critical State Soil Mechanics", McGraw-Hill Book Co., London.

Seed, H.B., 1979, "Soil liquefaction and cyclic mobility evaluation for level ground during earthquakes", *J. Geotech. Engng Div. Am. Soc. Civ. Engrs* 105, GT2, 201-255.

Shi, Q., 1988, "Centrifugal Modelling of Surface Footings subjected to Combined Loading", Ph.D. Thesis, Cambridge University.

Silva Perez, A.A., 1982, "Conical Footings under Combined Loads", MPhil. Thesis, Cambridge University.

Sokolovski, V.V., 1960, *Statics of Soil Media*, Butterworths Scientific Publications, London.

Steedman, R.S., 1984, Ph.D. Thesis, "Modelling the behaviour of retaining walls in earthquakes", Cambridge University

Tan, F.S.C., 1990, "Centrifuge and Theoretical Modelling of Conical Footings on Sand", Ph.D. Thesis, Cambridge University.

Taylor, D.W., 1948, *Fundamentals of Soil Mechanics*, Wiley, New York.

Taylor, R.N., 1979, "Stand up of a model tunnel in silt", MPhil., Cambridge University.

Taylor, R.N., 1995, *Geotechnical Centrifuge Technology*, Blackie Academic and Professional, London.

Terzaghi, K., 1943, *Theoretical Soil Mechanics*, Wiley, New York.

Tsukamoto, Y., 1994, "Drum Centrifuge Tests of Three-Leg Jack-ups on sand", Ph.D. Thesis, Cambridge University.

Vesic, A.S., 1973, "Analysis of Ultimate Loads of Shallow Foundations", J. of the Soil Mech. and Found. Div., ASCE, SM1, pp. 45-73.

Vugts, 1993, "Jack-ups in Perspective", Proc. of the 4th Int. Conf. on the Jack-up Platform, London, pp. 1-4.

Wong, P.C., Chao, J.C., Murff, J.D., Dean, E.T.R., James, R.G., and Schofield, A.N., 1993, "Jackup rig foundation modeling II", Paper OTC 7303, *Offshore Technology Conference*, pp. 411-420.

Zienkiewicz, O.C., 1977, The Finite Element Method, 3rd ed., McGraw-Hill, London.

Storm (hurricane)	Year	Structure name	Overload Ratio (est. load/design)	Comments
Hilda	1964	SS 274	3.17	Damaged
Hilda	1964	EI 276	4.50	Collapsed
Hilda	1964	SS 198-C	4.50	Collapsed
Betsy	1965	WD 133	2.41	Damaged
Camille	1969	SP 62	2.56	Undamage

Table 1.1 Selected Platform Survival Experience (Extracted from Efthymiou, 1990)

Event	G-level	Description	No. of Cycles	Hull Disp* (+/-), mm	Freq. Hz
01	1→80	Swing Up	-	-	-
02	80	Preloading	-	-	-
03	80	Rapid Horizontal Loading	50	0.24	0.5
04	80	Slow Horizontal Loading	3	0.23	0.05
05	80	Rapid Horizontal Loading	50	0.49	0.5
06	80	Slow Horizontal Loading	3	0.47	0.05
07	80	Rapid Horizontal Loading	50	0.87	0.5
08	80	Slow Horizontal Loading	3	0.82	0.05
09	80	Rapid Horizontal Loading	50	1.16	0.5
10	80	Slow Horizontal Loading	3	1.12	0.05
11	80	Slow Horizontal Loading	3	1.52	0.05
12	80	Slow Horizontal Loading	3	1.80	0.05
13	80	Slow Horizontal Loading	3	2.26	0.05
14	80	Slow Horizontal Loading	3	2.57	0.05
15	80	Rapid Horizontal Loading	50	1.53	0.5
16	80	Rapid Horizontal Loading	50	1.80	0.5
17	80	Rapid Horizontal Loading	50	2.26	0.5
18	80	Rapid Horizontal Loading	42	2.55	0.5
19	80	Various Horizontal Loading	-	-	-
20	80	Fast Horizontal Loading	50	1.31	1.0
21	80	Fast Horizontal Loading	50	0.40	2.0
22	80	Fast Horizontal Loading	50	0.21	4.0
23	80	Fast Horizontal Loading	50	0.45	4.0
24	80	Fast Horizontal Loading	50	0.78	4.0
25	80	Fast Horizontal Loading	200	0.90	2.0
26	80	Vertical Reloading, Unloading, Retraction	-	-	-
27	80→1	Swing down	-	-	-

* Horizontal Hull Displacements

Table 1.2 Test YSH3. Event Summary: 3-Leg Jackup model with conical spuds on dense sand

Event	G-level	Description	No. of Cycles	Hull Disp* (+/-), mm	Freq. Hz
01	1→80	Swing Up	-	-	-
02	80	Preloading	-	-	-
03	80	Rapid Horizontal Loading	50	0.39	0.5
04	80	Slow Horizontal Loading	3	0.37	0.05
05	80	Rapid Horizontal Loading	50	0.88	0.5
06	80	Slow Horizontal Loading	3	0.85	0.05
07	80	Rapid Horizontal Loading	50	1.40	0.5
08	80	Slow Horizontal Loading	3	1.36	0.05
09	80	Rapid Horizontal Loading	50	1.94	0.5
10	80	Slow Horizontal Loading	3	1.89	0.05
11	80	Slow Horizontal Loading	3	2.45	0.05
12	80	Various Horizontal Moves	-	-	-
13	80	Fast Horizontal Loading	50	1.88	1.0
14	80	Fast Horizontal Loading	50	1.36	2.0
15	80	Fast Horizontal Loading	50	2.01	2.0
16	80	Fast Horizontal Loading	200	2.09	2.0
17	80	Fast Horizontal Loading	200	1.59	3.0
18	80	Fast Horizontal Loading	200	0.69	3.0
19	80	Partial Vertical UnLoading	-	-	-
20	80	Fast Horizontal Loading	200	0.94	2.0
21	80	Fast Horizontal Loading	200	1.80	2.0
22	80	Fast Horizontal Loading	200	2.18	2.0
23	80	Slow Horizontal Loading	3	2.36	0.05
24	80	Slow Horizontal Loading	3	2.81	0.05
25	80	Vertical Reloading to Preload Value	-	-	-
26	80	Slow Horizontal Loading	1	2.29	0.05
27	80	Slow Horizontal Loading	3	1.41	0.05
28	80	Fast Horizontal Loading	200	1.06	2.0
29	80	Vert. Reloading, Unloading, Retraction	-	-	-
30	80→1	Swing down	-	-	-

* Horizontal Hull Displacements

Table 1.3 Test YSH4. Event Summary: 3-Leg Jackup model with flat spuds on medium dense sand

Event	G-level	Description	No. of Cycles	Hull Disp* (+/-), mm	Freq. Hz
01	1→80	Swing Up	-	-	-
02	80	Preloading	-	-	-
03	80	Rapid Horizontal Loading	50	0.37	0.5
04	80	Slow Horizontal Loading	3	0.36	0.05
05	80	Rapid Horizontal Loading	50	0.80	0.5
06	80	Slow Horizontal Loading	3	0.77	0.05
07	80	Rapid Horizontal Loading	50	1.26	0.5
08	80	Slow Horizontal Loading	3	1.23	0.05
09	80	Rapid Horizontal Loading	50	1.74	0.5
10	80	Slow Horizontal Loading	3	1.70	0.05
11	80	Slow Horizontal Loading	3	2.19	0.05
12	80	Slow Horizontal Loading	3	2.70	0.05
13	80	Slow Horizontal Loading	3	3.21	0.05
14	80	Slow Horizontal Loading	3	3.72	0.05
15	80	Slow Horizontal Loading	3-part cycles	3.70	0.05
16	80	Rapid Horizontal Loading	50	2.72	0.5
17	80	Rapid Horizontal Loading	1	3.64	0.5
18	80	Rapid Horizontal Loading	50	3.74	0.5
19	80	Fast Horizontal Loading	50	3.61	1
20	80	Fast Horizontal Loading	50	2.68	2.0
21	80	Fast Horizontal Loading	50	1.58	4.0
22	80	Fast Horizontal Loading	50	1.17	8.0
23	80	Slow Horizontal Loading	3	4.44	0.05
24	80	Rapid Horizontal Loading	50	4.53	0.5
25	80	Fast Horiznotal Loading	50	3.28	2.0
26	80	Slow Horizontal Loading	3	5.26	0.05
27	80	Rapid Horizontal Loading	50	5.32	0.5
28	80	Fast Horizontal Loading	50	3.87	2.0
29	80	Slow Horizontal Loading	3	6.46	0.05
30	80	Rapid Horizontal Loading	50	6.53	0.5
31	80	Fast Horizontal Loading	50	4.69	2.0
32	80	Vert. Reloading, Unloading, Retraction	-	-	-
33	80→1	Swing down	-	-	-

* Horizontal Hull Displacements

Table 1.4 Test YSH5. Event Summary: 3-Leg Jackup model with conical spuds on dense sand

Event	G-level	Description	No. of Cycles	Hull Disp* (+/-), mm	Freq. Hz
01	1→64	Swing Up	-	-	-
02	64	Landing and Preloading	-	-	-
03	64	Rapid Horizontal Loading	50	0.37	0.1
04	64	Rapid Horizontal Loading	50	0.35	0.1
05	64	Slow Horizontal Loading	3	0.70	0.01
06	64	Rapid Horizontal Loading	50	0.56	0.1
07	64	Slow Horizontal Loading	4	1.05	0.01
08	64	Rapid Horizontal Loading	50	0.82	0.1
09	64	Slow Horizontal Loading	4	1.67	0.01
10	64	Rapid Horizontal Loading	50	0.60	0.5
11	64	Fast Horizontal Loading	50	0.58	1.0
12	64	Fast Horizontal Loading	50	0.45	2.0
13	64	Rapid Horizontal Loading	50	1.30	0.5
14	64	Fast Horizontal Loading	50	1.26	1.0
15	64	Fast Horizontal Loading	50	0.91	2.0
16	64	Rapid Horizontal Loading	50	2.05	0.5
17	64	Fast Horizontal Loading	50	1.98	1.0
18	64	Fast Horizontal Loading	50	1.37	2.0
19	64	Slow Horizontal Loading	4	2.13	0.05
20	64	Vert. Reloading, Unloading, Retraction	-	-	-
21	64→1	Swing down	-	-	-

* Horizontal Hull Displacements

Table 1.5 Test YSH6. Event Summary: 3-Leg Jackup model with flat spuds on dense water-saturated sand

Event	G-level	Description	No. of Cycles	Hull Disp* (+/-), mm	Freq. Hz
01	1→40	Swing Up	-	-	-
02	40	Landing and Preloading	-	-	-
03	40	Rapid Horizontal Loading	50	0.27	0.5
04	40	Slow Horizontal Loading	3	0.26	0.05
05	40	Rapid Horizontal Loading	50	0.62	0.5
06	40	Slow Horizontal Loading	3	0.59	0.05
07	40	Rapid Horizontal Loading	50	0.97	0.5
08	40	Slow Horizontal Loading	3	0.94	0.05
09	40	Rapid Horizontal Loading	43	1.34	0.5
10	40	Slow Horizontal Loading	3	1.30	0.05
11	40	Slow Horizontal Loading	3	1.69	0.05
12	40	Slow Horizontal Loading	3	2.08	0.05
13	40	Fast Horizontal Loading	50	0.64	1
14	40	Fast Horizontal Loading	50	0.45	2
15	40	Fast Horizontal Loading	50	0.36	4
16	40	Fast Horizontal Loading	50	1.51	1
17	40	Fast Horizontal Loading	50	1.06	2
18	40	Fast Horizontal Loading	50	0.63	4
19	40	Fast Horizontal Loading	50	3.50	1
20	40	Fast Horizontal Loading	50	2.57	2
21	40	Fast Horizontal Loading	50	1.45	4
22	40	Rapid Horizontal Loading	50	4.84	0.5
23	40	Fast Horizontal Loading	50	4.67	1
24	40	Fast Horizontal Loading	50	3.39	2
25	40	Fast Horiznotal Loading	50	1.98	4
26	40	Rapid Horizontal Loading	200	4.83	0.5
27	40	Fast Horizontal Loading	200	4.97	1
28	40	Fast Horizontal Loading	200	3.93	2
29	40	Fast Horizontal Loading	200	2.36	4
30	40	Three Horizontal Movetos	-	-	-
31	40	Pullout and Retraction	-	-	-
32	40→1	Swing down	-	-	-

* Horizontal Hull Displacements

Table 1.6 Test YSH7. Event Summary: 3-Leg Jackup model with flat spuds on dense sand

Event	G-level	Description	No. of Cycles	Hull Disp* (+/-), mm	Freq. Hz
01	1→61	Swing Up	-	-	-
02	61	Landing and Preloading	-	-	-
03	61	Rapid Horizontal Loading	50	0.43	0.284
04	61	Slow Horizontal Loading	3	0.49	0.0284
05	61	Rapid Horizontal Loading	50	0.98	0.284
06	61	Slow Horizontal Loading	3	1.11	0.0284
07	61	Rapid Horizontal Loading	50	1.56	0.284
08	61	Slow Horizontal Loading	3	1.76	0.0284
09	61	Rapid Horizontal Loading	43	2.14	0.284
10	61	Slow Horizontal Loading	3	2.41	0.0284
11	61	Slow Horizontal Loading	3	3.13	0.0284
12	61	Slow Horizontal Loading	3	3.86	0.0284
13	61	Fast Horizontal Loading	50	1.03	0.568
14	61	Fast Horizontal Loading	50	0.97	1.12
15	61	Fast Horizontal Loading	50	0.69	2.24
16	61	Fast Horizontal Loading	50	1.66	0.568
17	61	Fast Horizontal Loading	50	1.56	1.12
18	61	Fast Horizontal Loading	50	1.13	2.24
19	61	Fast Horizontal Loading	50	3.66	0.568
20	61	Fast Horizontal Loading	50	3.46	1.12
21	61	Fast Horizontal Loading	50	2.40	2.24
22	61	Fast Horizontal Loading	50	4.97	0.568
23	61	Fast Horizontal Loading	50	4.71	1.12
24	61	Fast Horizontal Loading	50	3.44	2.24
25	61	Various Horizontal Movetos	-	-	-
26	61	Reduction in Vertical Load	-	-	-
27	61	Rapid Horizontal Loading	50	0.99	0.284
28	61	Slow Horizontal Loading	50	1.12	0.0284
29	61	Fast Horizontal Loading	50	1.05	0.568
30	61	Fast Horizontal Loading	50	0.99	1.12
31	61	Fast Horizontal Loading	50	0.68	2.24
32	61	Fast Horizontal Loading	50	1.10	2.24
33	61	Rapid Horizontal Loading	50	2.17	0.284
34	61	Slow Horizontal Loading	3	2.51	0.0284
35	61	Fast Horizontal Loading	50	2.35	0.568
36	61	Fast Horizontal Loading	50	2.24	1.12
37	61	Fast Horizontal Loading	50	1.66	2.24
38	61	Reduction of Vertical Load	-	-	-
39	61	Rapid Horizontal Loading	50	0.44	0.284
40	61	Slow Horizontal Loading	3	0.51	0.0284
41	61	Fast Horizontal Loading	50	0.47	0.568
42	61	Fast Horizontal Loading	50	0.43	1.12
43	61	Fast Horizontal Loading	50	0.32	2.24

Table 1.7a Test YSH8. Event Summary: 3-Leg Jackup model with large flat spuds on dense sand (Events 01-43)

Cont'd

Event	G-level	Description	No. of Cycles	Hull Disp* (+/-), mm	Freq. Hz
44	61	Rapid Horizontal Loading	50	1.02	0.284
45	61	Slow Horizontal Loading	3	1.20	0.0284
46	61	Fast Horizontal Loading	50	1.11	0.568
47	61	Fast Horizontal Loading	50	1.05	1.12
48	61	Fast Horizontal Loading	50	0.73	2.24
49	61	Fast Horizontal Loading	50	1.69	1.12
50	61	Fast Horizontal Loading	50	2.36	1.12
51	61	Fast Horizontal Loading	50	3.02	1.12
52	61	Fast Horizontal Loading	50	3.68	1.12
53	61	Fast Horizontal Loading	50	4.25	1.12
54	61	Fast Horizontal Loading	50	4.90	1.12
55	61	Slow Horizontal Loading	3	4.91	0.0284
56	61	Vert.Reload,Unload, Retraction	-	-	-
57	61→1	Swing down	-	-	-

* Horizontal Hull Displacements

Table 1.7b Test YSH8. Event Summary: 3-Leg Jackup model with large flat spuds on dense sand (Events 44-57)

Event	G-level	Description	No. of Cycles	Hull Disp* (+/-), mm	Freq. Hz
01	1→61	Swing Up	-	-	-
02	61	Landing and Preloading	-	-	-
03	61	Rapid Horizontal Loading	50	0.50	0.284
04	61	Slow Horizontal Loading	3	0.57	0.0284
05	61	Rapid Horizontal Loading	50	0.98	0.284
06	61	Slow Horizontal Loading	3	1.11	0.0284
07	61	Rapid Horizontal Loading	50	1.55	0.284
08	61	Slow Horizontal Loading	3	1.76	0.0284
09	61	Rapid Horizontal Loading	43	2.12	0.284
10	61	Slow Horizontal Loading	3	2.43	0.0284
11	61	Slow Horizontal Loading	3	3.12	0.0284
12	61	Slow Horizontal Loading	3	3.86	0.0284
13	61	Fast Horizontal Loading	50	1.04	0.568
14	61	Fast Horizontal Loading	50	0.97	1.12
15	61	Fast Horizontal Loading	50	0.70	2.24
16	61	Fast Horizontal Loading	50	1.65	0.568
17	61	Fast Horizontal Loading	50	1.56	1.12
18	61	Fast Horizontal Loading	50	1.11	2.24
19	61	Fast Horizontal Loading	50	3.65	0.568
20	61	Fast Horizontal Loading	50	3.44	1.12
21	61	Fast Horizontal Loading	50	2.51	2.24
22	61	Fast Horizontal Loading	50	5.06	0.568
23	61	Fast Horizontal Loading	50	4.83	1.12
24	61	Various Horizontal Movetos	-	-	-
25	61	Fast Horizontal Loading	50	3.43	2.24
26	61	Reduction in Vertical Load	-	-	-
27	61	Rapid Horizontal Loading	50	1.09	0.284
28	61	Slow Horizontal Loading	50	1.17	0.0284
29	61	Fast Horizontal Loading	50	1.11	0.568
30	61	Fast Horizontal Loading	50	1.06	1.12
31	61	Fast Horizontal Loading	50	0.82	2.24
32	61	Fast Horizontal Loading	50	1.20	2.24
33	61	Rapid Horizontal Loading	50	2.24	0.284
34	61	Slow Horizontal Loading	3	2.57	0.0284
35	61	Fast Horizontal Loading	50	2.41	0.568
36	61	Fast Horizontal Loading	50	2.30	1.12
37	61	Fast Horizontal Loading	50	1.67	2.24
38	61	Horizontal Moveto	-	-	-
39	61	Reduction of Vertical Load	-	-	-
40	61	Rapid Horizontal Loading	50	0.43	0.284
41	61	Slow Horizontal Loading	3	0.49	0.0284
42	61	Fast Horizontal Loading	50	0.46	0.568
43	61	Fast Horizontal Loading	50	0.43	1.12
44	61	Fast Horizontal Loading	50	0.32	2.24

Table 1.8a Test YSH9. Event Summary: 3-Leg Jackup model with large flat skirted spuds on dense sand (Events 01-43)

Cont'd

Event	G-level	Description	No. of Cycles	Hull Disp* (+/-), mm	Freq. Hz
45	61	Rapid Horizontal Loading	50	1.01	0.284
46	61	Slow Horizontal Loading	3	1.17	0.0284
47	61	Fast Horizontal Loading	50	1.04	1.12
48	61	Fast Horizontal Loading	50	0.72	2.24
49	61	Fast Horizontal Loading	50	1.04	1.12
50	61	Fast Horizontal Loading	50	1.68	1.12
51	61	Fast Horizontal Loading	50	2.32	1.12
52	61	Fast Horizontal Loading	50	2.99	1.12
53	61	Fast Horizontal Loading	50	3.68	1.12
54	61	Fast Horizontal Loading	50	4.35	1.12
55	61	Fast Horizontal Loading	50	5.03	1.12
56	61	Slow Horizontal Loading	3	5.73	0.0284
57	61	Fast Horizontal Loading	50	5.77	1.12
58	61	Fast Horizontal Loading	50	5.88	1.12
59	61	Horizontal Moveto	-	-	-
60	61	Slow Horizontal Loading	3	6.50	0.0284
61	61	Four Horizontal Movetos	-	-	-
62	61	Vert.Reload,Unload, Retraction	-	-	-
63	61→1	Swing down	-	-	-

* Horizontal Hull Displacements

Table 1.8b Test YSH9. Event Summary: 3-Leg Jackup model with large flat skirted spuds on dense sand (Events 44-63)

Category	Sub-Division	Characteristics	Method of Parameter Determination
1	–	Empirical – not based on soil mechanics principles	Simple in-situ or laboratory tests, with correlations
2	2A	Based on simplified theory or charts – uses soil mechanics principles – amenable to hand calculation. Theory is linear elastic (deformation) or rigid plastic (stability)	Routine relevant in-situ tests – may require some correlations
	2B	As for 2A, but theory is non-linear (deformation) or elasto-plastic (stability)	
3	3A	Based on theory using site-specific analysis, uses soil mechanics principles. Theory is linear elastic (deformation) or rigid plastic (stability)	Careful laboratory and/or in-situ tests which follow the appropriate stress paths
	3B	As for 3A, but non-linearity is allowed for in a relatively simple manner	
	3C	As for 3A, but non-linearity is allowed for via proper constitutive models of soil behavior	

Table 2.1 Categories of Analysis/Design Procedures
(Extracted from Poulos and Hull,1992)

Entity	Model	Prototype
Length	1	N
Area	1	N^2
Volume	1	N^3
Angles	1	1
Soil Density	1	1
Void Ratio	1	1
Relative Density	1	1
Forces	1	N^2
Energy or Weight	1	N^3
Pressure or Stress	1	1
Soil Element Stiffness= σ_v'/ε	1	1
Shear Force, H	1	N^2
Moment, M	1	N^3
Vertical Force, V	1	N^2
Vertical Stiffness, K_v	1	N
Shear Stiffness, K_h	1	N
Moment Stiffness, M/t	1	N^3
$M/(BT)$	1	N^2
Leg Axial Stiffness, EA	1	N^2
Leg Shear Stiffness, GA	1	N^2
Flexural Rigidity, $M/curv$	1	N^4
Elastic Beam Flexural Rigidity, EI	1	N^4
Time (Consolidation)	1	N^2
Time (Dynamic)	1	N
Viscosity	1	N^{-1}

Table 3.1 Summary of scaling relations

Leigton Buzzard 100/170 Sand

D_{10} grain size	0.095 mm
D_{50} grain size	0.14 mm
D_{60} grain size	0.15 mm
Specific Gravity, G_s	2.65
Minimum Voids Ratio, e_{min}	0.613
Maximum Void Ratio, e_{max}	1.014
Permeability to water ($e=0.72$)	0.98×10^{-4} m/s
Angle of Shearing Resistance at Critical State, ϕ_{crit}	32° (estimated value)

Table 3.2 Properties of BS 100/170 sand (extracted from Tan, 1990)

Test no.	G-Level G=Ng	Description of Prototype	No. of Horiz. loading events, total
YSH1	60g	19.1 m high jackup with three 3.47 m dia. flats spuds on drained sand, RD=75%. Cyclic loading periods up to 10 hours. Proof test for experimental apparatus.	24,29
YSH2	80g	25.4 m high jackup with three 4.62 m dia. flat spuds on oil saturated sand, RD=76%. Cyclic loading periods from 12 to 496 seconds.	16,21
YSH3	80g	25.4 m high jackup with three 4.62 m dia. conical spuds on oil saturated sand, RD=80%. Cyclic loading periods from 6 to 486 seconds.	23,27
YSH4	80g	25.4 m high jackup with three 4.62 m dia. flat spuds on oil saturated sand, RD=62%. Cyclic loading periods from 8 to 520 seconds.	24,30
YSH5	80g	25.4 m high jackup with three 4.62 m dia. conical spuds on oil saturated sand, RD=74%. Cyclic loading periods from 14 to 578 seconds.	29,33
YSH6	64g	20.4 m high jackup with three 3.7 m dia. flat spuds on drained sand, RD=58%. Cyclic loading periods up to 23 hours. Water saturated to ensure no generation of excess pore pressure.	17,21
YSH7	40g	12.7 m high jackup with three 2.3 m dia. flat spuds on oil saturated sand, RD=69%. Cyclic loading periods from 1.5 to 123 seconds.	28,32
YSH8	61g	19.6 m high jackup with three 4.68 m dia. flat spuds on oil saturated sand, RD=78%. Cyclic loading periods from 6 to 486 seconds. Modelling of models.	53,57
YSH9	61g	19.6 m high jackup with three 4.68 m dia. skirted flat spuds on oil saturated sand, RD=69%. Cyclic loading periods from 6 to 465 seconds.	57,63

Table 4.1 Description of the nine tests

Leg 1

Test Code	Pull-out Strength (kN/m^2)	Pull-out Displ. Rate (mm/s)	Model Penetration Depth (mm)	Max. Reload stress (kN/m^2)	Max. -ve Pore (kPa) Pressure
YSH3	15.24	0.42	3.92	1044.25	3
YSH4	15.24	0.2333	4.67	941.35	4.42
YSH5	34.3	0.372	9.25	945.16	20.6
YSH6	0				0
YSH7	119.67	0.503	15.3	560.62	81.8
YSH8	17.31	0.276	4.48	709.89	16.175
YSH9	112.54	0.341	22.1	725.04	101.4

Leg 2

Test Code	Pull-out Strength (kN/m^2)	Pull-out Displ. Rate (mm/s)	Model Penetration Depth (mm)	Max. Reload stress (kN/m^2)	Max. -ve Pore (kPa) Pressure
YSH3	7.62	0.3111	4.3	1074.74	7.83
YSH4	3.81	0.2283	4.89	827.02	3.08
YSH5	34.3	0.351	9.05	884.18	9.34
YSH6	0				0
YSH7	92.23	0.558	15.1	524.79	88.7
YSH8	28.14	0.235	7.05	720.72	30
YSH9	125.53	0.3665	21.99	731.54	100.9

Leg 3

Test Code	Pull-out Strength (kN/m^2)	Pull-out Displ. Rate (mm/s)	Model Penetration Depth (mm)	Max. Reload stress (kN/m^2)	Max. -ve Pore (kPa) Pressure
YSH3	7.62	0.4	4.17	960.41	4.81
YSH4	19.06	0.2283	5.22	918.48	8.55
YSH5	38.11	0.316	8.51	895.62	26.5
YSH6	0				0
YSH7	83.46	0.527	16.3	519.84	62.5
YSH8	45.45	0.249	7.35	753.18	60.2
YSH9	123.37	0.318	21.69	748.85	69.4

Table 4.2 Summary of the Pull-out results for Tests YSH3-9

Leg 1

Test Code	Event No.	No. of cycles	Model freq, Hz	Integral of area ∫(PA-PB)dt per cycle	Estimated Settlement (mm)	Experimental Settlement (mm)	% of error
YSH8	19	50	0.568	4.106	0.772	0.9	14
YSH9	19	50	0.568	6.175	0.570	0.575	0.87
YSH8	12	3	0.0284	15.845	0.1787	0.1375	20
YSH9	12	3	0.0284	16.953	0.0738	0.08	7.7

Leg 2

Test Code	Event No.	No. of cycles	Model freq, Hz	Integral of area ∫(PA-PB)dt per cycle	Estimated Settlement (mm)	Experimental Settlement (mm)	% of error
YSH8	19	50	0.568	4.91	0.923	1	7.7
YSH9	19	50	0.568	8.504	0.615	0.625	1.6
YSH8	12	3	0.0284	15.13	0.163	0.12	35.8
YSH9	12	3	0.0284	24.405	0.106	0.1	6

Table 4.3 Estimation of Permanent vertical deformation using Pore Pressure data at positions A and B

Test	Test YSH8			Test YSH9		
Legs	1	2	3	1	2	3
Elasto-plastic vertical stiffness (Kep), MN/mm	0.51	0.48	0.57	0.47	0.45	0.52
Plastic vertical stiffness (Kp), MN/mm	0.10	0.10	0.10	0.095	0.097	0.11
Vertical Load at preload, MN	9.16	9.08	9.11	8.26	9.48	9.55
Kep/Kp	5.08	4.60	5.56	4.92	4.63	4.76

Table 5.1 Comparison of Prototype Vertical Elasto-plastic and Plastic Stiffness

Leg No.	Max. Tension Force (MN) for Pull-out Event		Ratio of tension Forces (YSH9/YSH8)
	Test YSH8	Test YSH9	
1	0.283	2.046	7.23
2	0.316	2.154	6.81
3	0.783	2.147	2.74
Average	0.461	2.116	4.59

Table 5.2 Comparison of Prototype Suction Forces

	Skirted Spud (YSH9)			Non-skirted Spud (YSH8)		
PPT	Estimated P. press.(kPa)	Leg 3 Experi	% of error	Estimated P. press.(kPa)	Leg 3 Experi	% of error
A	-50	-47.4	5.5	-35.05	-33.2	5.6
B	-13	-14.6	11	-5.5	-7.4	25.7
C	15	14.2	5.6	14.5	18.36	21
D	14	14.3	2.1	25.5	39.03	34.8

Table 5.3 Comparison of the Estimated Pore suction via simple seepage analysis and the Leg3 Experimental pore pressure data

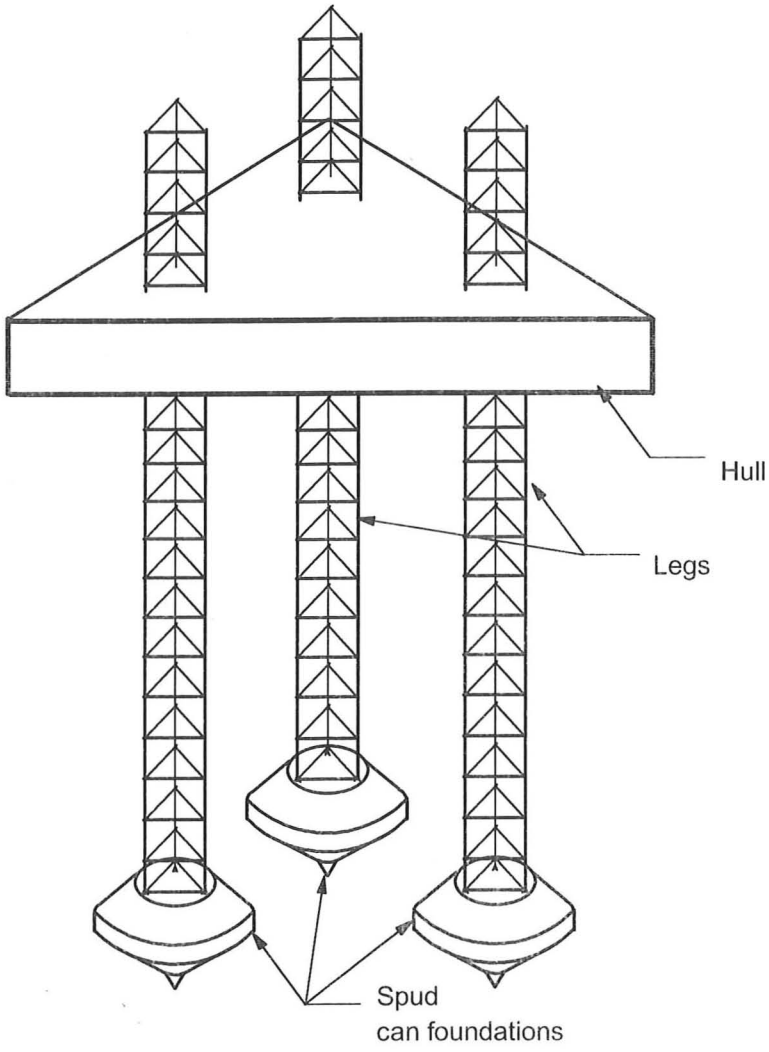

Fig. 1.1 Three-leg jack up installation

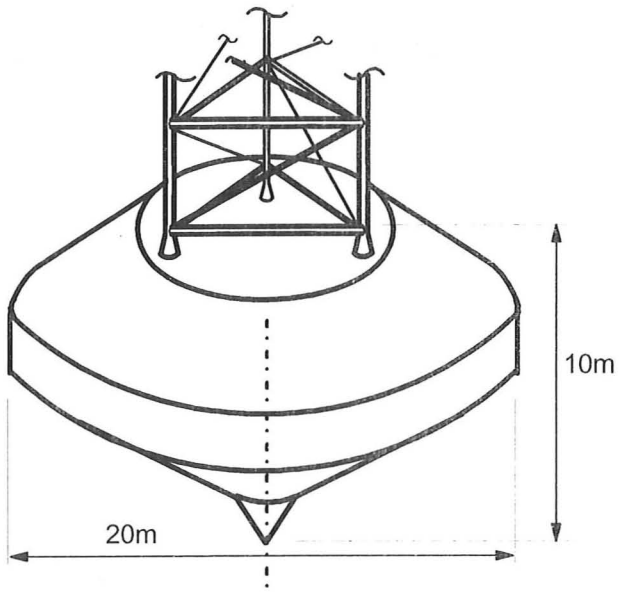

Fig. 1.2 Typical large conical spud can foundation

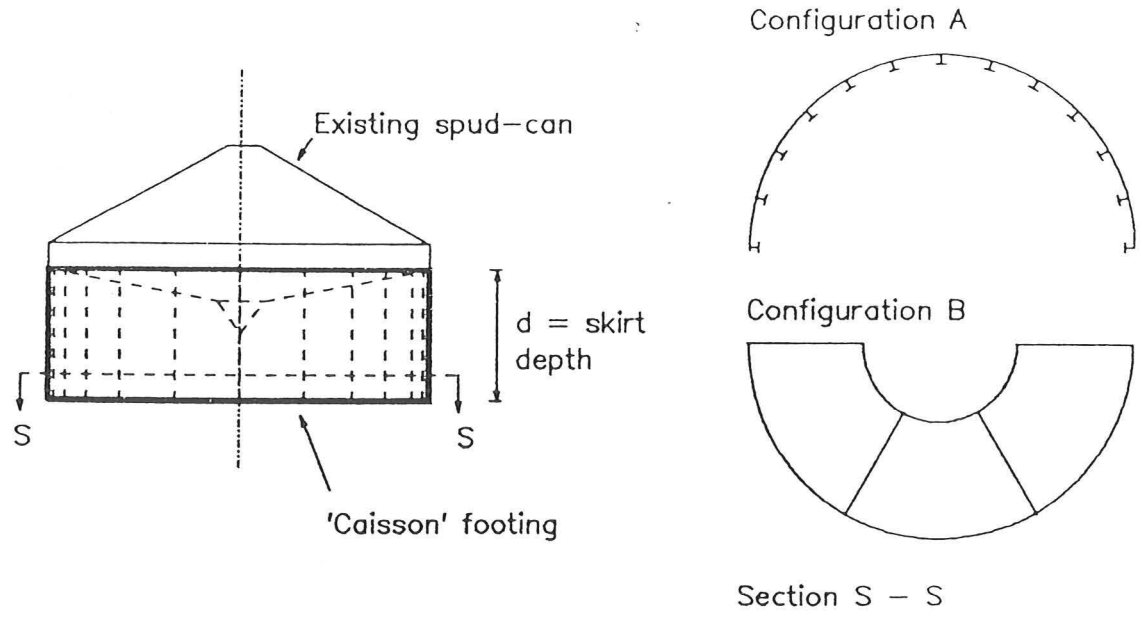

A) Skirt cylinder added to an existing spud–can

B) Possible configurations of skirt stiffeners

Fig. 1.3 Skirted conical spud can foundation
(Extracted from Geir Svanϕ, 1993)

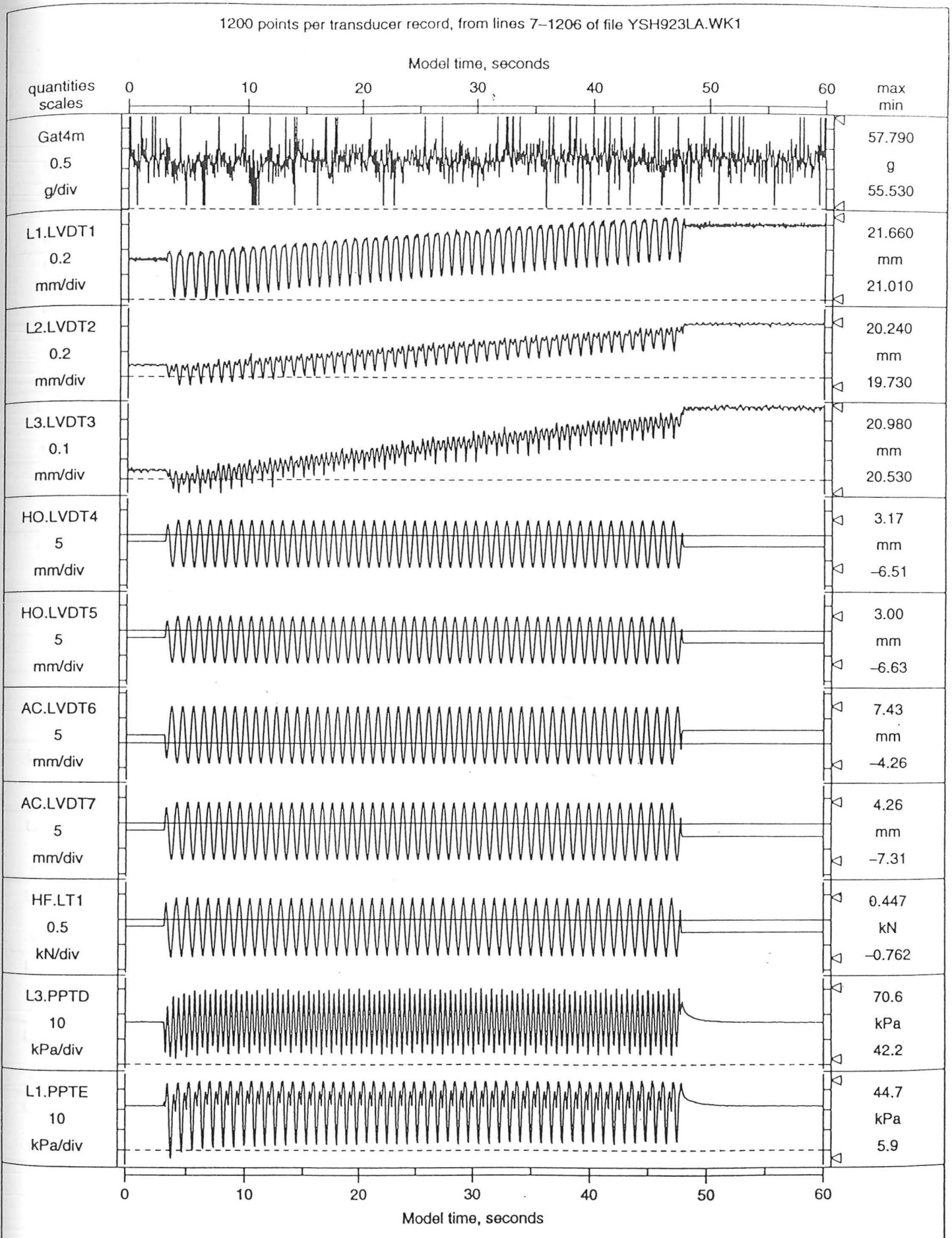

Time on this plot is synchronised with time on the corresponding Labtech B plot in Fig.9.23.LB

TEST YSH9 EVENT 23 G=61g	Skirted flat spuds Dense LB100/170 sand 200cS Silicone Oil	TIME RECORDS – LABTECH A FAST HORIZONTAL LOADING 50 cycles, ± 4.83mm at 1.12Hz	FIG NO. 1.4a

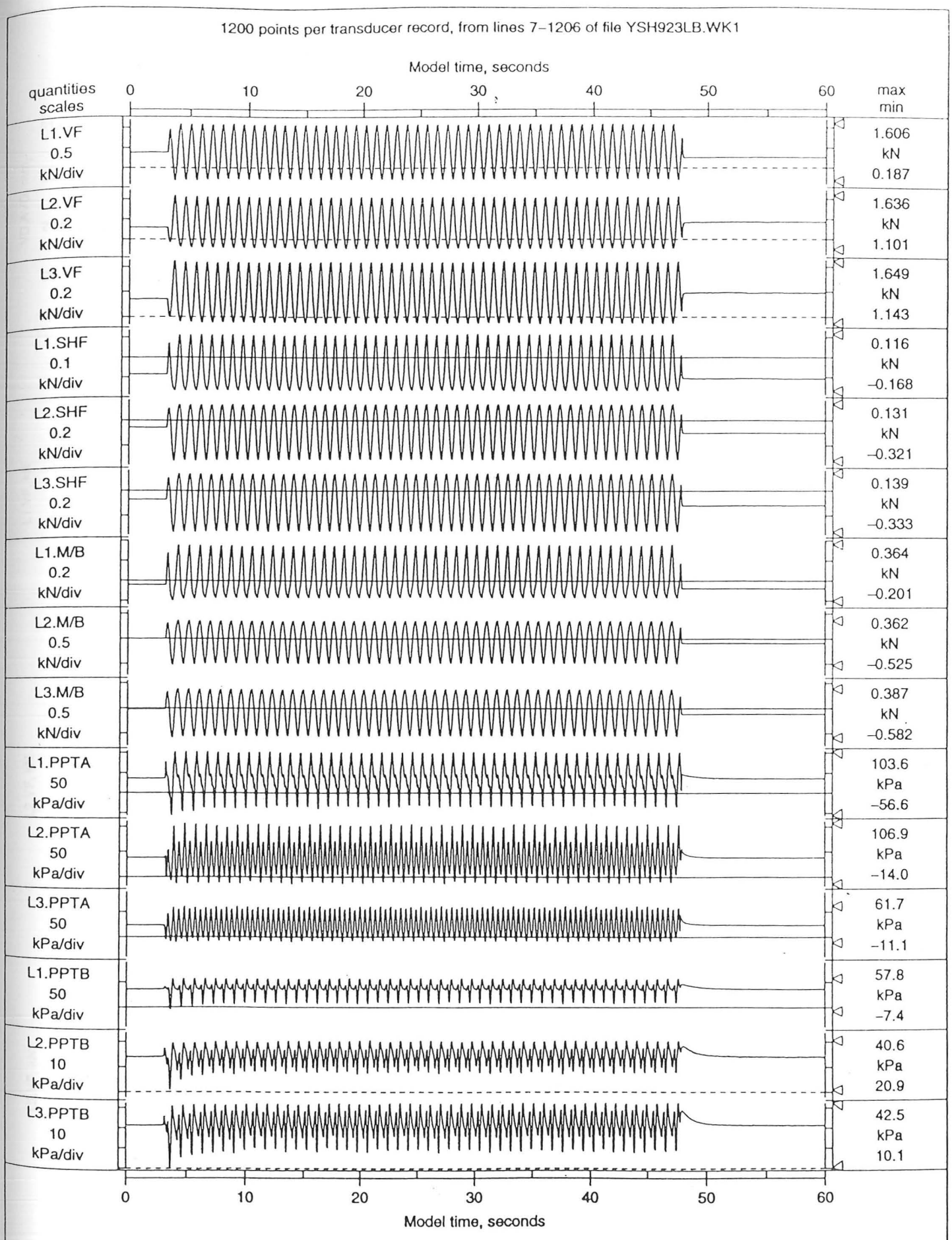

Time on this plot is synchronised with time on the corresponding Labtech A plot in Fig.9.23.LA

TEST YSH9 EVENT 23 G=61g	Skirted flat spuds Dense LB100/170 sand 200cS Silicone Oil	TIME RECORDS – LABTECH B FAST HORIZONTAL LOADING 50 cycles, ± 4.83mm at 1.12Hz	FIG.NO. 1.4b

Data from lines 7–1206 of files YSH923LA.WK1 and YSH923LB.WK1

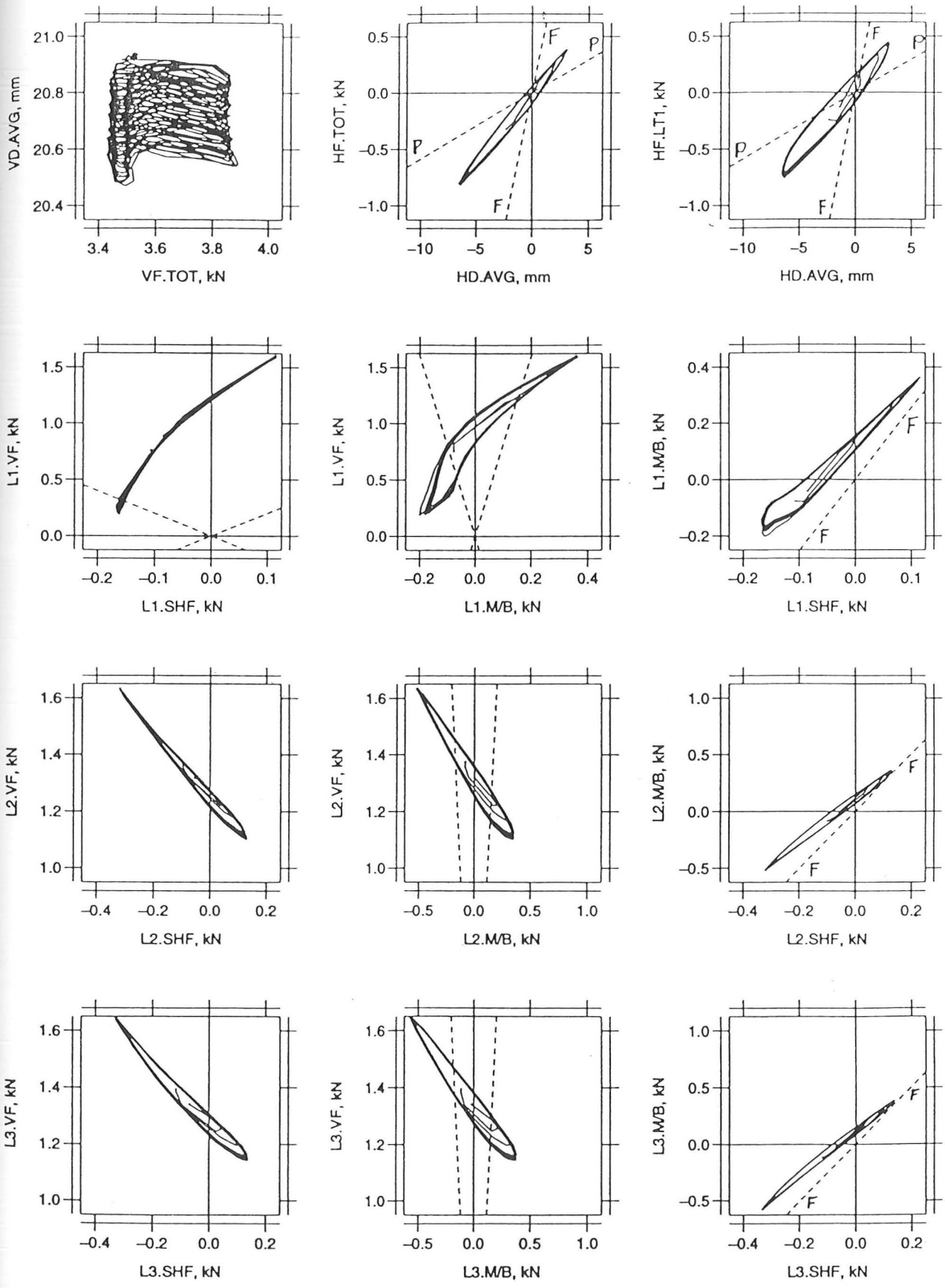

TEST YSH9 EVENT 23 G=61g	Skirted flat spuds Dense LB100/170 sand 200cS Silicone Oil	DISPS AND LOADS (LABTECH) FAST HORIZONTAL LOADING 50 cycles, ± 4.83mm at 1.12Hz	FIG.NO. 1.4c

Data from lines 7–1206 of file YSH923LB.WK1

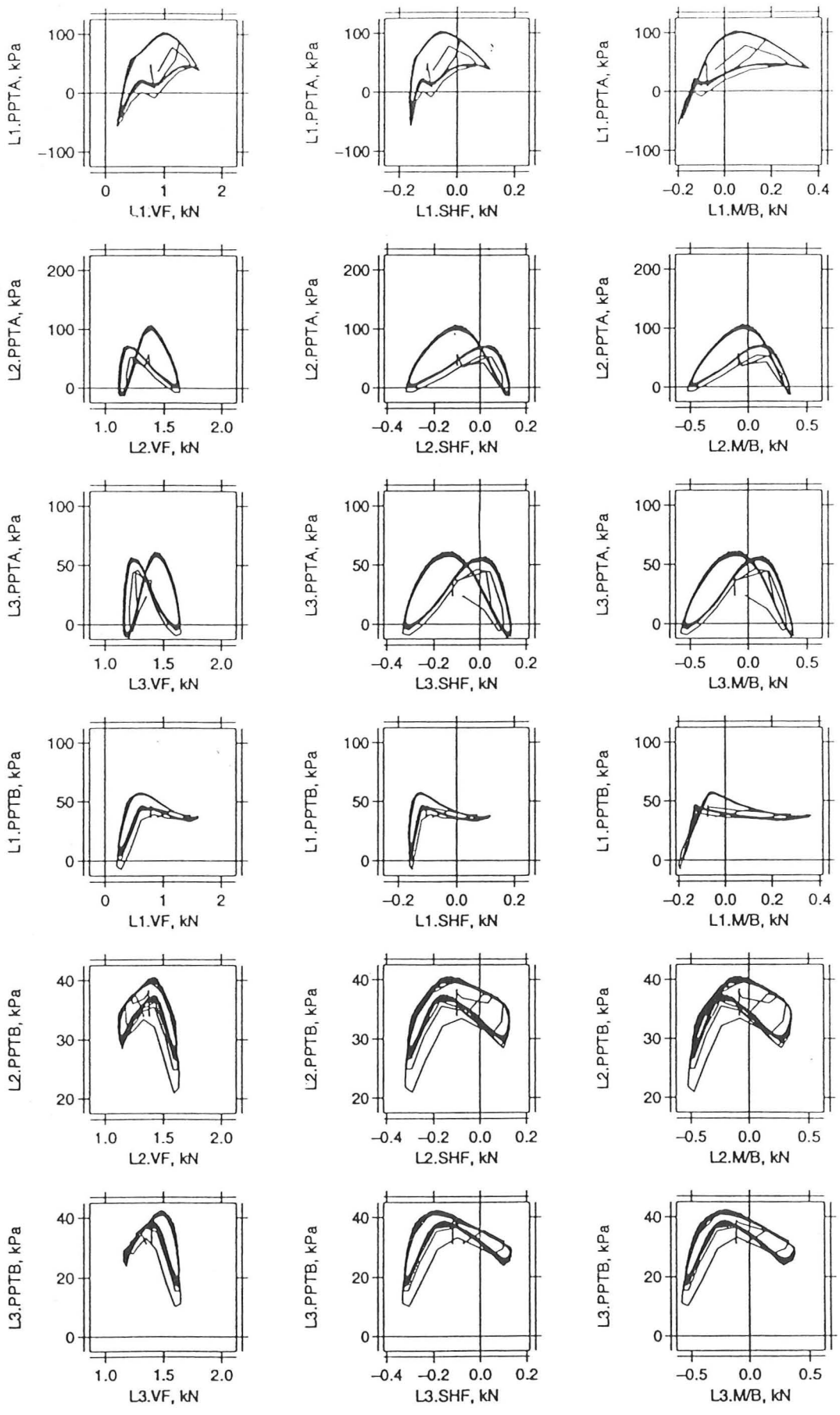

TEST YSH9 EVENT 23 G=61g	Skirted flat spuds Dense LB100/170 sand 200cS Silicone Oil	PORE PRESSURES (LABTECH) FAST HORIZONTAL LOADING 50 cycles, ± 4.83mm at 1.12Hz	FIG.NO. 1.4d

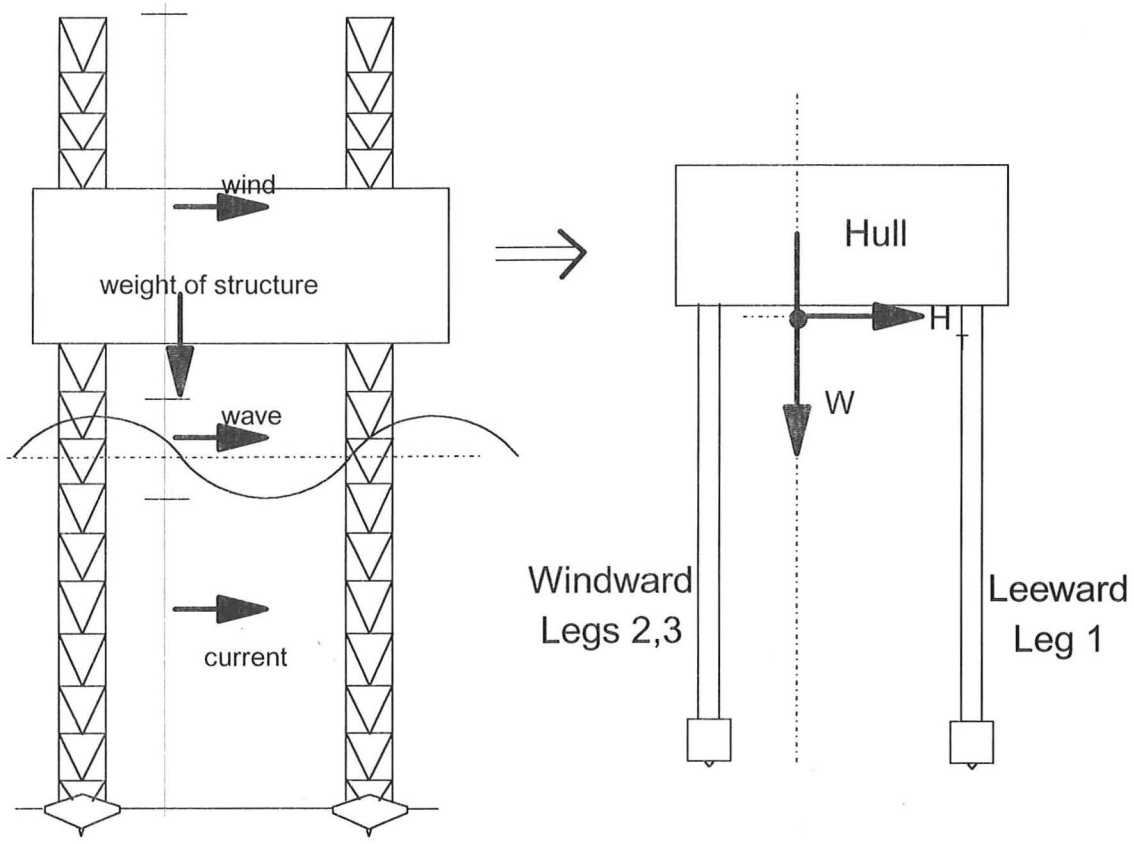

Fig. 1.5 Environmental Forces on structure and its equivalent for Modelling

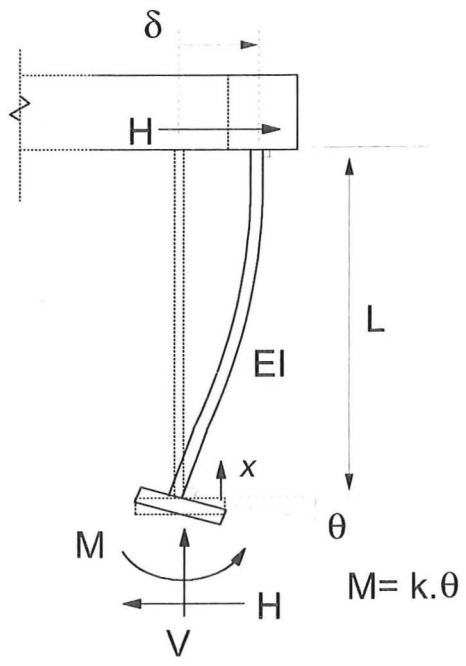

$$M(x) = M - H.x = EI.\frac{d^2\delta}{dx^2}$$

where M is moment at foundation. Integrating,

$$EI.\frac{d\delta}{dx} = M.x - \frac{Hx^2}{2} + \text{const.}$$

when $\frac{d\delta}{dx} = \theta$ at x=0,

$$\text{const.} = EI.\theta$$

when $\frac{d\delta}{dx} = 0$ at x=L,

$$0 = k\theta L - \frac{HL^2}{2} + EI.\theta$$

$$\theta = \frac{HL^2}{2(kL + EI)}$$ (same as equation 1.2)

Fig. 1.6 Single leg subjected to horizontal force at top of leg

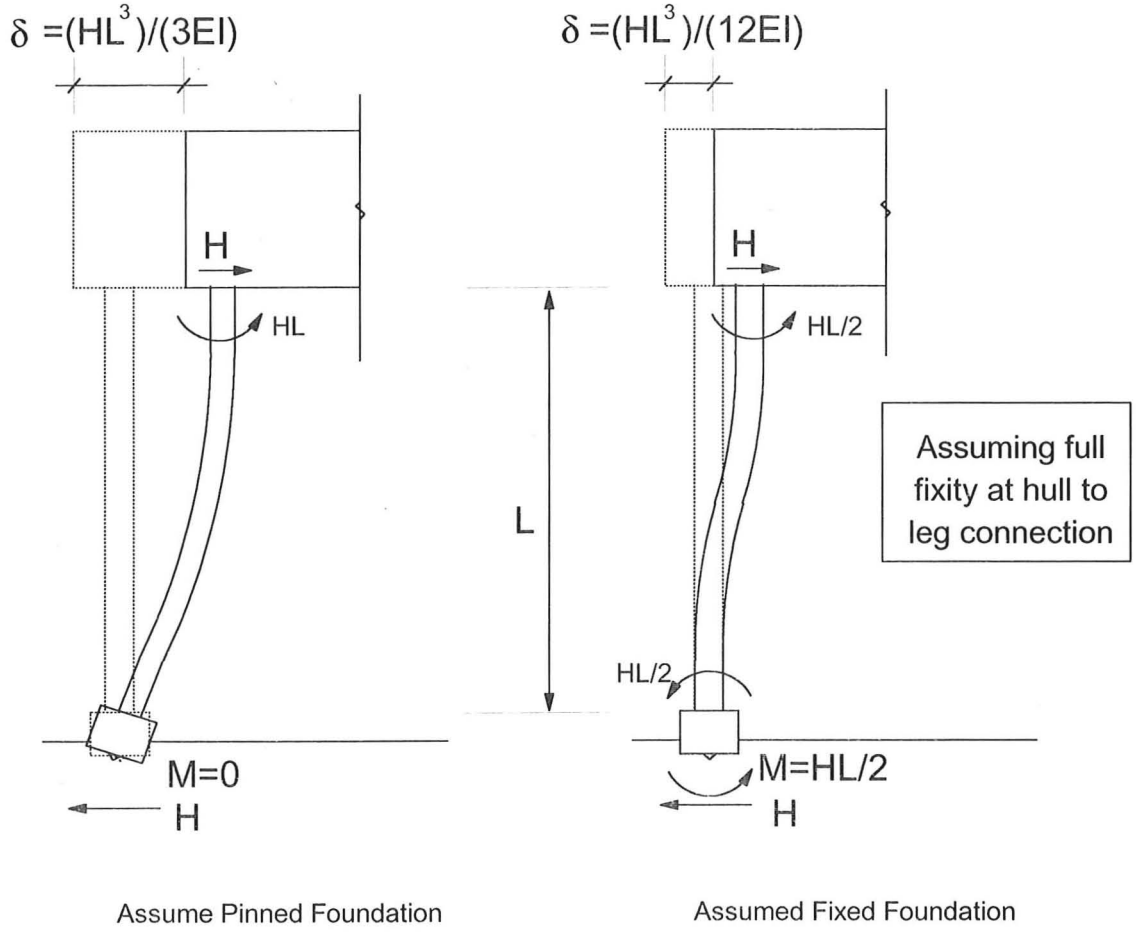

Fig. 1.7 Pinned and Fixed or Encastre Foundation

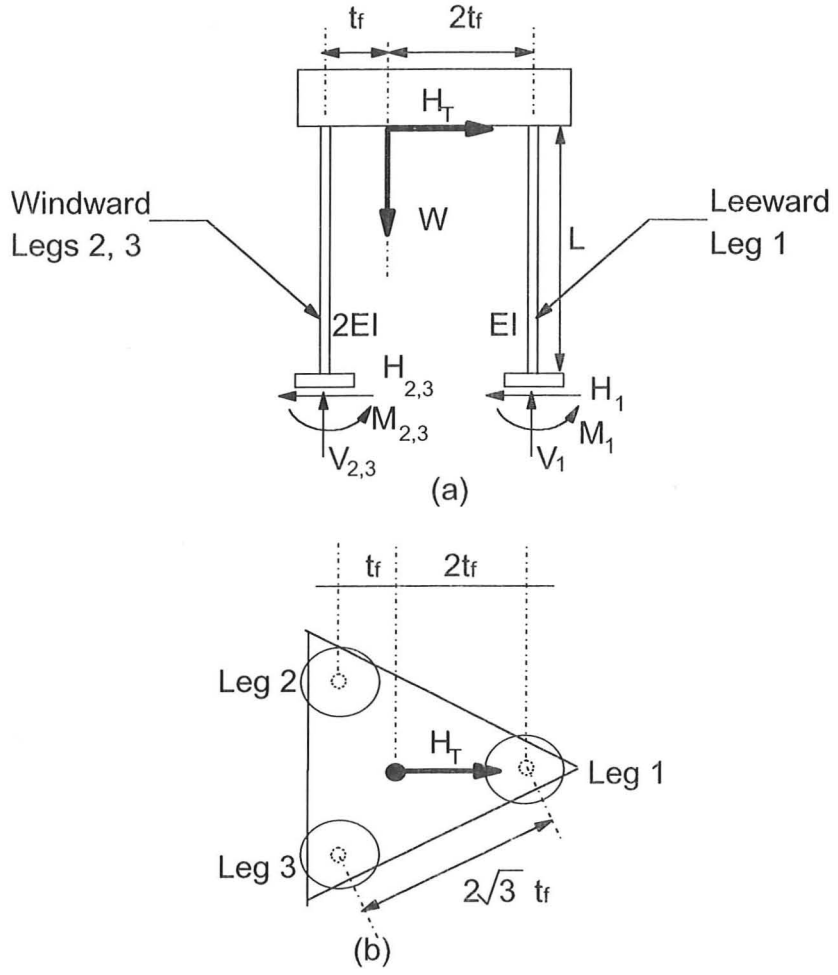

$$V_1 = \frac{W.(t + \delta - M_2/V_2) + H_T.L}{3t + (M_1/V_1 - M_2/V_2)} \qquad \text{Equation (1.5)}$$

$$2V_2 = \frac{W.(2t - \delta + M_1/V_1) - H_T.L}{3t + (M_1/V_1 - M_2/V_2)} \qquad \text{Equation (1.6)}$$

$W = V_1 + V_2 + V_3 = V_1 + 2V_2$, assume $V_1 = V_2 = W/3$, $H_1 = H_2 = H_T/3$, $\delta \approx 0$.

Pinned Conditions

$M_1 = M_2 = 0$,

$$V_1 = \frac{W.(t + \overcancel{\delta}^{0} - \overcancel{M_2}^{0}/V_2) + H_T.L}{3t + (\overcancel{M_1/V_1}^{0} - \overcancel{M_2/V_2}^{0})}$$

$$2V_2 = \frac{W.(2t - \overcancel{\delta}^{0} + \overcancel{M_1}^{0}/V_1) - H_T.L}{3t + (\overcancel{M_1/V_1}^{0} - \overcancel{M_2/V_2}^{0})}$$

Fixed Conditions

$M_1 / V_1 = H_1.L/(2V_1) = H_T/3.L/(2.W/3) = M_2/V_2$

$$V_1 = \frac{W.(t + \overcancel{\delta}^{0} - M_2/V_2) + H_T.L}{3t + (\overcancel{M_1/V_1 - M_2/V_2}^{0})}$$

$$2V_2 = \frac{W.(2t - \overcancel{\delta}^{0} + M_1/V_1) - H_T.L}{3t + (\overcancel{M_1/V_1 - M_2/V_2}^{0})}$$

Fig. 1.8 Simplified three-leg jack up

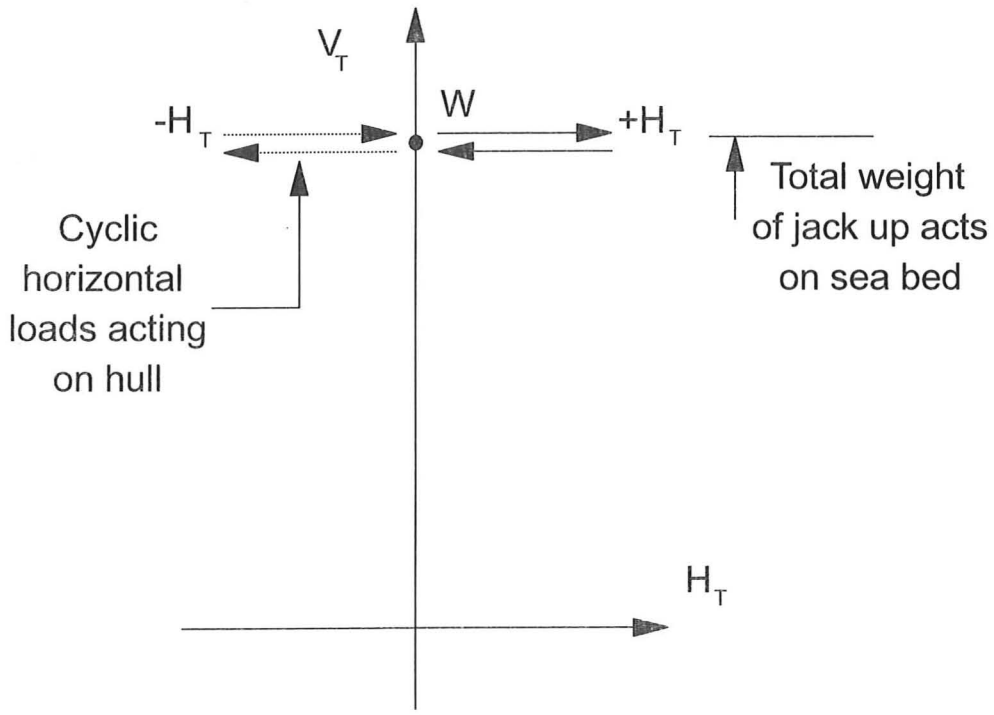

(a)

$$|\Delta V_{1max}| \approx 2. |\Delta V_{2,3min}|$$

$$|\Delta H_{1max}| \approx |\Delta H_{2,3min}| \approx H_T/3$$

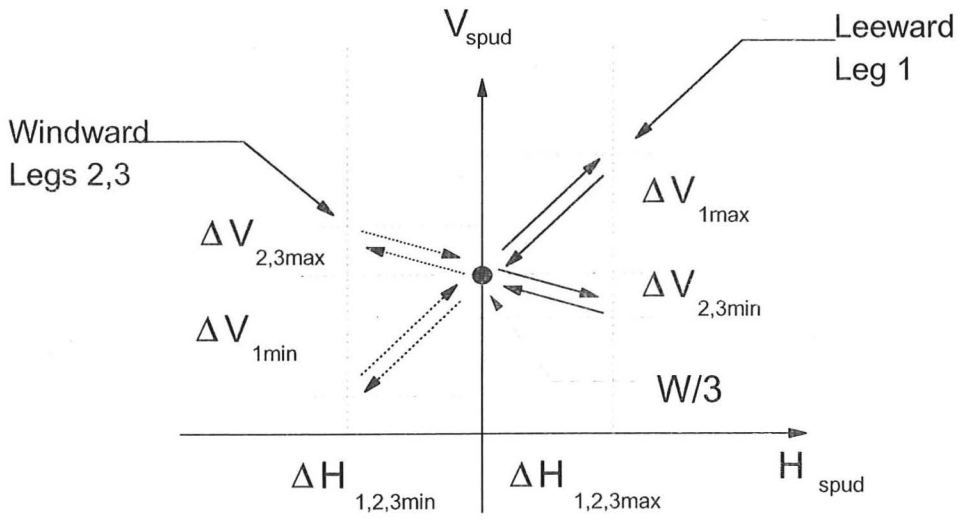

(b)

Fig. 1.9 Load paths of Structure and respective individual spud foundation

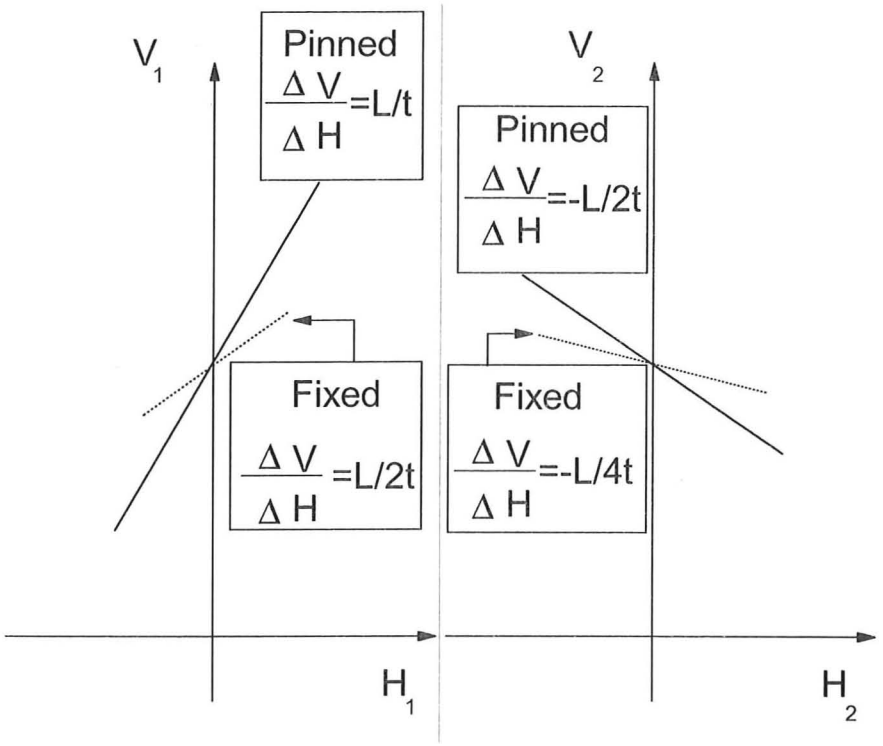

(a)

——	Pinned	$\delta = \frac{HL^3}{3EI}$	$M_1=M_2=M_3=0$
.....	Fixed	$\delta = \frac{HL^3}{12EI}$	$M_1=M_2=M_3=\frac{HL}{2}$

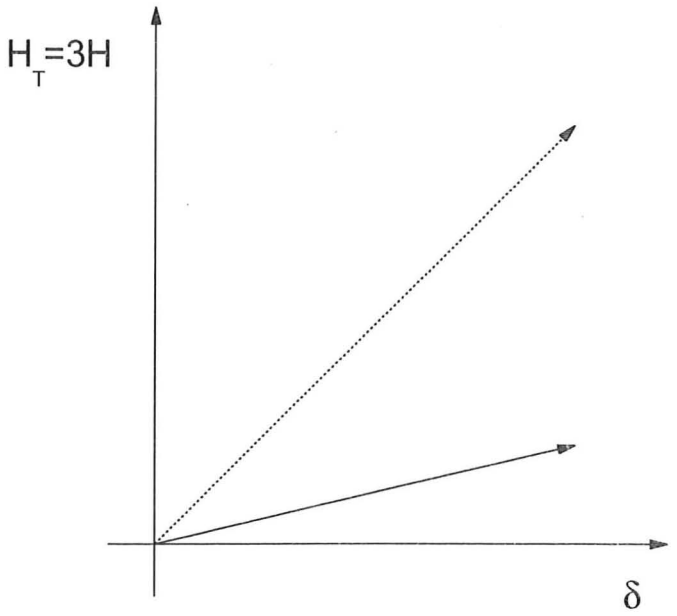

(b)

Fig. 1.10 Secant Load paths and Lateral Displacements vs. Force
(Extracted from Dean et. al, 1992)

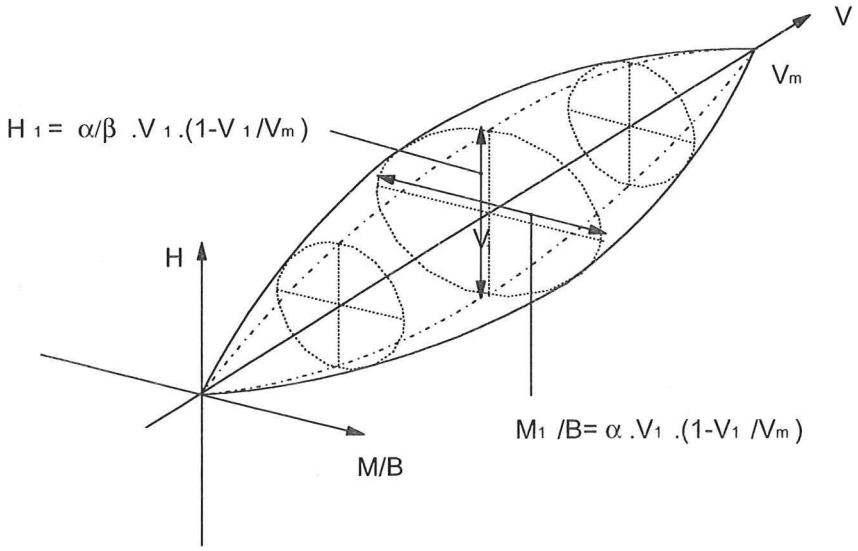

Fig. 1.11 Three dimensional yield locus developed by Osborne et al (1990) and Dean et al (1992)

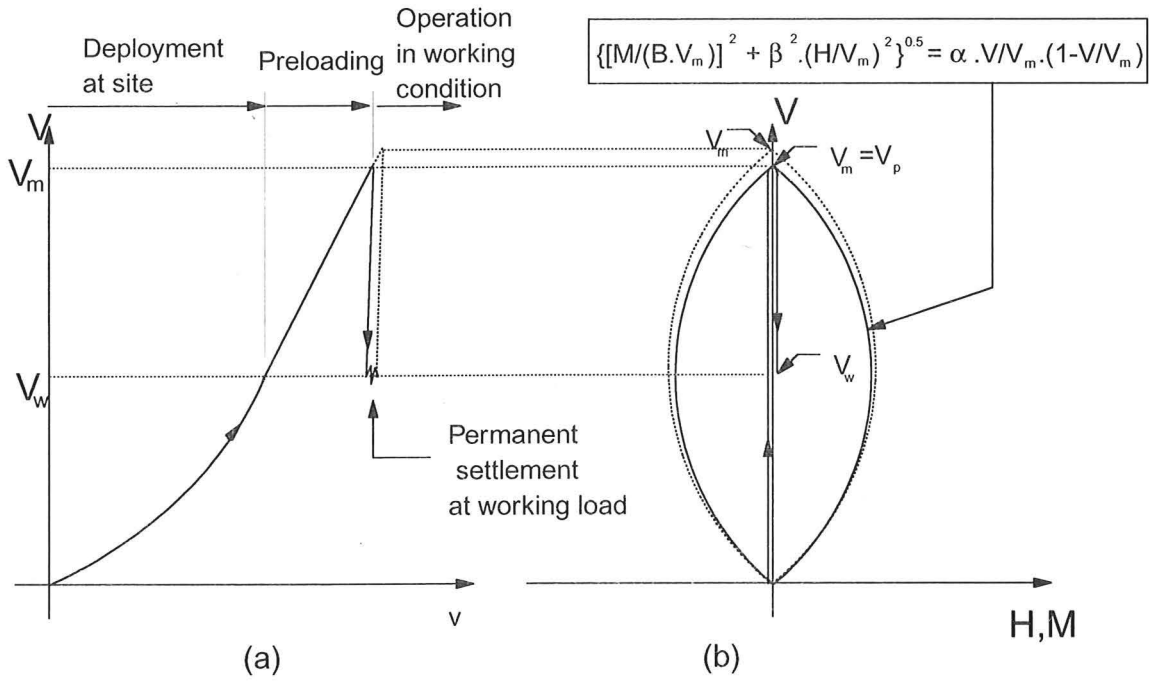

Fig. 1.12 Preloading and unloading operation

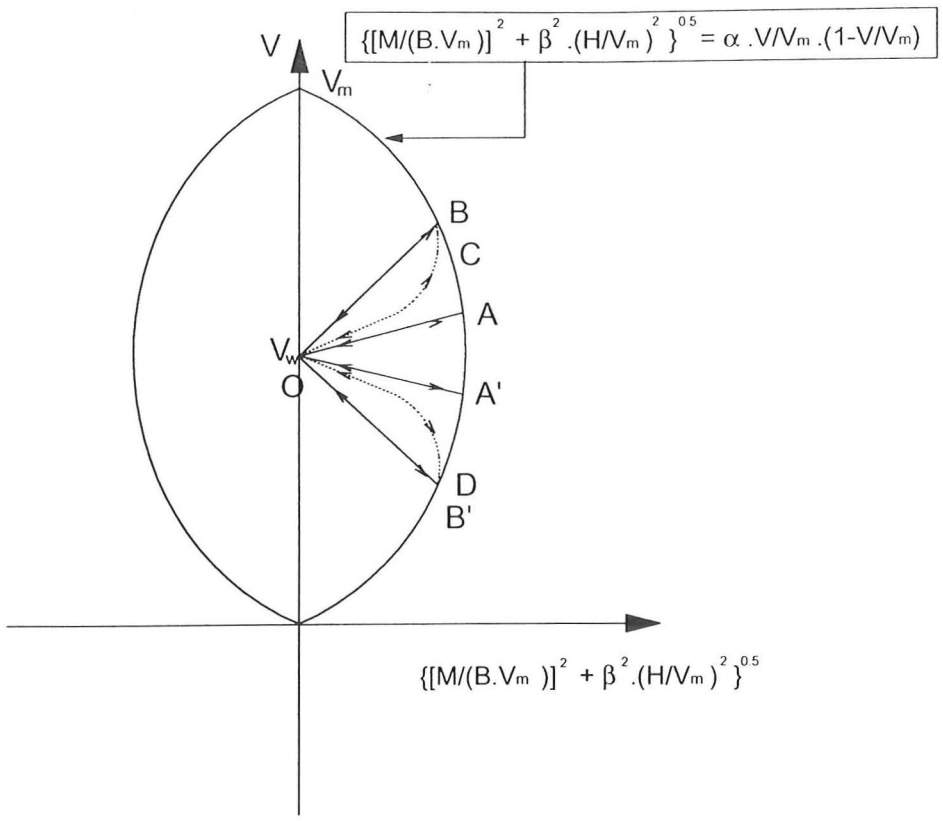

Fig. 1.13 Load paths within the yield limiting locus

Vertical displacements and excess pore pressures

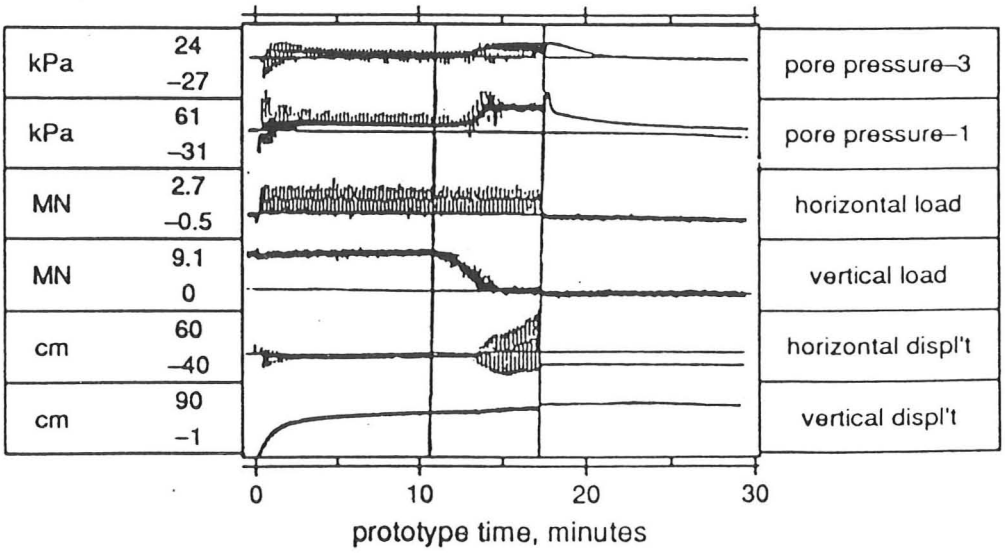

3.2m diameter footing on medium dense sand

Fig. 1.14 Liquefaction under spud can foundation
(extracted from Tan, 1990 and Dean et al., 1995)

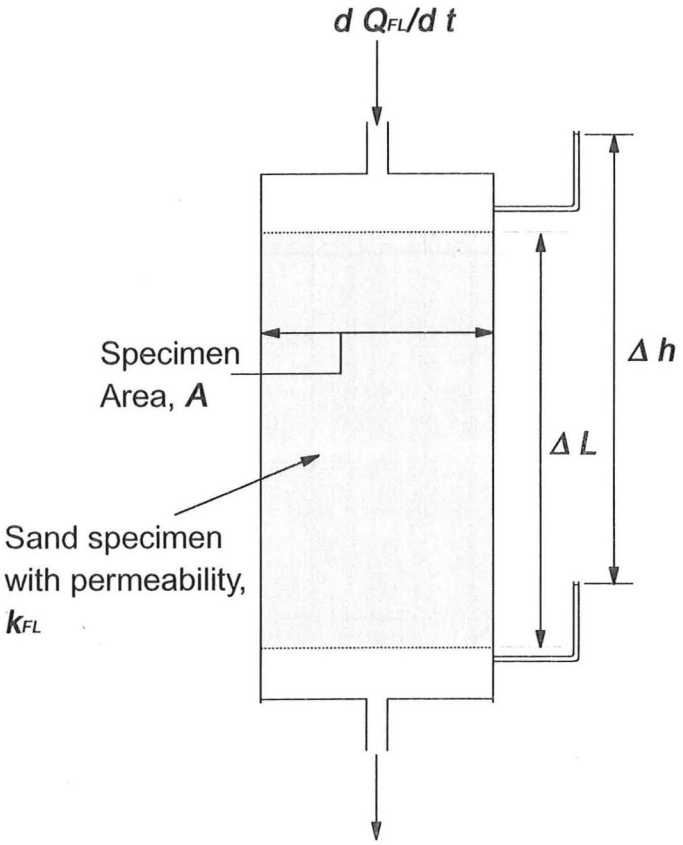

Fig. 2.1 Darcy's Experiment

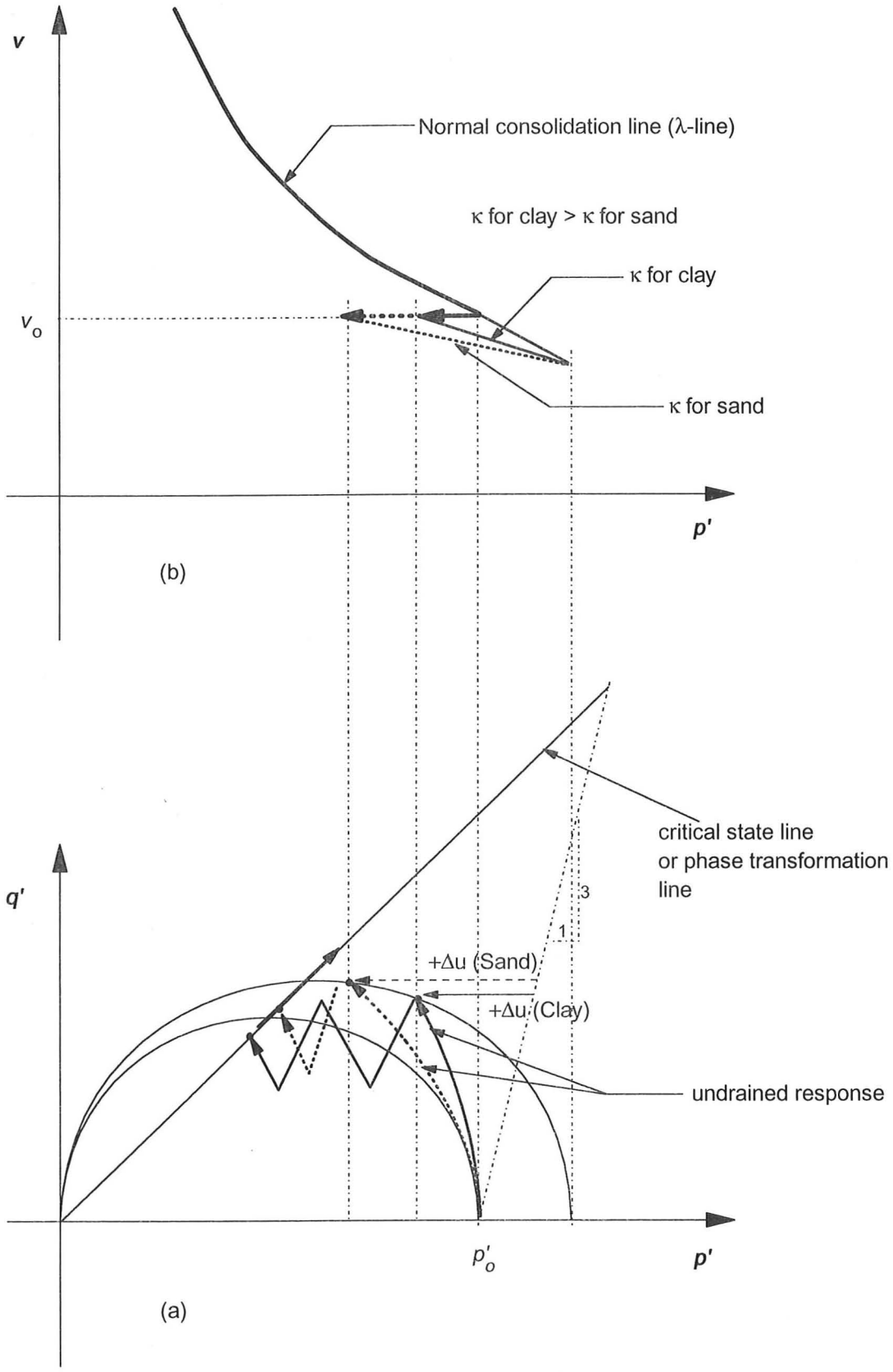

Fig. 2.2 Cyclic mobility

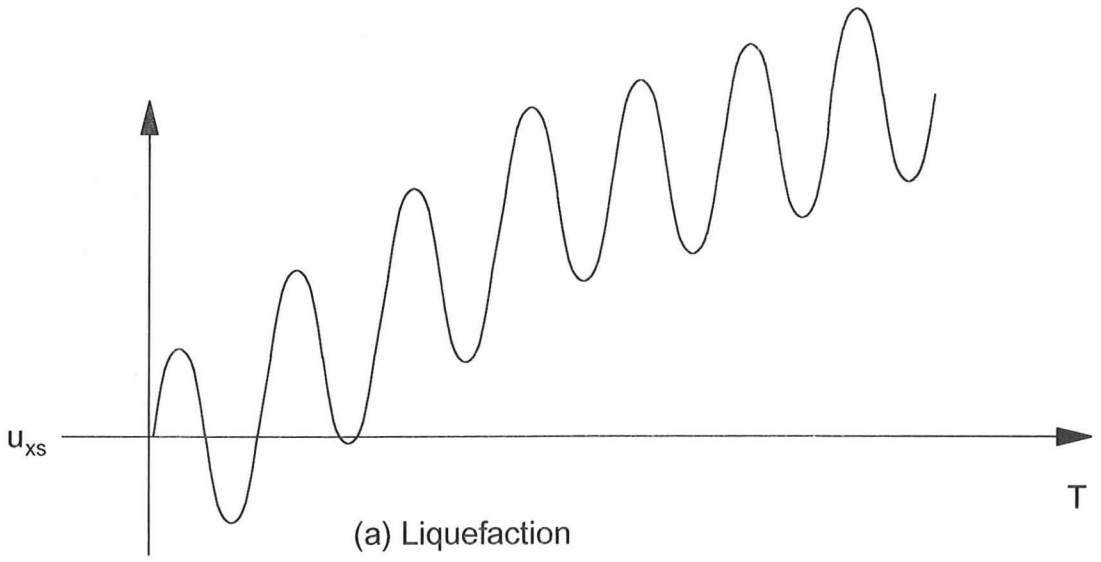

(a) Liquefaction

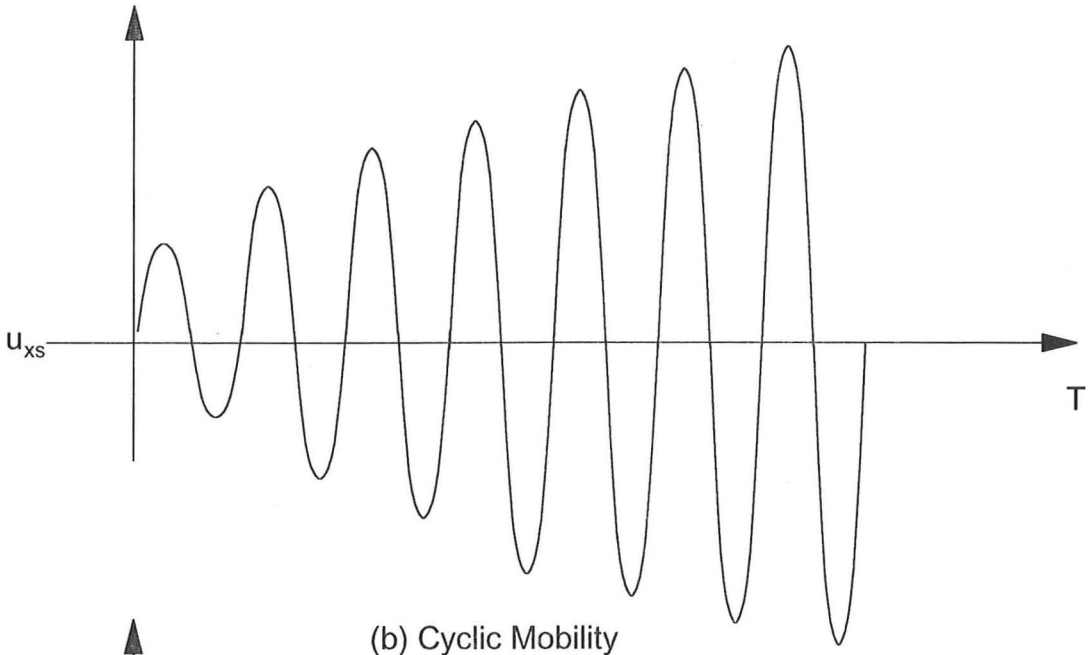

(b) Cyclic Mobility

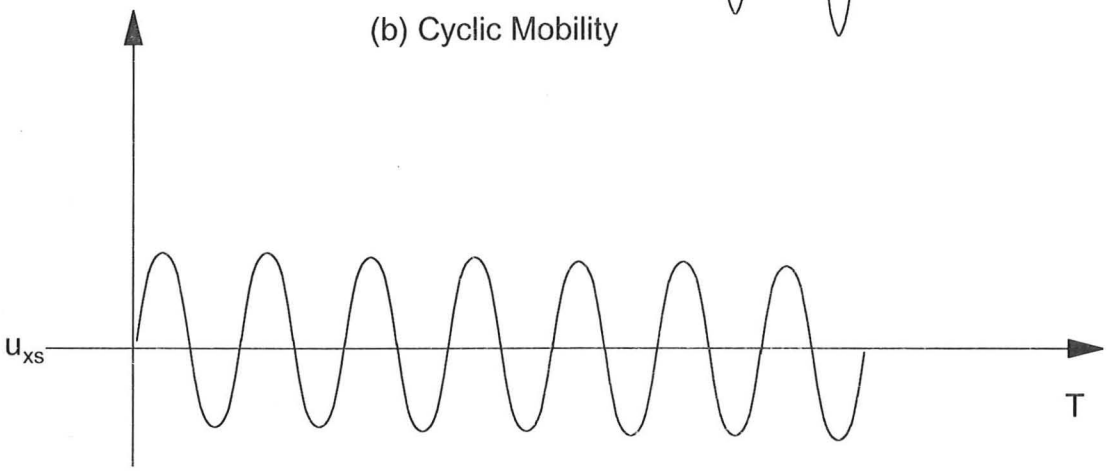

(c) partially drained cyclic loading

Fig. 2.3 Excess pore pressure due to cyclic loading

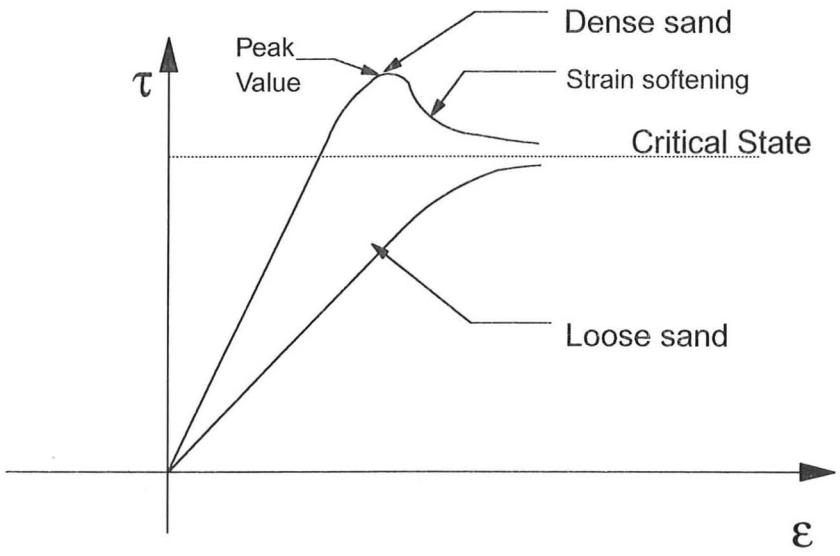

Fig. 2.4 Dense, Loose and Critical State Soils

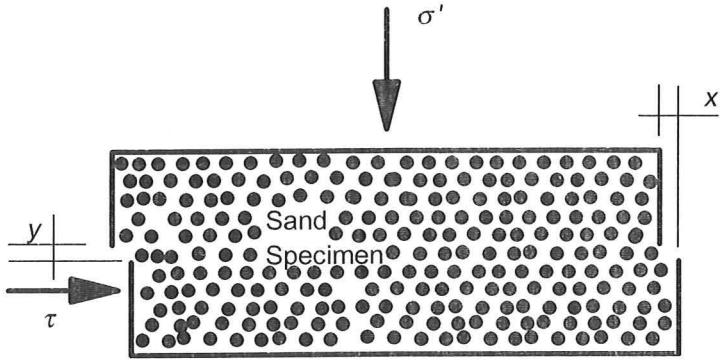

Fig. 2.5 Shearing of soil sample

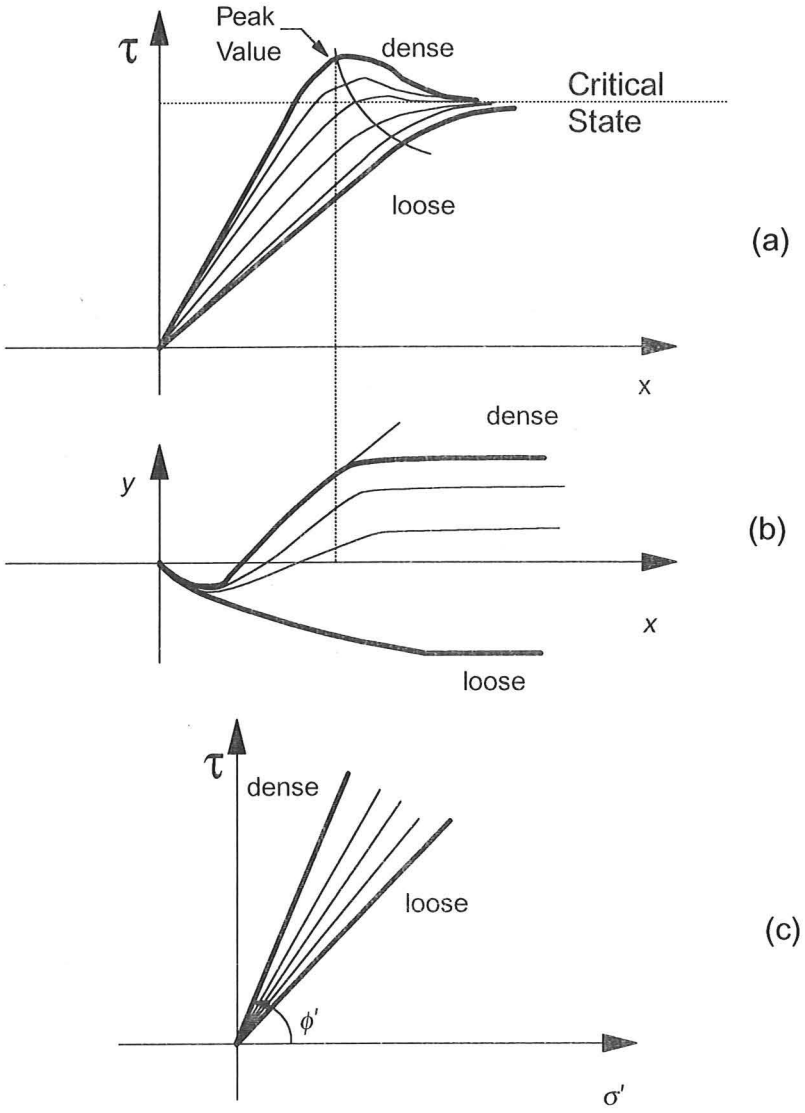

Fig. 2.6 Shearing of dense and loose soil sample

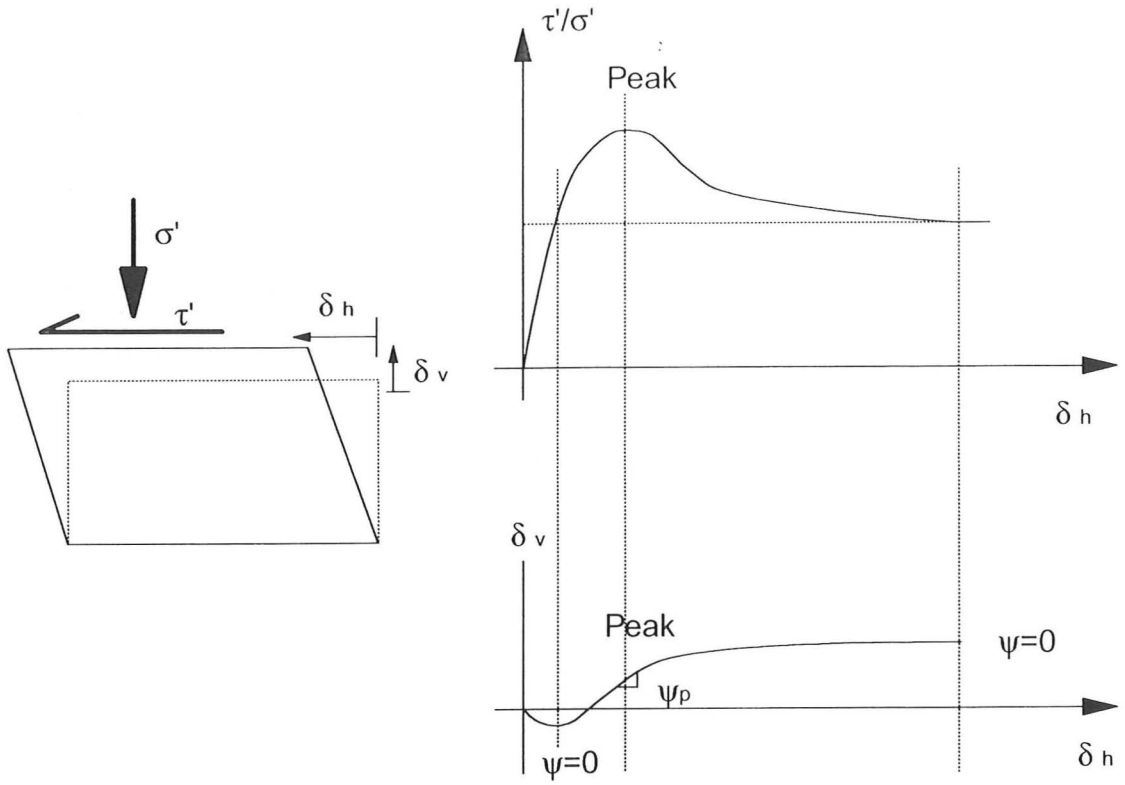

Fig. 2.7 Shearing of an overconslidated or dense soil sample

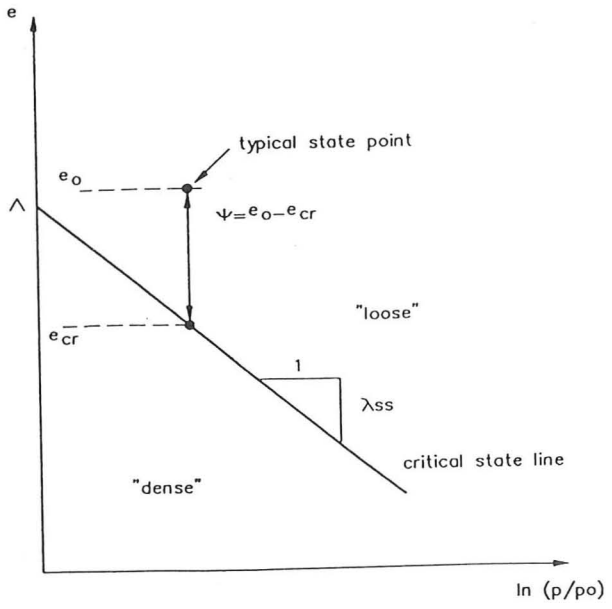

Fig. 2.8 Critical state line and state parameter (Been and Jefferies, 1985)

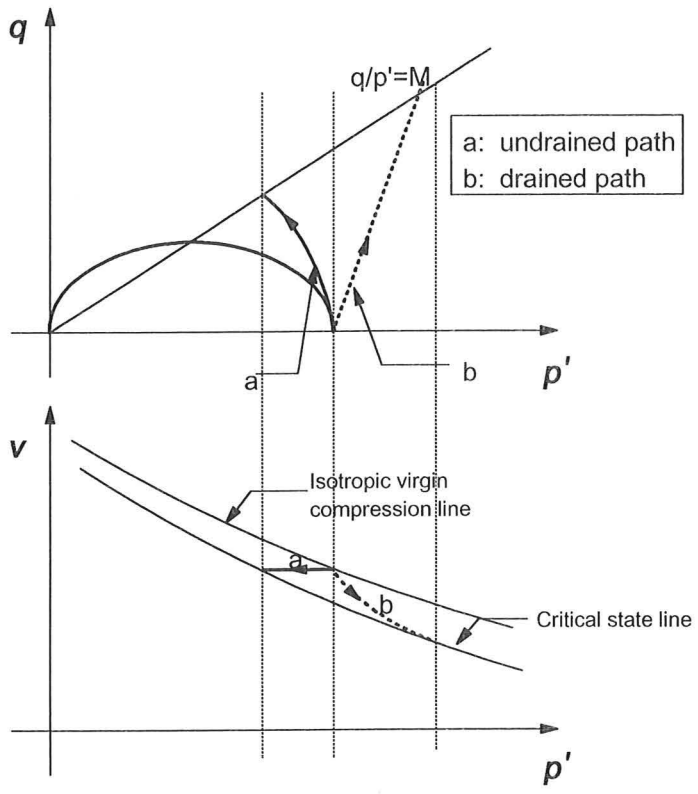

Fig. 2.9a Typical undrained and drained state paths

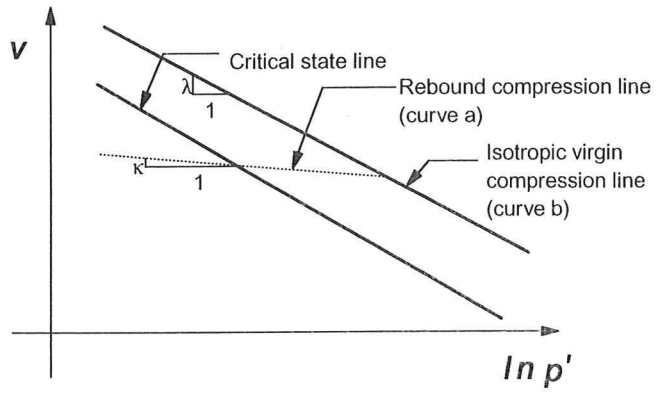

Fig. 2.9b Rebound and Isotropic compression lines

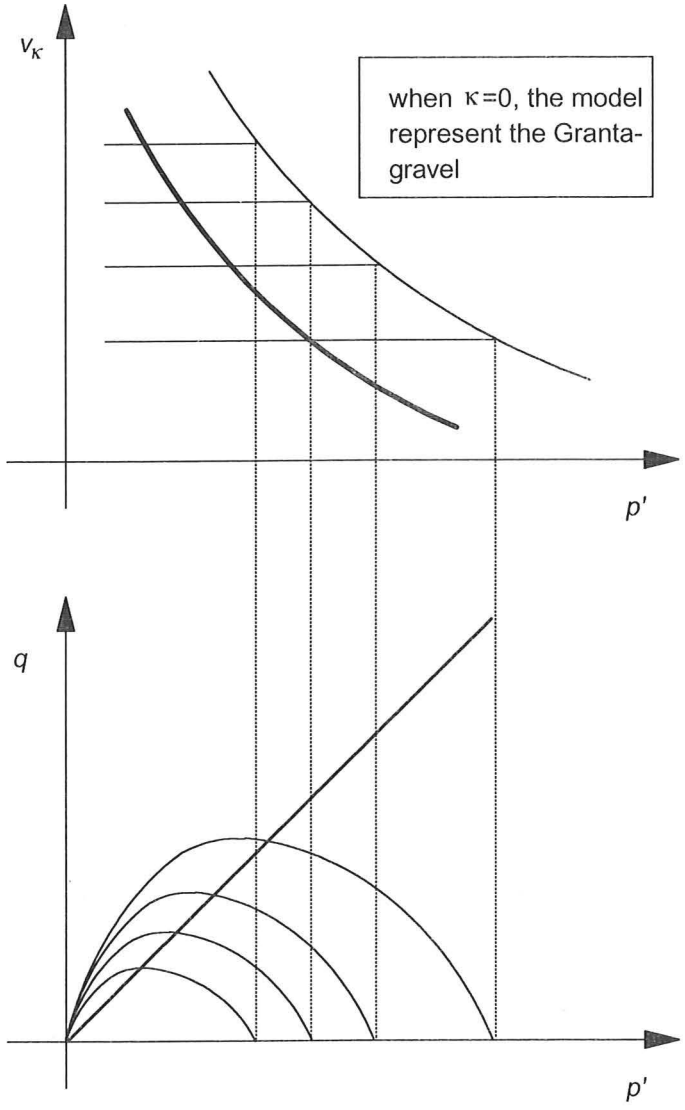

Fig. 2.10 Simplified rebound and isotropic lines

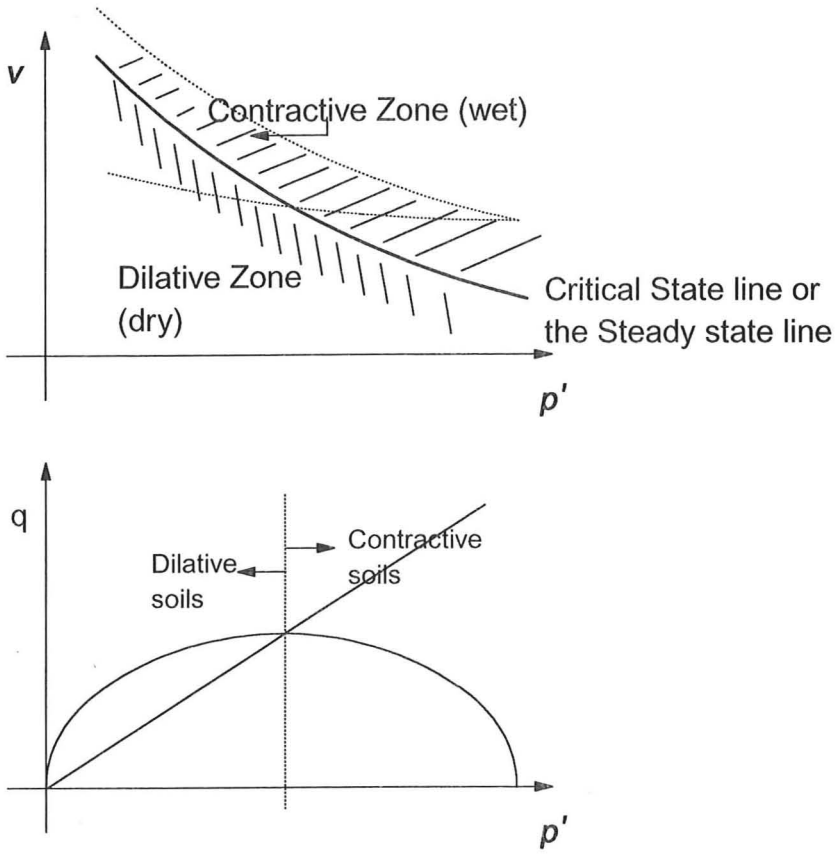

Fig. 2.11 Steady state line, approximate division between dilative and contractive soil (after Schofield and Wroth, 1968)

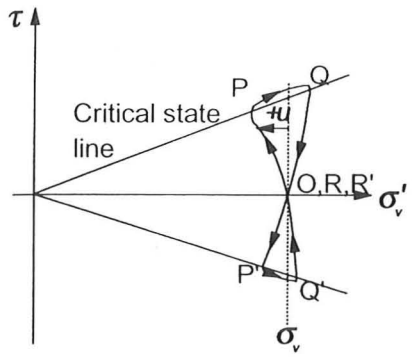

(a) Shear Stress vs effective stress plot

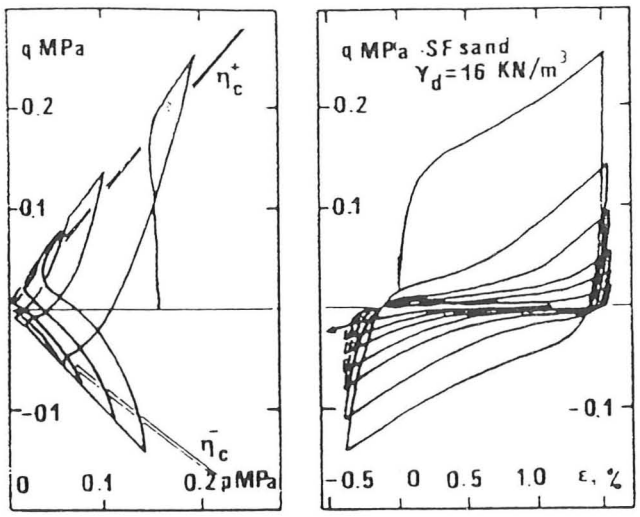

(b) Liquefaction of a dense sand under undrained shearing controlled by axial strains

Fig. 2.12 Shear stress vs. effective stress plot and laboratory liquefaction data (Extracted from Luong and Sidaner, 1981)

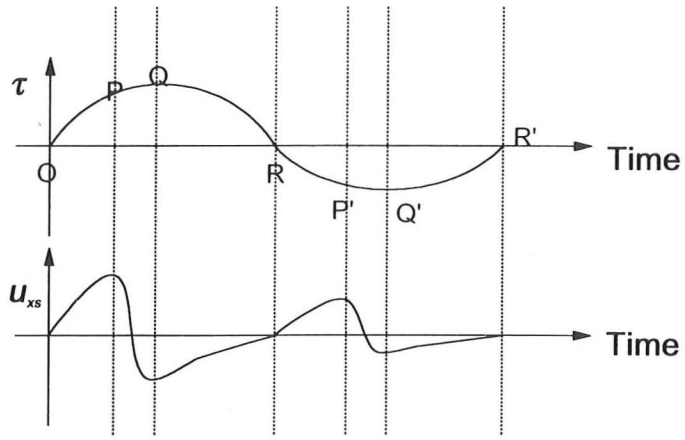

Fig. 2.13 Pore pressure and shear stress time plots

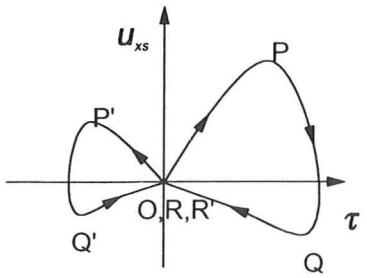

Fig. 2.14 Shear stress and pore pressure cross plot

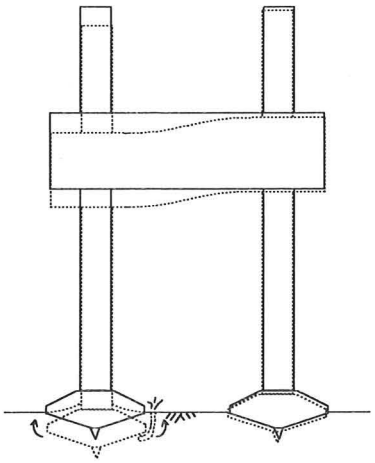

(a) Failure by liquefaction

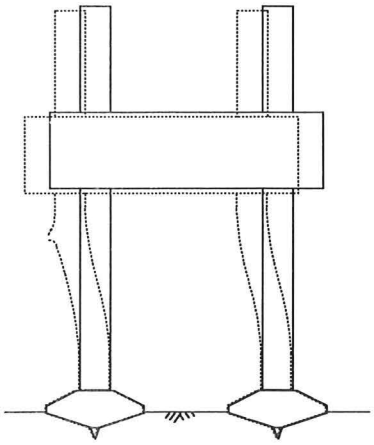

(b) Failure of structure

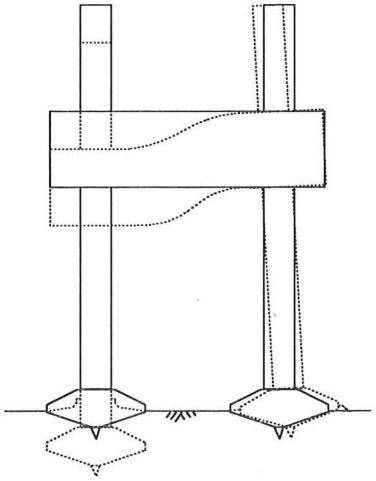

(c) Failure by punchthrough

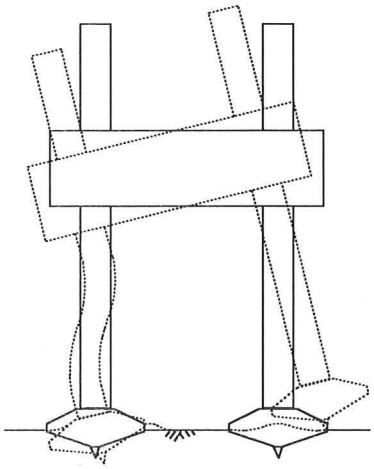

(d) Failure by overturning

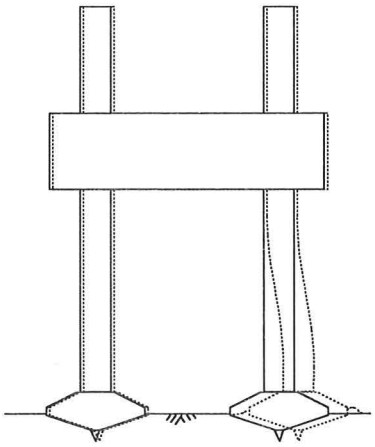

(e) Failure by partial sliding

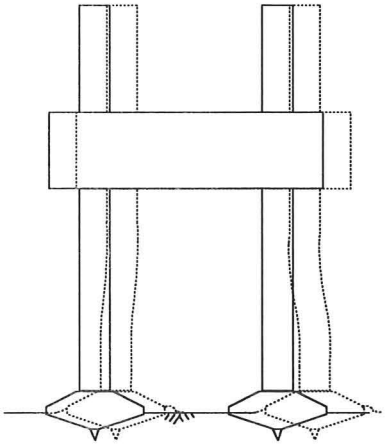

(f) Failure by full sliding

Fig. 2.15 Modes of failure

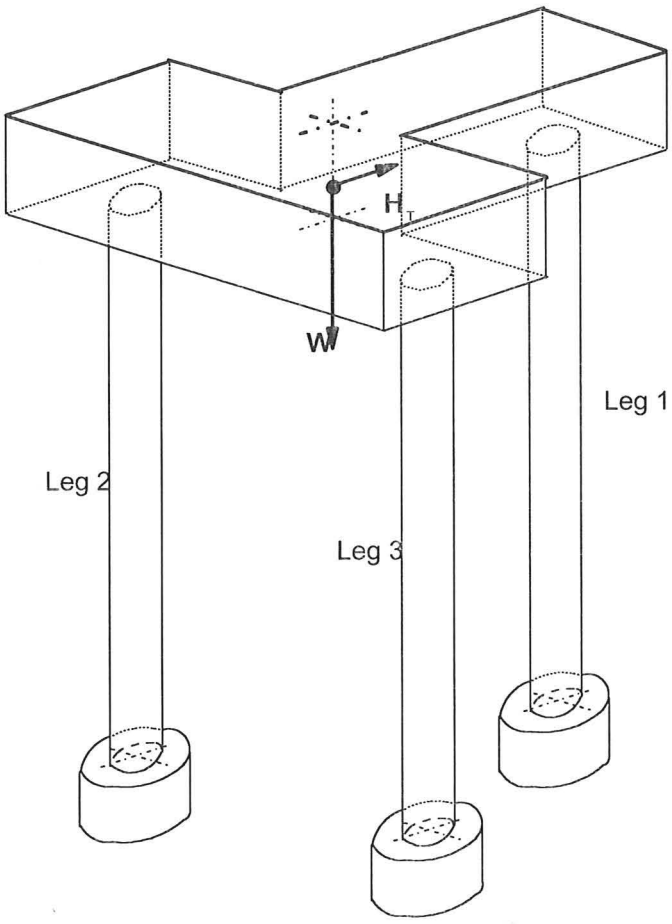

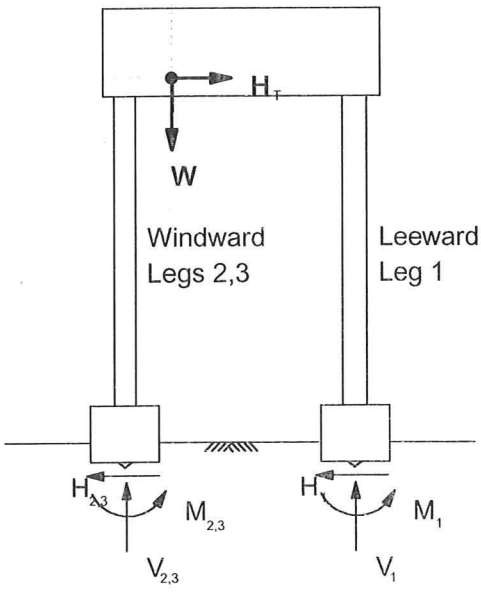

Fig. 2.16 Load application on three leg model and sign conventions of load and reactions

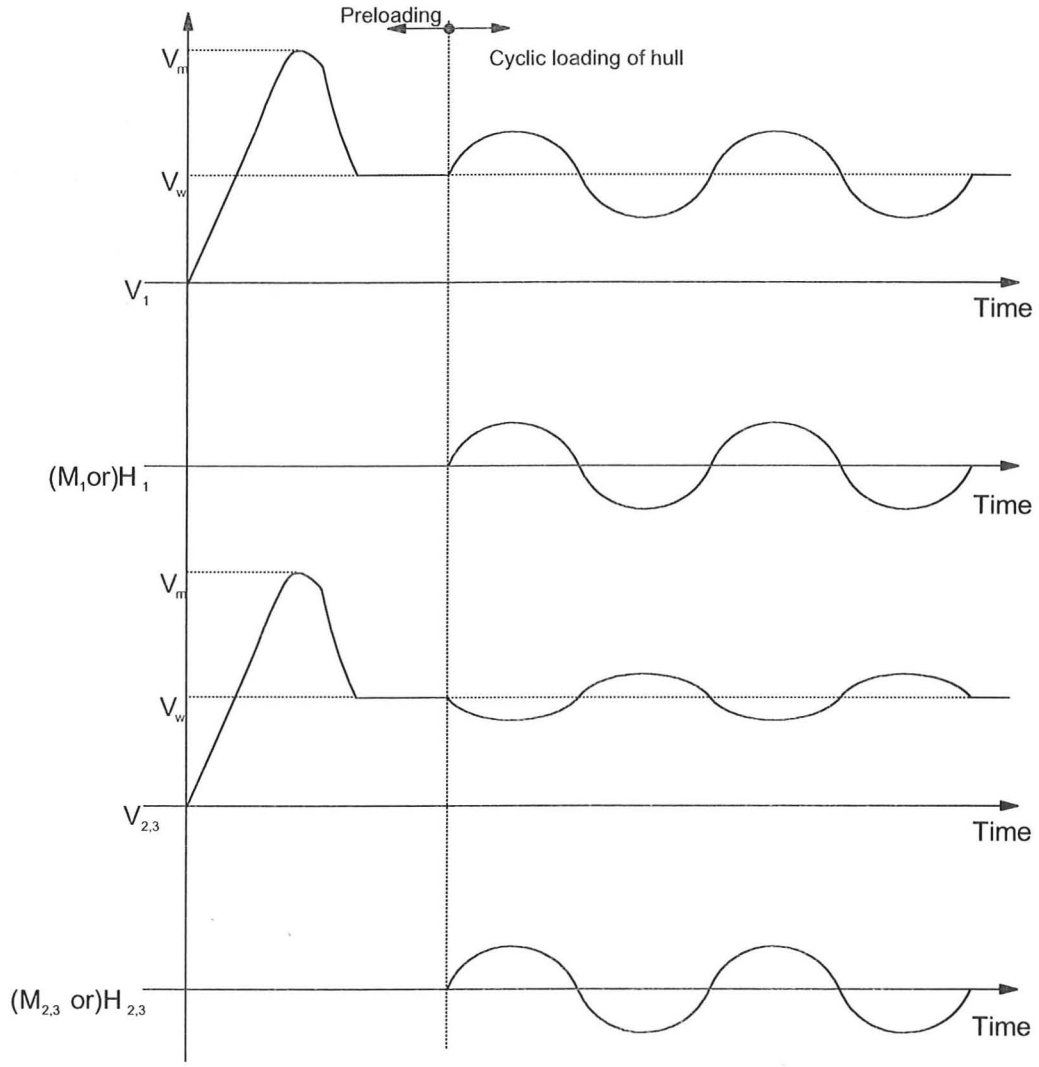

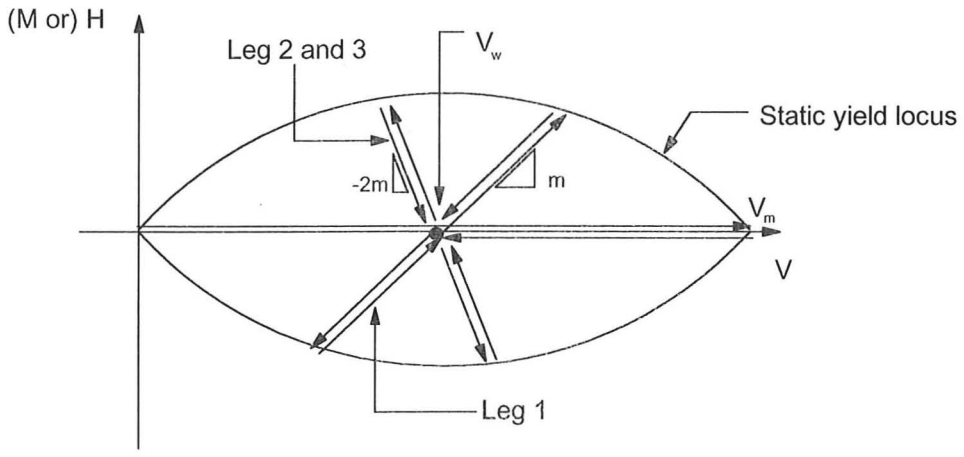

Fig. 2.17 Typical load paths for Legs 1 and 2,3 subjected to cyclic loading

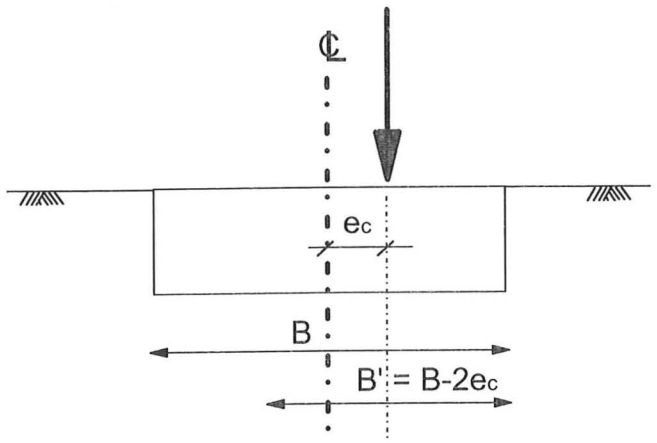

Fig. 2.18 Effective contact width for an eccentric load

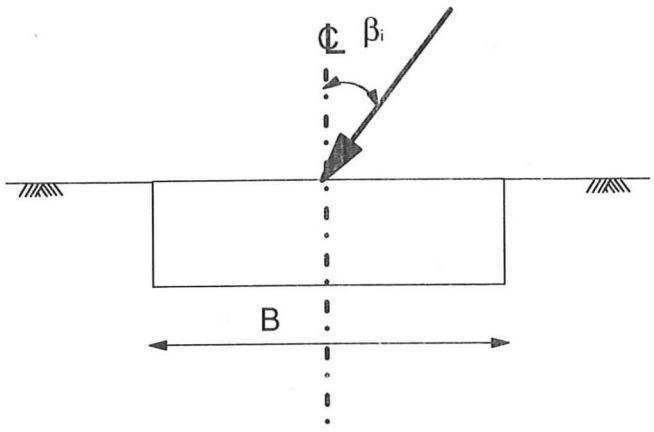

Fig. 2.19 Inclined load applied on foundation

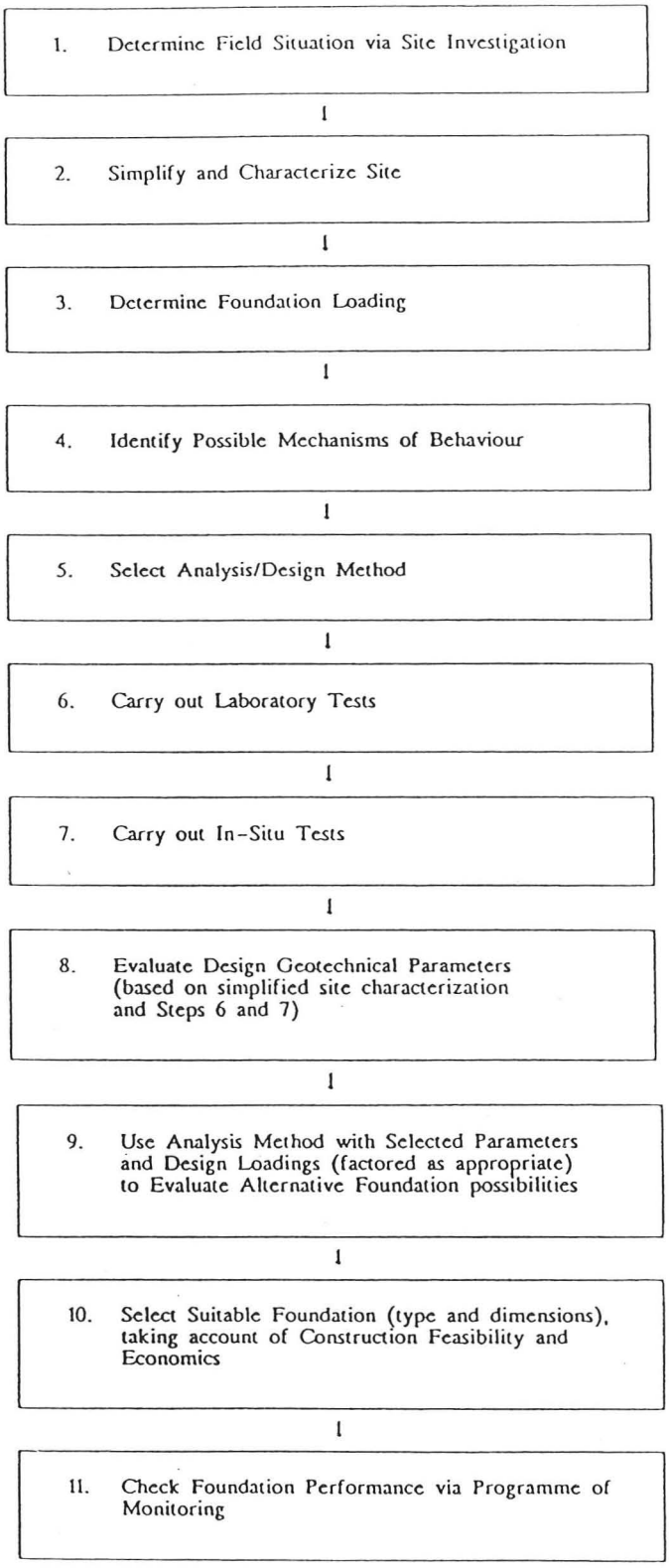

Fig. 2.20 Steps in Foundation Design Process (Poulos and Hull, 1994)

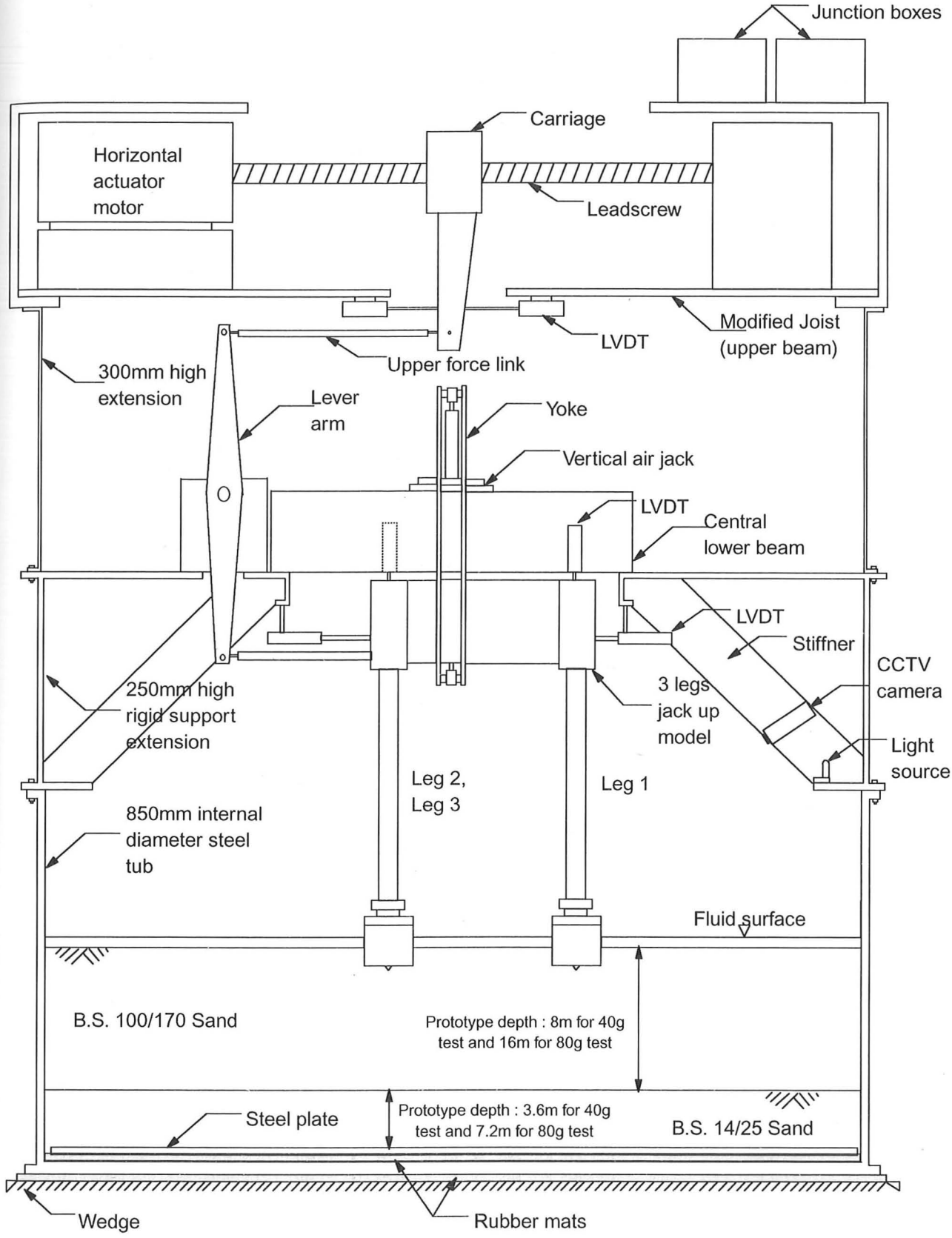

Fig. 3.1a General arrangement of the apparatus

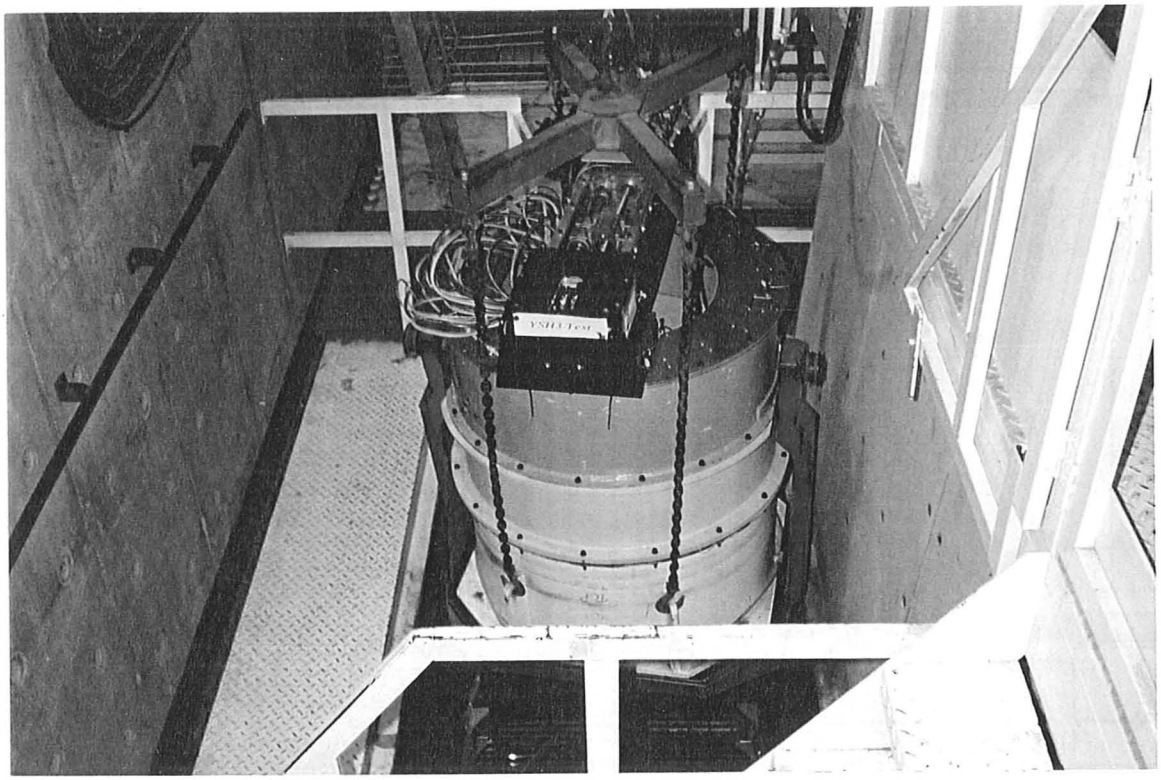

Fig. 3.1b Assembled package before it is lowered into the centrifuge pit

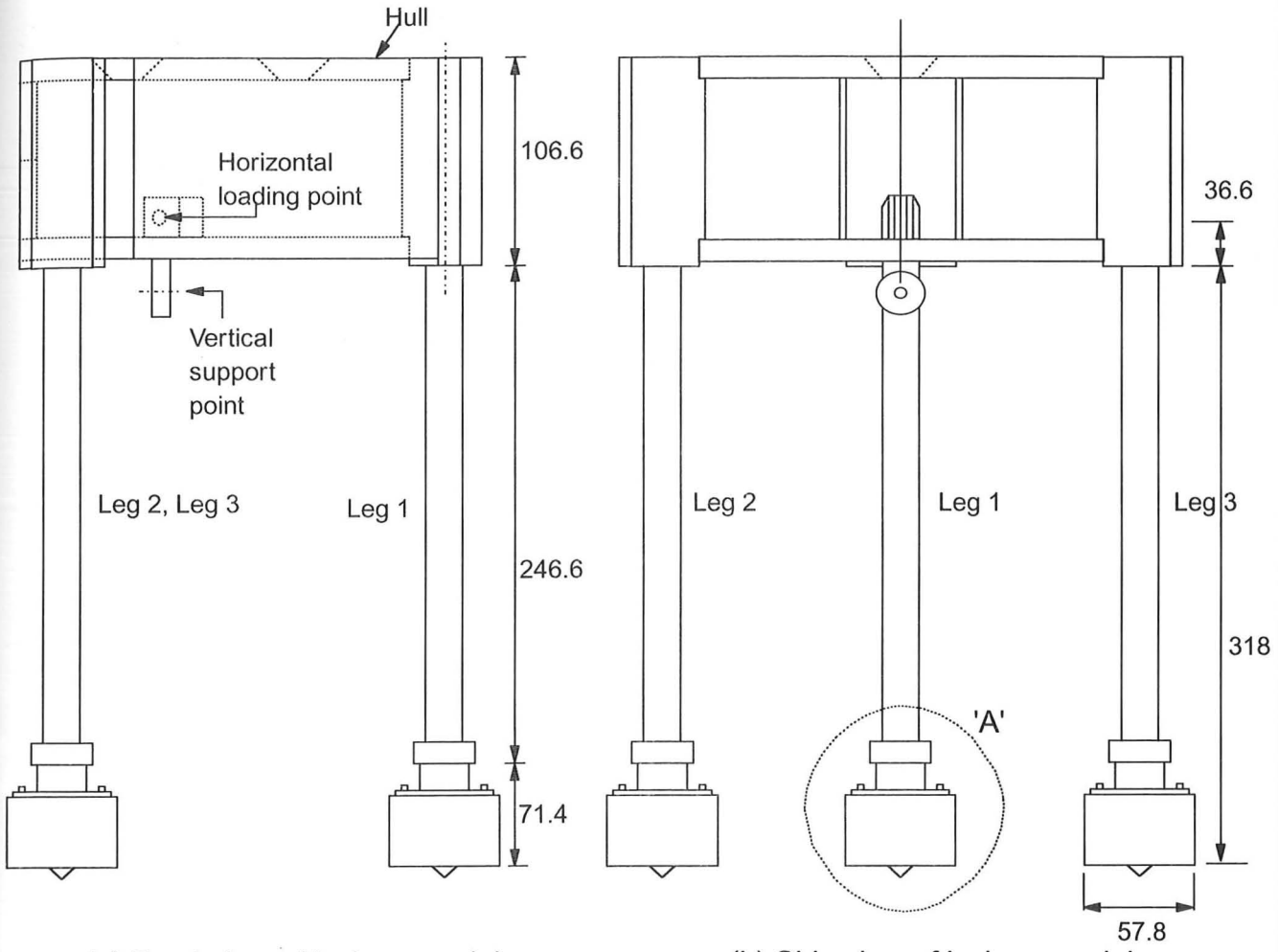

(a) Front view of jack up model

(b) Side view of jack up model

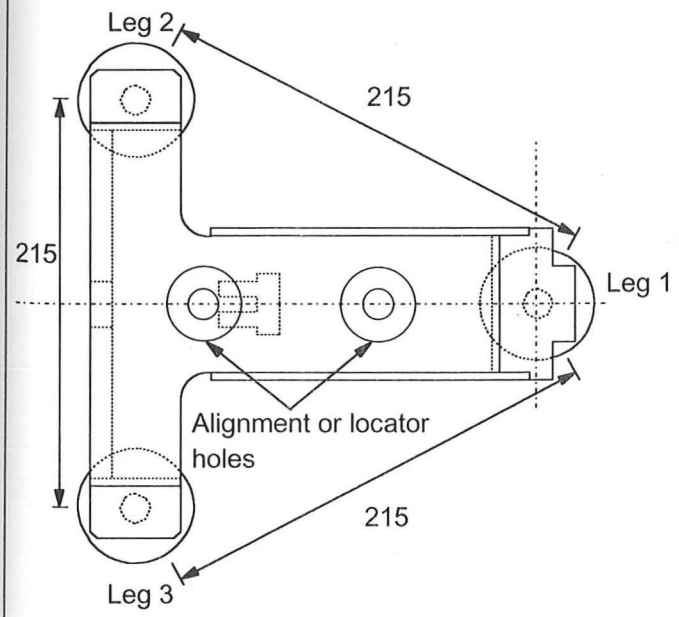

(c) Plan view of jack up model

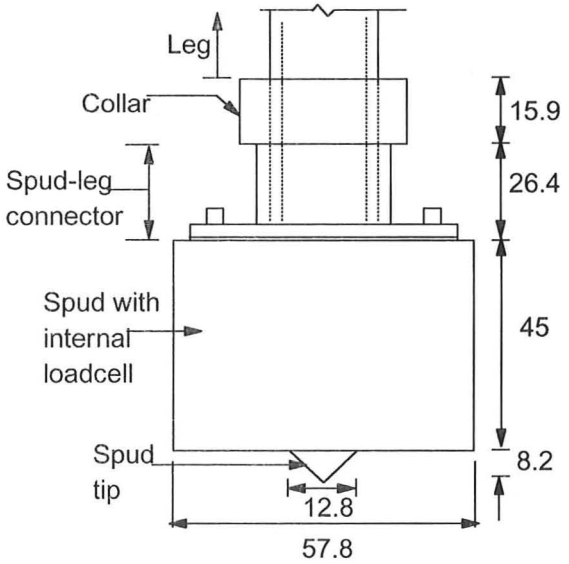

(d) Detail of 'A' Spud can foundation

Fig. 3.2 Details of the three-leg jack up model

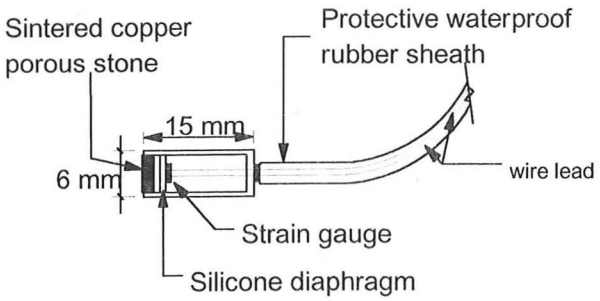

Fig. 3.3 Pore pressure transducer

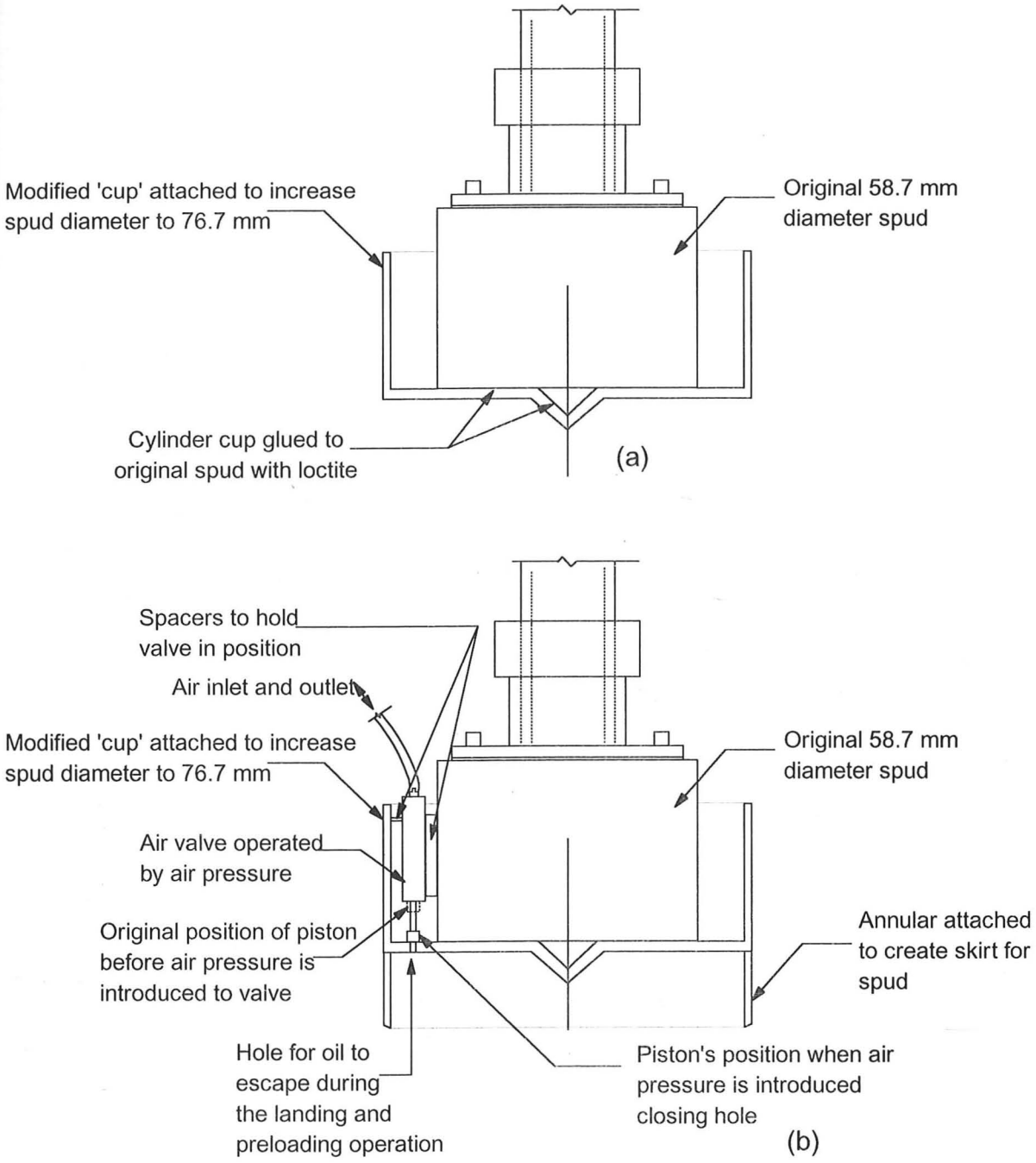

Fig. 3.4 Modified 58.7 mm Flat Spud for 76.7 mm skirted spud foundation

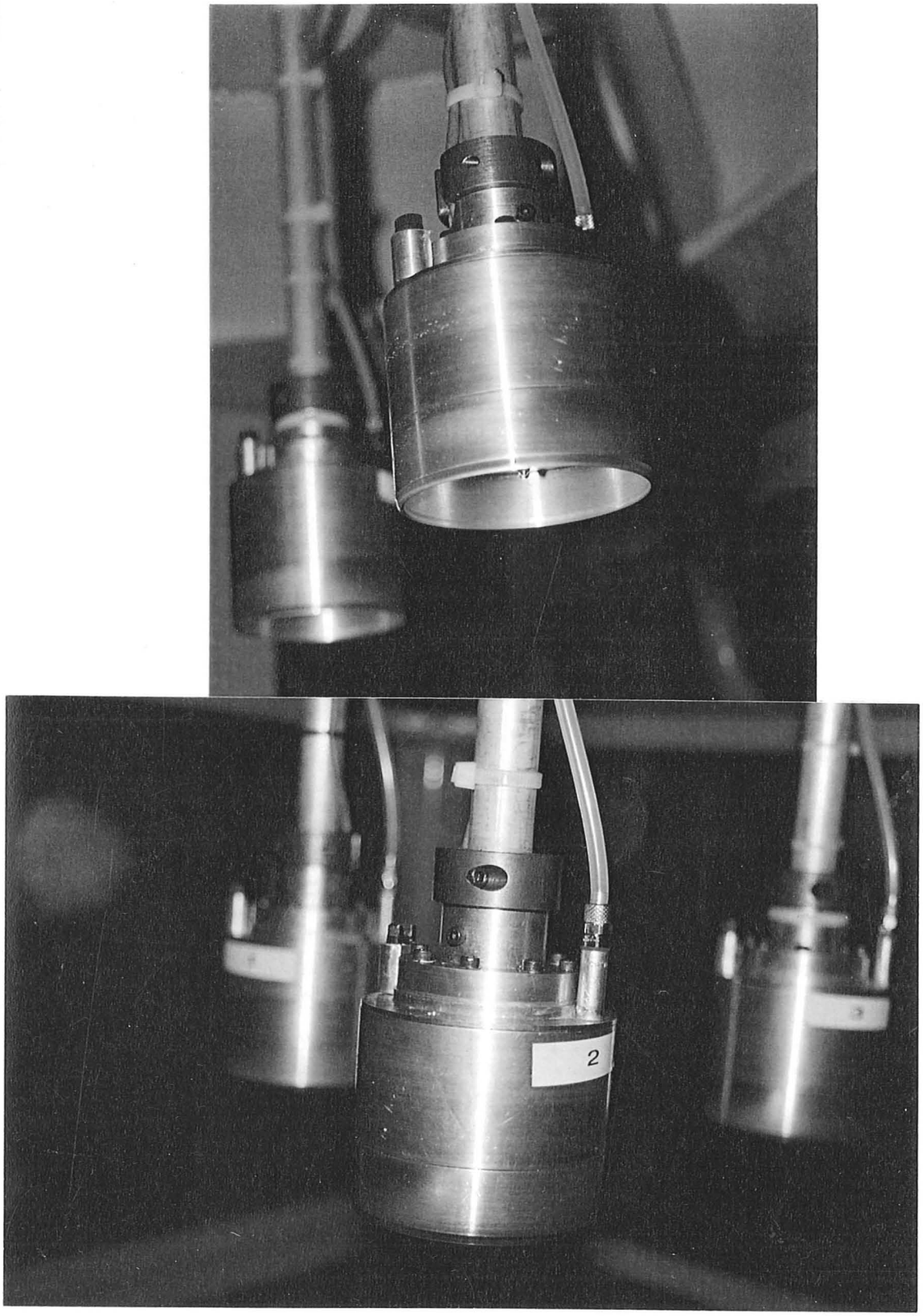

Fig. 3.4c Picture of modified skirted spuds
for test YSH9

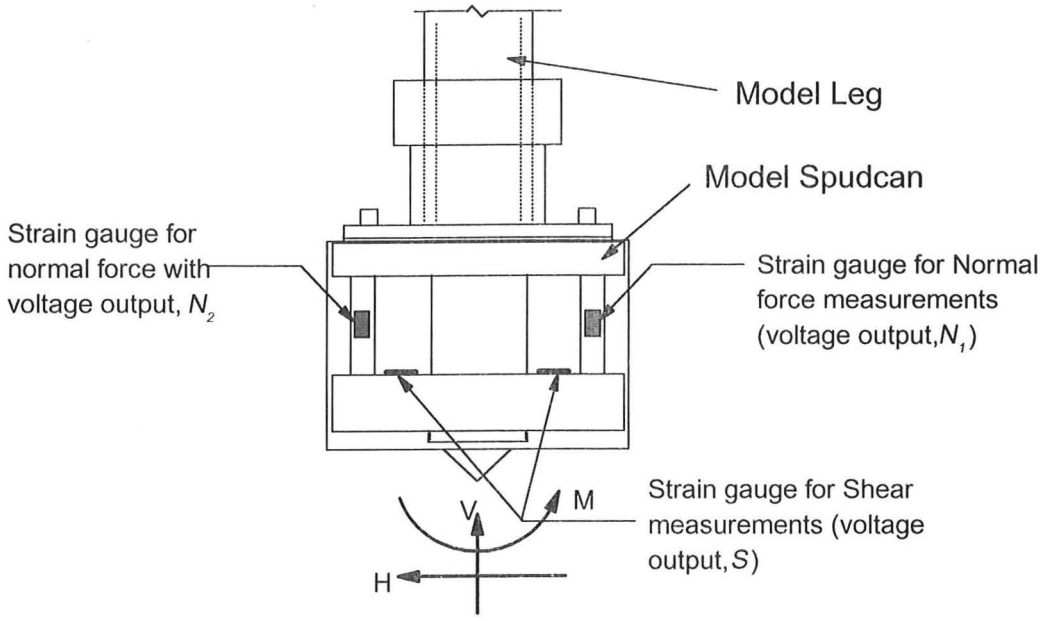

$$\begin{bmatrix} V \\ M \\ H \end{bmatrix} = \begin{bmatrix} c_{11} & c_{12} & c_{13} \\ c_{21} & c_{22} & c_{23} \\ c_{31} & c_{32} & c_{33} \end{bmatrix} \times \begin{bmatrix} N_1 \\ N_2 \\ S \end{bmatrix}$$

Calibration Matrix

Fig. 3.5 Schematic diagram of Load cell

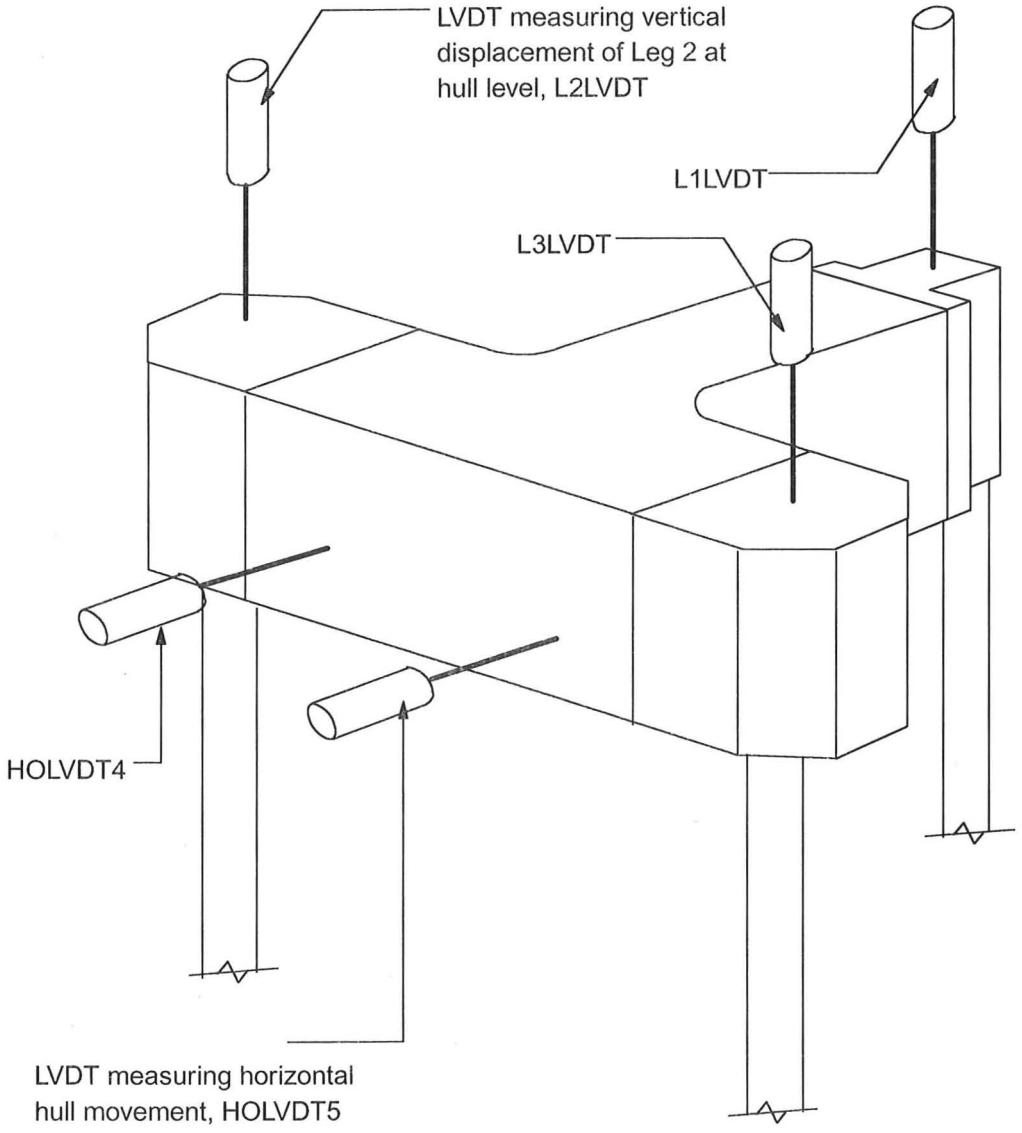

Fig. 3.6 Positions of LVDTs

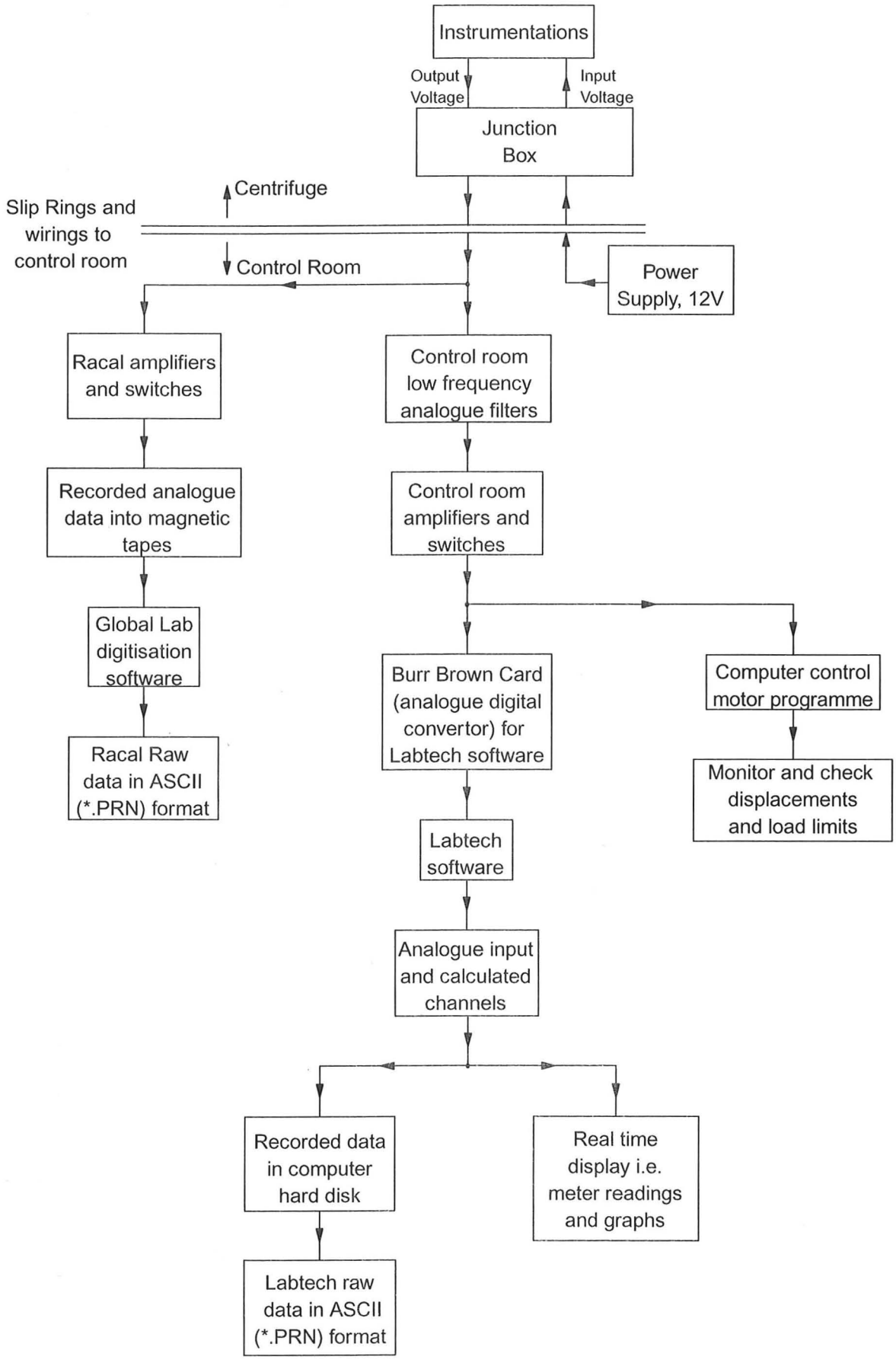

Fig. 3.7 Data signal processing format

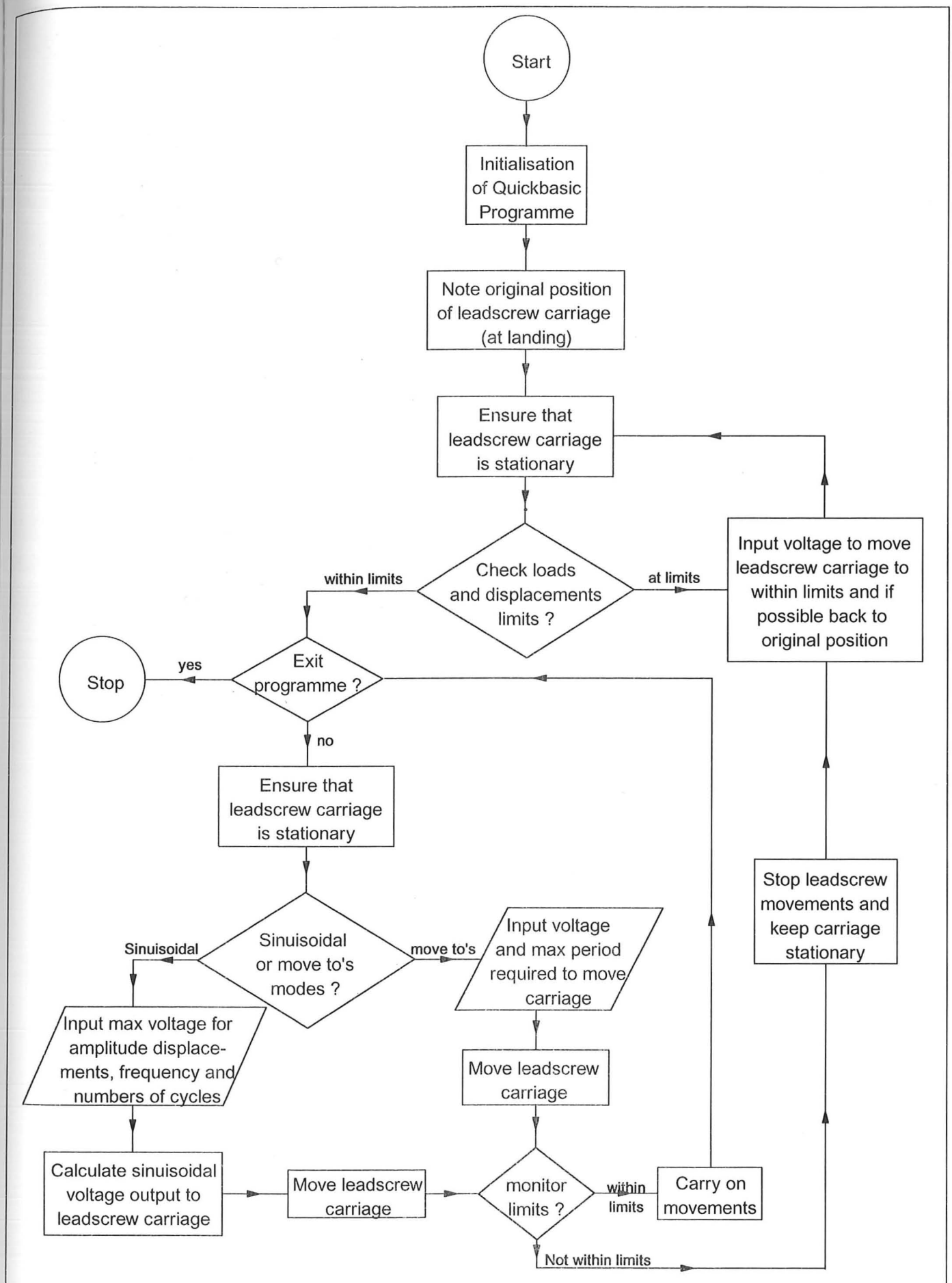

Fig. 3.8a Flowchart of Quickbasic Programme for computer motor control

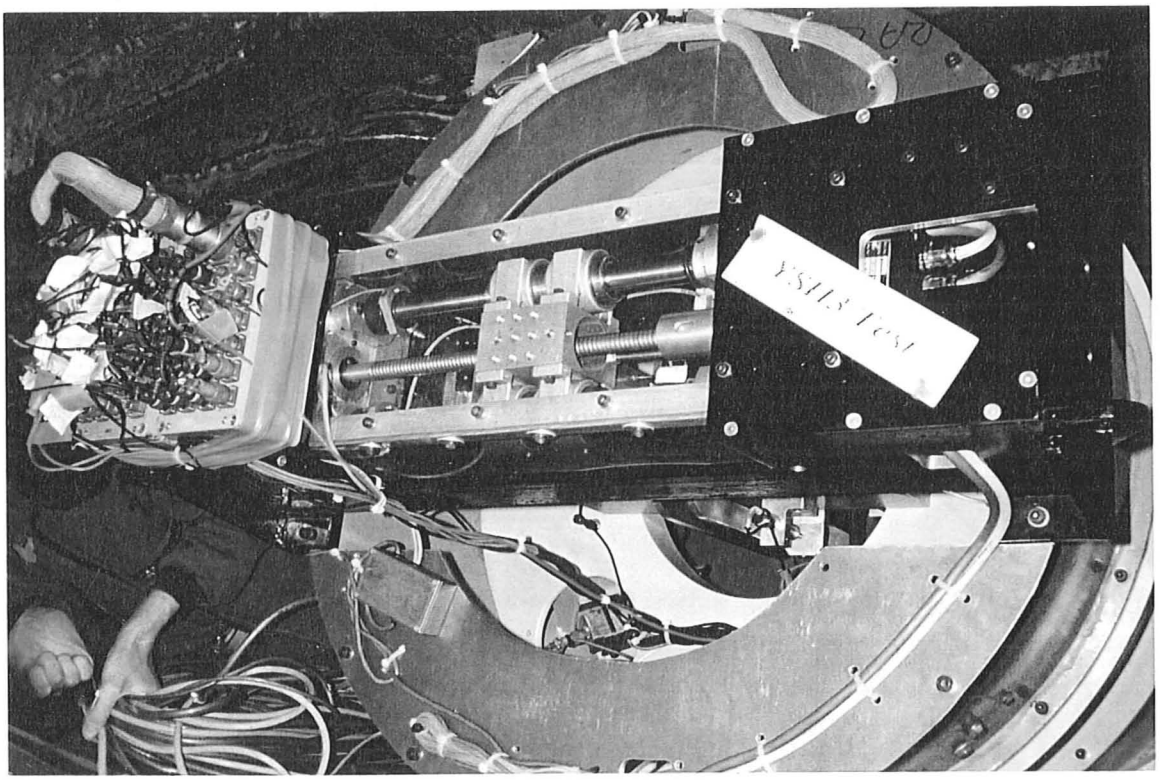

Fig. 3.8b Picture of horizontal Actuator

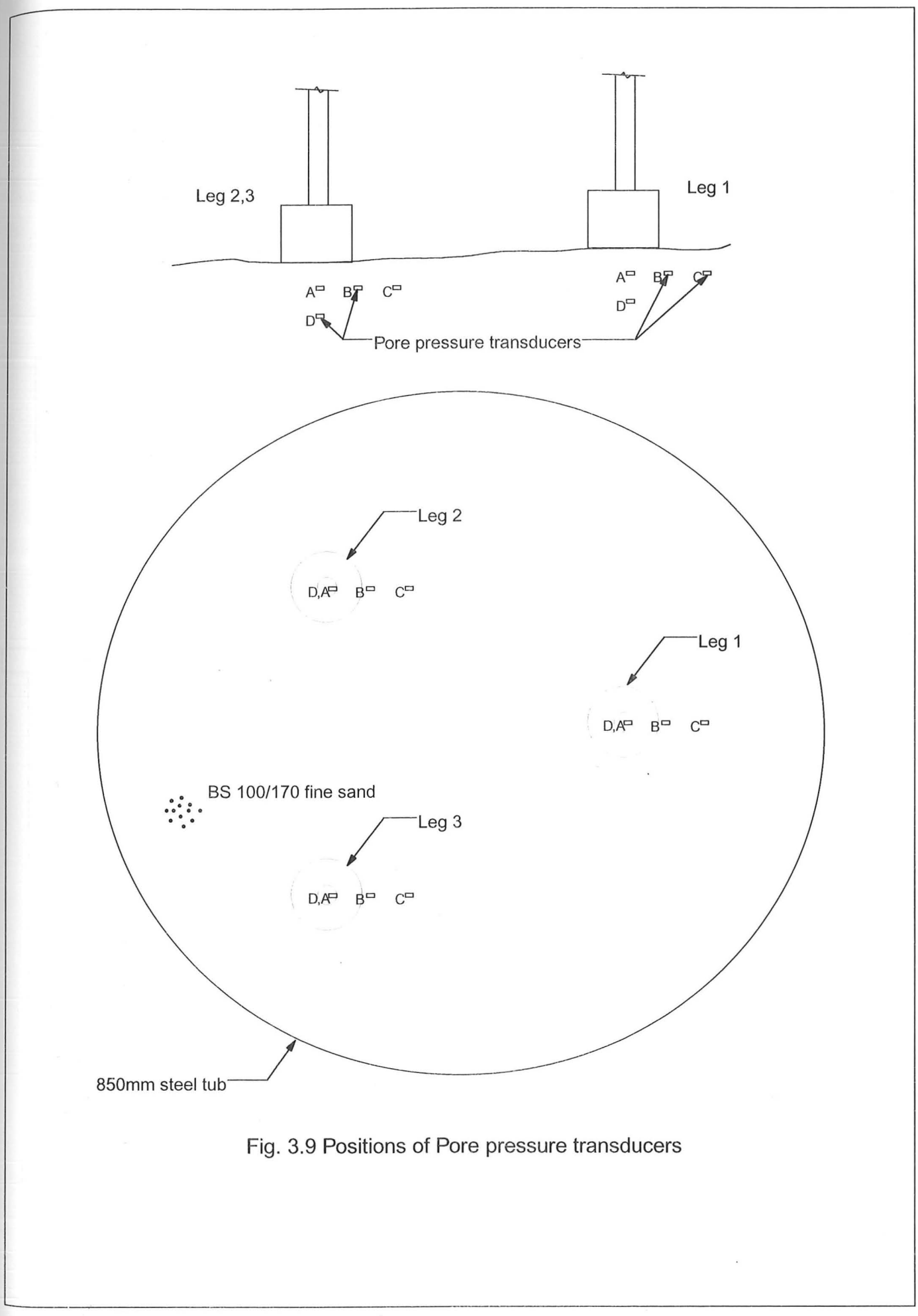

Fig. 3.9 Positions of Pore pressure transducers

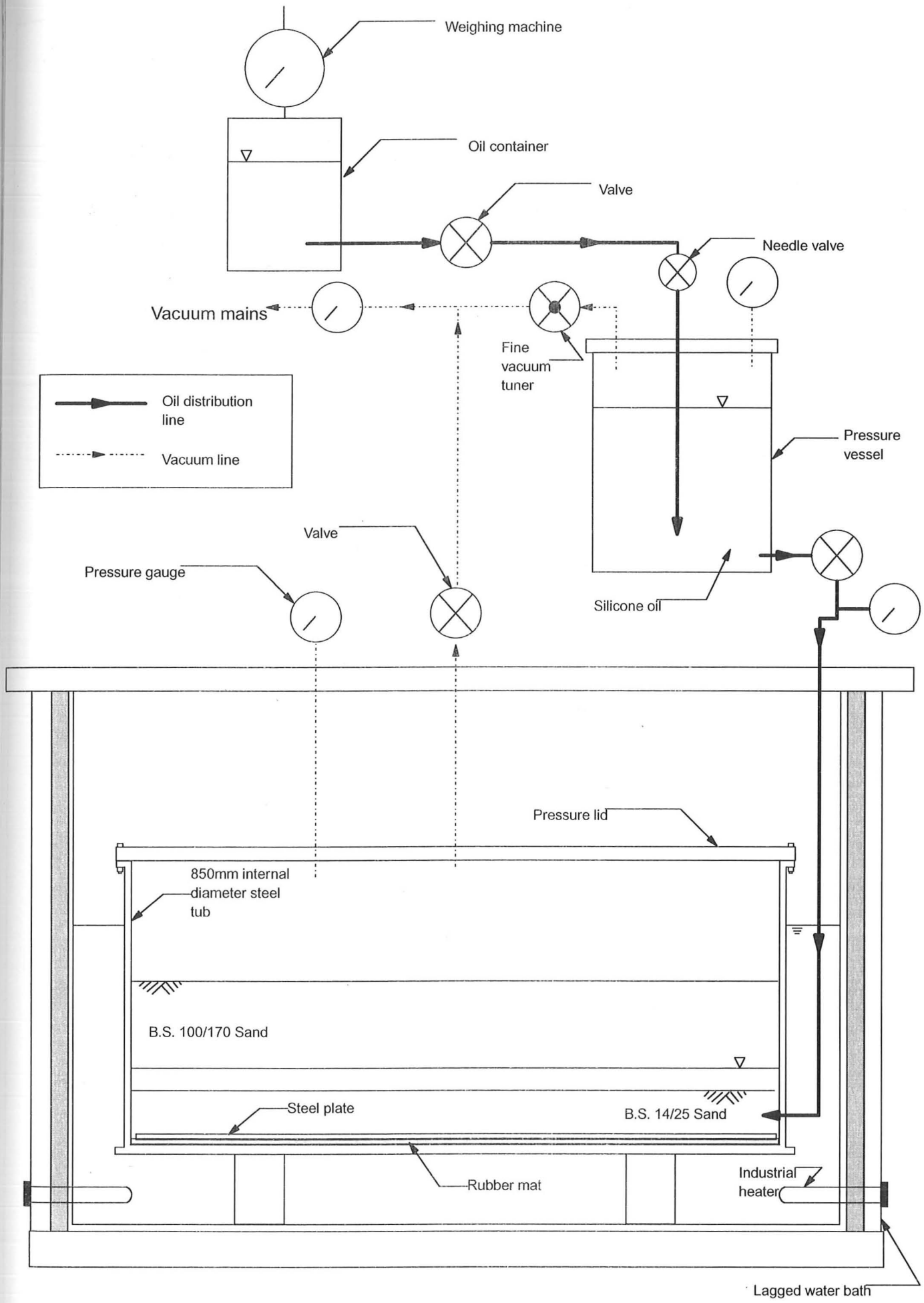

Fig. 3.10 Oil Saturation Process

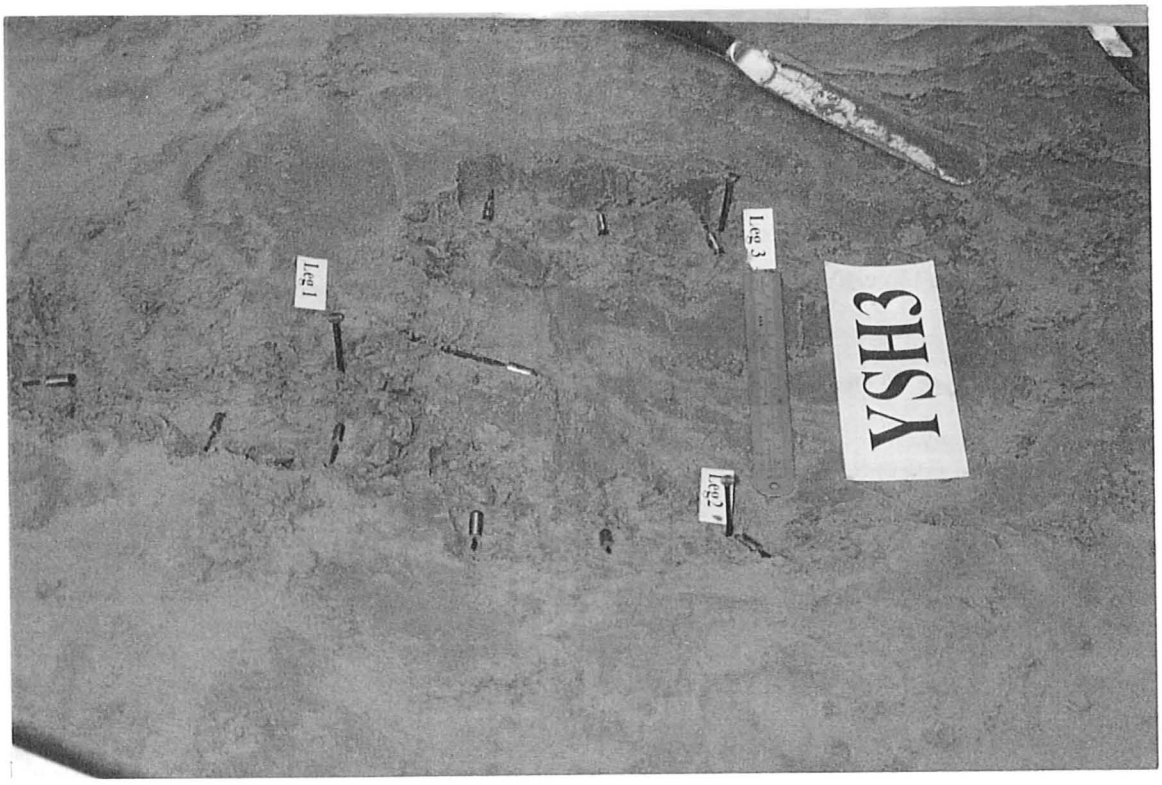

Fig. 3.11 Picture of the Post-test investigation

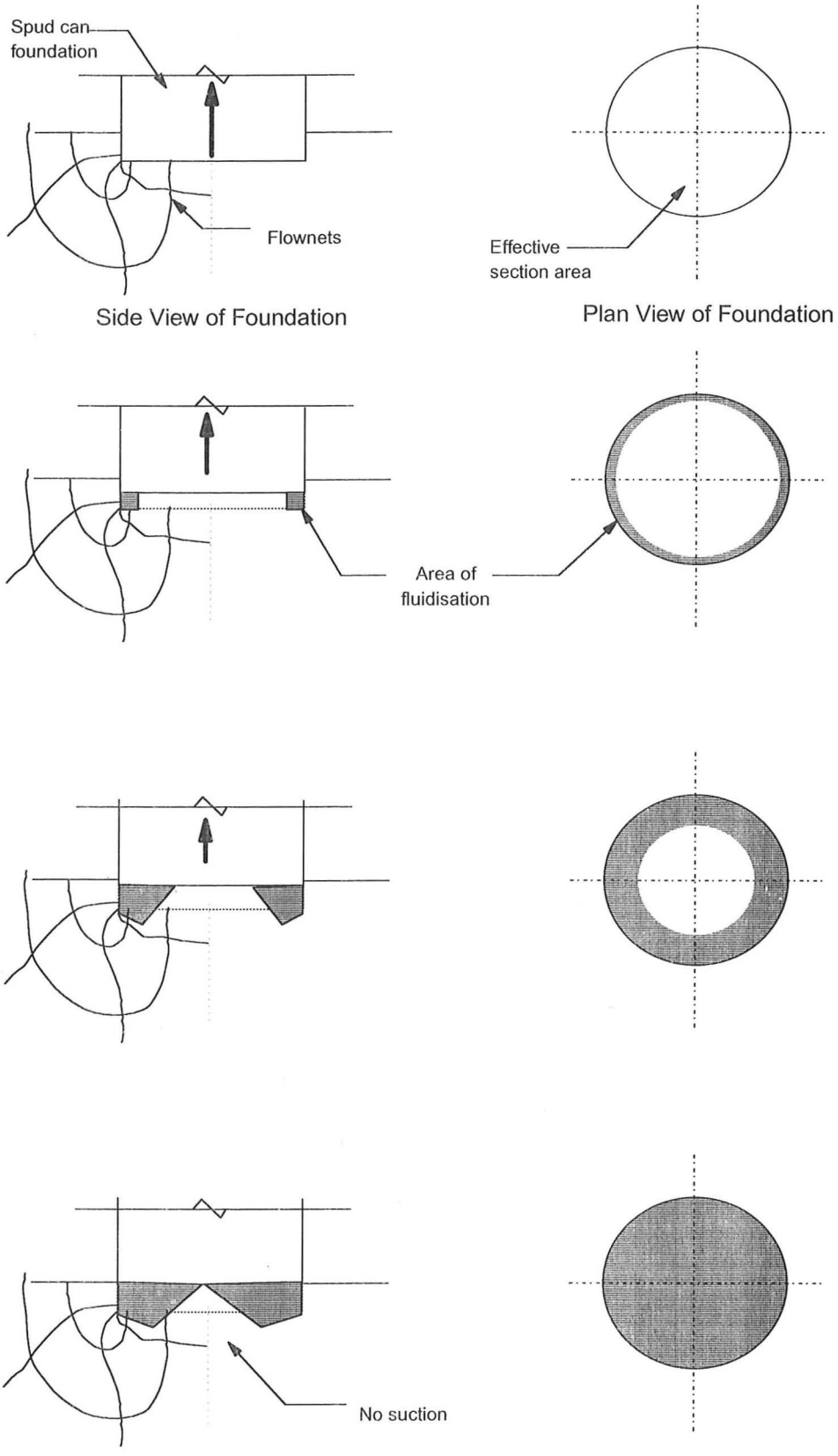

Fig. 4.1 Progressive Failure due to Pull-out
(Schematics only)

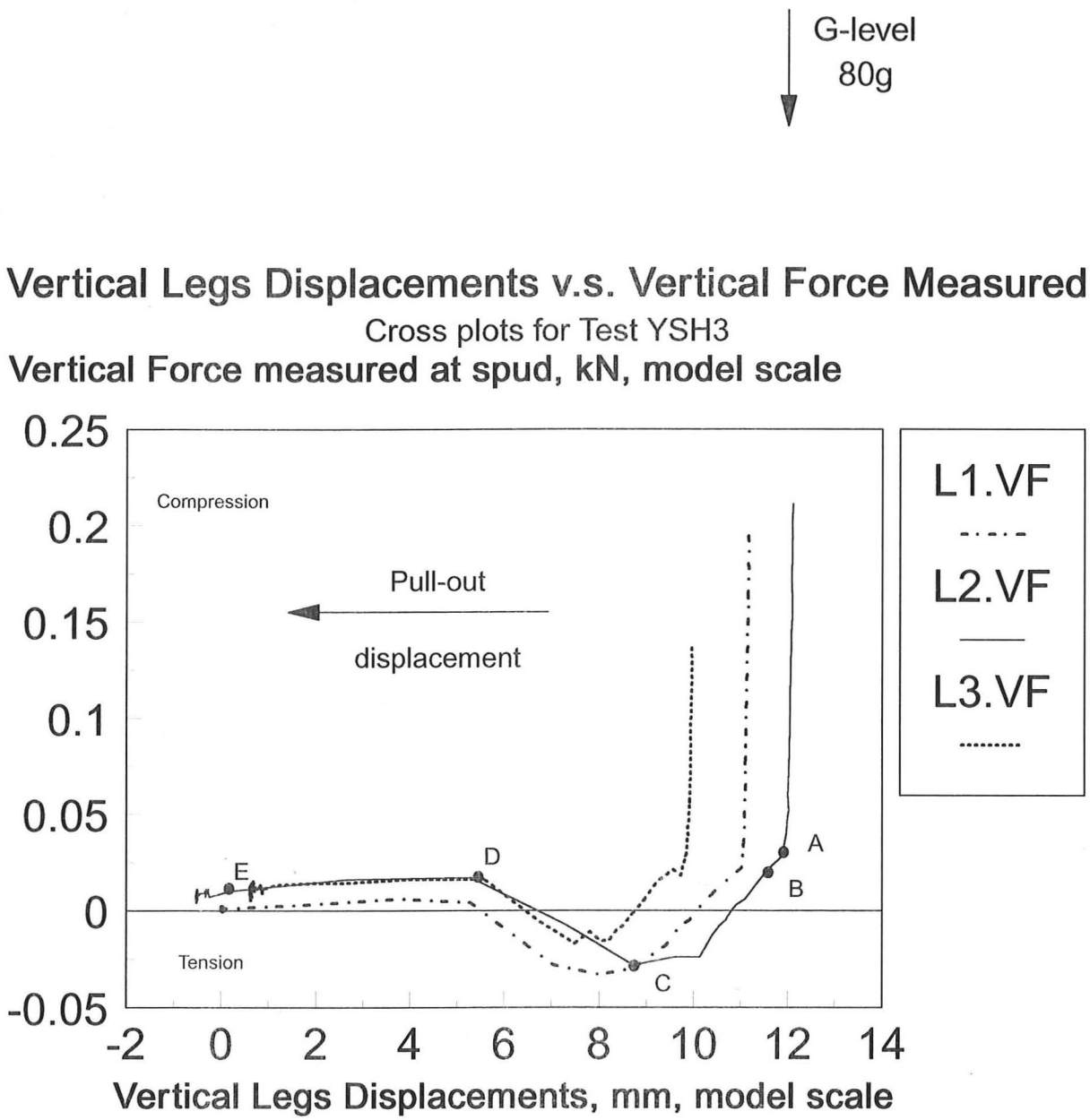

Fig. 4.2 Retraction process for Test YSH3
(Load v.s. displacements plot)

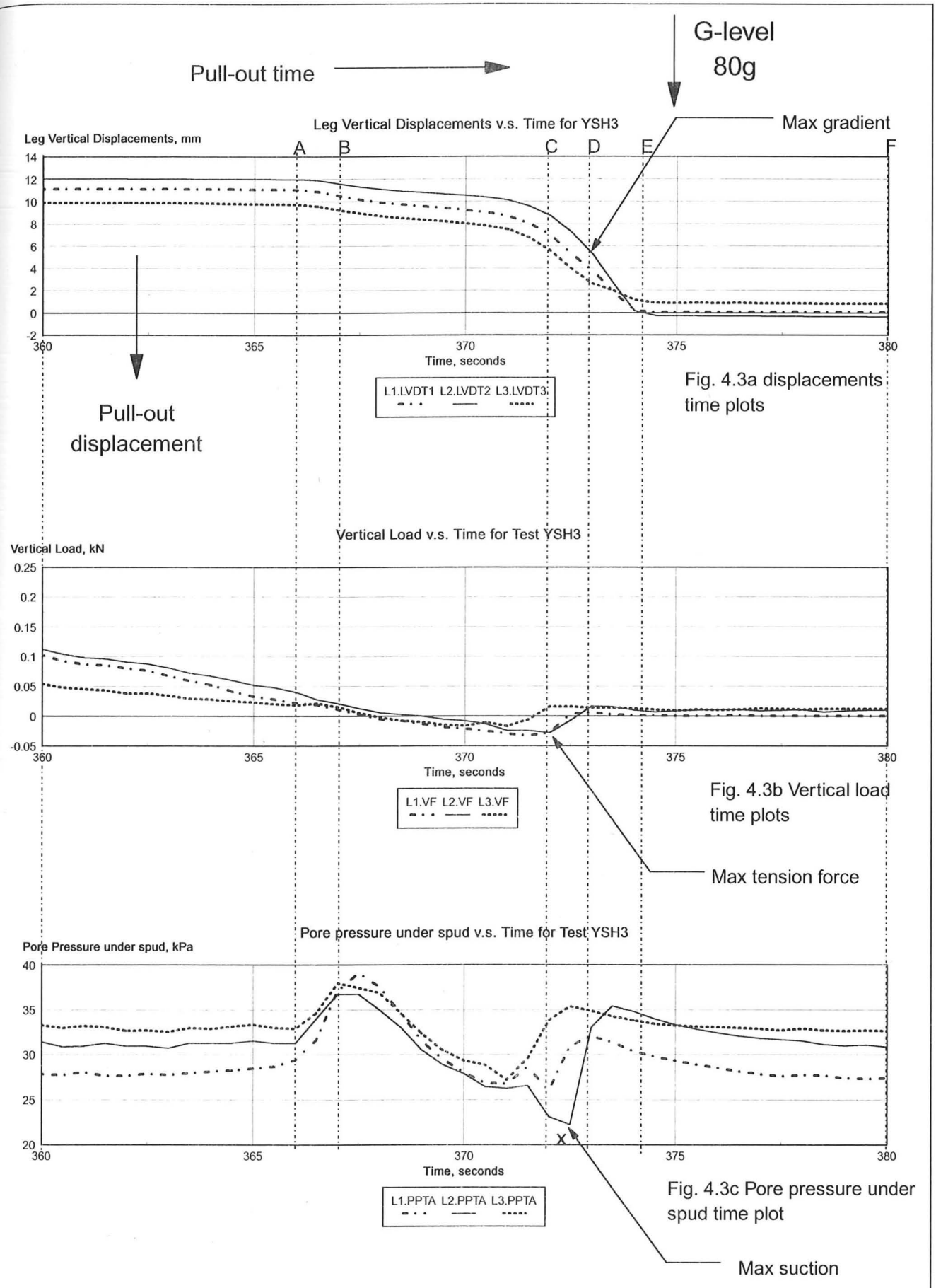

Fig. 4.3 Retraction process for Test YSH3 (Time Plots)

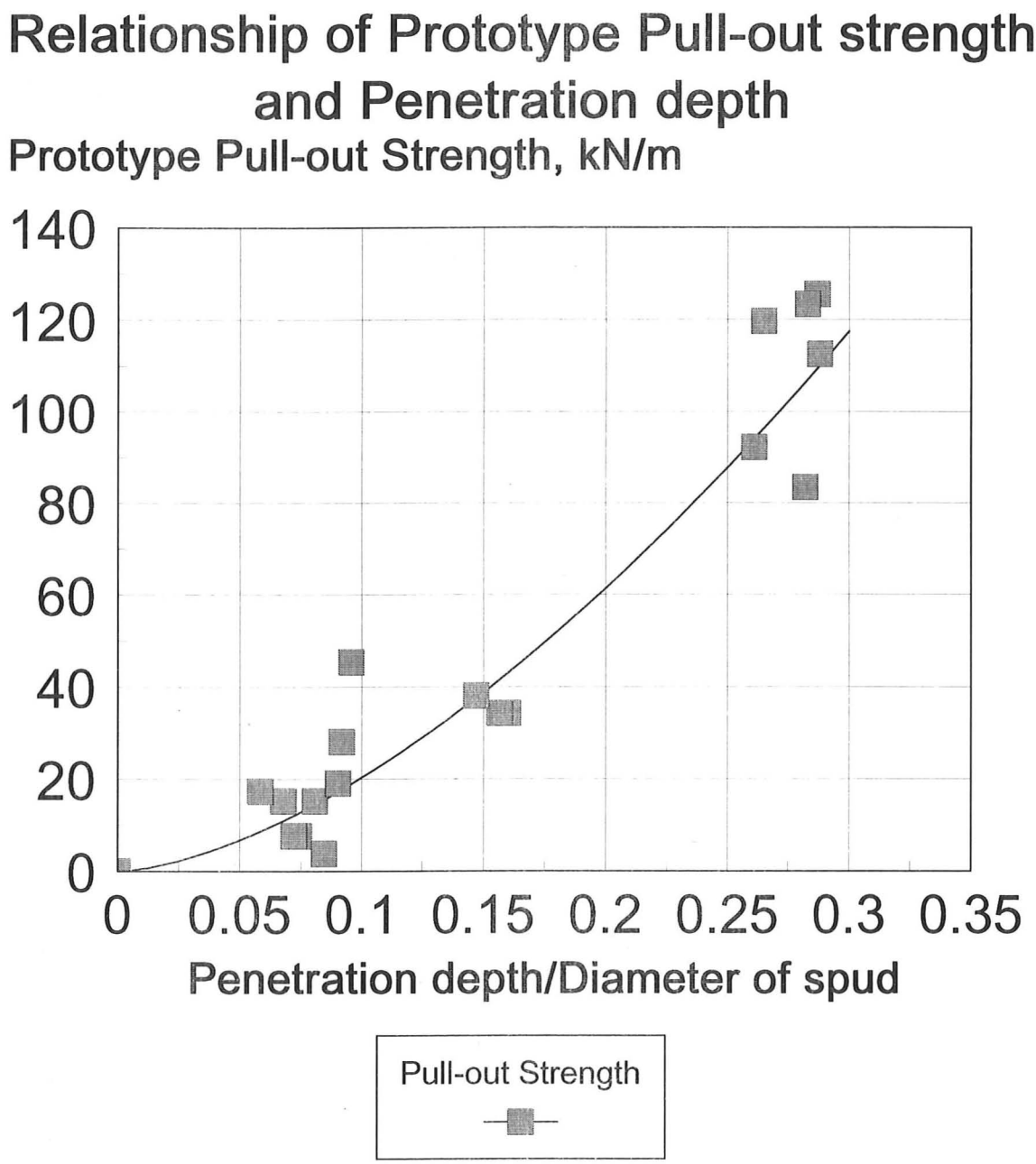

Fig. 4.4 Pull-out Strength Relationship with Penetration Depth over Diameter of Spud

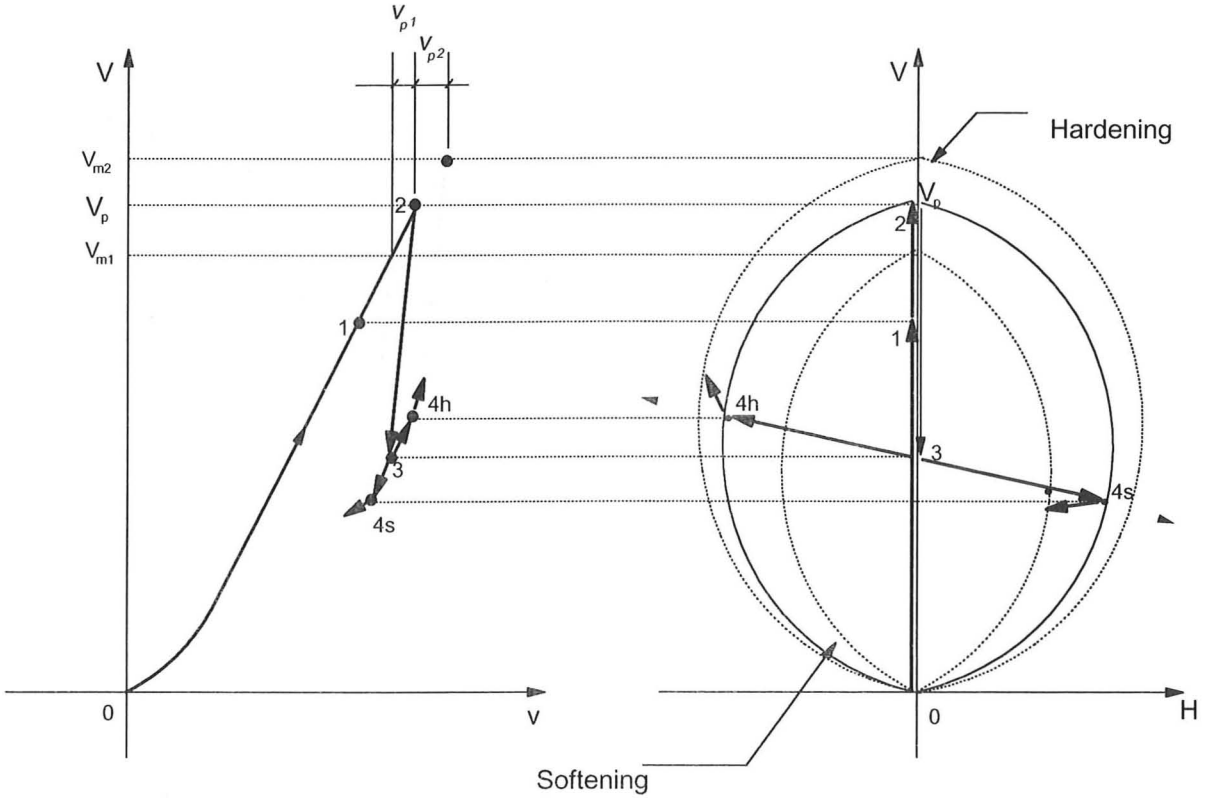

(a) (b)

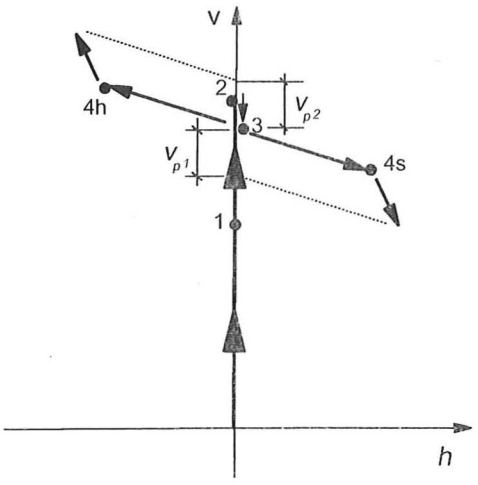

(c)

Fig. 4.5 Work-hardening and softening concept

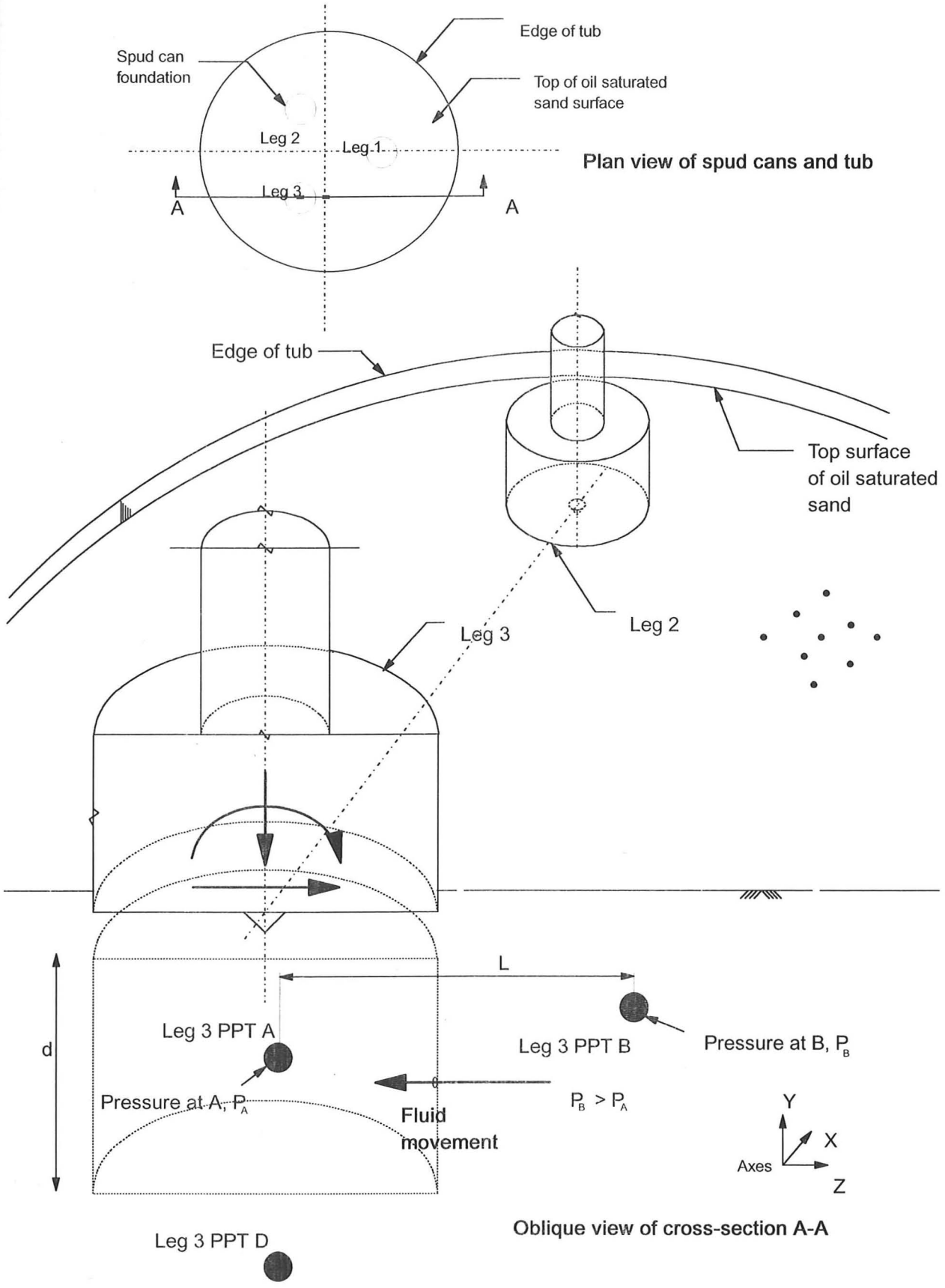

Fig. 4.6 Simple approach to estimation of permanent vertical displacements

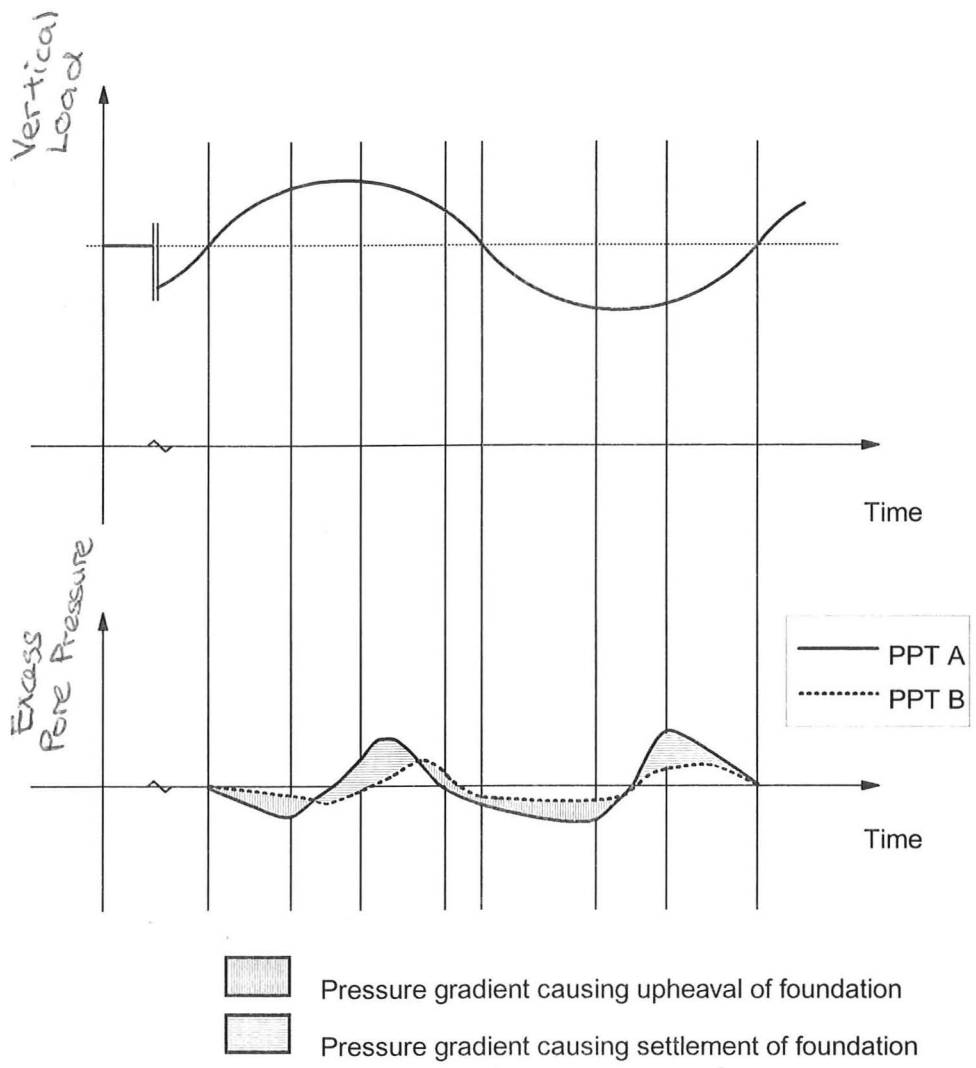

Fig. 4.7 Pore pressure effects at positions A and B causing permanent upheaval or settlement of foundation

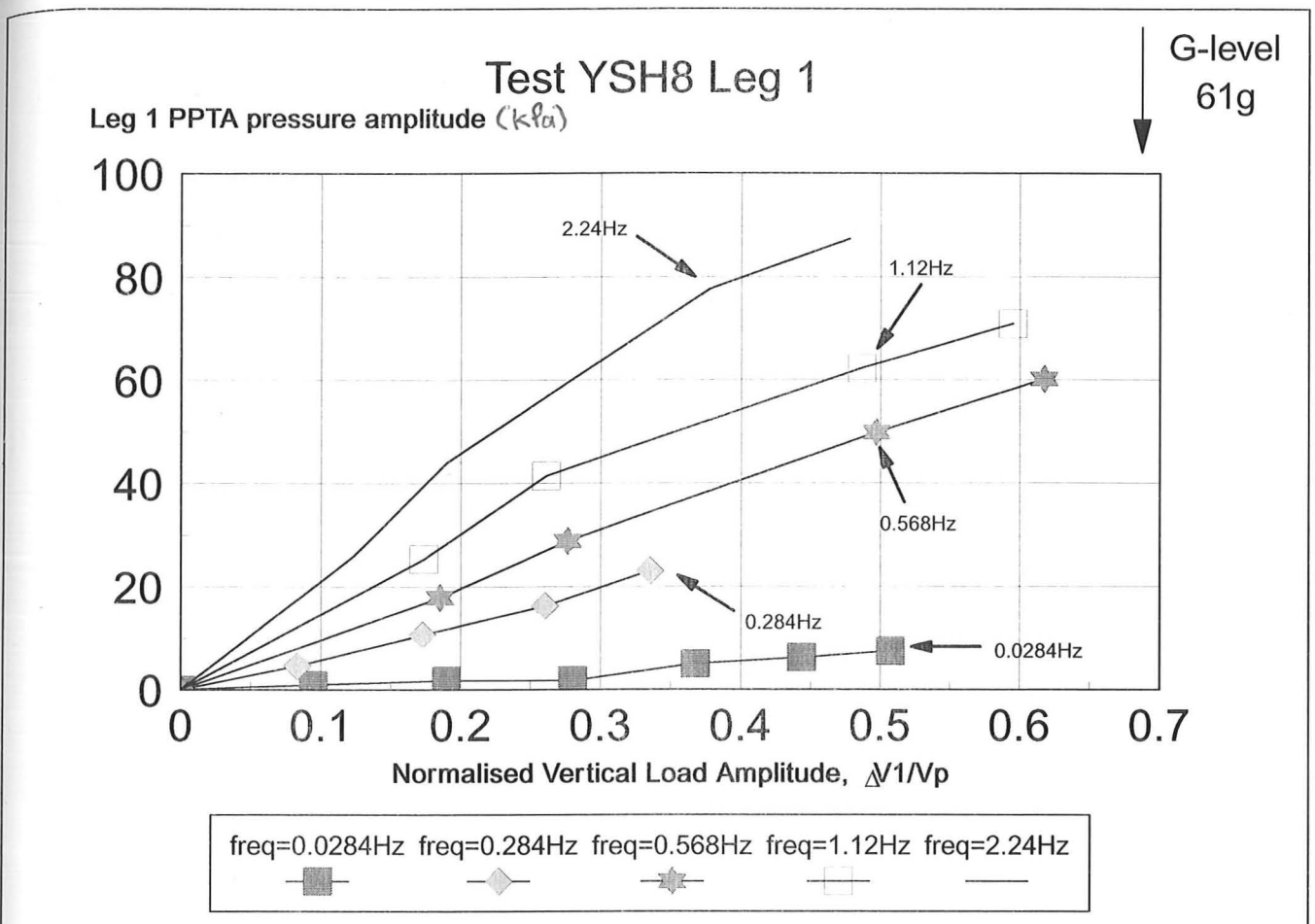

(a)

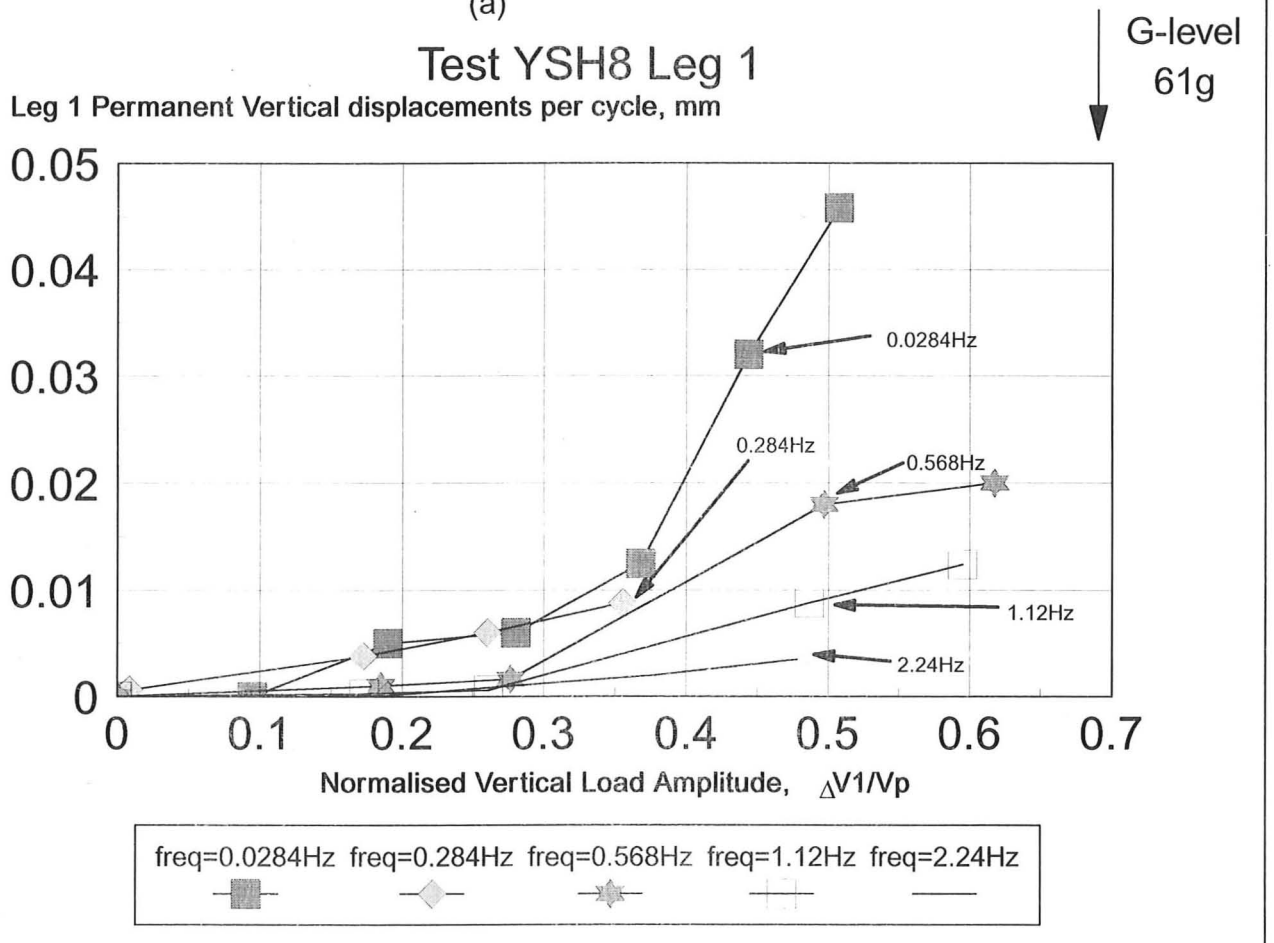

(b)

Fig. 4.8 Excess Pore Pressure and Settlement with respect to Vertical Cyclic loads

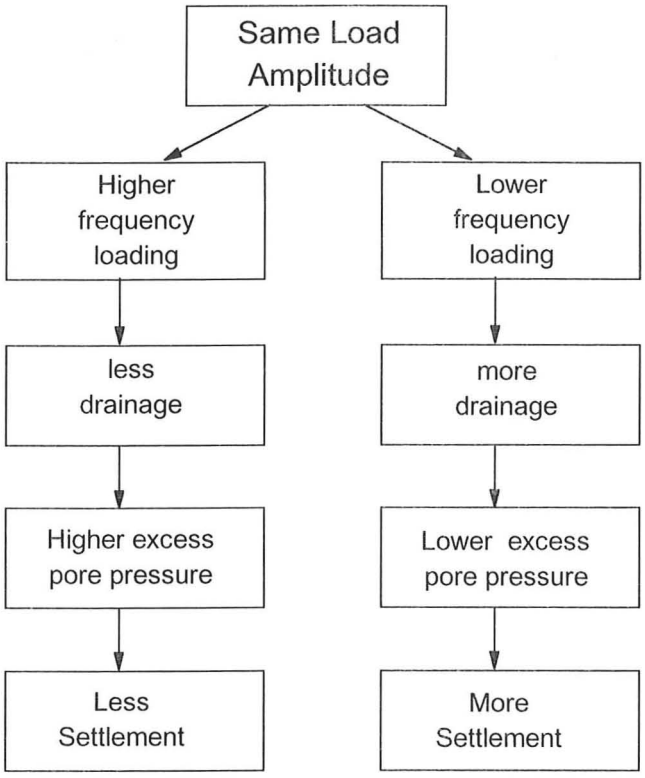

(a)

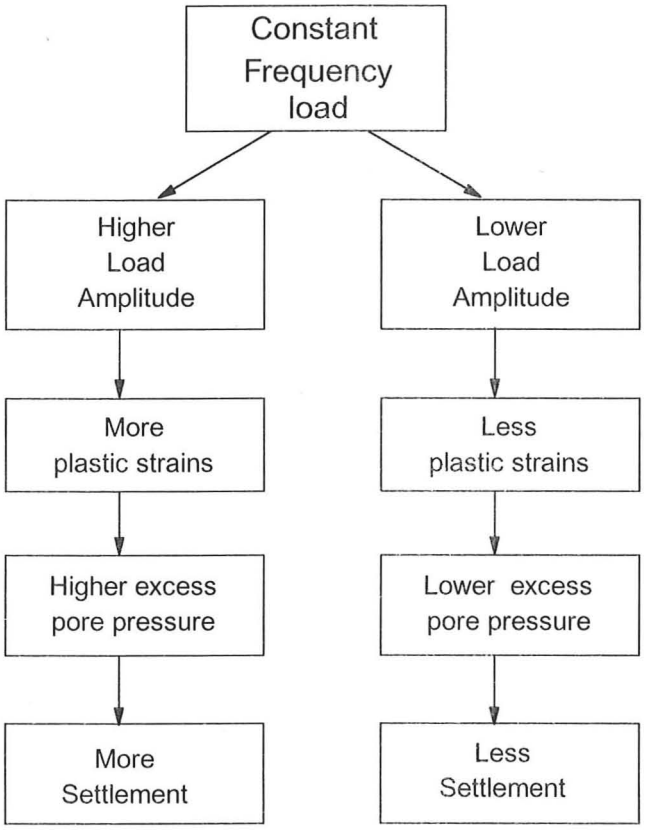

(b)

Fig. 4.9 Hypothesis for excess pore pressure generation and settlement

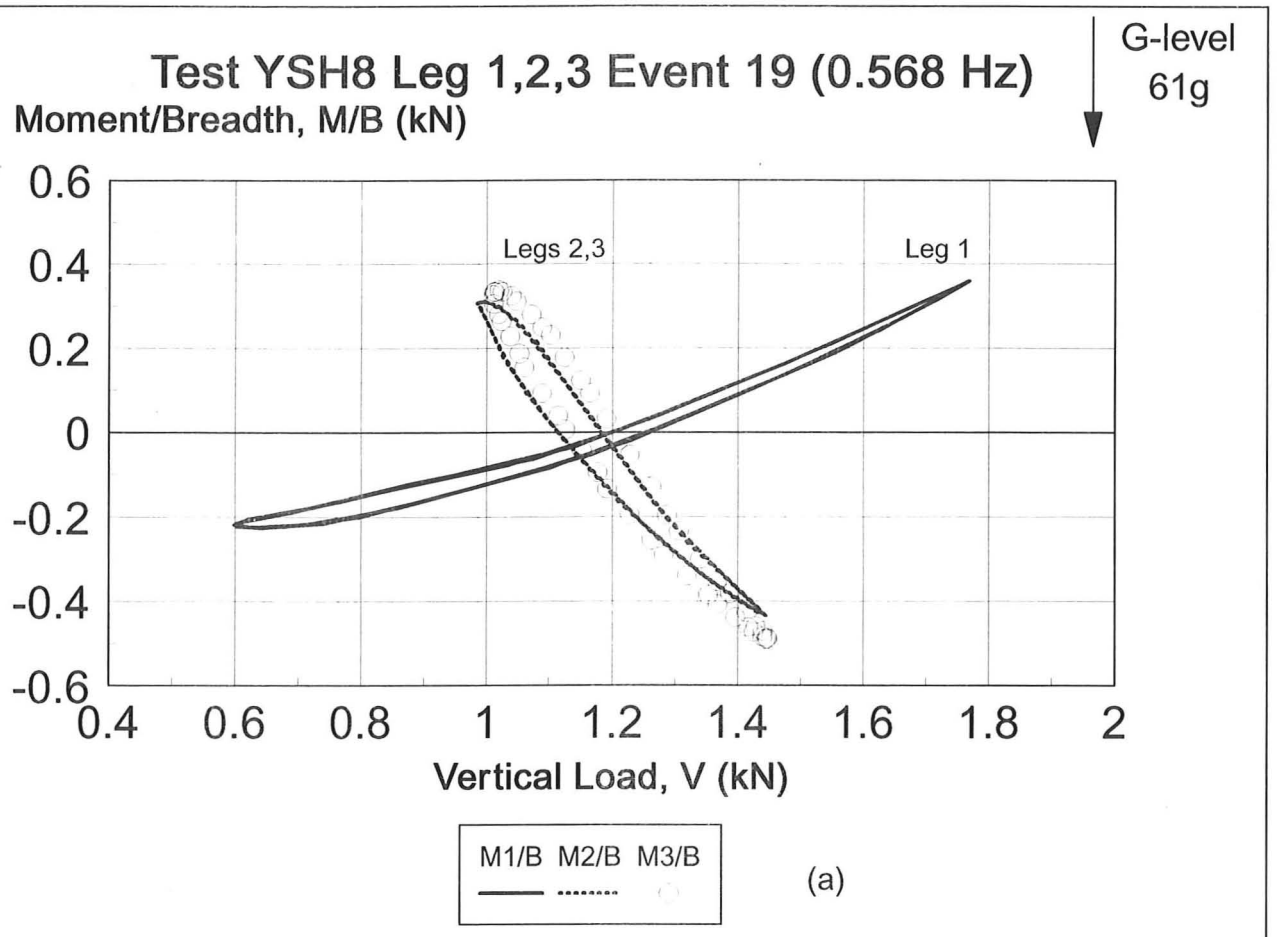

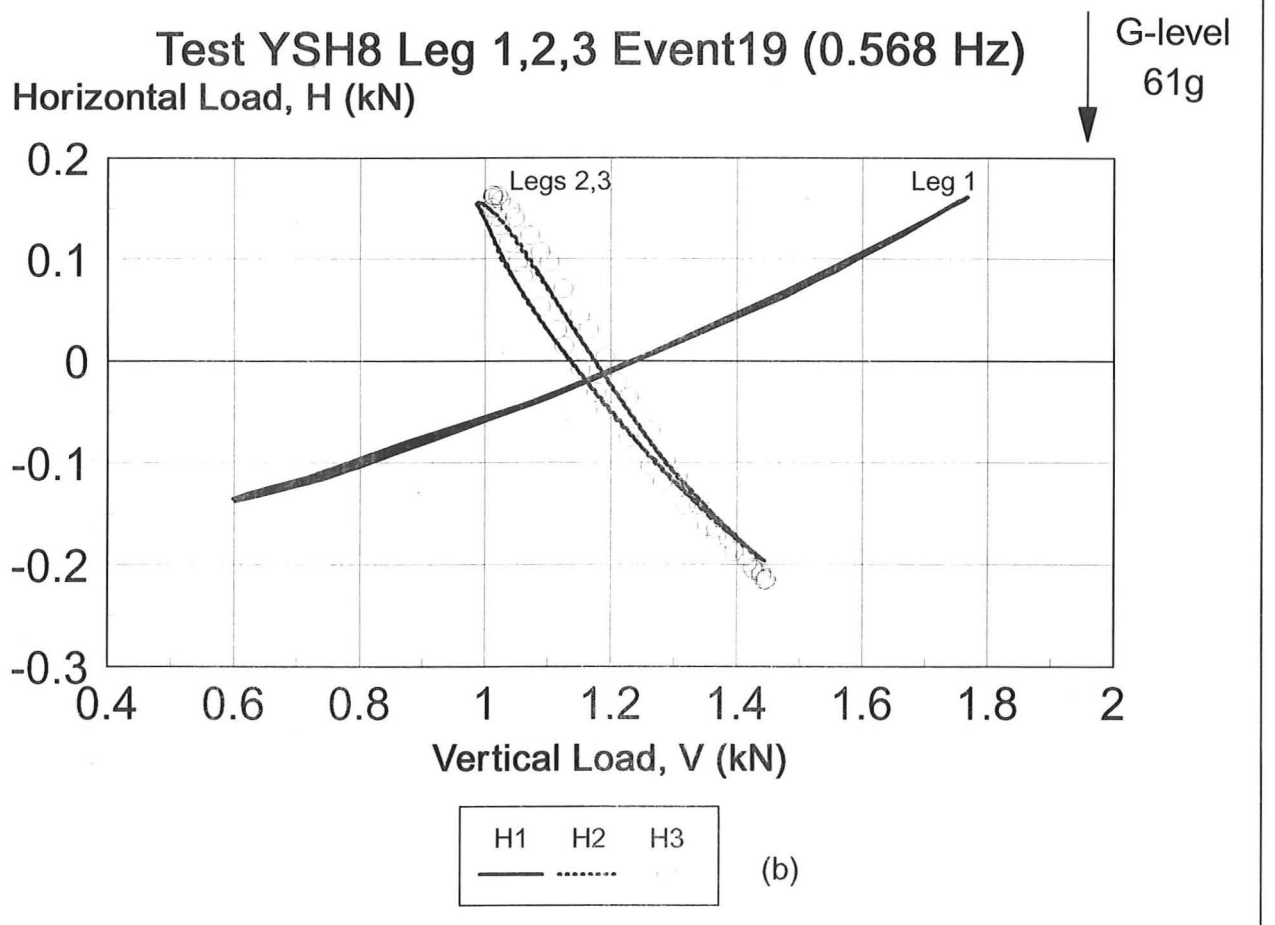

Fig. 4.10 Load path (load freq., 0.568Hz)

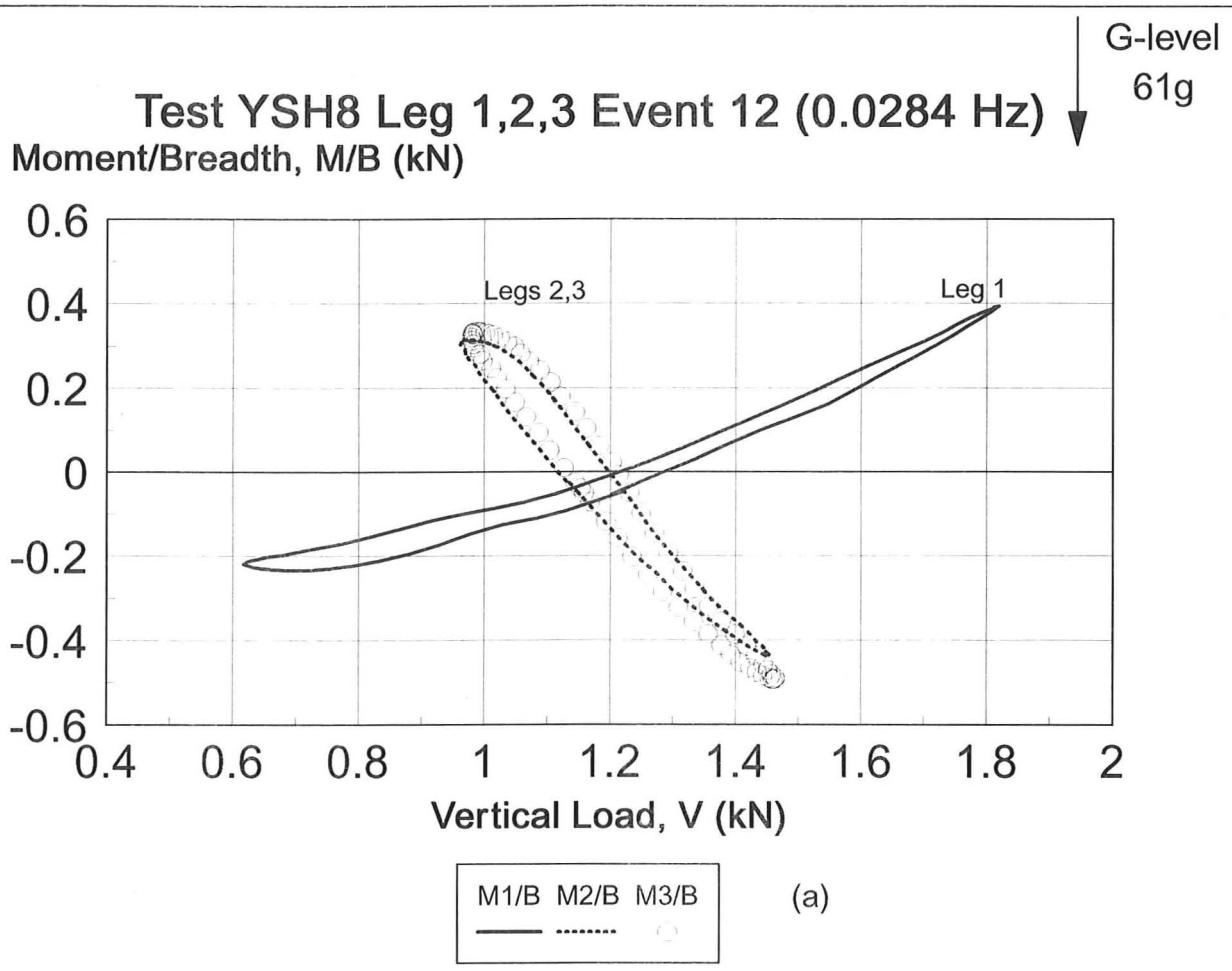

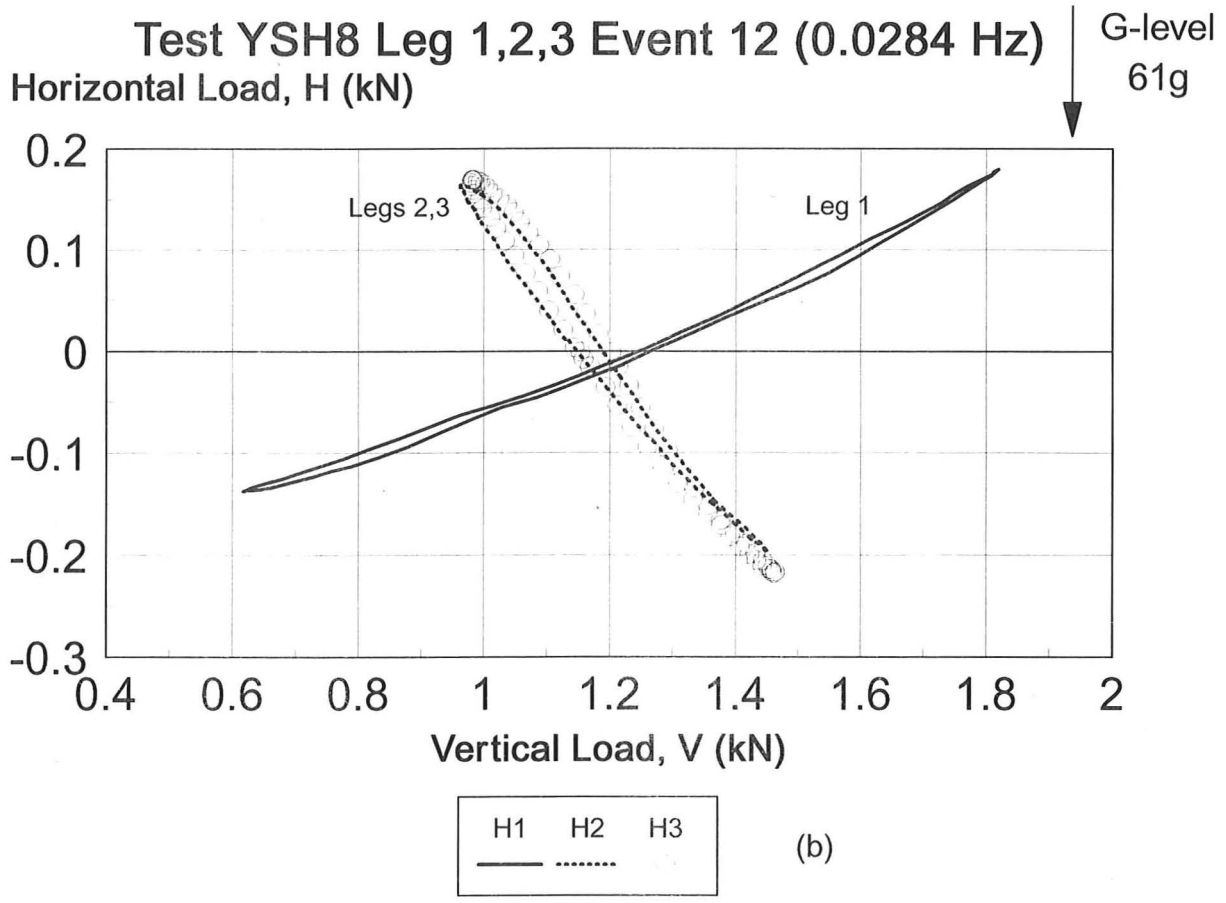

Fig. 4.11 Load paths (load freq., 0.0284Hz)

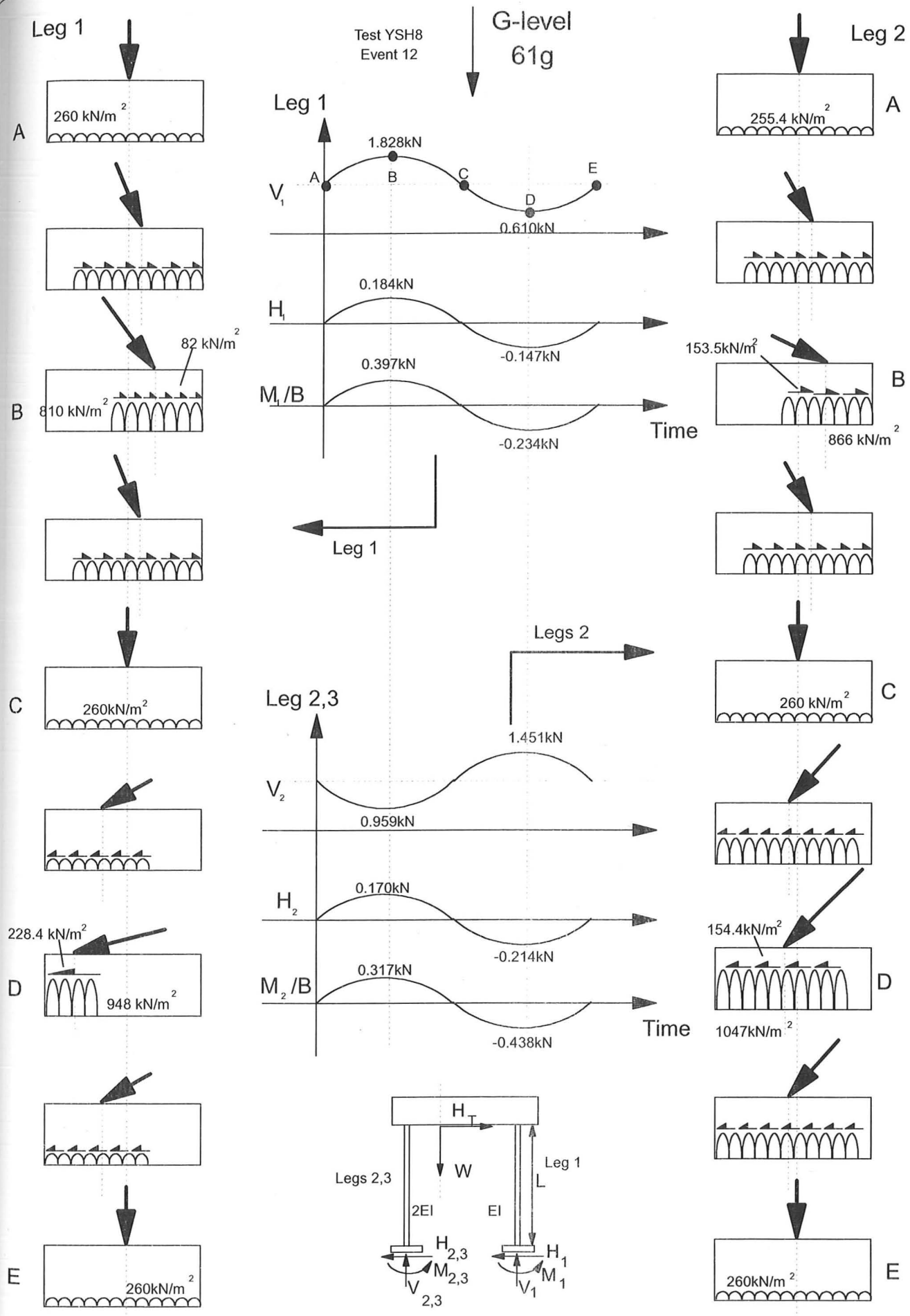

Fig. 4.12 Stresses transferred to soil

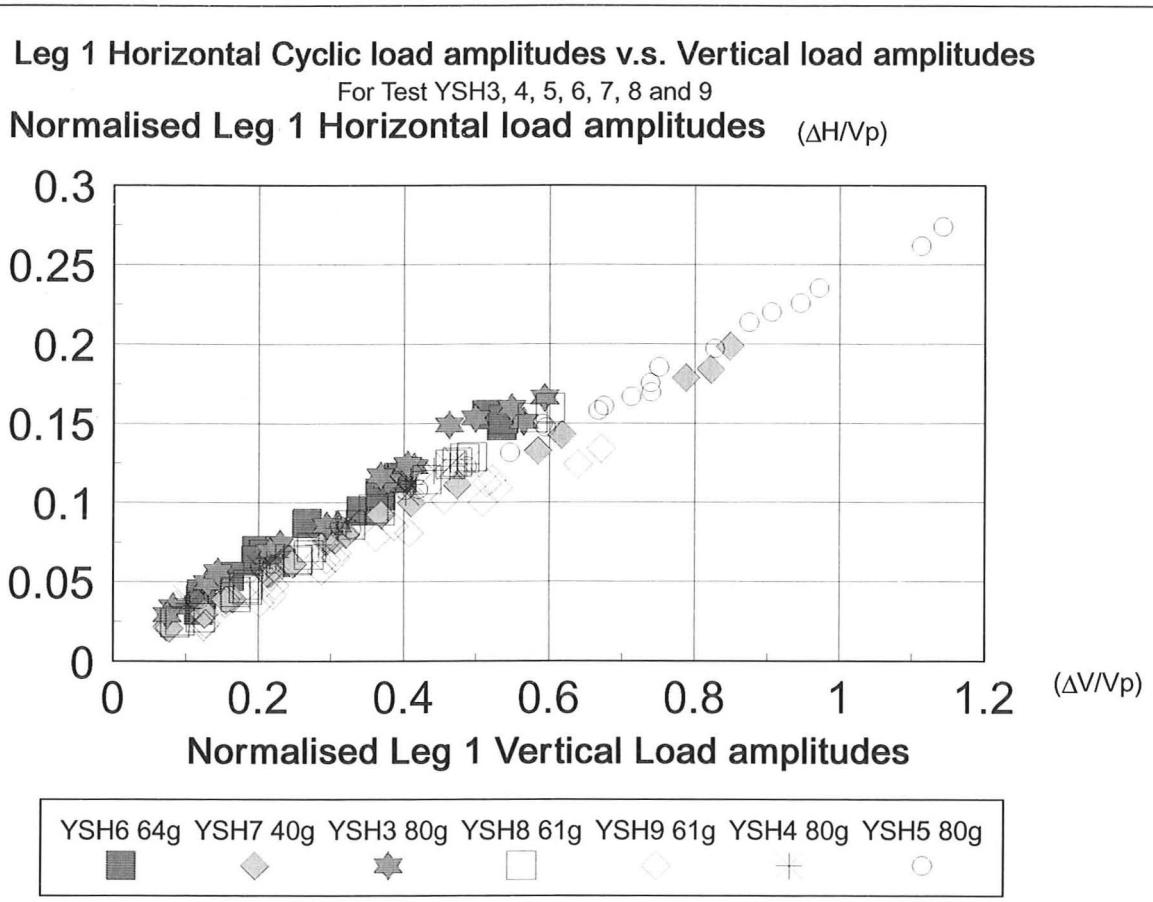

(a)

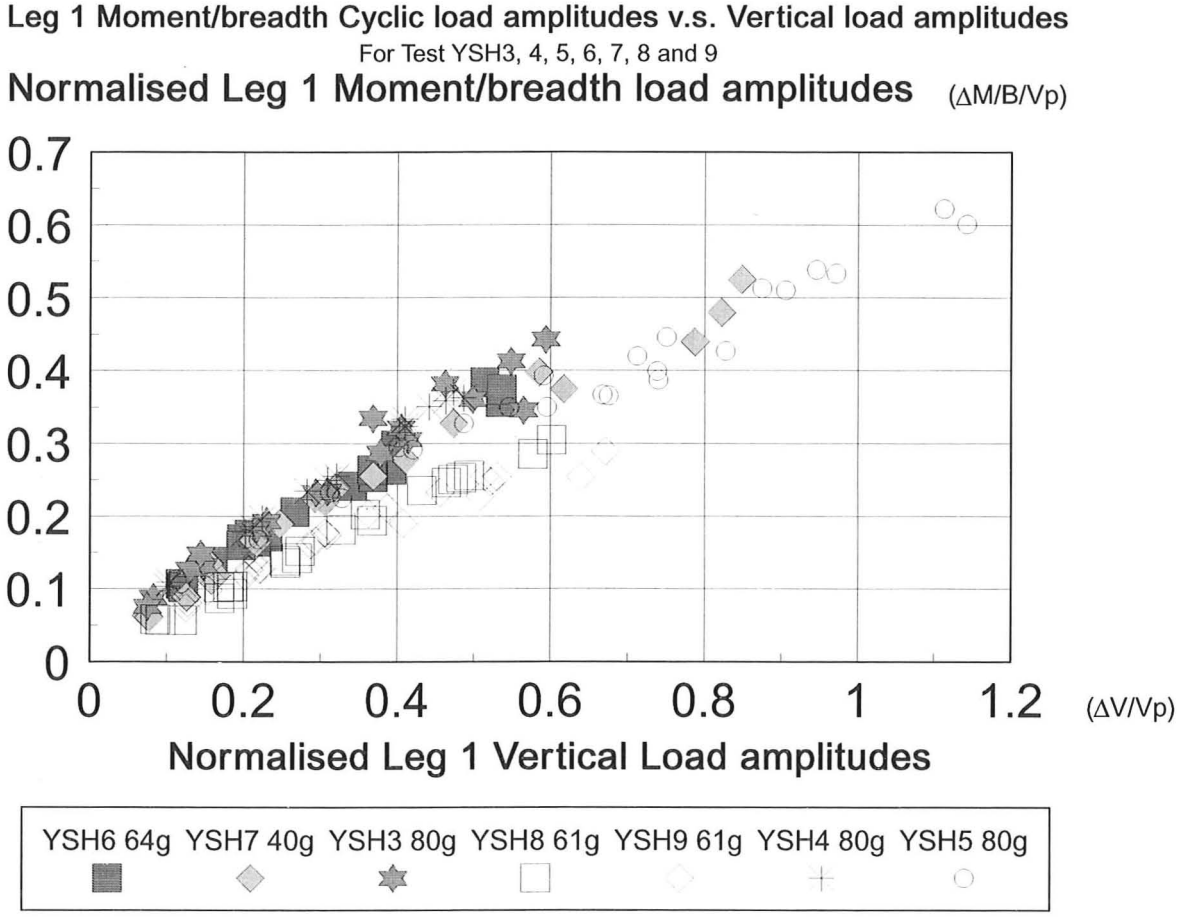

(b)

Fig. 4.13 Normalised load amplitude plots for Leg 1

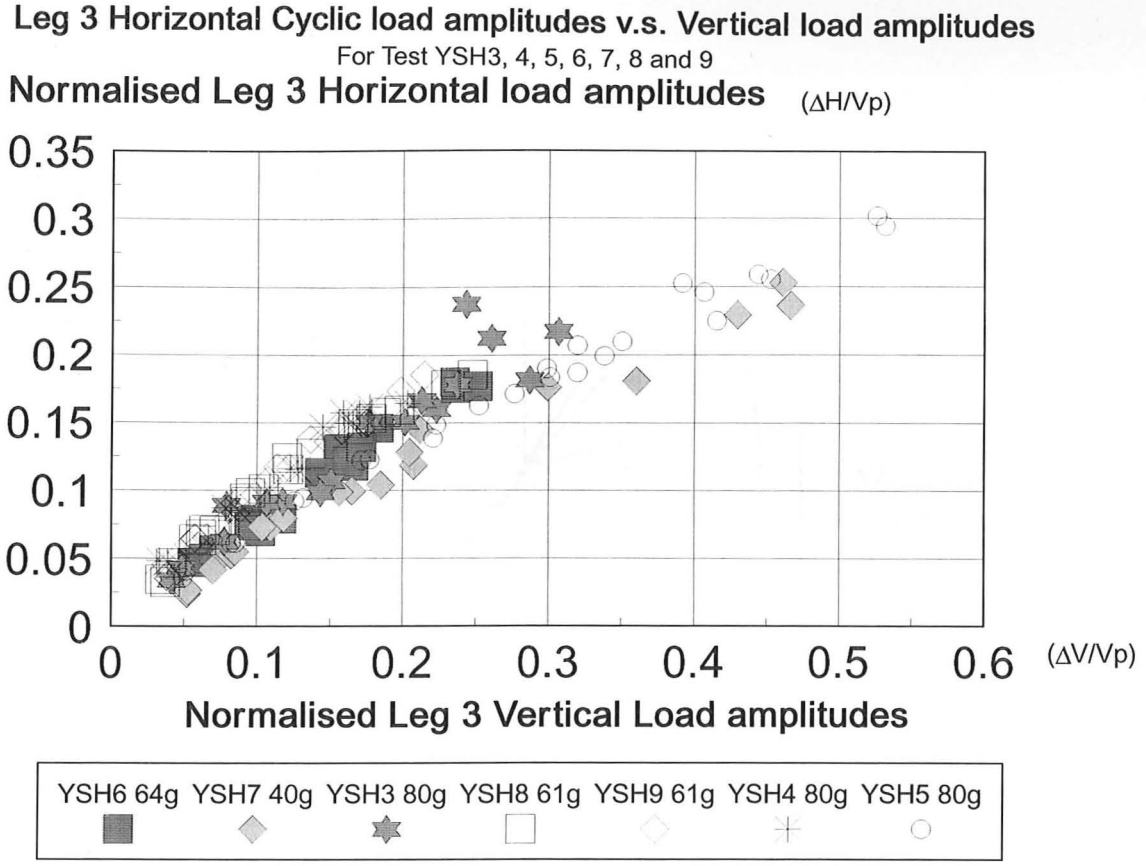

(a)

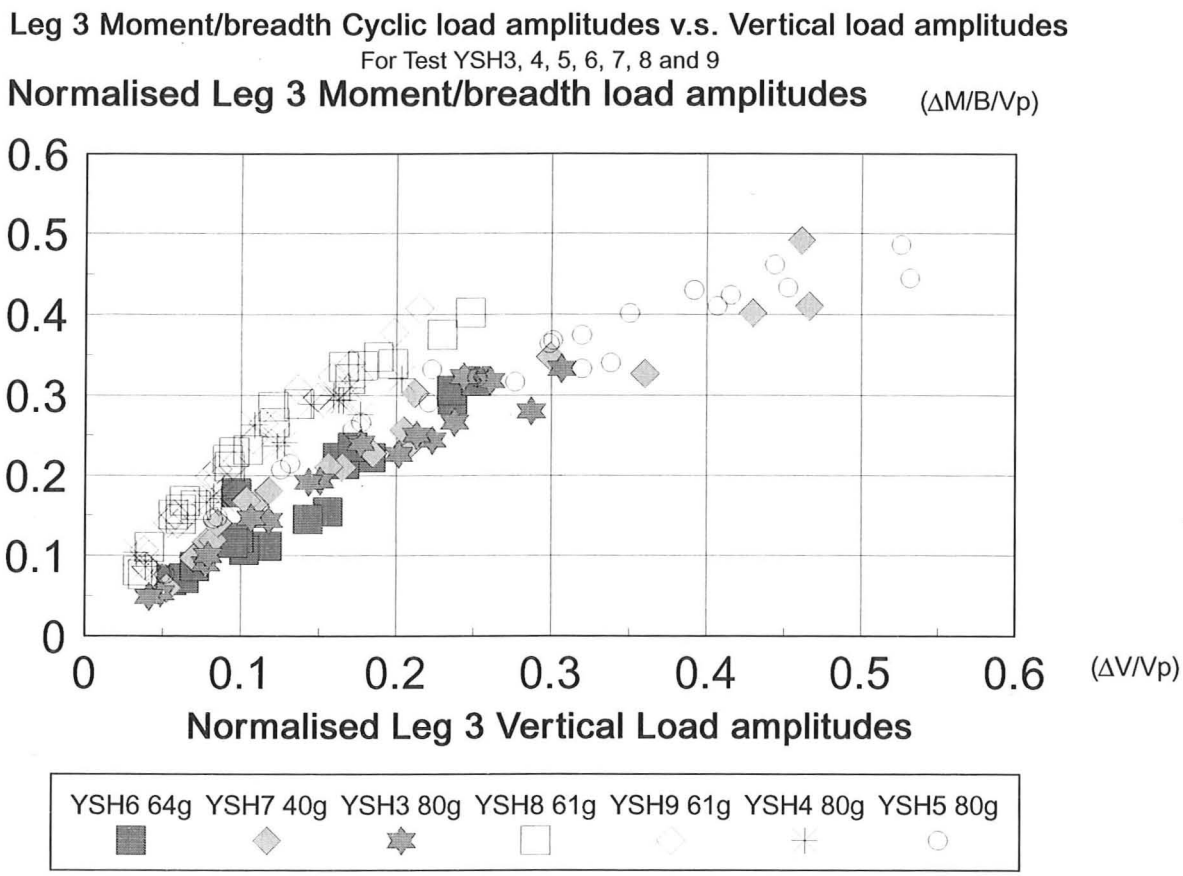

(b)

Fig. 4.14 Normalised load amplitude plots for Leg 3

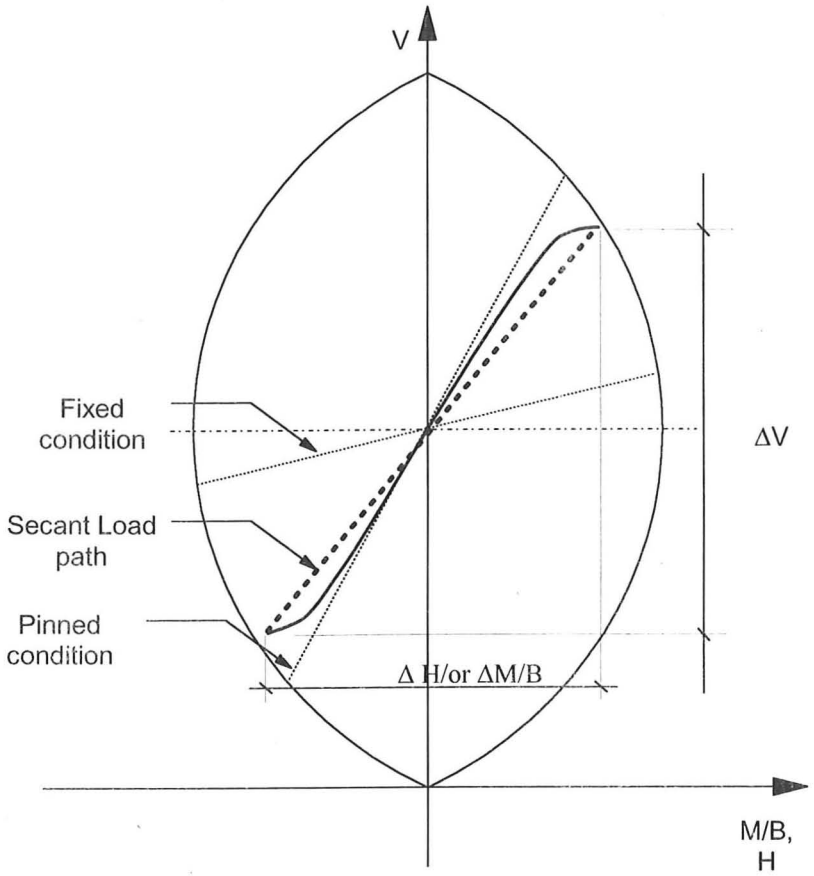

Fig. 4.15a Simplified Secant Load Path

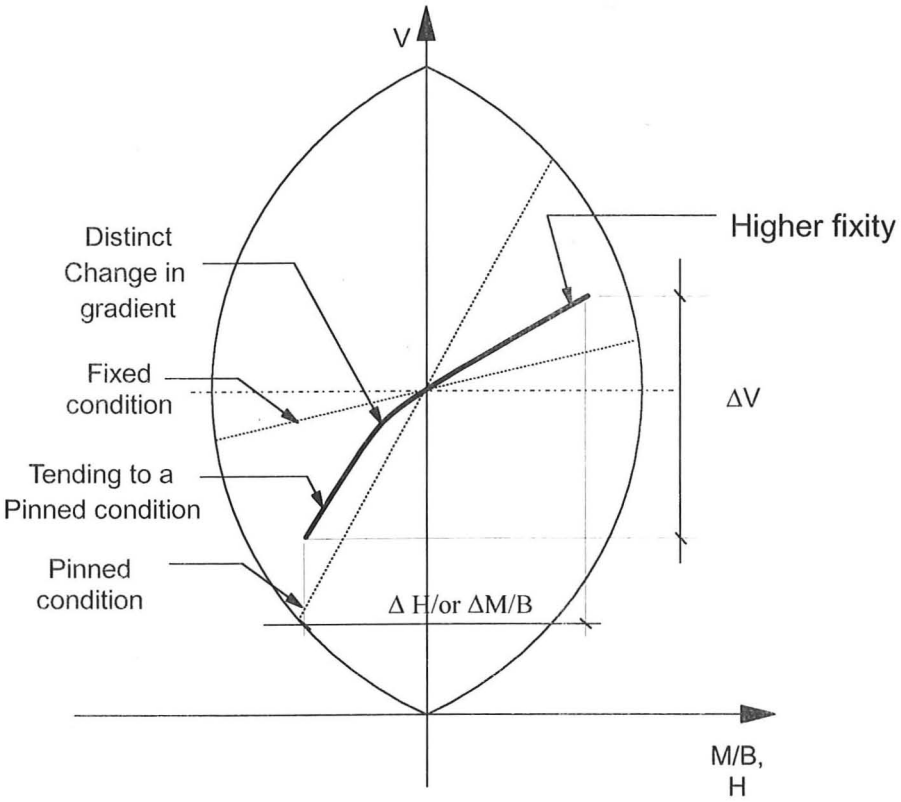

Fig. 4.15b Typical Load Path reducing in stiffness

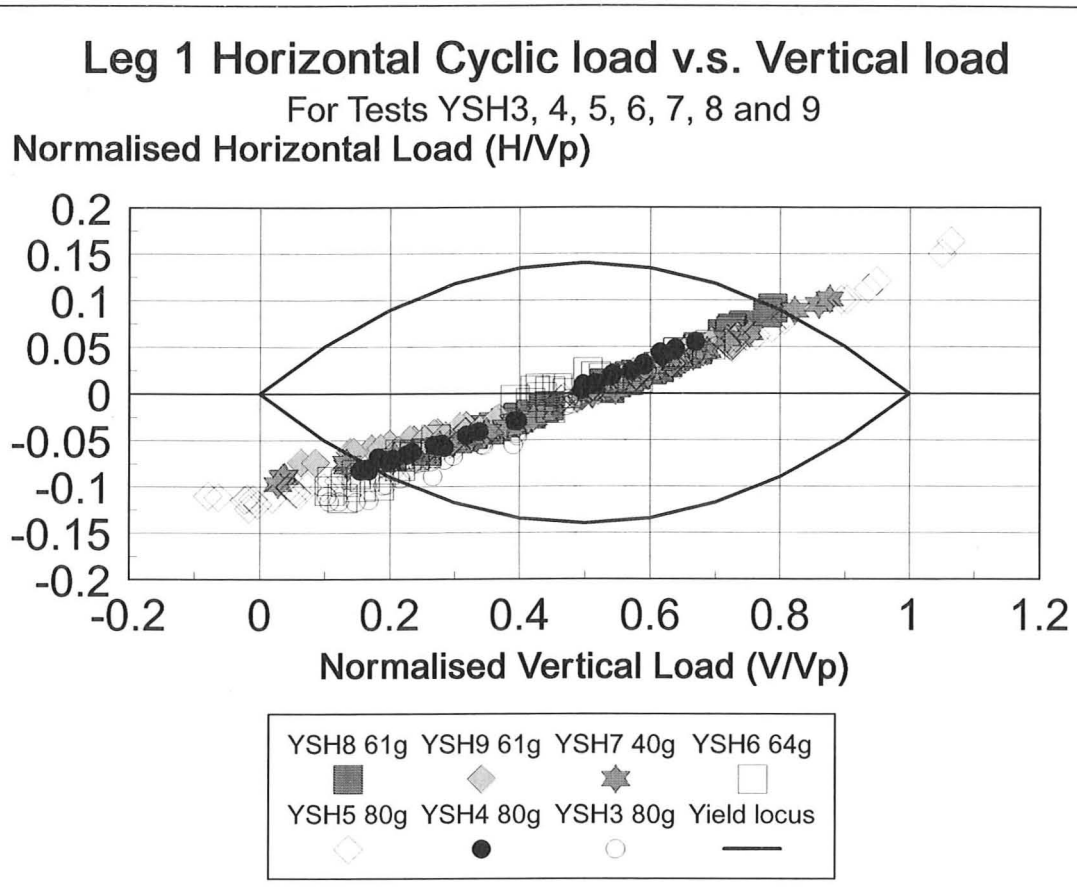

(a)

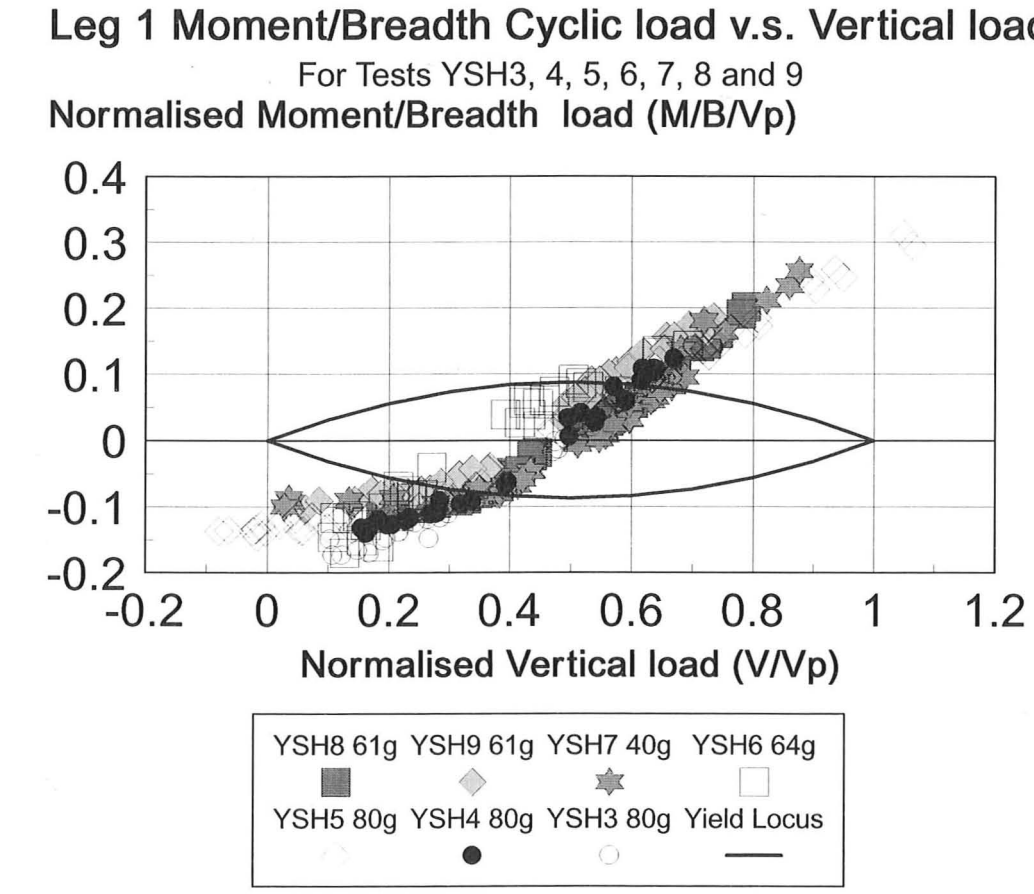

(b)

Fig. 4.16 General Load Path pattern for Leg 1

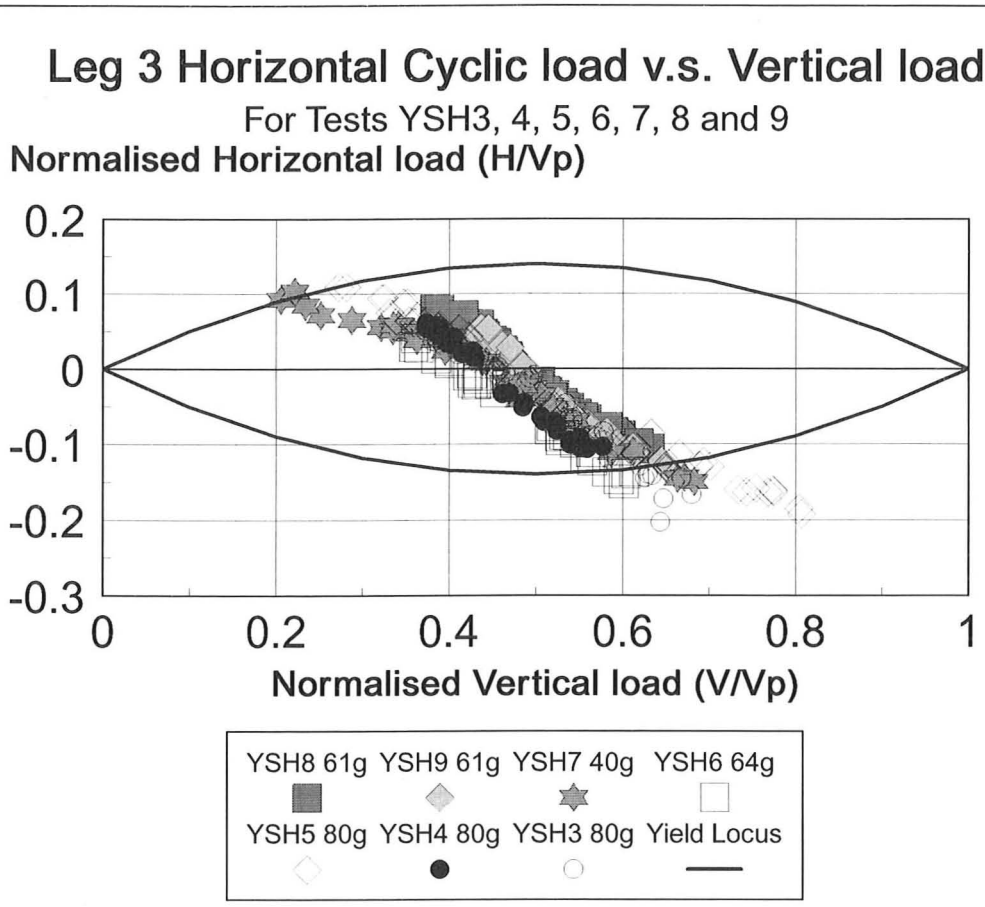

(a)

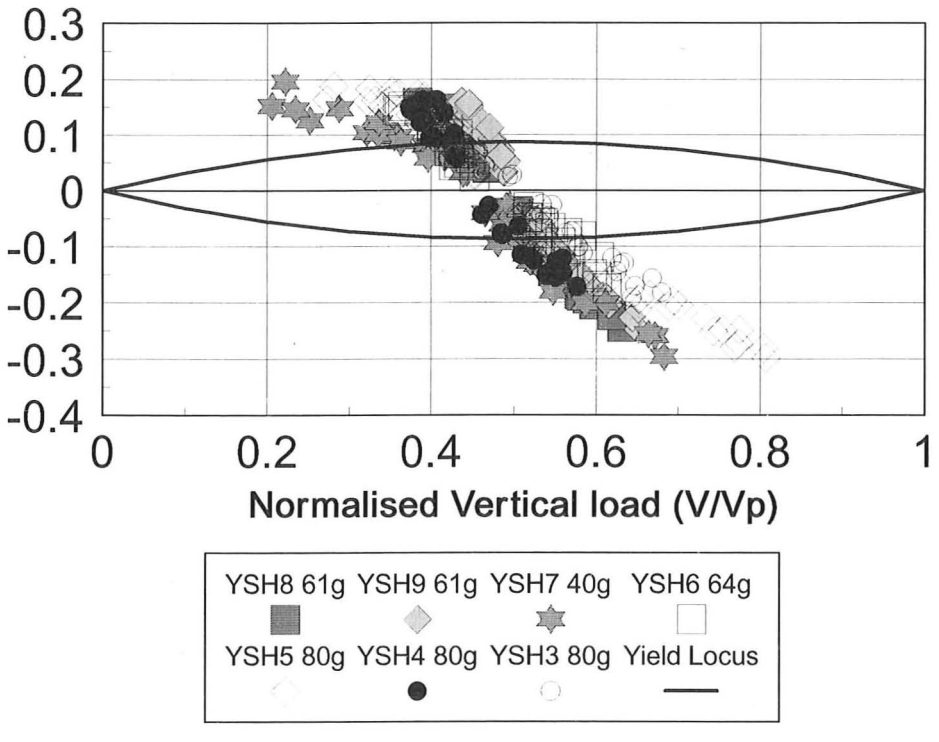

(b)

Fig. 4.17 General Load Path pattern for Leg 3

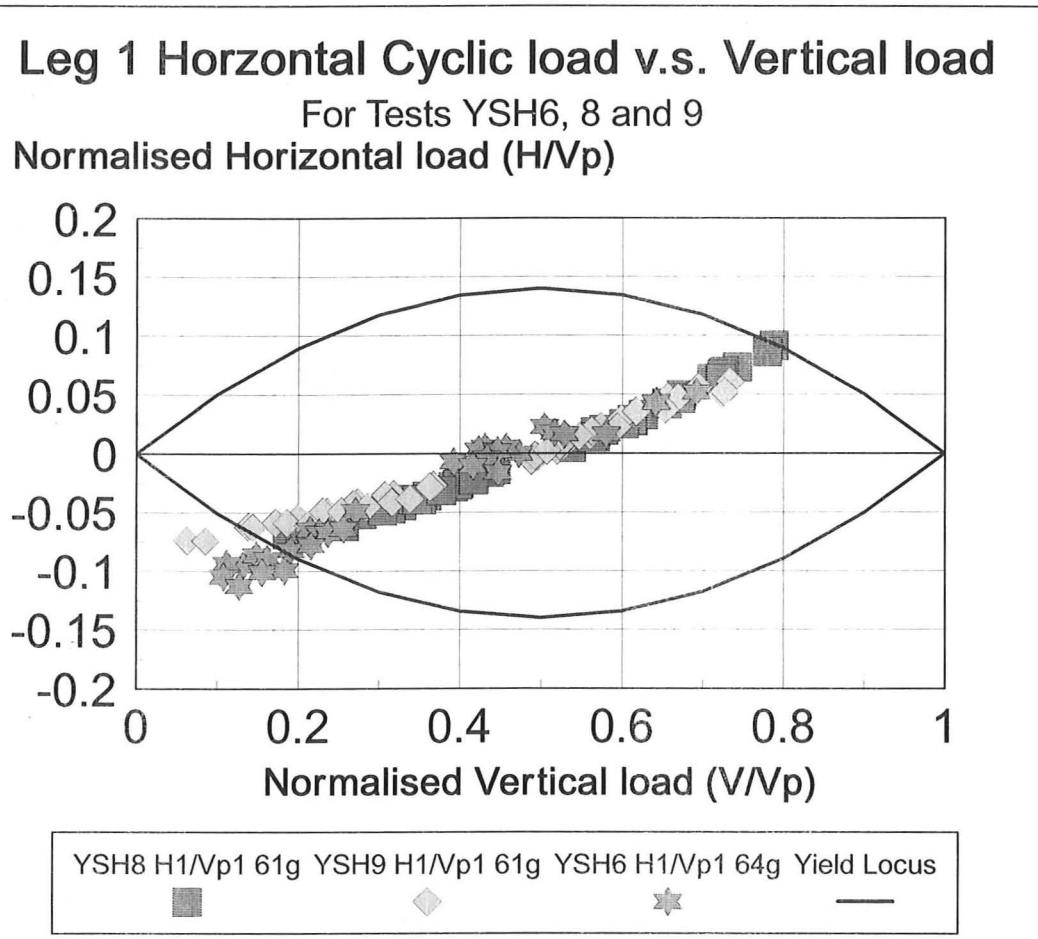

(a)

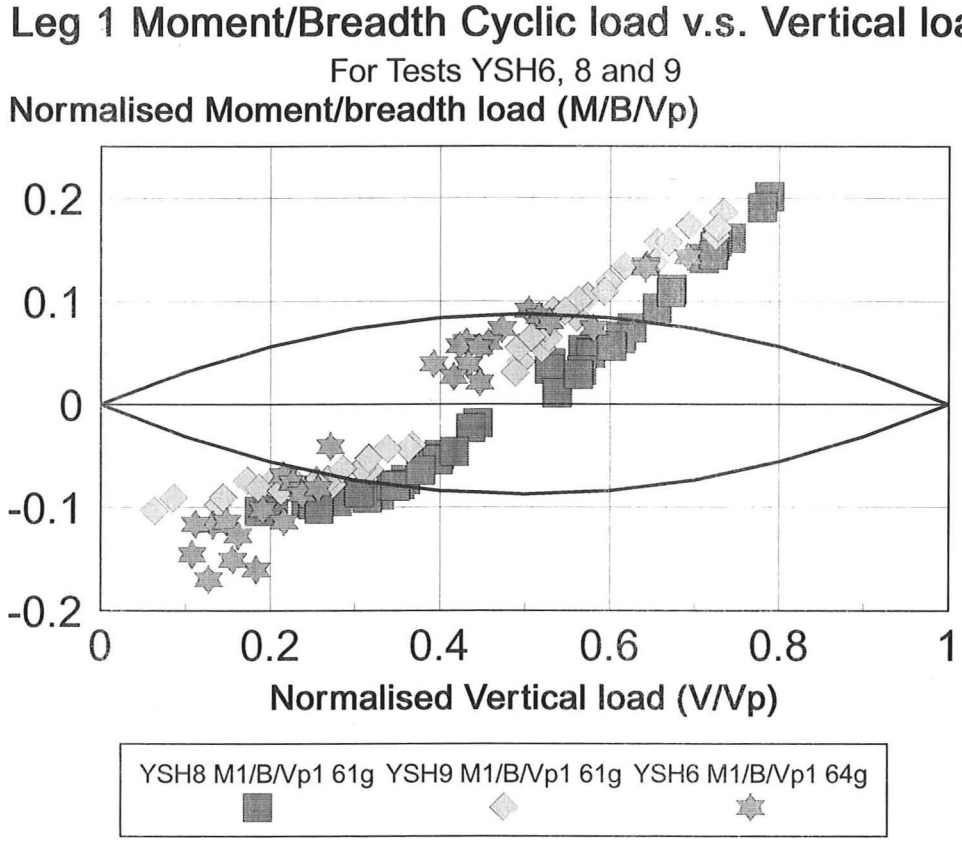

(b)

Fig. 4.18 Partially Drained and Drained Comparison for Leg 1

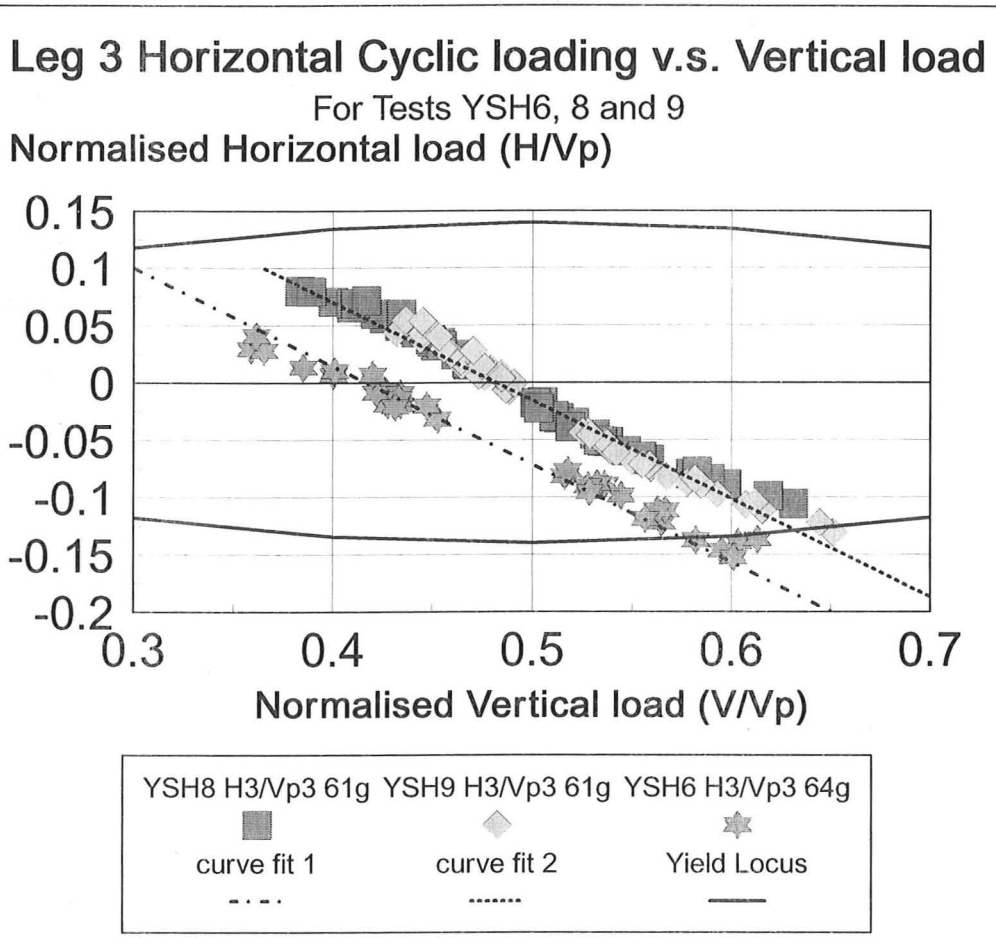

(a)

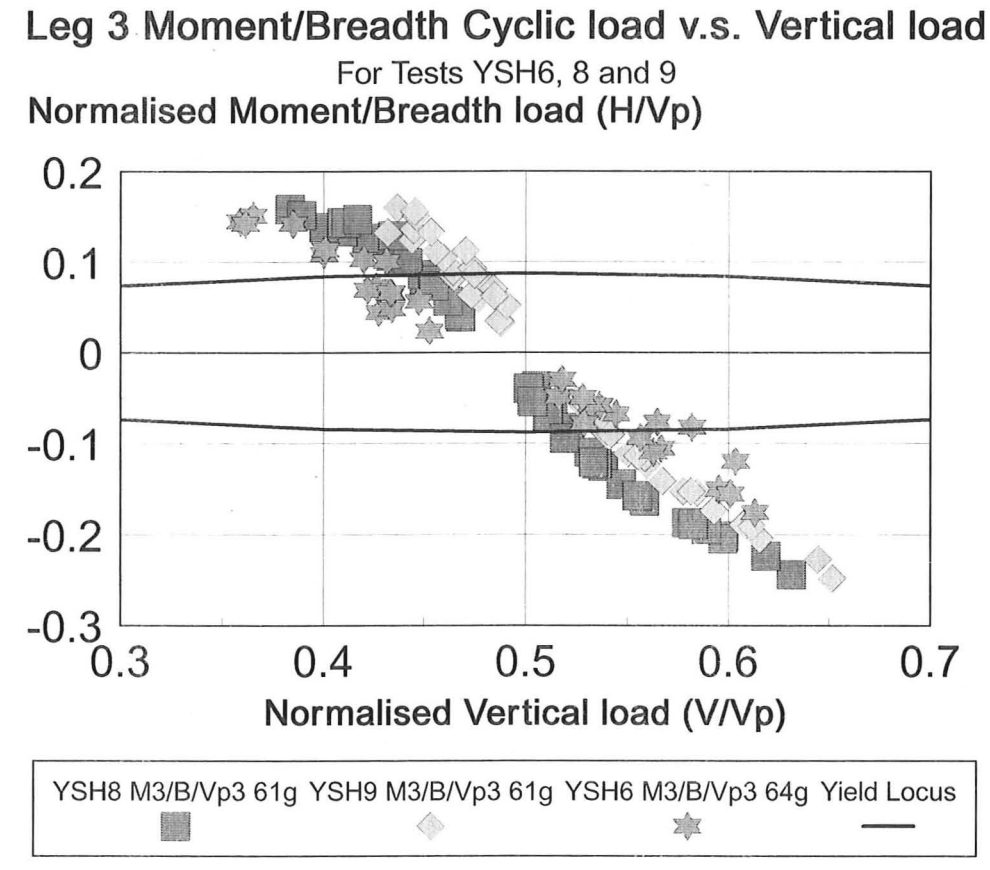

(b)

Fig. 4.19 Partially Drained and Drained Comparison for Leg 3

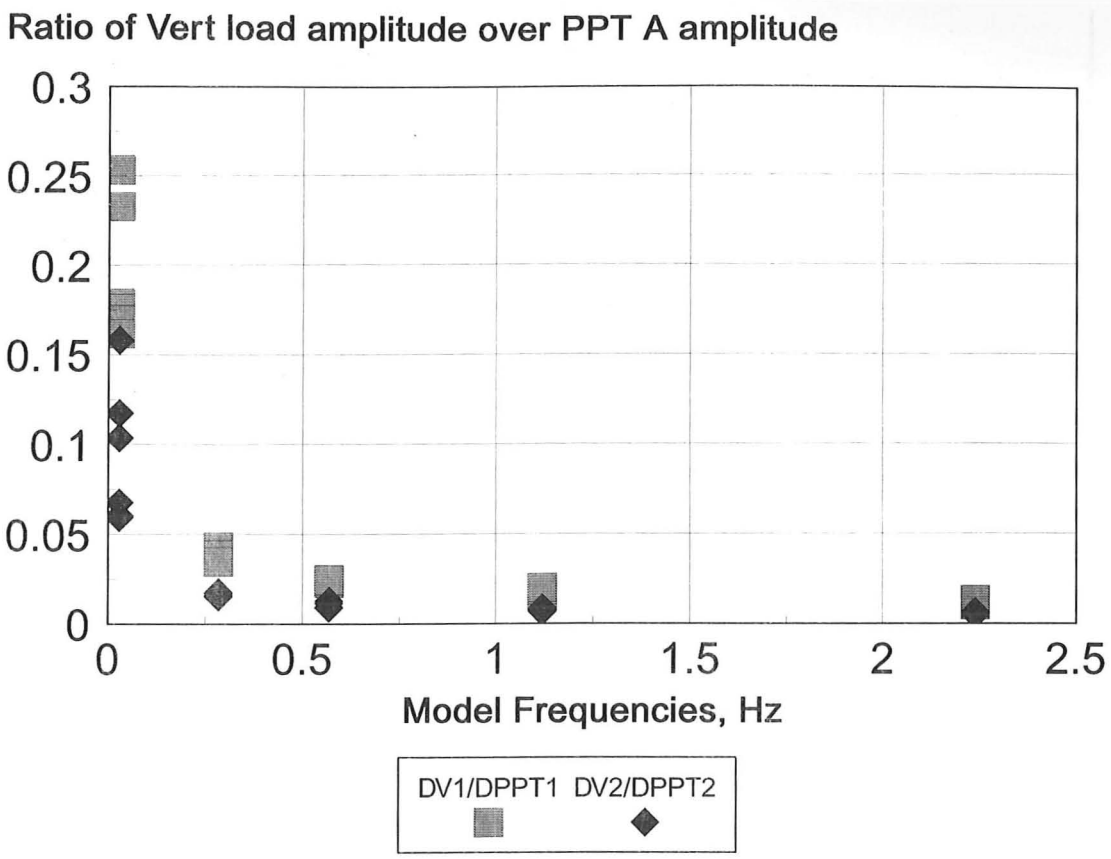
Ratio of Vert load amplitude over PPT A amplitude
0.3
0.25
0.2
0.15
0.1
0.05
0
0
0.5
1
1.5
2
2.5
Model Frequencies, Hz
DV1/DPPT1
DV2/DPPT2

(a)

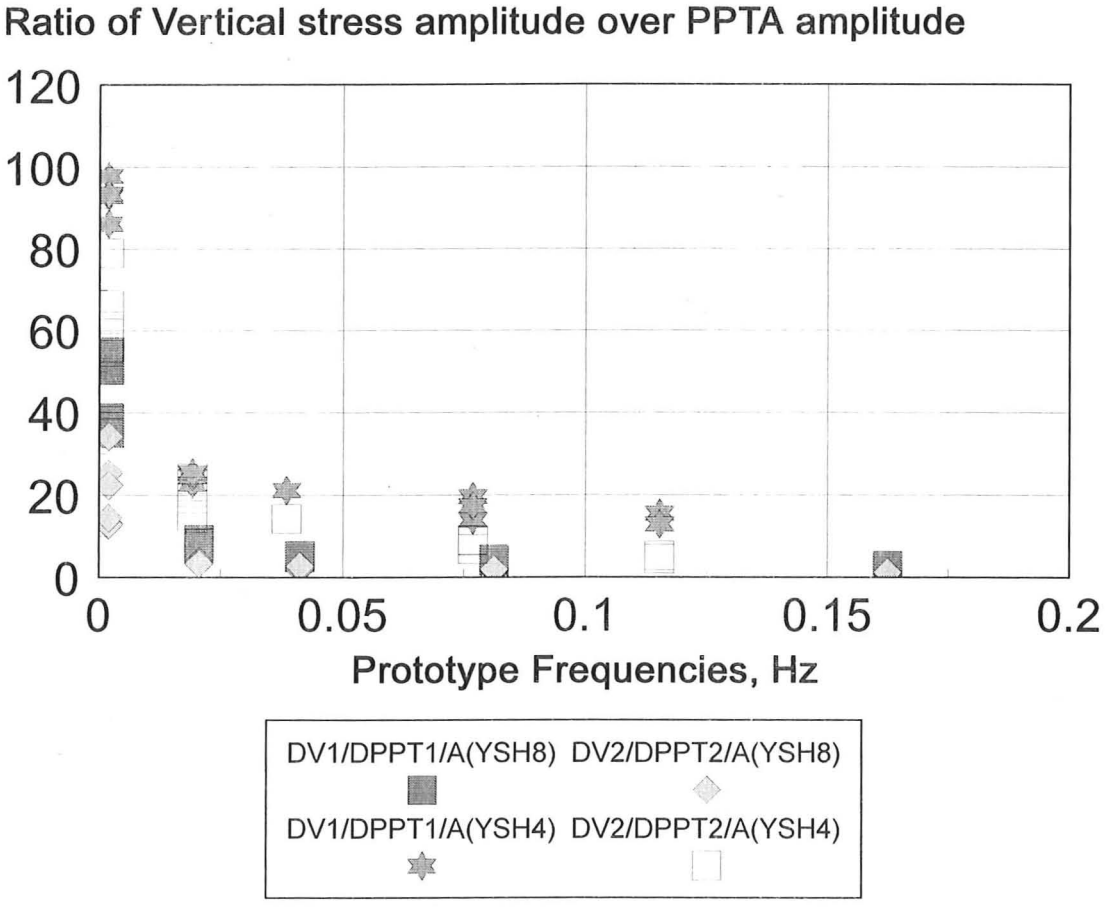
Ratio of Vertical stress amplitude over PPTA amplitude
120
100
80
60
40
20
0
0
0.05
0.1
0.15
0.2
Prototype Frequencies, Hz
DV1/DPPT1/A(YSH8)
DV2/DPPT2/A(YSH8)
DV1/DPPT1/A(YSH4)
DV2/DPPT2/A(YSH4)

(b)

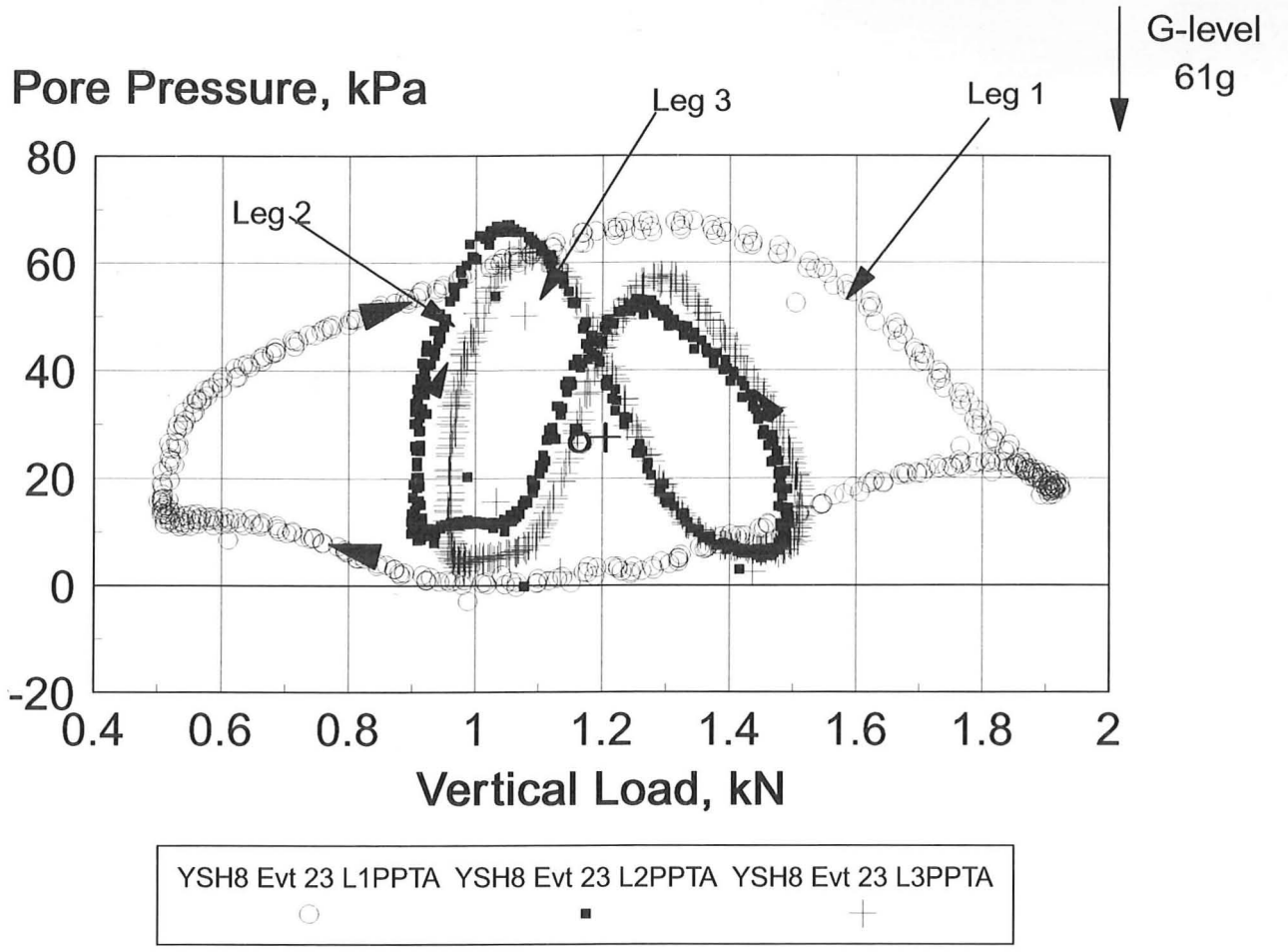

(a)

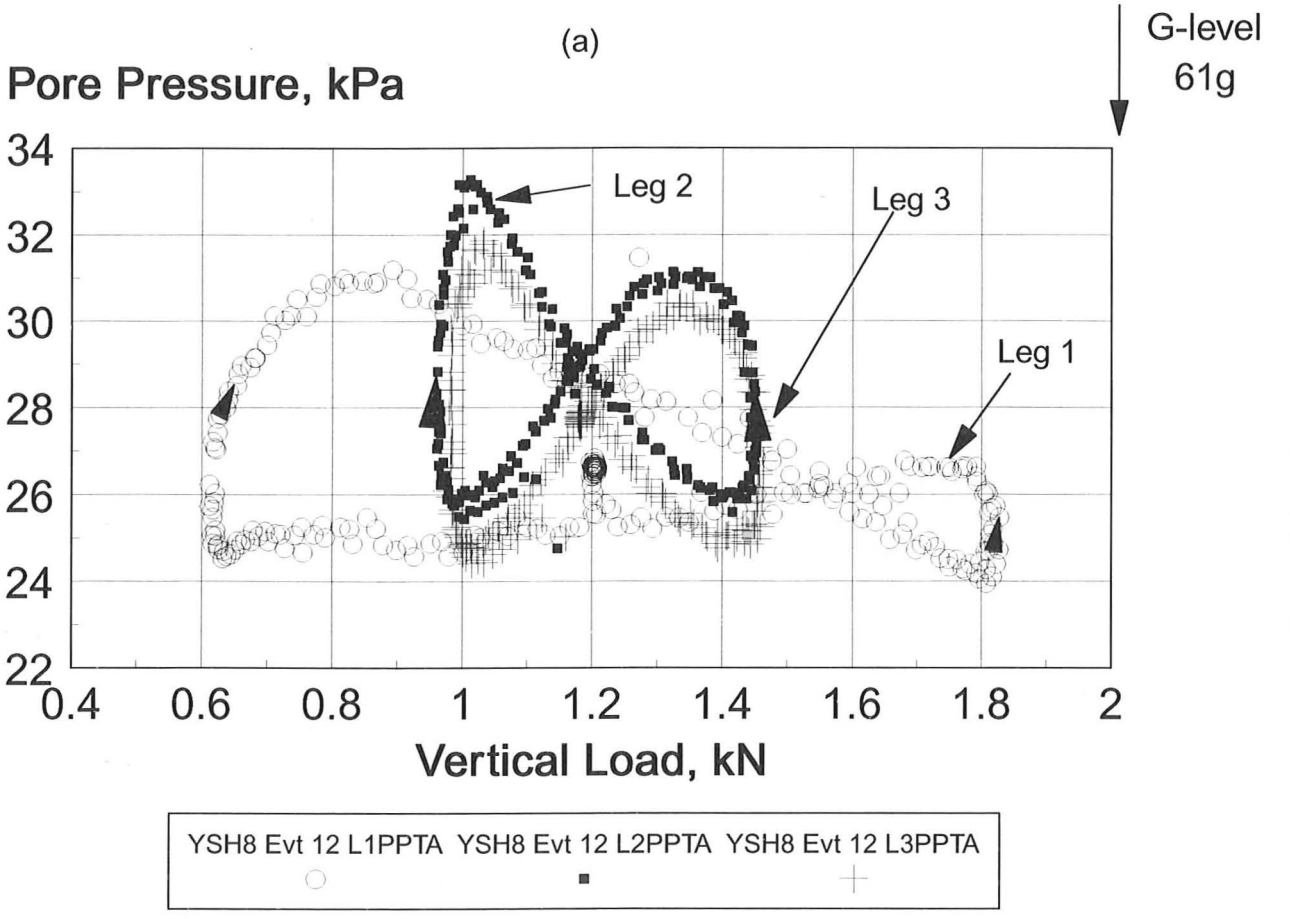

(b)

Fig. 4.21 Pore Pressure Patterns for Fast and Slow Cyclic loading

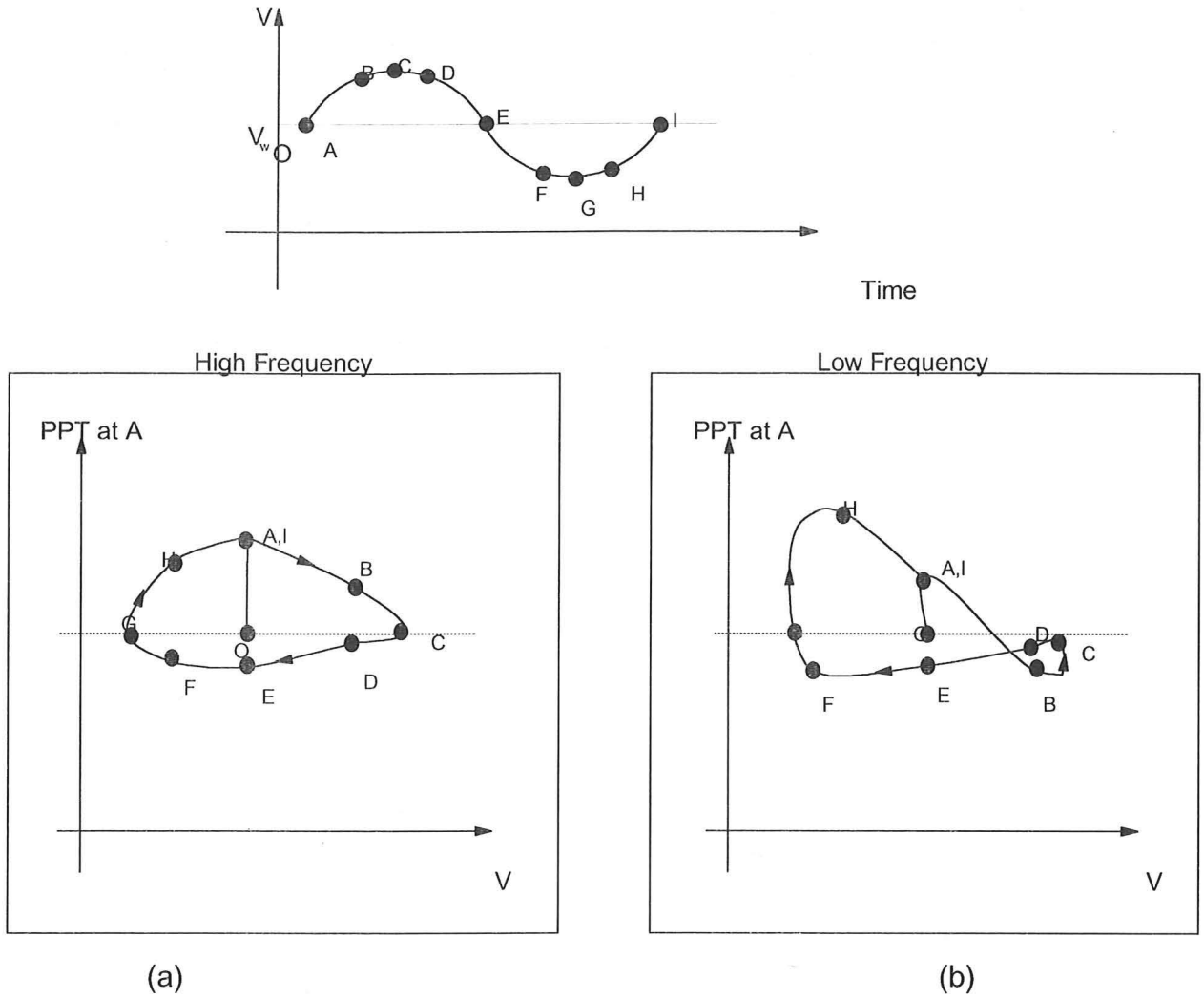

Fig. 4.22 Hypothesis for Pore pressure Patterns

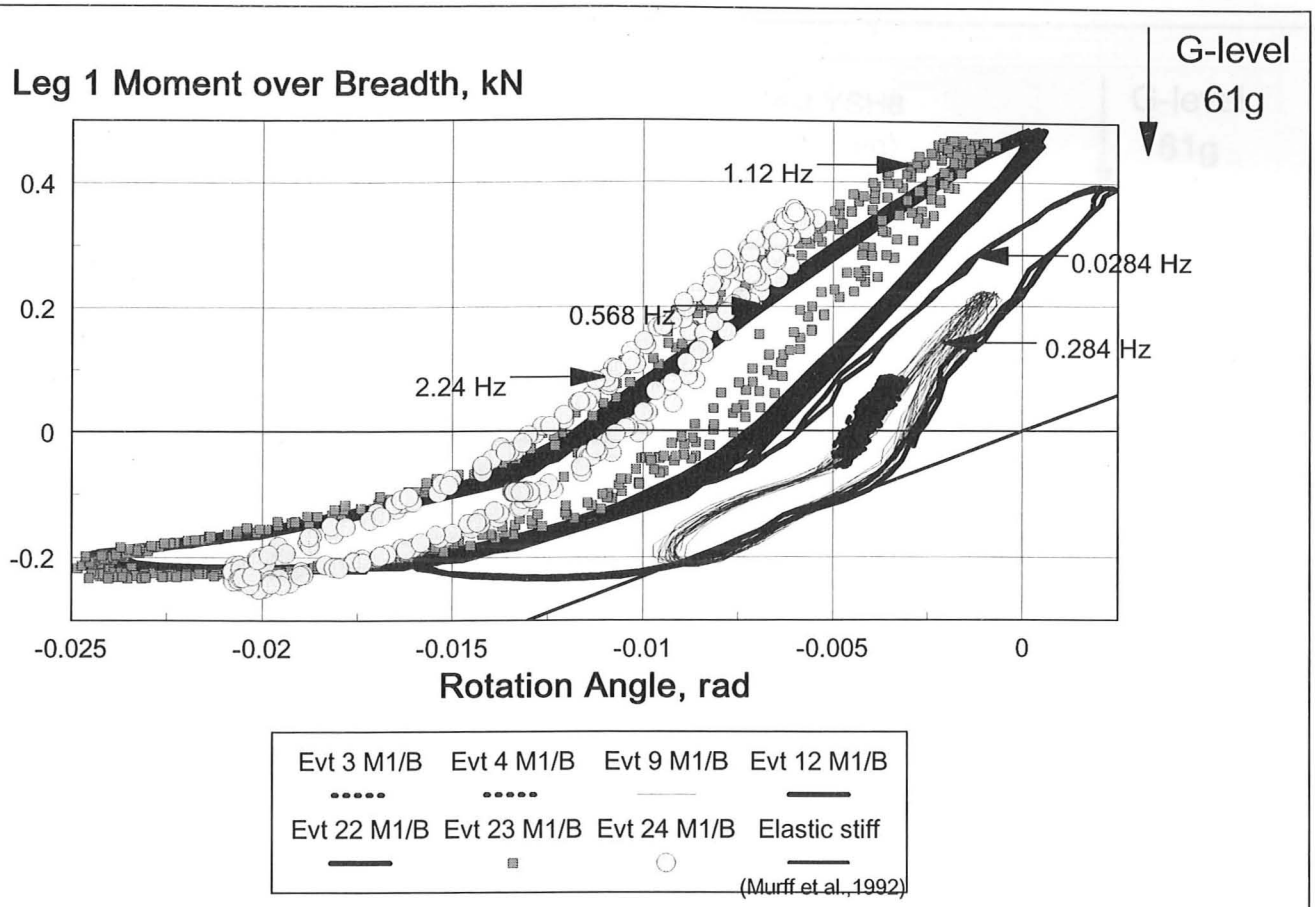

(a)

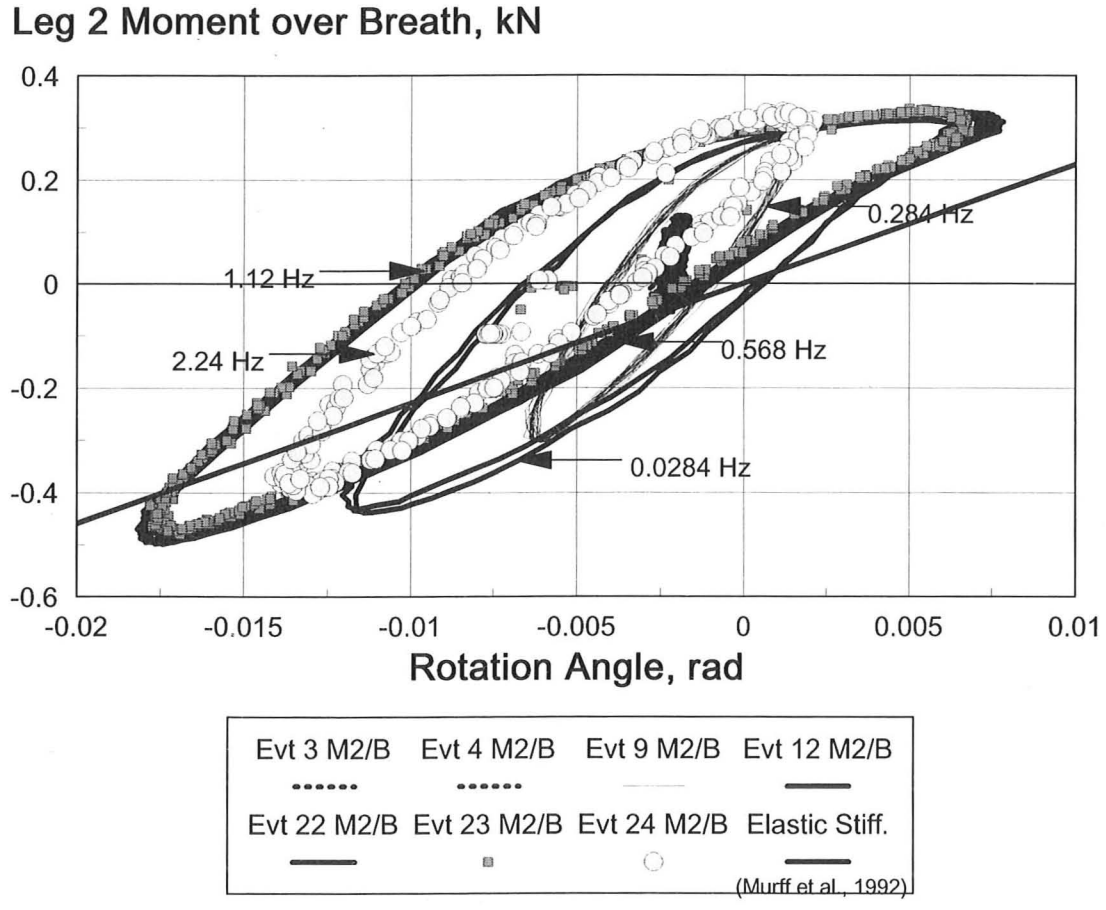

(b)

Fig. 4.23 Moment Stiffness for Leg 1 and Leg 2

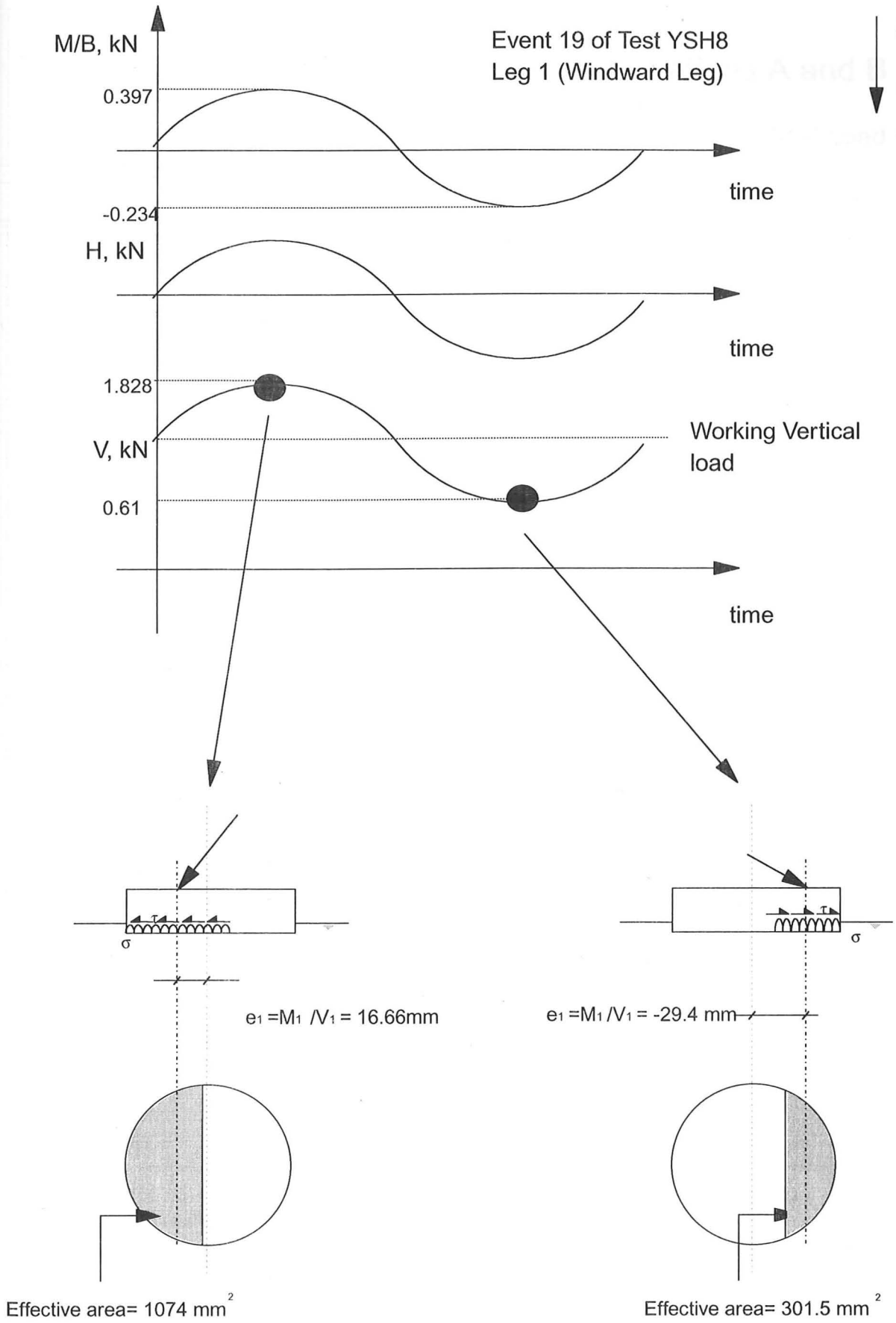

Fig. 4.24 Variation of Effective area with Load Sequence

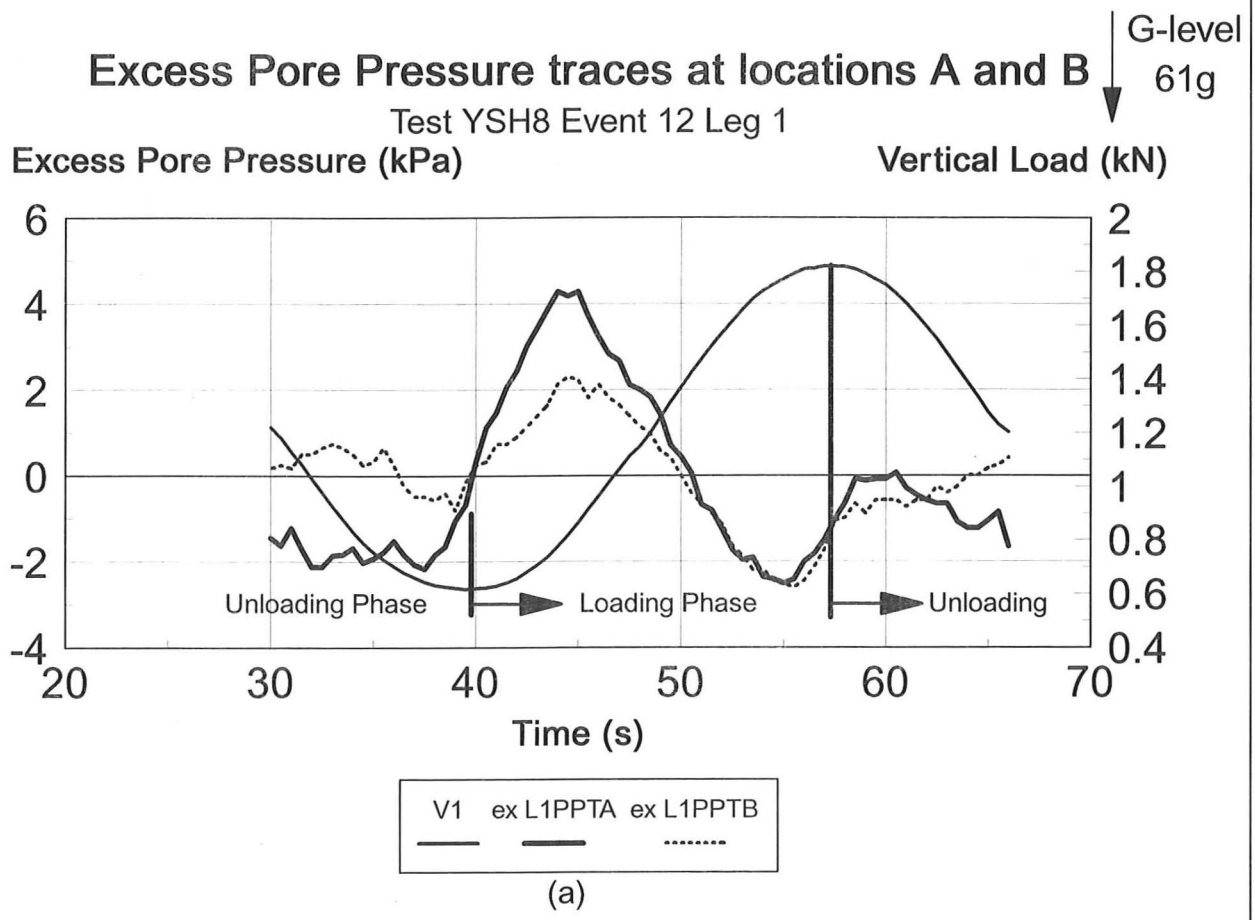

(a)

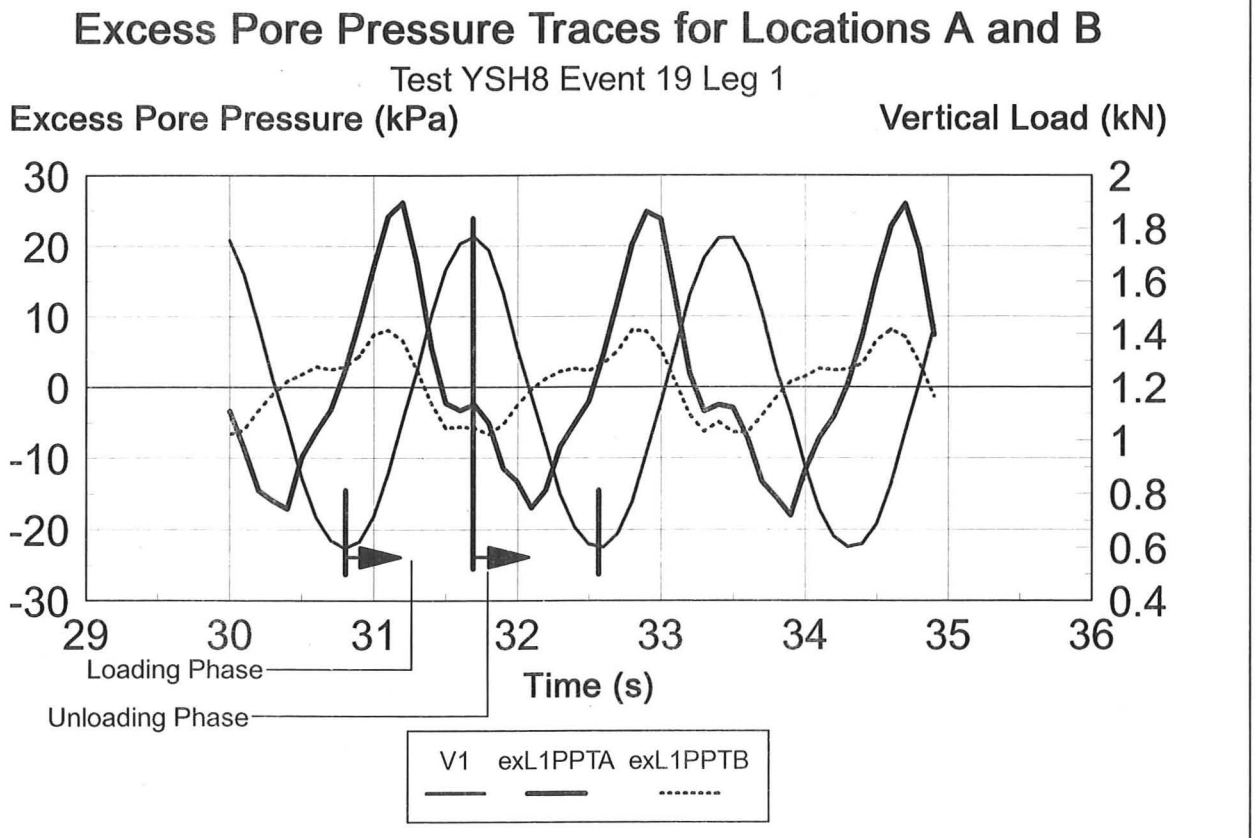

(b)

Fig. 4.25 Traces of Excess Pore Pressure at A and B superimposed with the vertical load variation

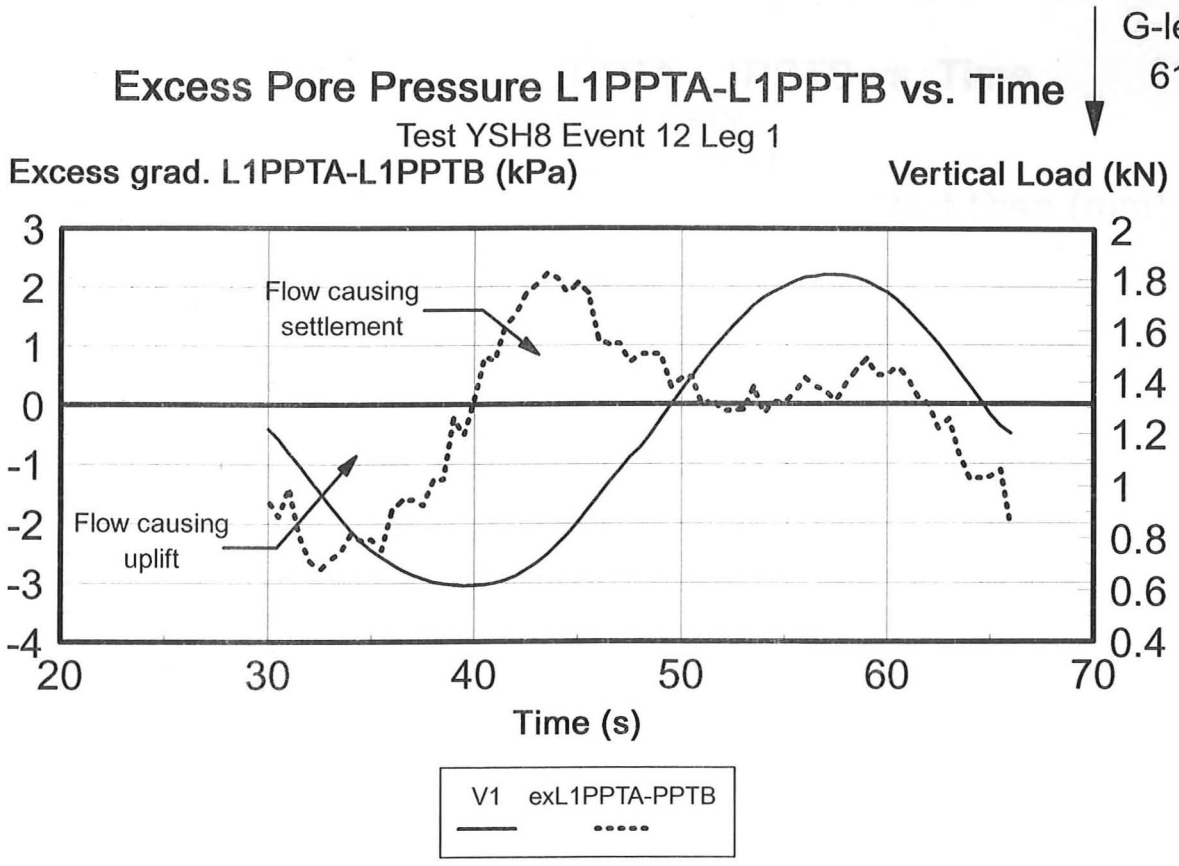

(a)

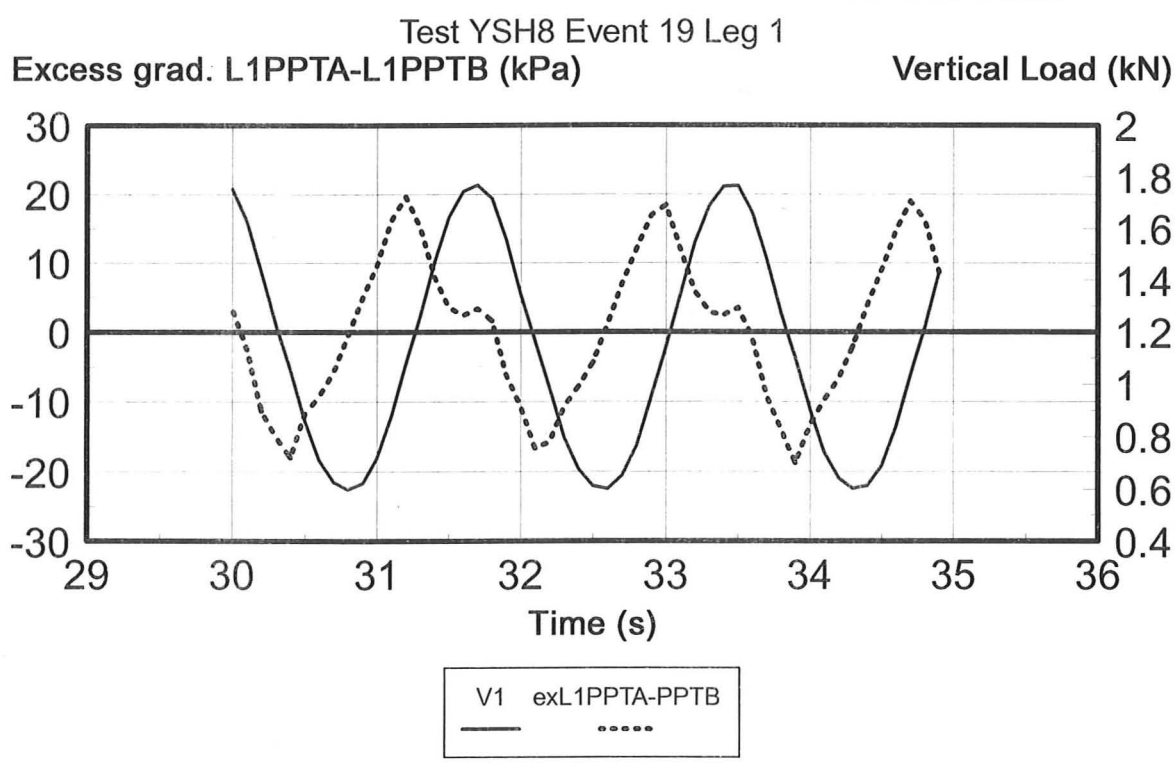

(b)

Fig. 4.26 Difference in Pore Pressure between A and B related to the hydraulic gradient

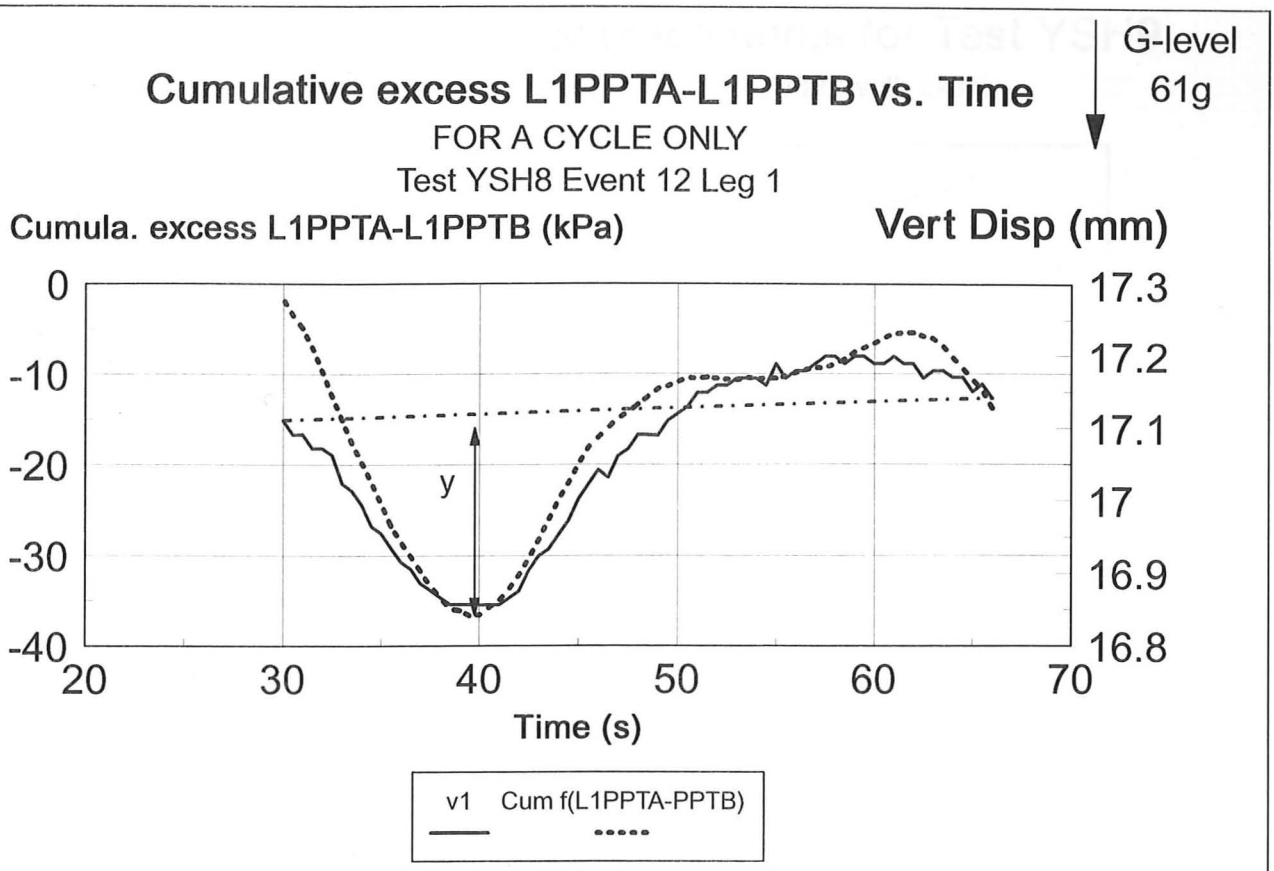

(a)

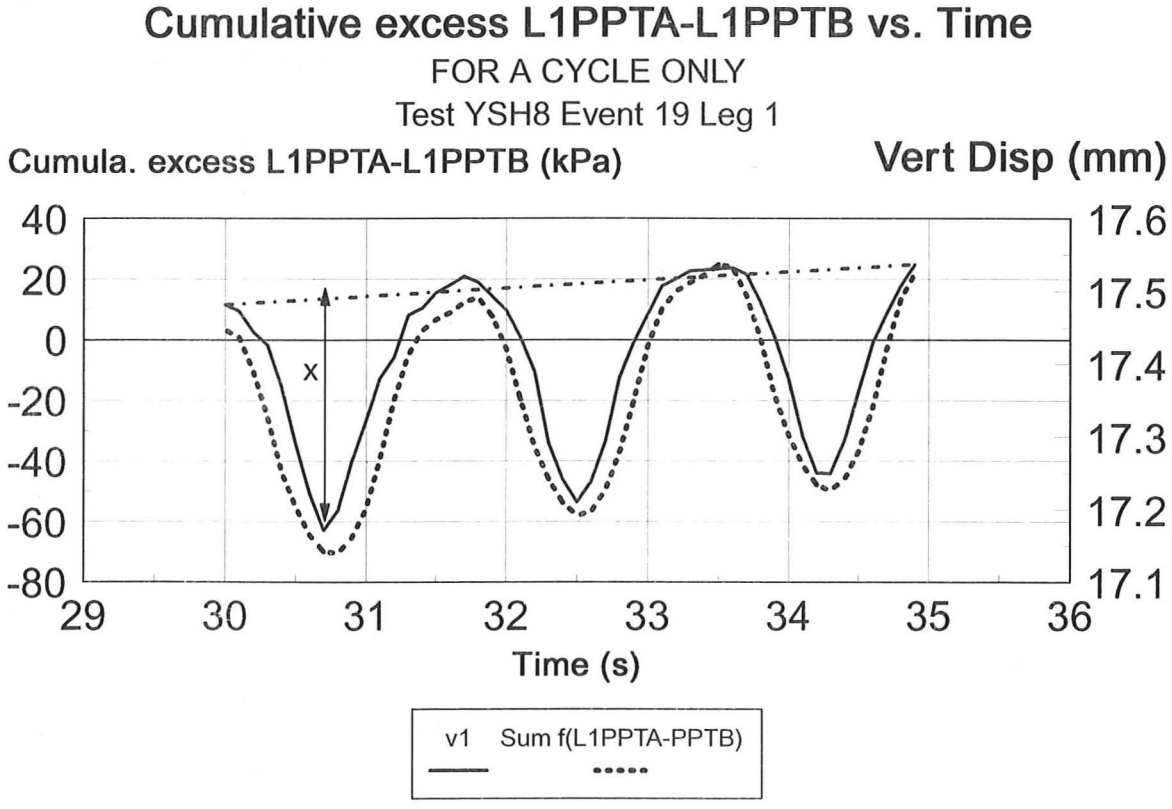

(b)

Fig. 4.27 Sum of diff. of Pore Pressure between A and B superimposed with the vertical settlements under Leg 1

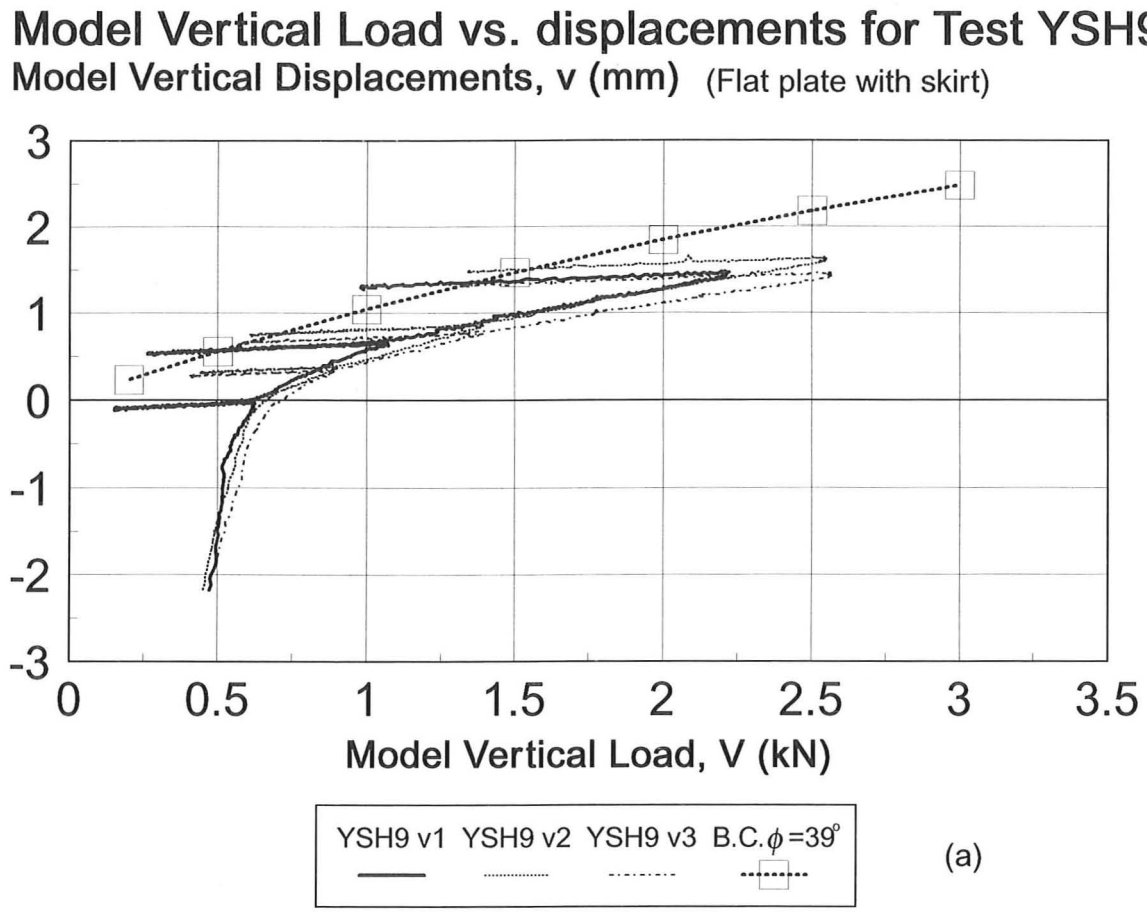

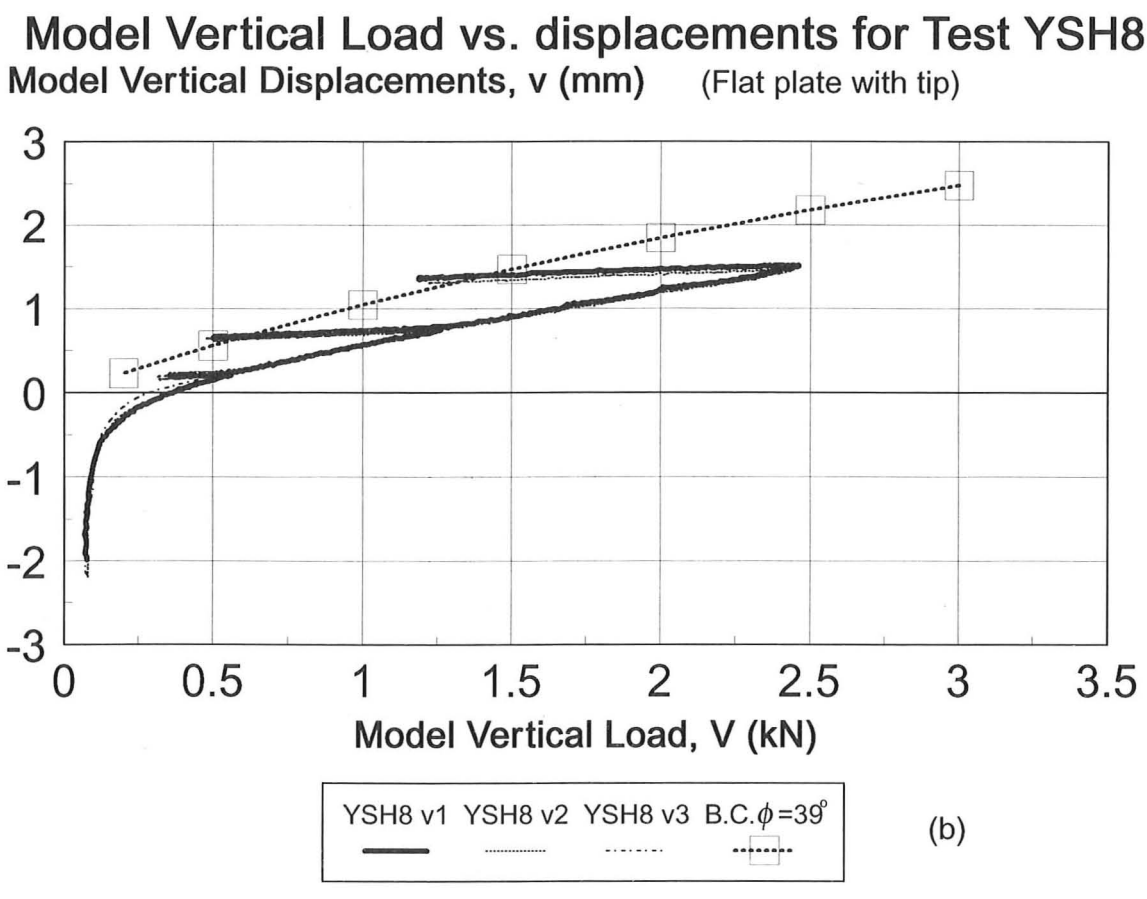

Fig. 5.1 Vertical displacements and vertical load profile for preload event

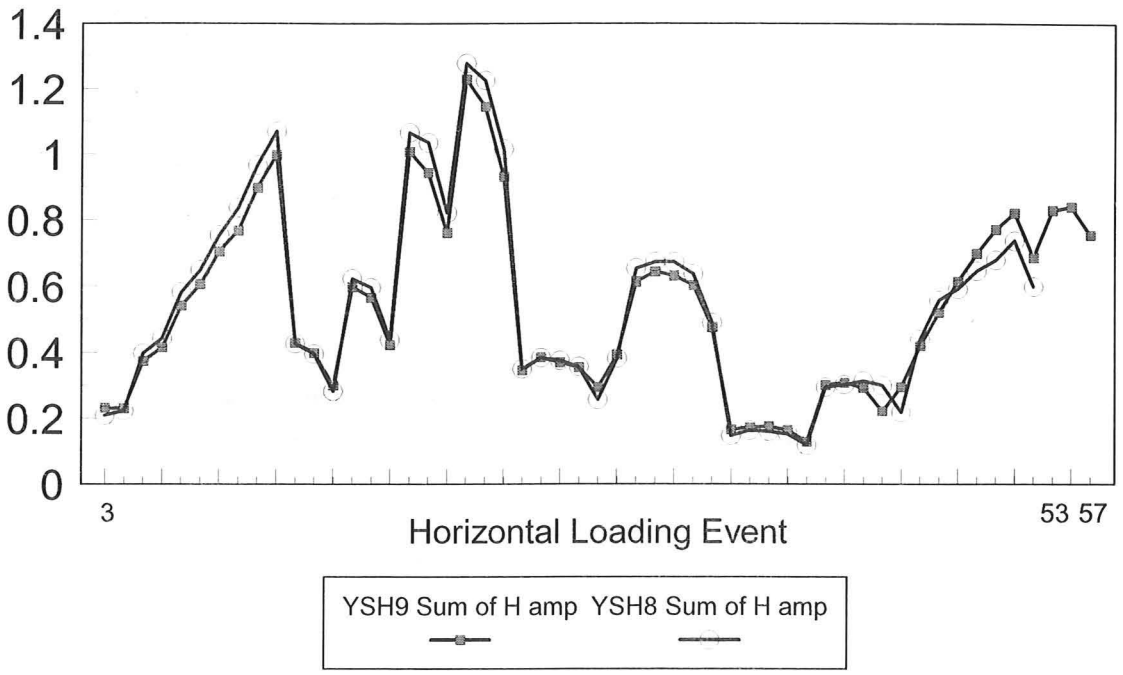

Fig. 5.2 Total horizontal load amplitude for test YSH8 and YSH9

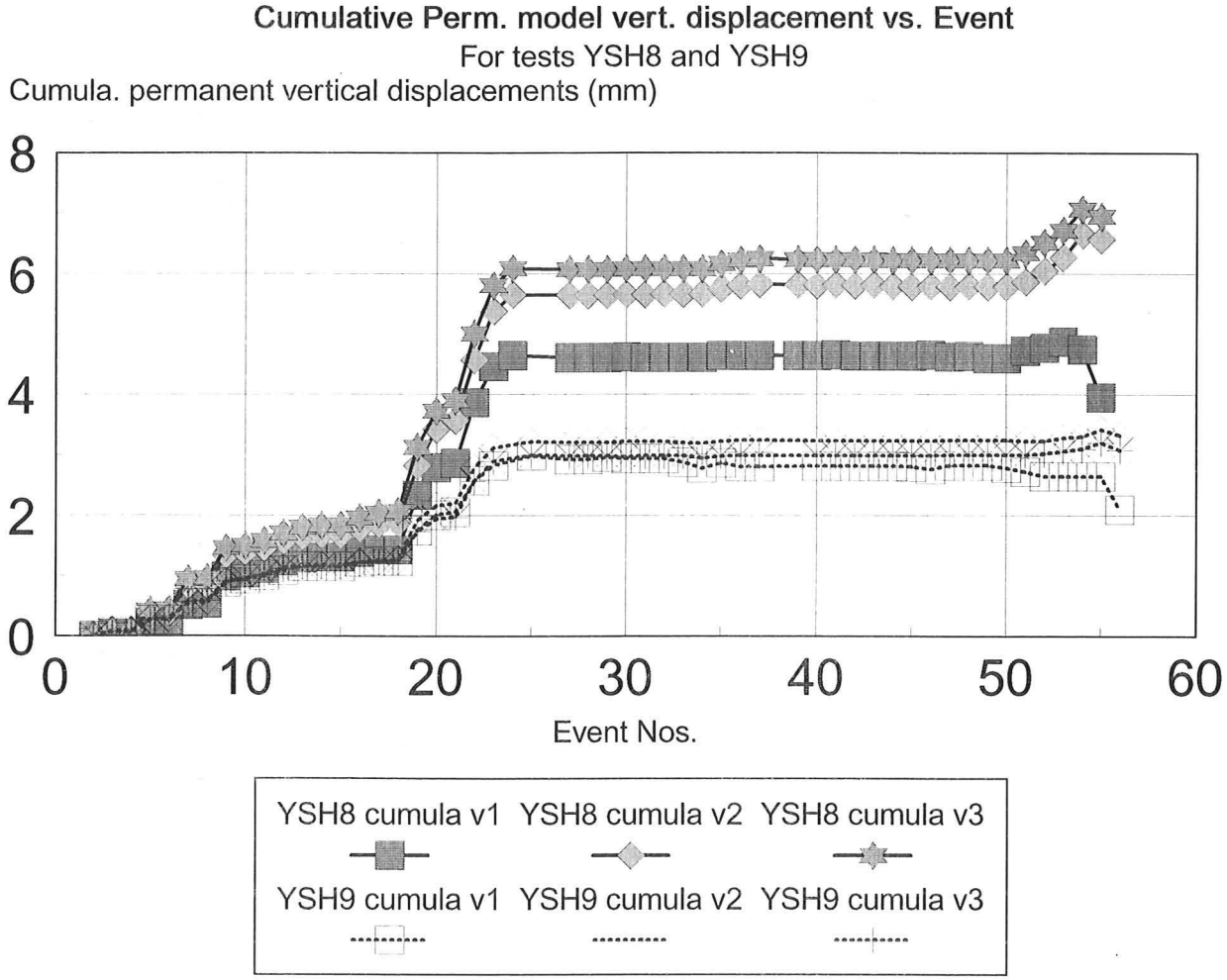

Fig. 5.3 Cumulative settlement profile for both tests YSH8 and YSH9

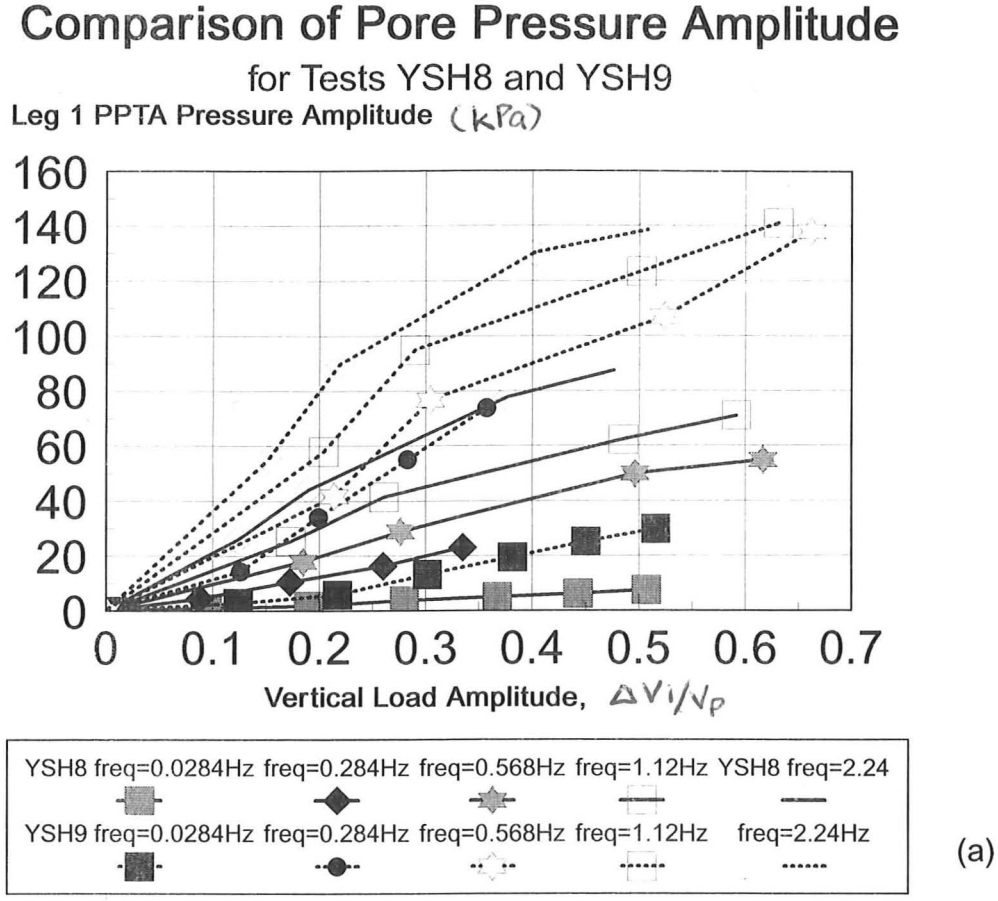

(a)

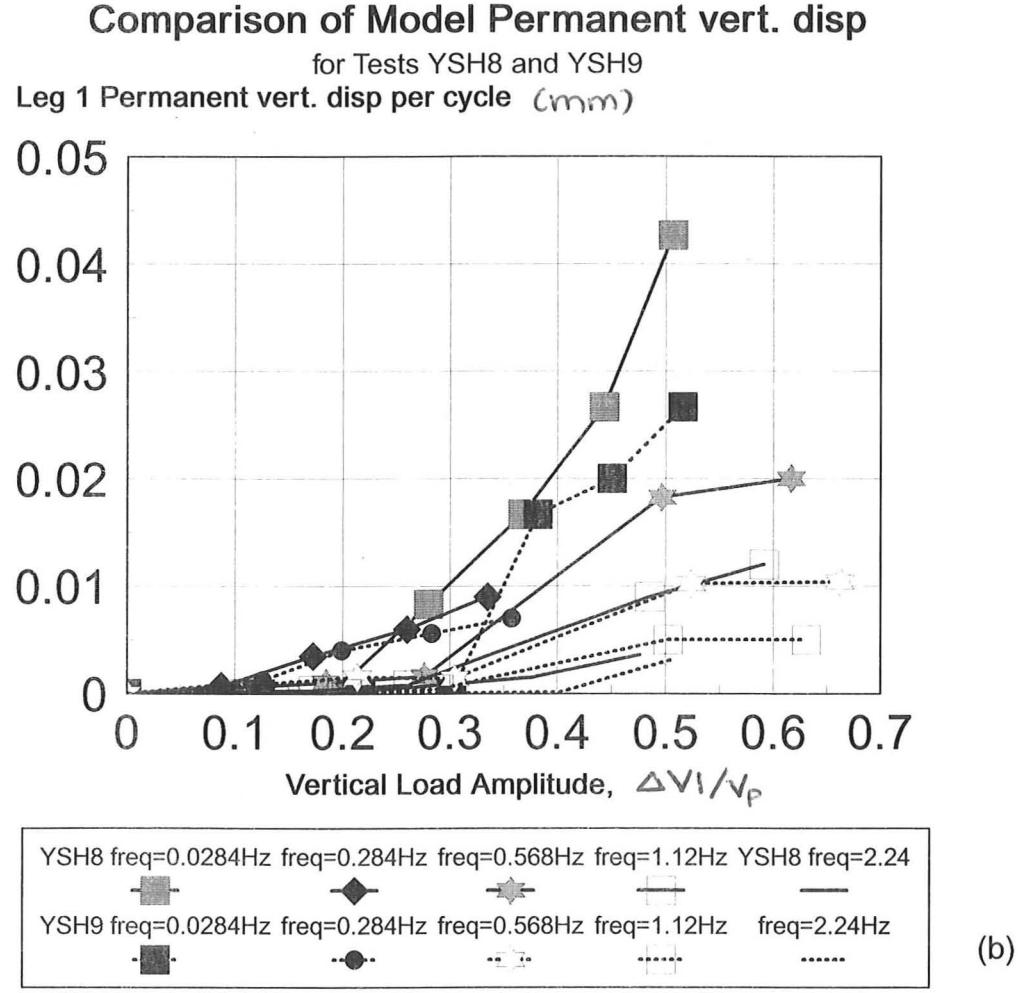

(b)

Fig. 5.4 Effects on settlement and excess pore pressure amplitude with respect to vertical load amplitude

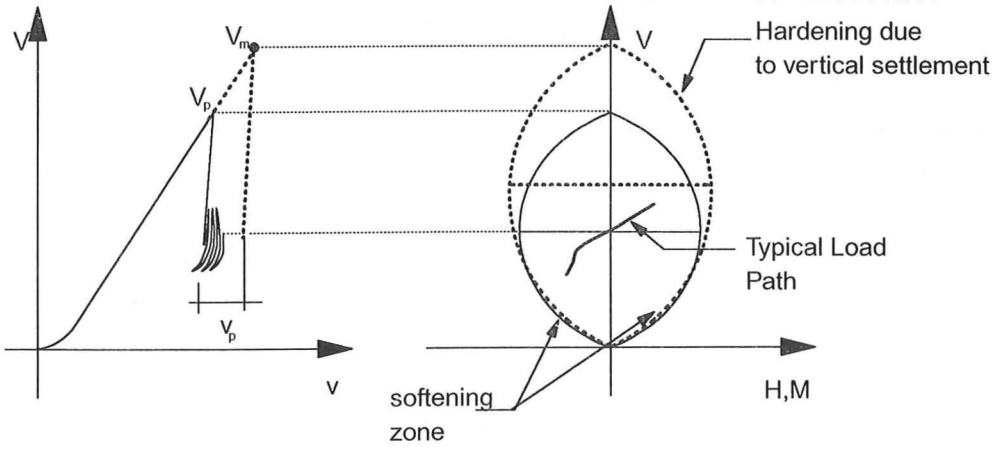

Fig. 5.5 Settlement causing hardening ie. expansion of yield locus

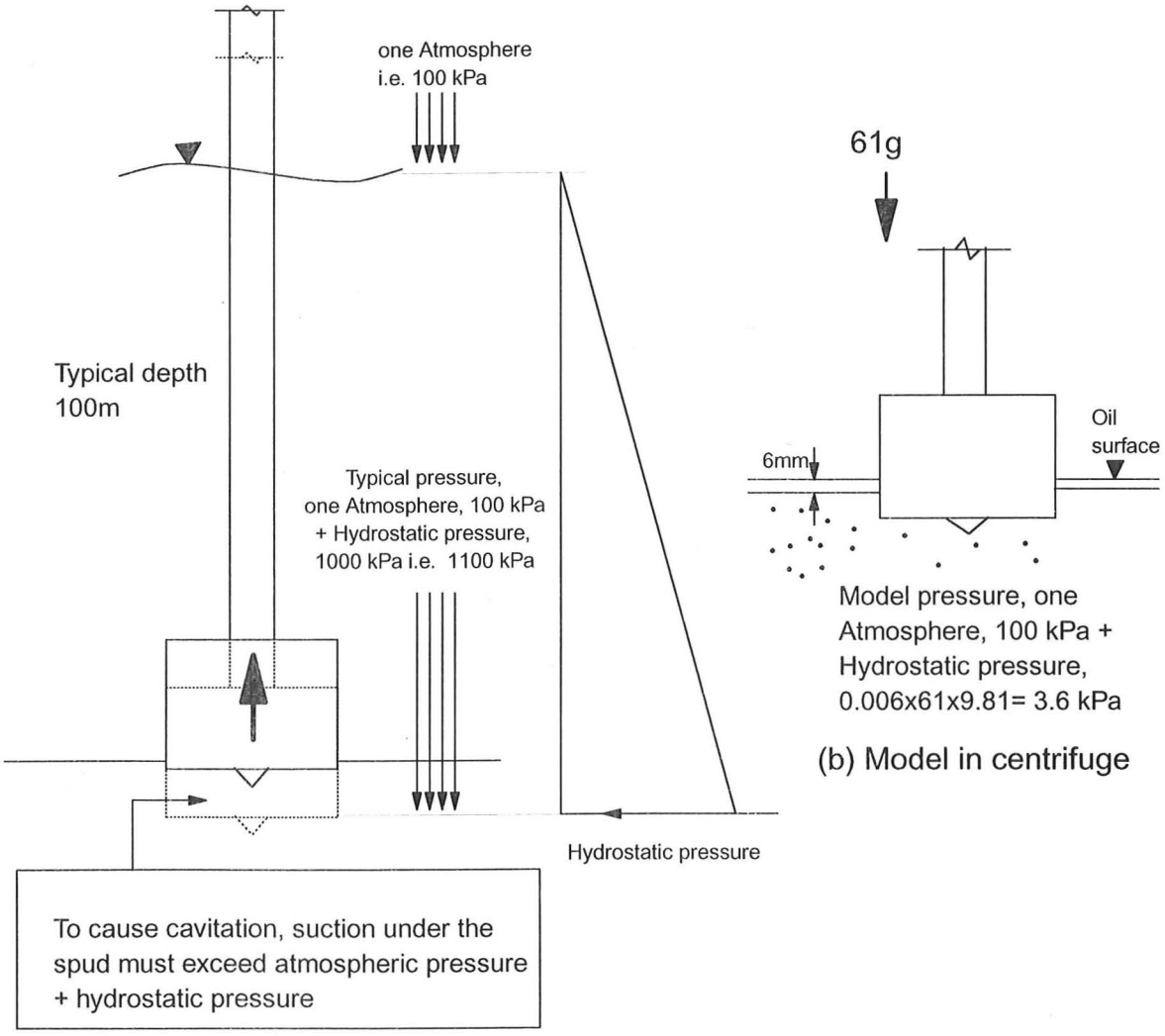

Fig. 5.6 Creation of cavitation under the spud can foundation

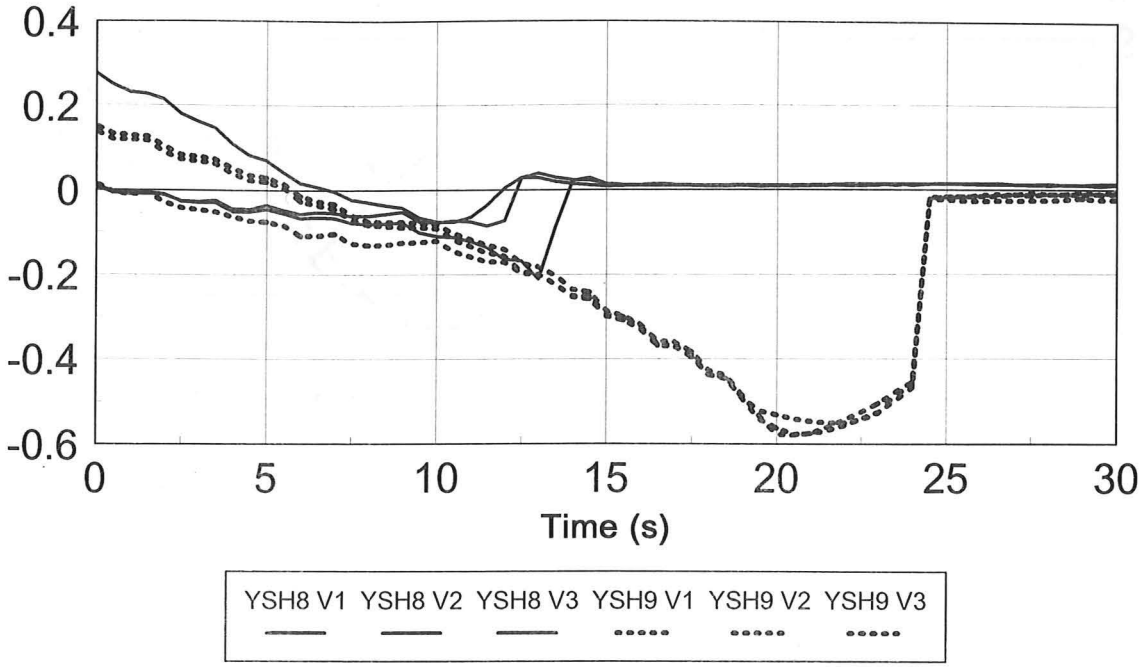

Fig. 5.7 Pull out Time plot for tests YSH8 and YSH9

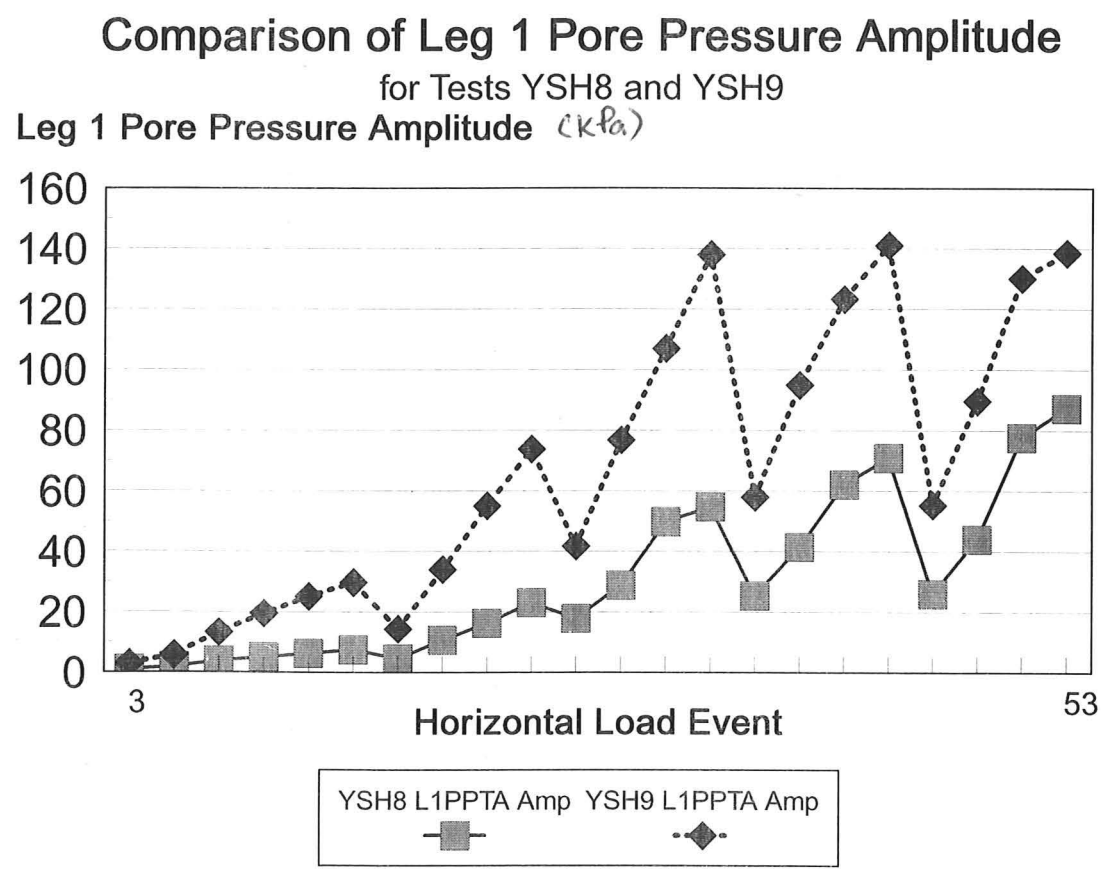

Fig. 5.8 Excess pore pressure amplitude comparison for tests YSH8 and YSH9

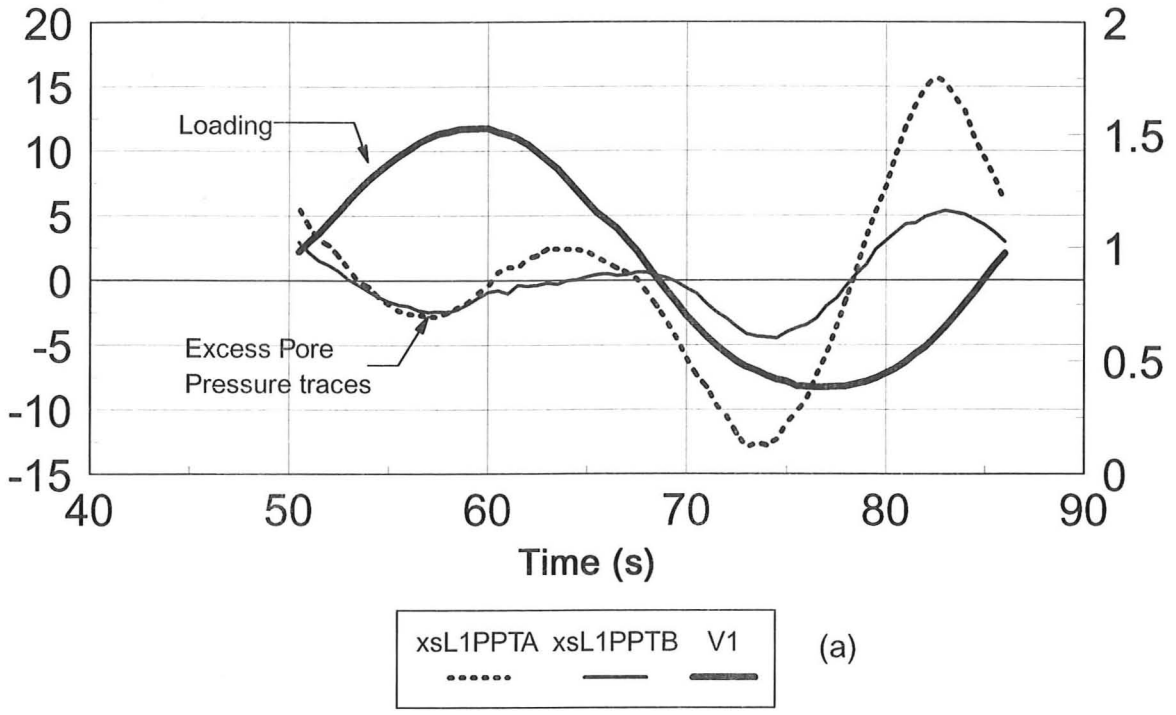

(a)

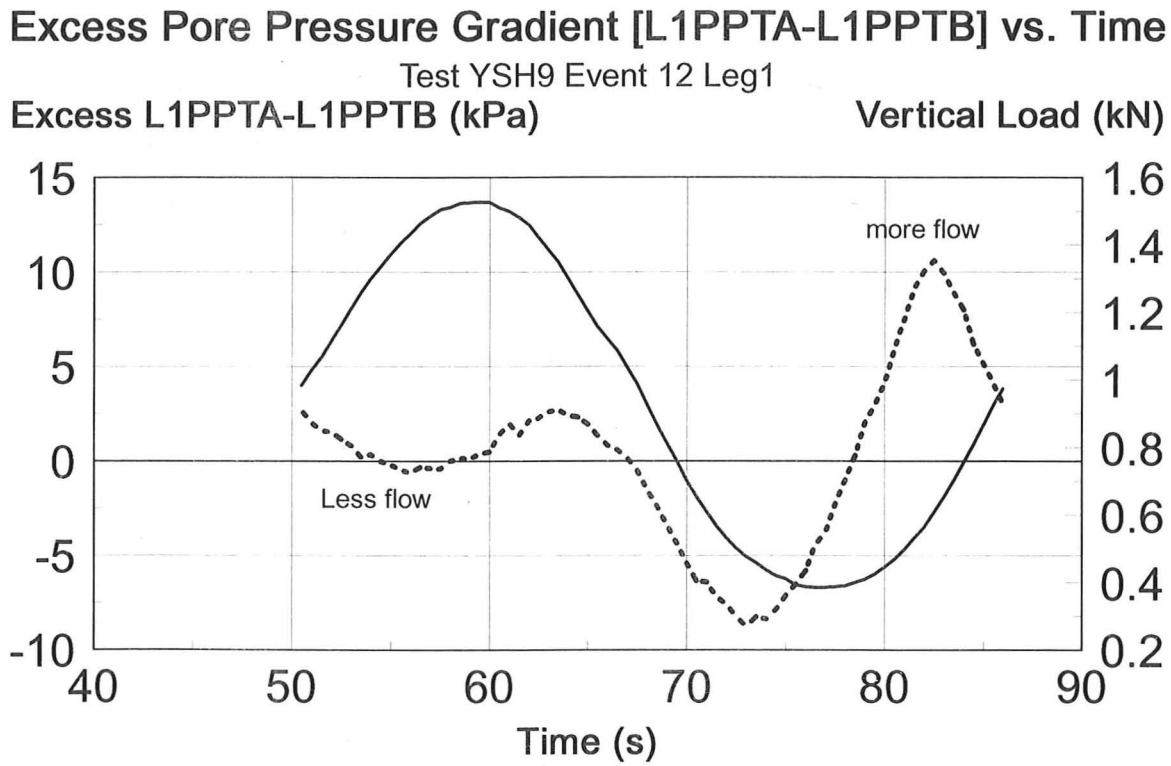

(b)

Fig. 5.9 Effects of Excess pore pressure at A and B

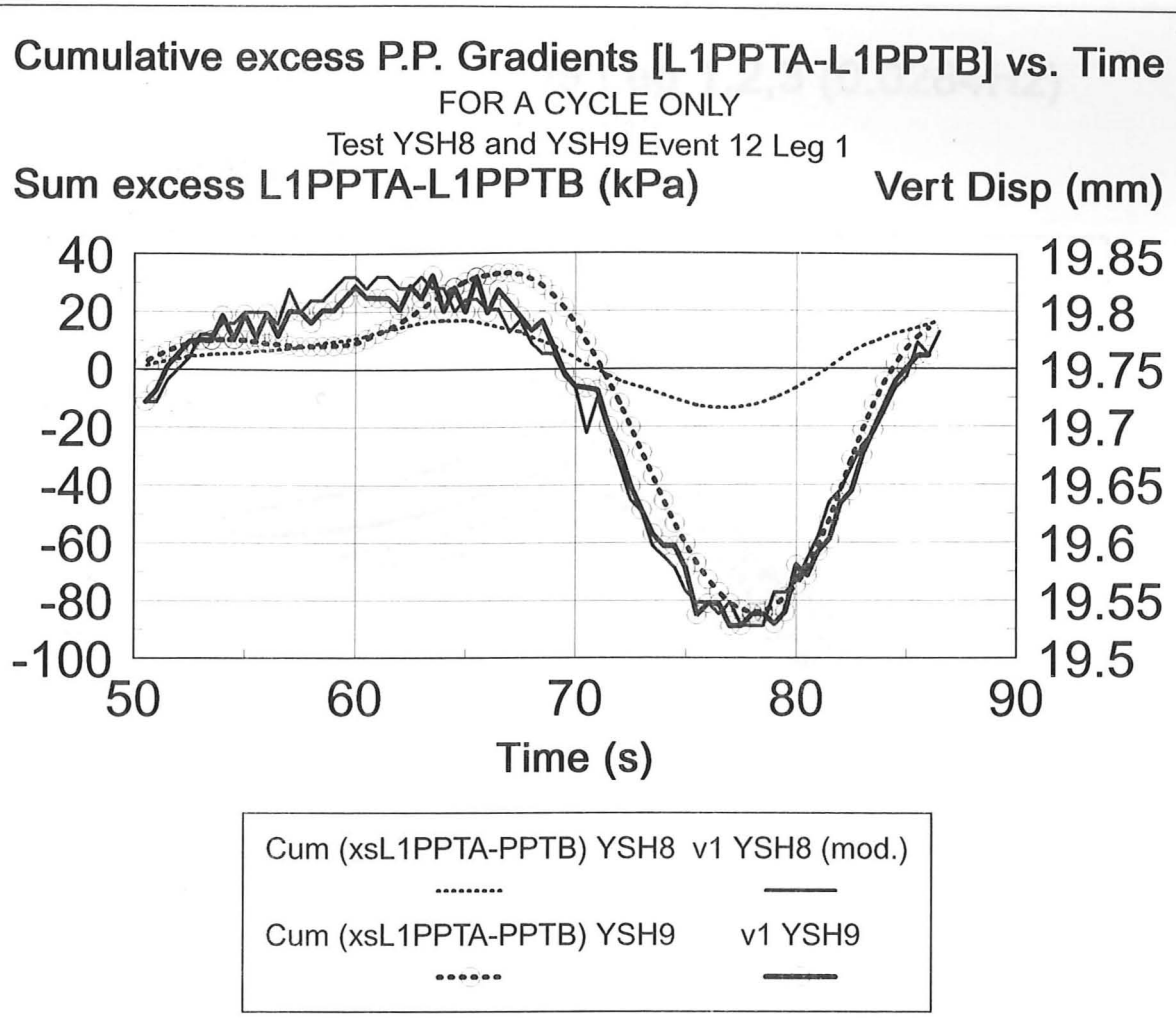

Fig. 5.10 Sum of difference of excess pore pressure between A and B superimposed with settlement profile

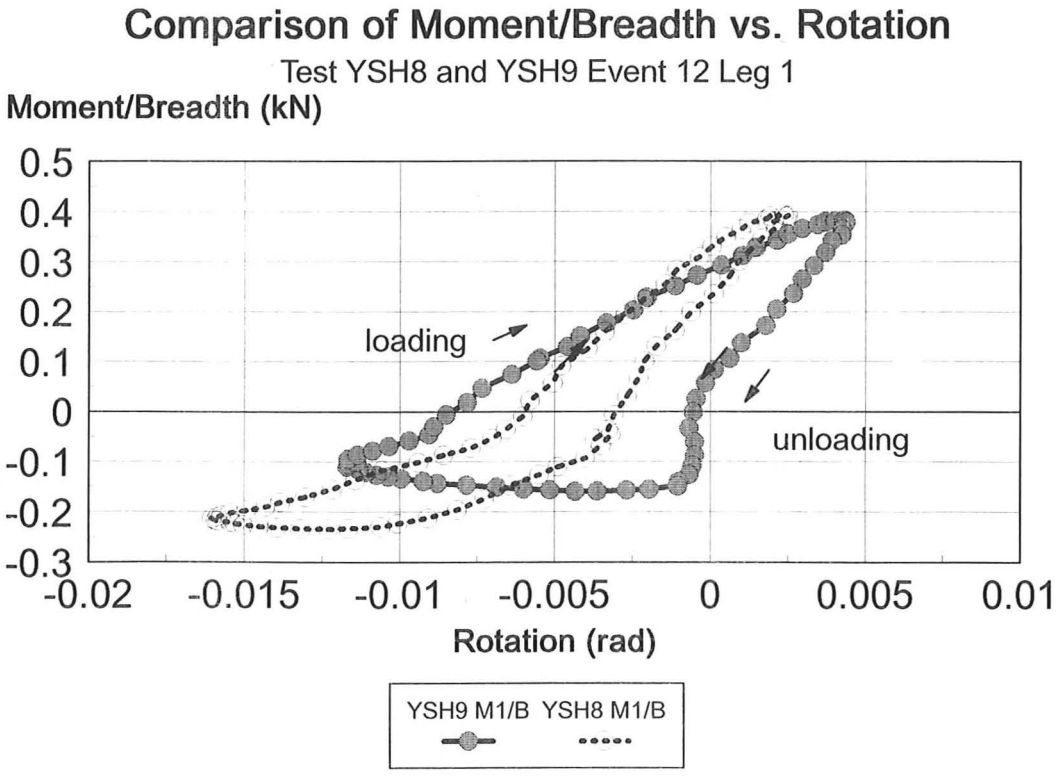

Fig. 5.11 Moment vs. Rotation plot for YSH8 and YSH9

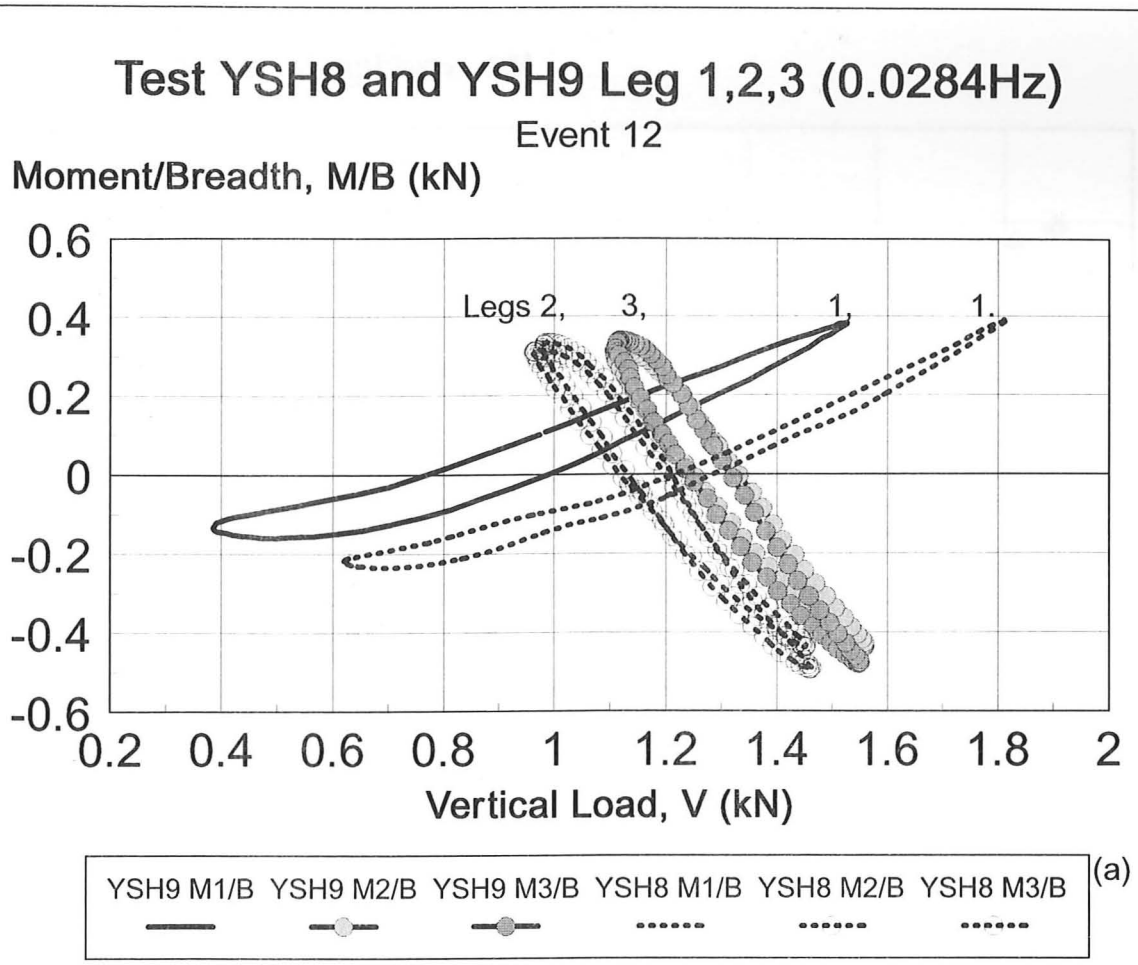

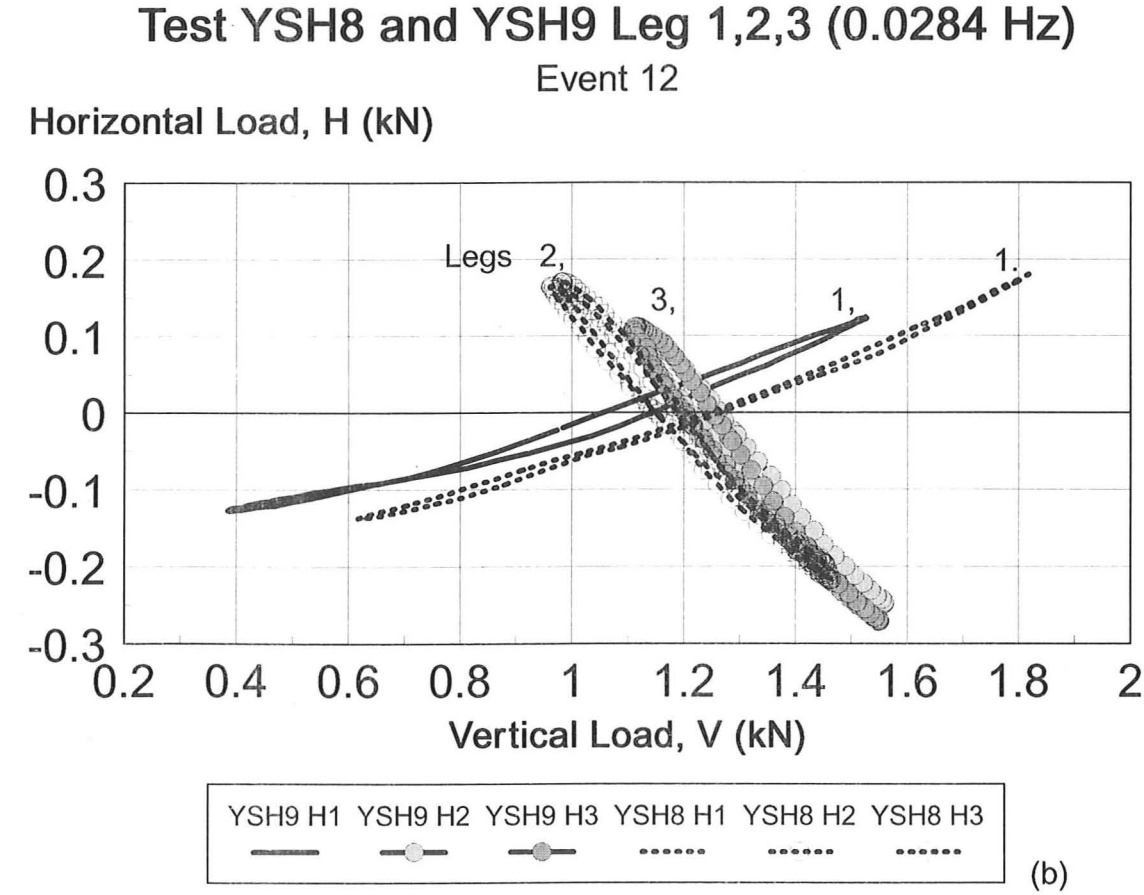

Fig. 5.12 Load Paths comparison for Test YSH8 and YSH9

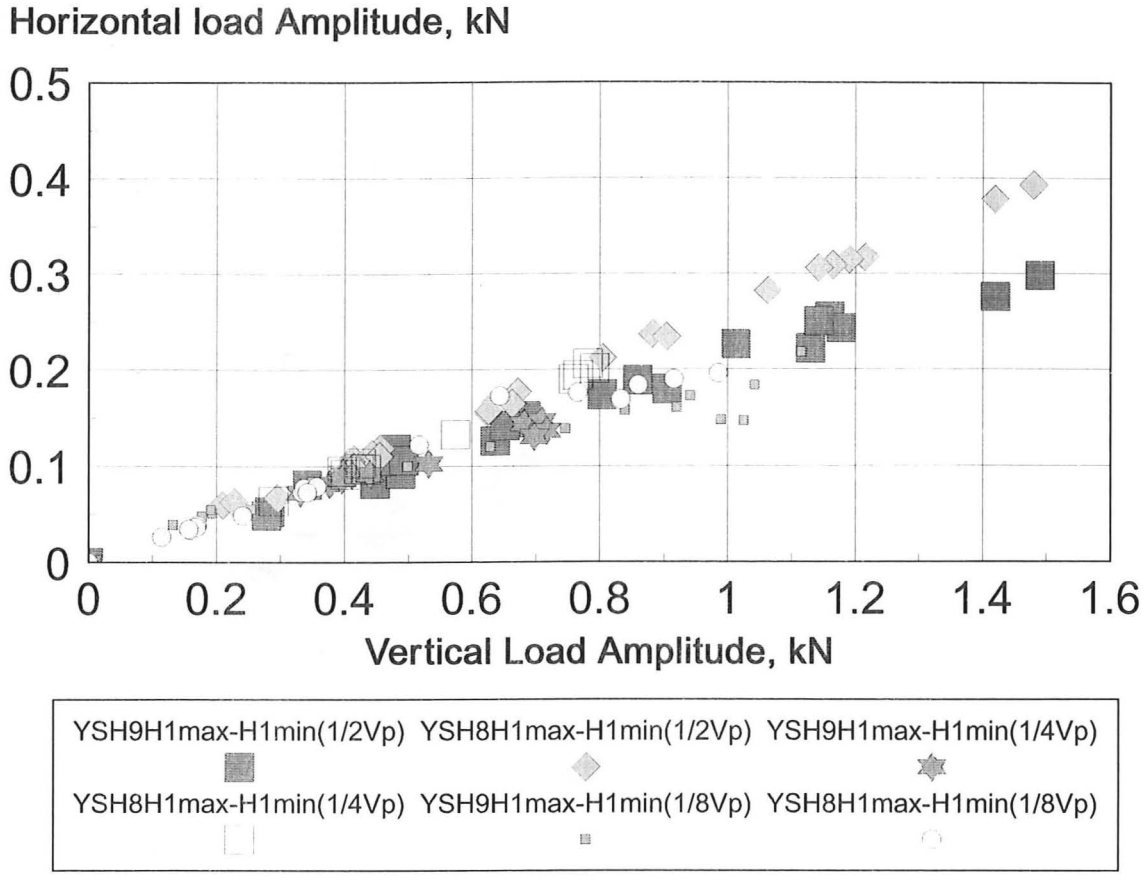

(a)

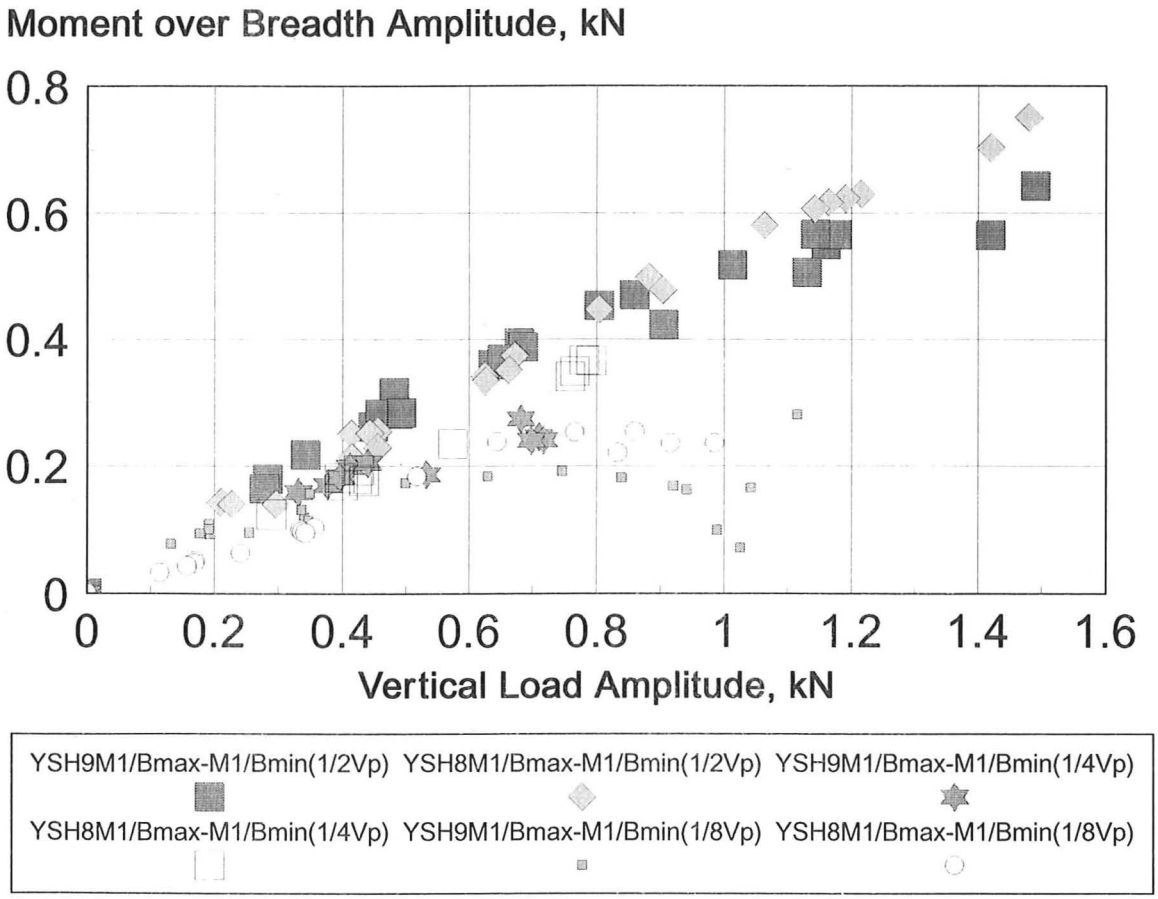

(b)

Fig. 5.13 Simplified secant load paths

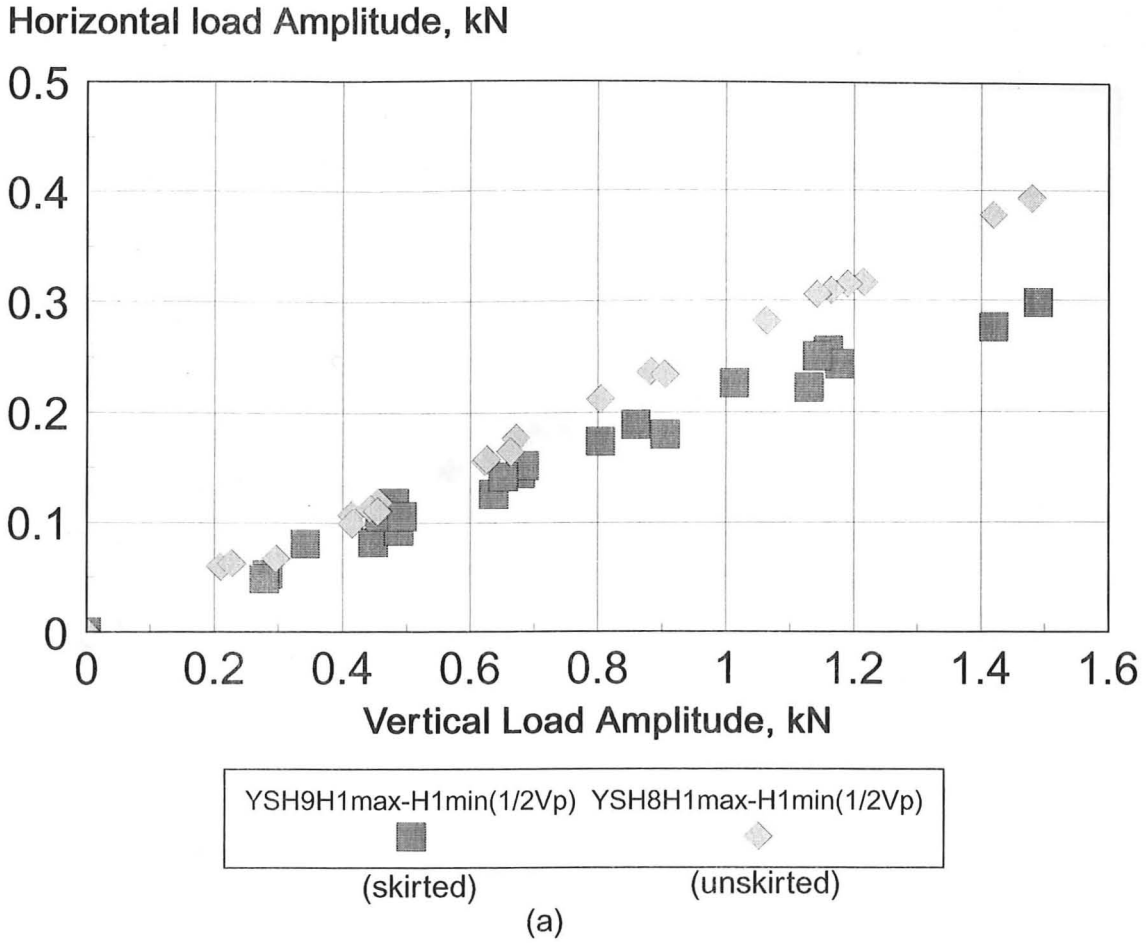

(a)

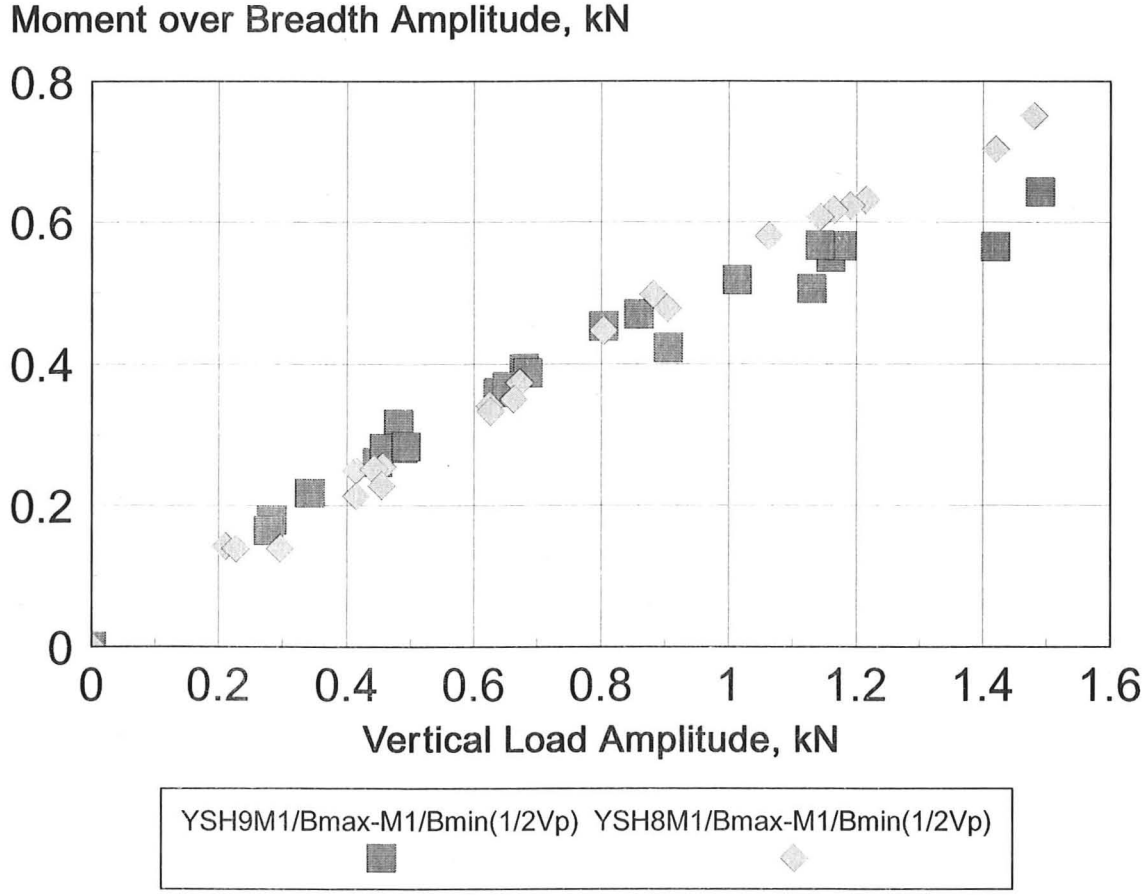

(b)

Fig. 5.14 Simplified secant load paths at 1/2 Preload working load

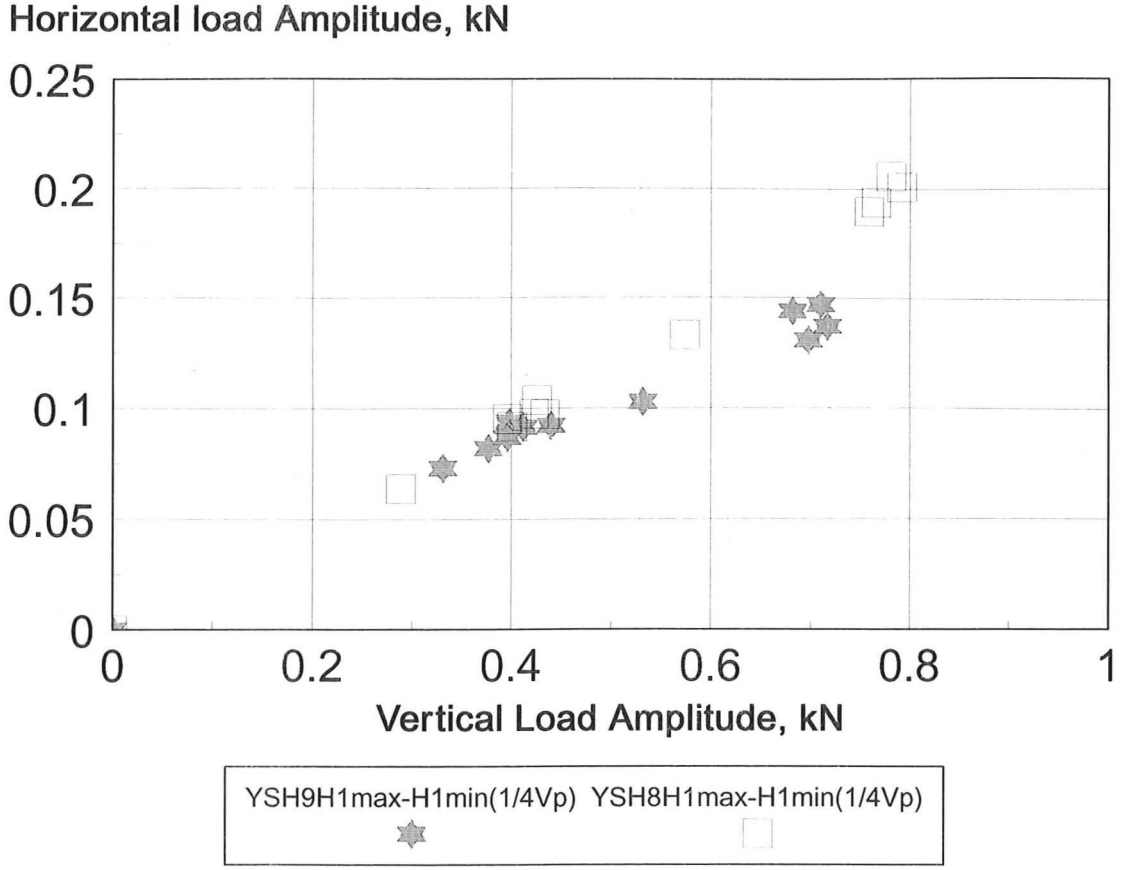

(a)

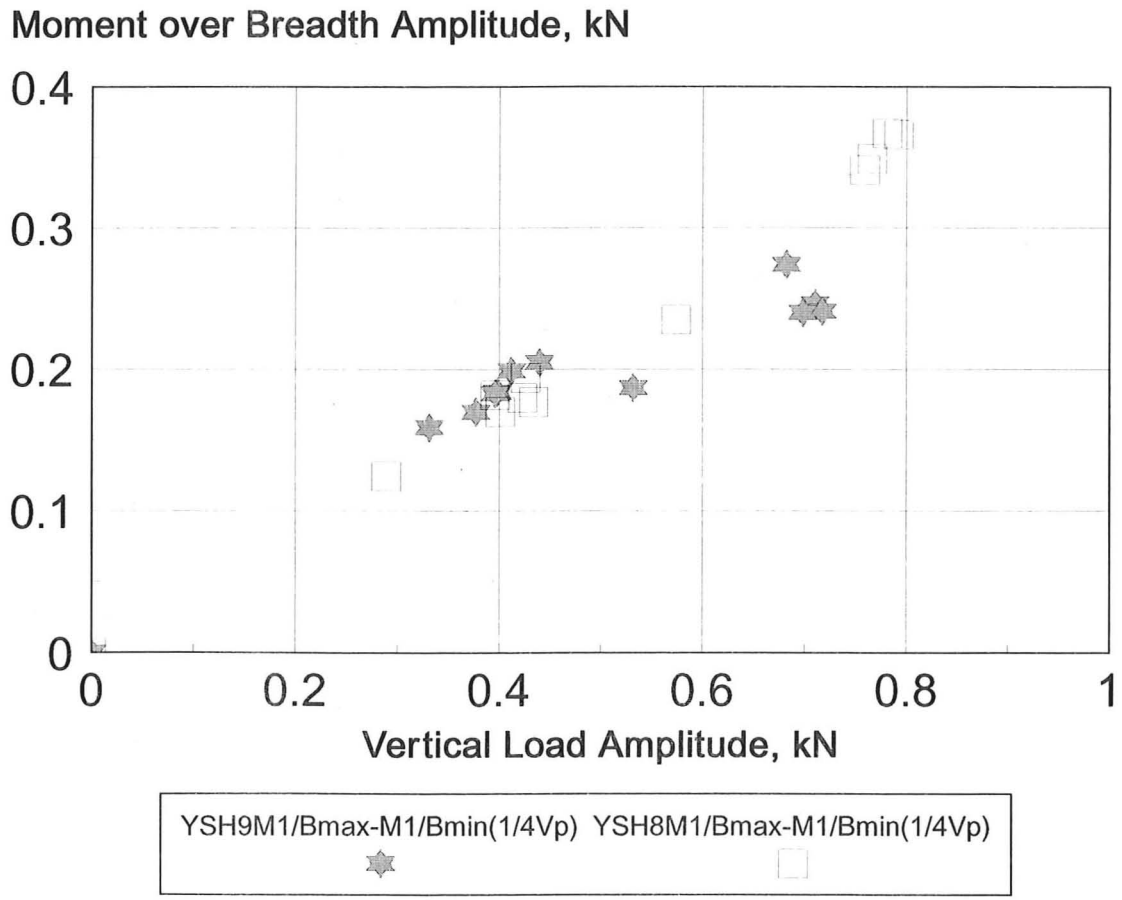

(b)

Fig. 5.15 Simplified secant load paths at 1/4 Preload working load

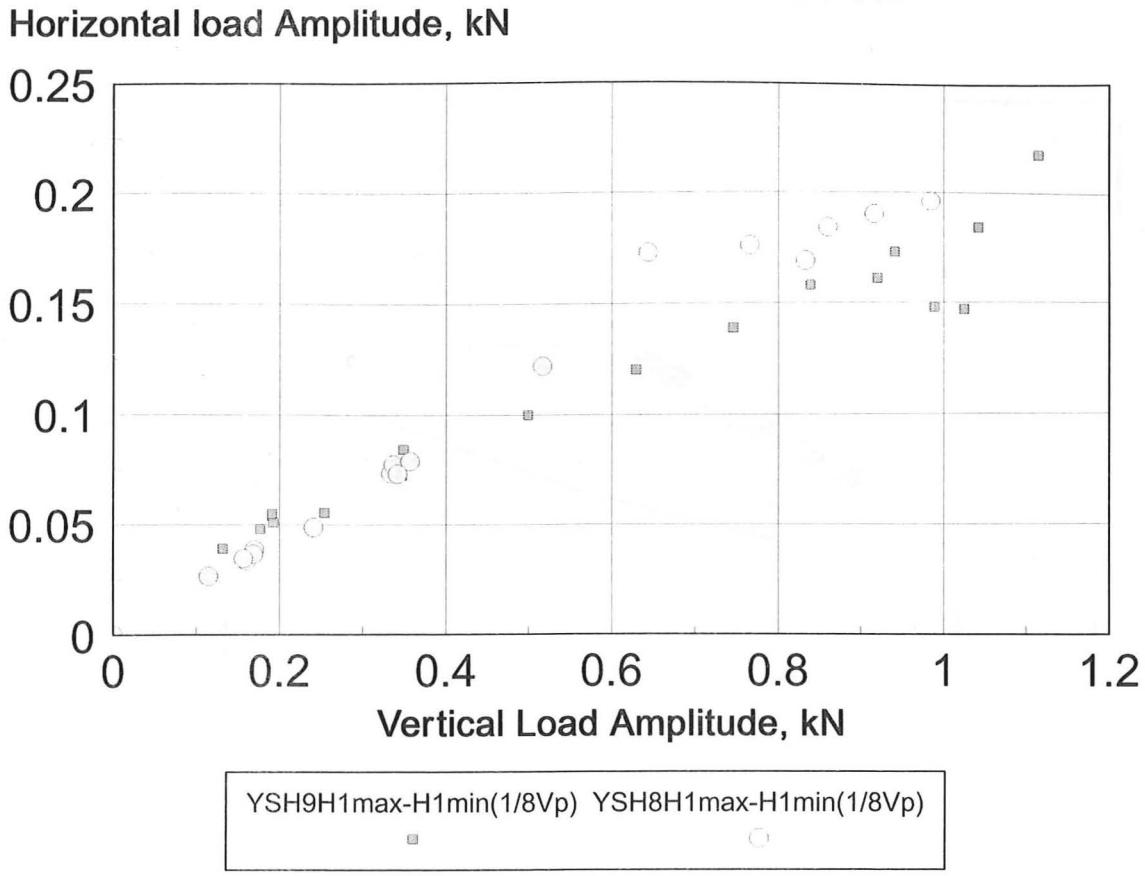

(a)

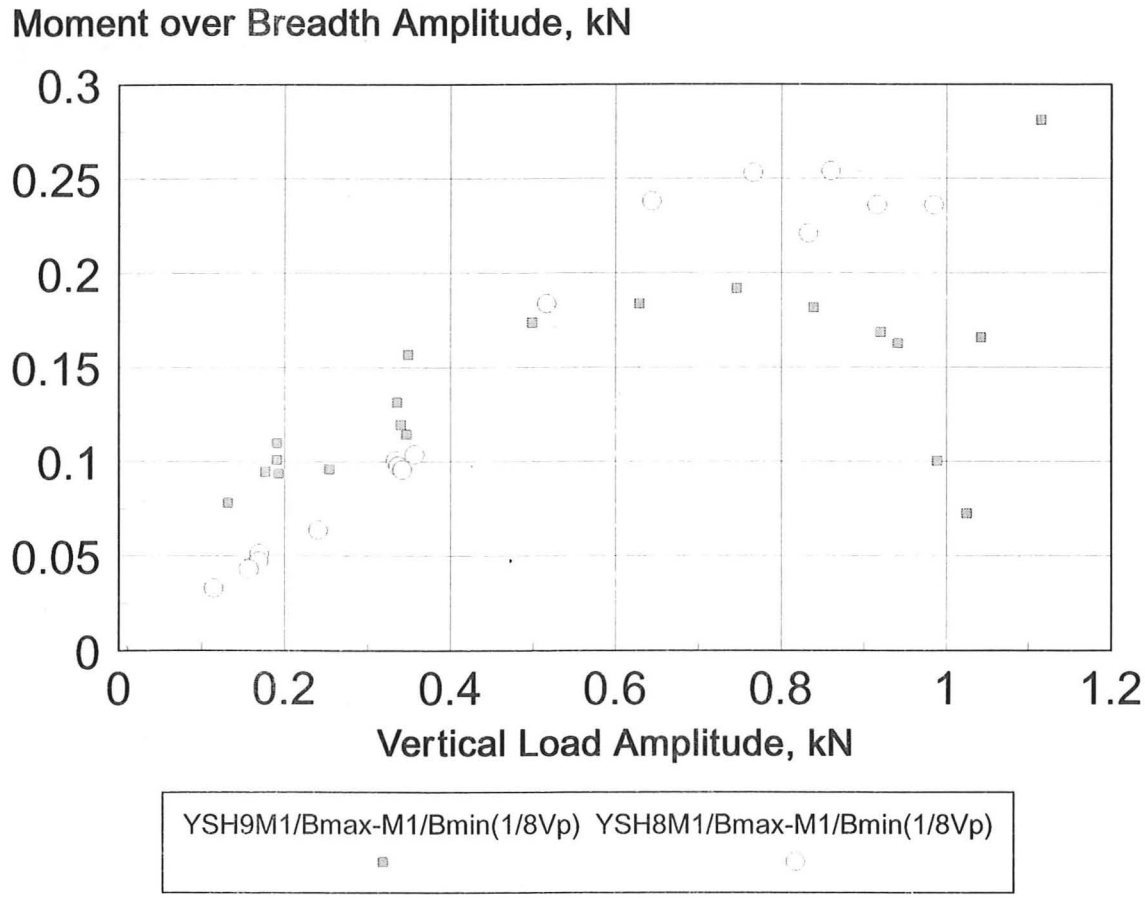

(b)

Fig. 5.16 Simplified secant load paths at 1/8 Preload working load

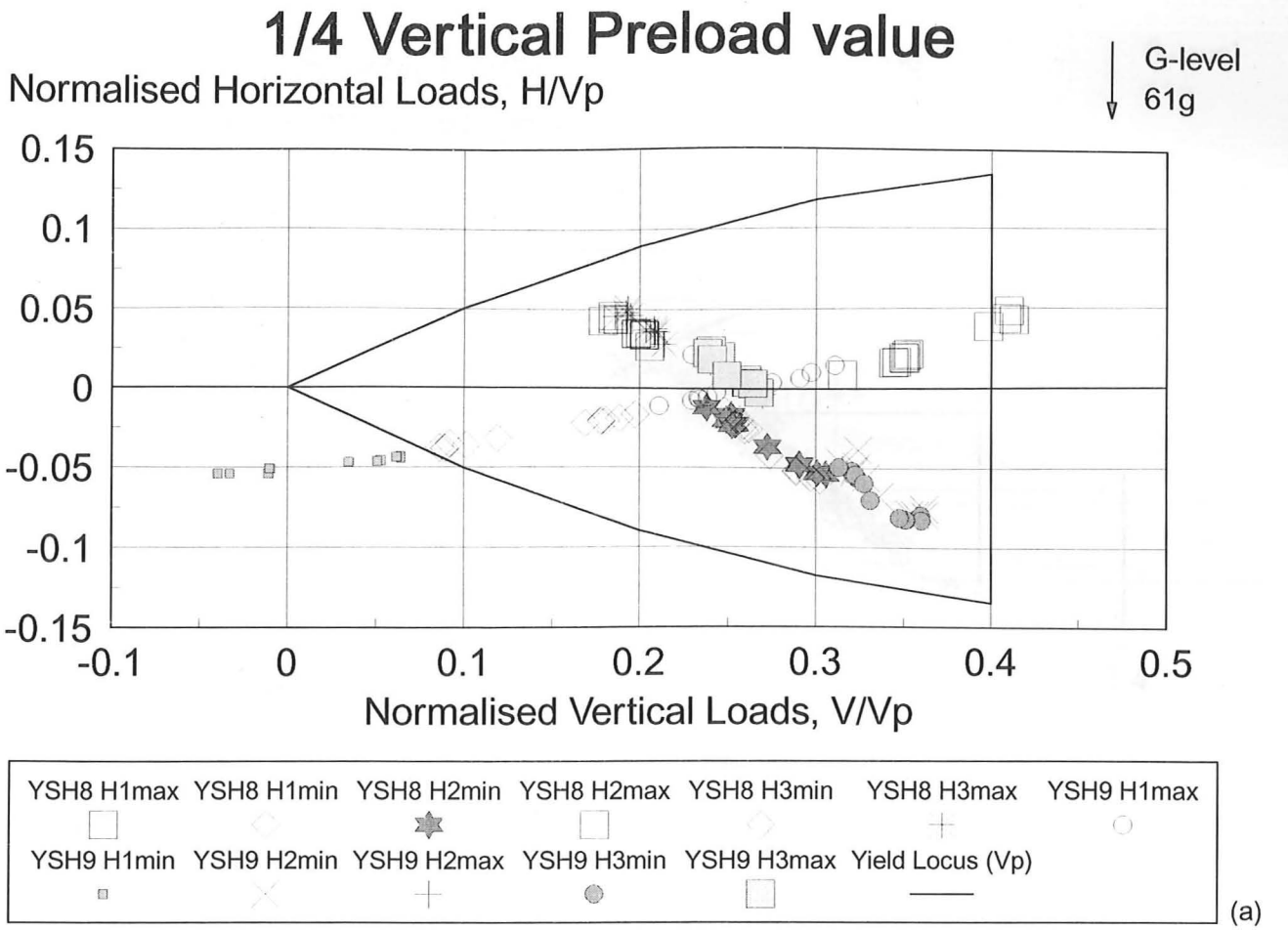

(a)

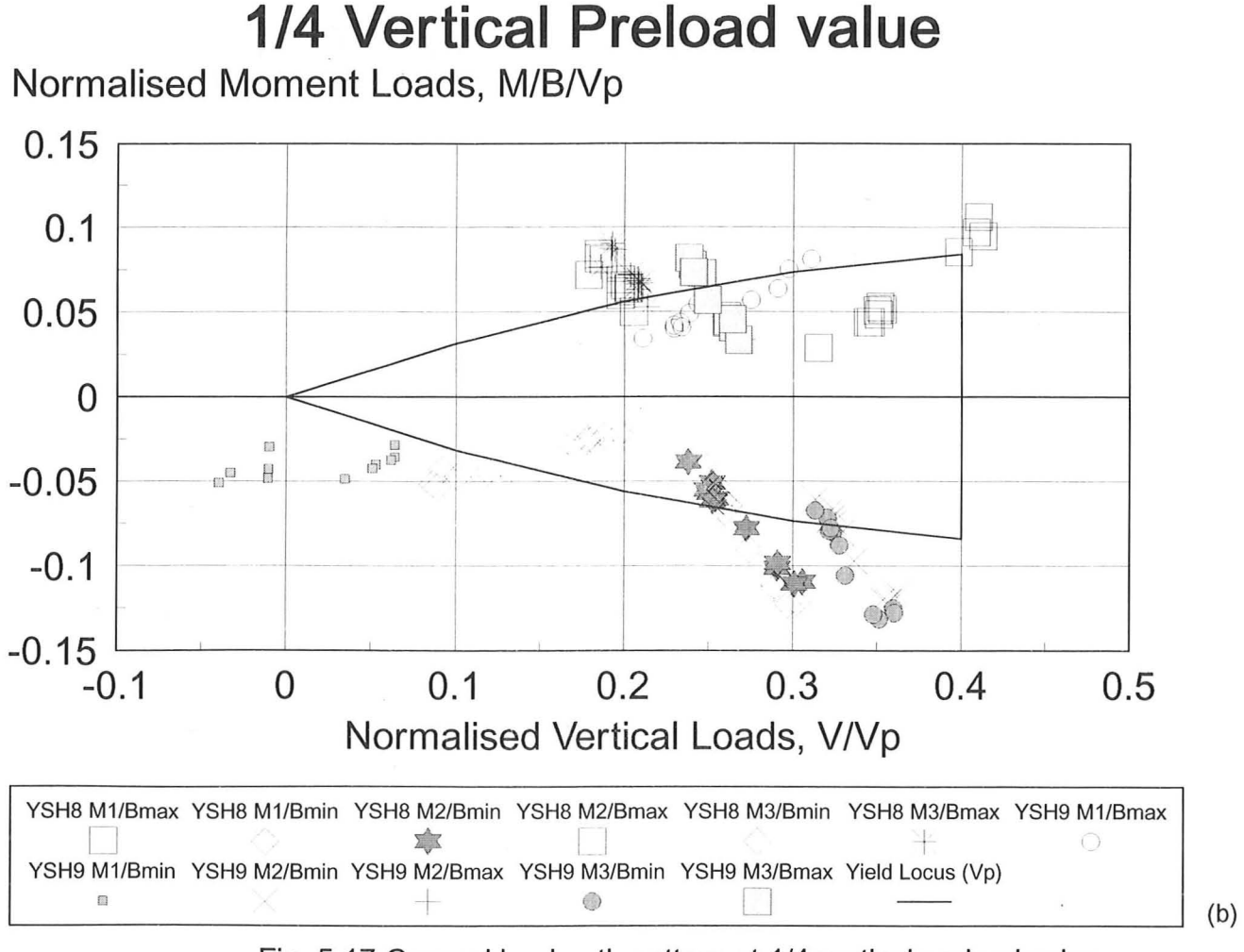

(b)

Fig. 5.17 General load path pattern at 1/4 vertical preload value

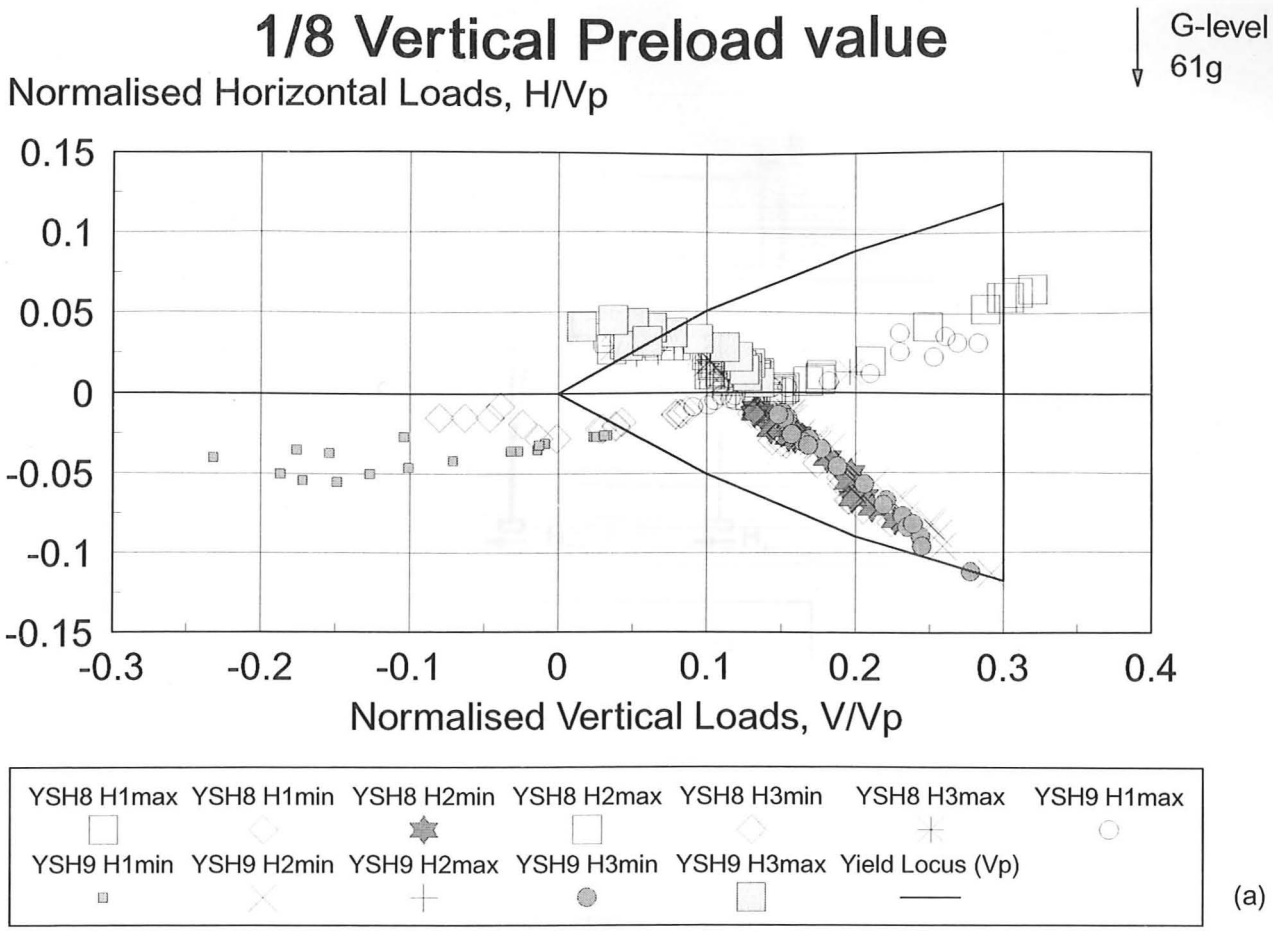

(a)

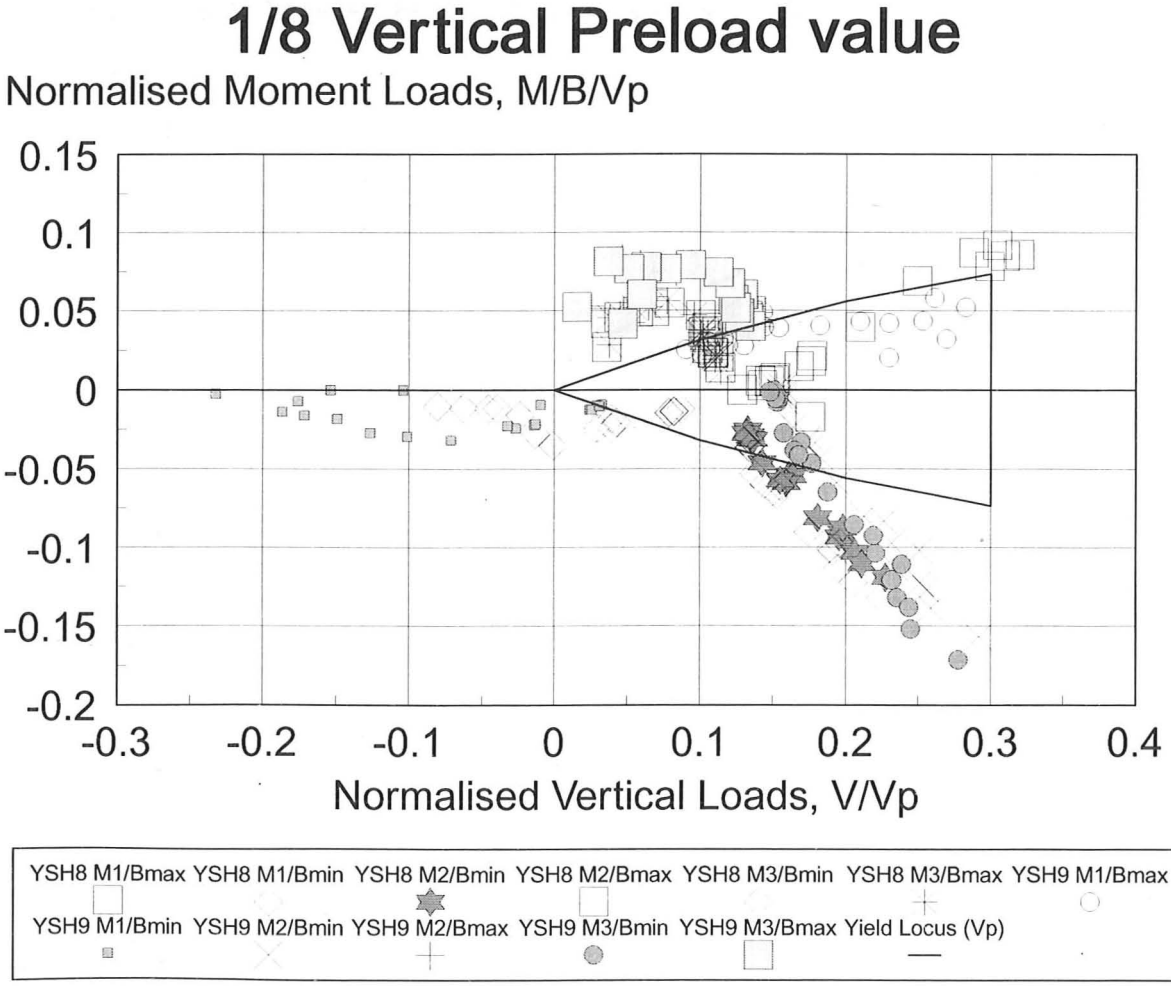

(b)

Fig. 5.18 General load path pattern at 1/8 vertical preload value

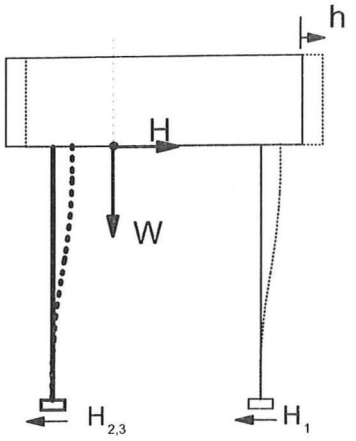

$H = H_1 + H_2 + H_3$

Hull Stiffness= H/h

fig. 5.19 Hull Horizontal stiffness

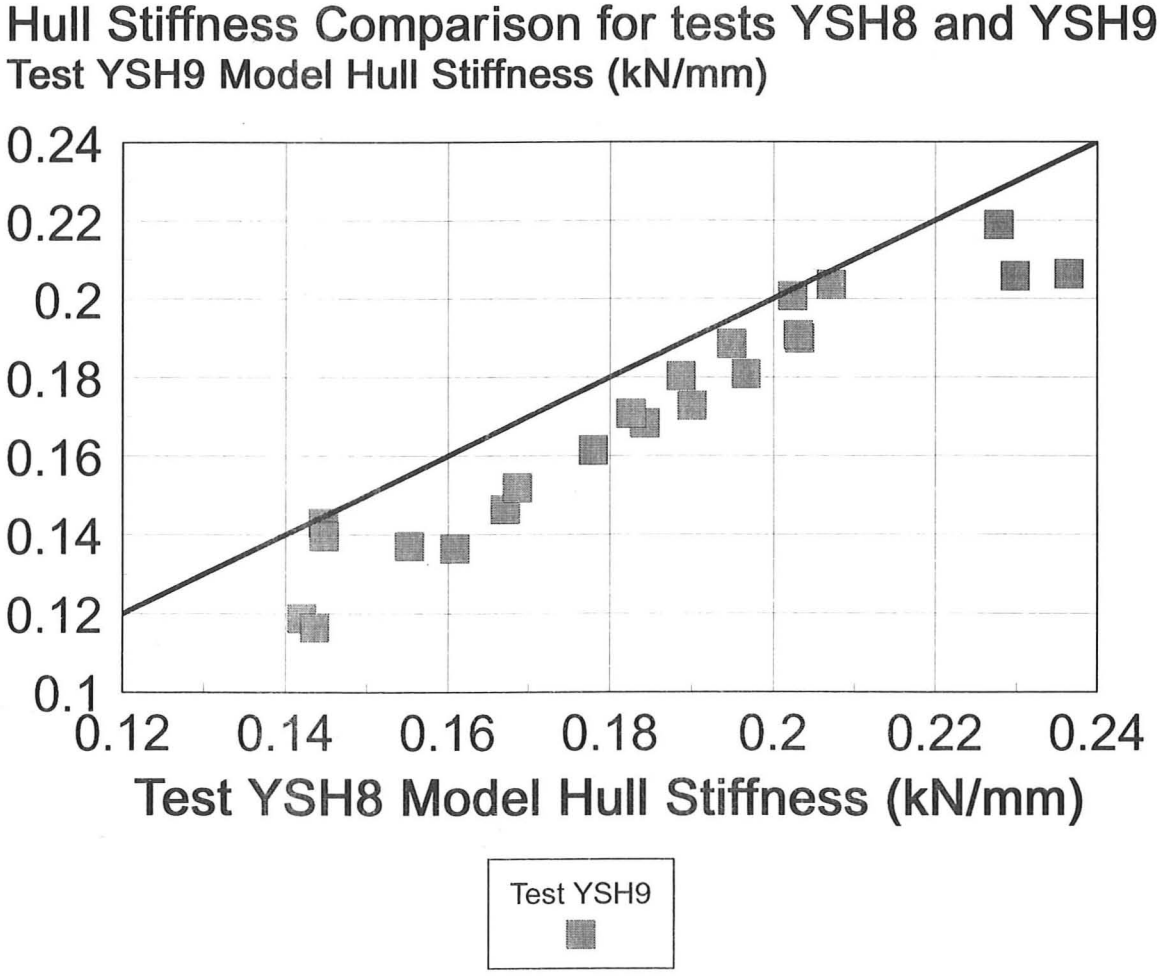

Fig. 5.20 Comparison of Hull stiffness between tests YSH8 and YSH9